University of Reading

Dynamic variations in anthropogenic heat flux: a model and its implications

Isabella Capel-Timms

Department of Meteorology and School of Built Environment

A thesis submitted for the degree of Doctor of Philosophy

December 2020

Abstract

Recent advances in urban climate modelling and weather forecasting have allowed for the integration of multiple processes at fine resolutions. Anthropogenic heat flux (Q_F) is the thermal emission due to human activity and is therefore most relevant in urban areas. It can impact aspects of urban meteorology through the modification of other surface energy balance fluxes. Despite this, Q_F is often underrepresented in forecasting and urban land surface studies. Whilst current modelling approaches provide reasonable estimates, they do not have the capability for detailed scenario modelling.

This thesis presents a novel, agent-based Q_F modelling approach (**D**ynamic **A**nthropogenic activitie**S** impacting **H**eat emissions – DASH) with human behaviours governing its fundamental dynamics, integrating simple building energy and transport models. This model can be used to investigate a city's response to scenarios such as population growth or climate change. To facilitate inclusion with broader urban land surface studies and weather models, DASH is adapted to two more computationally efficient schemes in such a way that spatial, temporal and thermal response behaviours are still represented. DASH is also coupled to an urban land surface model, SUEWS, to allow for feedback with the outdoor environment, e.g. temperature response.

DASH is developed for Greater London for October 2014 – September 2015 at a local resolution. It is evaluated against both an existing model and energy statistics for the same area and period. Expected diurnal, weekly and seasonal patterns are observed, along with variations due to building use and demographics. Areally weighted mean annual Q_F is 6.43 W m^{-2} in the evaluated instance, and 8.47 W m^{-2} when coupled to SUEWS (under different forcing meteorology). The two more efficient schemes, with parameters derived from DASH, show means of 6.68 and 7.44 W m^{-2}, but broader distributions overall.

Declaration of original authorship

I confirm that this is my own work and the use of all material from other sources has been properly and fully acknowledged. This work contains one publication, presented as:

Capel-Timms, I., Smith, S. T., Sun, T. and Grimmond, S.: Dynamic Anthropogenic activitieS impacting Heat emissions (DASHv1.0): Development and evaluation, *Geoscientific Model Development*, 13(10), 4891–4924, doi:10.5194/gmd-13-4891-2020, 2020.

Contributions are as stated in the publication: The project was conceptualised by Grimmond, Smith, and Capel-Timms. Capel-Timms, Smith, Sun, and Grimmond developed the methods. Capel-Timms, Sun, Smith, and Grimmond undertook the analyses. Capel-Timms wrote the first draft and created the figures. Grimmond, Smith, Capel-Timms, and Sun reviewed and edited the paper for submission. Resources were supplied by Grimmond and Smith. This project was conducted as part of a PhD with supervision from Grimmond, Smith, and Sun.

I Capel-Timms

Acknowledgements

I would first like to thank my lead supervisors Sue Grimmond and Stefán Smith. They have provided guidance and insight throughout my PhD, and of course gave me the opportunity to undertake this research in the first place. I also thank my third supervisor, Ting Sun, who has been patient and helpful with my coding issues and given lots of useful assistance. Weekly discussions with my three supervisors have been invaluable, and I appreciate all the time and advice they have given me. Needless to say, I have learnt a lot from them and their expertise.

Li Shao, Sylvia Bohnenstengel and Humphrey Lean have all provided valuable feedback throughout my monitoring committee meetings. Andy Gabey guided me through GQF in the early stages which benefitted my understanding of Q_F modelling. Thanks also go to my examiners Li Shao and Richard Snape for their enthusiastic conversation during my viva.

I would also like to thank past and present members of the Micromet group here in the Department of Meteorology. Their advice during meetings has helped improve a lot of my 'plots of the week', and it was enjoyable going along with some of them to various conferences and workshops. Members of the EEE Research Group at the School of Built Environment have also provided insightful suggestions. It has been fascinating to learn about the research from people in both of these groups, I hope to work with them in the future.

Other PhD students, especially those in 2U06, have been a great support throughout my time here. The events throughout the year keep us going and office chats are an ideal way to break up the day. Beth Saunders and David Meyer have been great friends, both during lunchtimes and in life outside of uni.

Imogen Capel-Timms, Joe Platonoff and Rose Hubbard all helped with the proof-reading, I thank them all for their time in doing this, as well their motivation and help these past years!

Finally, my family have given me boundless support and encouragement my through my whole life and education. I am infinitely grateful for this, without it I would not be where I am today, nor would this thesis exist.

Table of Contents

List of Figures

List of Tables

List of Abbreviations

Abbreviation	Definition
AADT	Annual Average Daily Traffic
ABM	Agent-based model, agent-based modelling
API	Application programming interface
BEM	Building energy model
BUS	Bottom-up simulation
CBD	Central business district
CDD	Cooling degree-days
DASH	**D**ynamic **A**nthropogenic activitie**S** impacting **H**eat emissions
DHW	Domestic hot water
DM	Daytime median
DOY	Day of year
EBC	Energy balance closure
GIS	Geographical information system
GL	Greater London
GQF	GQF model (Iamarino et al., 2012; Gabey et al., 2019)
HDD	Heating degree-days
HVAC	Heating, ventilation and air conditioning
IQR	Interquartile range
LA	Local authority
LOWESS	Locally Weighted Scatterplot Smoothing
LSOA	Lower layer super output area
MAE	Mean absolute error
MBE	Mean bias error
MM	Midday median
MSOA	Middle layer super output area
NS	Non-school weekday
NWP	Numerical weather prediction
OA	Output area
RMSE	Root mean square error
SEB	Surface energy balance
SR	Statistical relations
STEBBS	**S**implified **T**hermal **E**nergy **B**alance for **B**uilding **S**cheme
SW	School/work-day
TDI	Top-down inventory
TKE	Turbulent kinetic energy
ToU	Time of use
TUS	Time use survey
UBL	Urban boundary layer

UCM	Urban canopy model
UHI	Urban heat island
UK	United Kingdom
ULSM	Urban land surface model
USA	United States of America
WD	Weekday
WWR	Window-to-wall ratio

Notation

With location of 1st mention.

	Description	First section
$\alpha_{j,A_N}, \alpha_{j,k}, \alpha_{j,u}$	Characteristic of appliance α of type j: quantity in A_N, domestic usage factor u, market permeation k	3.2.4.3
$a_D^N, a_E^N, a_H^N, a_O^N, a_R^N, a_W^N$	Domestic, primary school, secondary school, other (e.g. leisure) shop and work subareas	3.2.1
$a_D^{senior}, a_D^{working}, a_D^{young}$	Dominant age cohort characteristics of subareas (analysed): seniors, working adults and young people (infants, children or teenagers)	3.4
$a_{F,0}$, $a_{F,1}$, $a_{F,2}$	V scheme regression coefficients for base, cooling and heating energy demand response	4.2
a_S^N	Subarea of A_N with specific activity s occurring	3.2.1
A	Building surface area (m^2)	App. B
AADT	Annual Average Daily Traffic	3.3.1
ABM	Agent-based model	3.2
A_c, A_h	U scheme coefficients for cooling and heating energy demand response	4.2
AE_i	Absolute error ($\lvert\Delta_i\rvert$)	3.3.2
A_N	Spatially discrete agent	3.2
AnE_i	Absolute normalised error	3.3.2
AO	Consumption class: active only	3.2.4.3
API	Application programming interface	3.2.4.2
AS	Consumption class: active/standby	3.2.4.3
β	Bowen ratio (Q_H/Q_E)	3.2.4.1
b_b, b_c, b_h	U scheme base energy demand coefficients for zero heating or cooling response (b), maximum cooling response (c) and maximum heating response (h)	4.2
B	Spatial unit, may be coarser than A_N	3.2.2
C	Consumption class: continuous	3.2.4.3
CBD	Central business district	3.6
$C_{m,r}$	Mode-appropriate ratio for m on r ($n_{o,m,r}$ vehicle^{-1})	3.2.4.2
c, c_p	Specific heat capacity, specific heat capacity of air at constant pressure (J kg^{-1} K^{-1})	3.2.4.3
Δ_i	Model-observation (reference) difference for variable i	3.3.2
DASH	***D**ynamic **A**nthropogenic activitie**S** impacting **H**eat emissions*	3.1
DHW	Domestic hot water	3.2.4.3
$d_{i,j}$	Distance between origin i and destination j (m)	3.2.2
ε	Emissivity	App. B
f	Fuel type	3.2.4.2
f_{x,α_j}	Fraction of households with x active occupants using α_j	3.2.4.3
$F_{m,f}$	Heat emission with fuel type f for m (W m^{-1})	3.2.4.2
$\Gamma_{i,j}$	Gravity weighting for all potential trips between origin i and destination j	3.2.2
GIS	Geographical information system	3.2.4.2
GL	Greater London	3.3.1
GQF	GQF model (Gabey et al., 2019)	3.3.2
h	Convection coefficient (W m^{-2} K^{-1})	3.3.1
HC	Heating and cooling usage	3.2.4.3
HW	Hot water usage	3.2.4.3
IQR	Interquartile range	3.3.2
κ	System efficiency	3.2.4.3
$K_\downarrow$	Downwelling shortwave radiation (W m^{-2})	3.2.4.3
k_e	Effective thermal conductivity (W m^{-1} K^{-1})	3.3.1
λ_i	Urban land cover (building + paved) fraction	4.2
l	Lighting (lm m^{-2})	3.2.4.3
l_{base} (l_{min}/l_{max})	Base (min/max) luminous intensity	3.2.4.3
L	Thickness of building component (m)	App. B
LA	Local Authority	3.3.1
L_m	Length of unit vehicle for m (m)	3.2.4.2
LOWESS	Locally Weighted Scatterplot Smoothing	3.2.4.2
$L_{r,t}$	Distance travelled in t (m)	3.2.4.2
LSOA	Lower-layer super output area	3.3.1
m	Travel mode (e.g. car, bus, train, walk)	3.2.4.2
M	Metabolic rate (W)	3.2.4.1

MSOA	Middle layer super output area	3.3.1
n_b ($n_{b,x}$)	Number of households (with x active occupants)	3.2.4.3
$n_{o,m,r}$	Number of occupants for m on r	3.2.4.2
nE_i	Normalised error	3.3.2
$nMax$	Maximum-normalised value	3.3.2
NS	Non-school weekday	3.4
OA	Output area	3.3.1
O_C	Occupant	3.2
$\pi(t)$	Stationary distribution for state at time step t	App. A
$\psi_{b/g/s/i}$	View factor for buildings/ground/sky/surface i	App. B
P, P_{max}	Power rating, maximum power rating (W)	3.2.4.3
$p(t)_{m,n}$	Transition probability from state m to state n at time step t	App. A
q, q_H, q_C	Energy use (for heating, cooling) (W)	3.2.4.3
q_{cd}	Building conductive flux (W)	App. B
q_{cv}	Building convective flux (W)	App. B
Q^*	Net all-wave radiation (W m^{-2})	3.1
Q_E	Turbulent latent flux (W m^{-2})	3.1
$Q_{F(,B/M/T)}$	Anthropogenic heat flux (emissions from buildings/metabolic activity/transport) (W m^{-2})	3.1
$Q^{\alpha}_{F,B}, Q^{HC}_{F,B}, Q^{HW}_{F,B}, Q^{l}_{F,B}$	$Q_{F,B}$ from: appliance usage, heating and cooling, hot water demand, lighting (W m^{-2})	3.2.4.3
$Q^{elec}_{F,B}, Q^{gas}_{F,B}$	$Q_{F,B}$ from: electricity, gas consumption	3.5
Q_H	Turbulent sensible flux (W m^{-2})	3.1
Q_{L*}, $Q_{L\uparrow}$	Net longwave radiation. Outgoing longwave radiation (W m^{-2})	App. B
ΔQ_S	Net storage heat flux (W m^{-2})	3.1
q_{vent}	Energy loss/gain from ventilation (W)	3.2.4.3
ρ (ρ_a)	Density (of air) (kg m^{-3})	3.2.4.3
r	Route type *r* (e.g. minor- or major-road, over-ground- or below-ground-rail)	3.2.4.2
R_{lim}	Route capacity limit	3.2.4.2
σ	Stefan-Boltzmann constant (W m^{-2} K^{-4})	App. B
STEBBS	**S**implified **T**hermal **E**nergy **B**alance for **B**uilding **S**cheme	3.2.4.3
SW	School/work-day	3.4
t	Time step (e.g. ten minutes)	3.2.3
τ	Effective transmissivity	App. B
Θ	Albedo	App. B
t_b	Journey specific time bin	3.2.4.2
T_b	Temperature threshold point for V scheme heating and cooling	4.2
T_c, T_h	Temperature threshold points for U scheme heating (*h*) and cooling (*c*)	4.2
$T_{f/s/si/so}$	Temperature or fluid *f*/surface *s*/indoor surface *si*/outdoor surface *so* (K)	App. B
T_i	Internal water/air temperature (K)	3.2.4.3
T_{max}, T_{min}	Temperature threshold points for U scheme maximum heating (*min*) and cooling (*max*) use at extreme temperatures	4.2
T_o	Outdoor air temperature (K)	3.2.4.3
ToU	Time of use	3.3.1
T_{set}	Setpoint temperature (K)	3.2.4.3
TUS	Time Use Survey	3.3.1
UK	United Kingdom	3.3.1
V_{FR}, V_R	Volumetric flow rate, ventilation rate (m^3 s^{-1})	3.2.4.3
$V_{m,r}$	Number of unit vehicles for m on r	3.2.4.2
$v, v_r, v_{r,lim}$	Speed, speed of travelling vehicle on r, speed limit on r (m s^{-1})	3.2.4.2
V_T	Volume of water tank (m^3)	3.3.1
WD	Weekday	3.3.2
ws	Wind speed (m s^{-1})	3.3.1
WWR	Window-to-wall ratio	3.3.1
X_i ($X_{M,i}, X_{O,i}$)	Output (M: modelled, O: observed/reference) value	3.3.2

Chapter 1 Introduction

1.1 Motivation

The urban climate is a result of the distinctive interactions between built-up areas and the atmospheric boundary layer, characterised by increased temperatures, reduced evapotranspiration, and changes in the energy and radiation balances compared to the rural surroundings. Populations are increasingly shifting from rural areas to cities and towns, with urban expansion rates increasing beyond this (Liu et al., 2020). As of 2018, 50% of the world's population was living in urban areas, with this proportion expected to increase to 68% by 2050 (United Nations, 2018). These dense populations are already vulnerable to weather events, and, along with the prospect of climate change, further growth presents challenges for the resilience of city services and infrastructure (HABITAT-III, 2016). A more detailed understanding of urban meteorology is therefore becoming more critical, not only with regards to the interplay between a city's morphology and the atmosphere, but also in the associations and feedbacks between urban inhabitants and city infrastructure, resources and meteorology.

As the urban landscape and climate are a result of anthropogenic change, the activities and practices of inhabitants directly interact with and influence a city's meteorology. At larger scales, the need for housing and transport networks alters the urban form and surface cover. At smaller scales, local changes in anthropogenic heat and water emissions interact with surface energy exchanges, with implications for urban meteorology. These compound factors act with complex heterogeneity across the city and have impacts on the everyday life of urban populations. Further inclusion of such processes in weather and climate models will help to address the vulnerabilities that could be faced by dense urban populations, such as increased risk of heat stress, poor air quality and flooding that may occur as a result of dynamic changes between anthropogenic adaptations and meteorology.

These matters, and the wider, global issue of climate change mitigation, drive changes in everyday behaviour and policy as cities and people adapt. This has implications for urban planning, energy demand and infrastructure (IPCC, 2014; Hatvani-Kovacs et al., 2018). For example, increasing global temperatures will lead to changes in the energy demand and load profiles related to heating and cooling buildings (Li et al., 2012; Takane et al., 2019). Building stock is replenished or retrofitted as countries aim to reduce carbon emissions (Lowe, 2007; Kelly, 2009), resulting in modifications in energy use and urban morphology. Emergent policies and trends surrounding fuel use, such as the movement towards more widespread use of electric vehicles, will have consequences for energy demand and fuel emissions. These adaptations, and other changes that may occur as the population

grows, should be examined before they are implemented in order to assess their efficacy and identify any feedbacks that may develop as a result (Martilli, 2002; Barlow, 2014).

Advances in modelling have led to a better understanding across many areas of urban meteorology over the past few decades (Arnfield, 2003; Barlow, 2014; Masson et al., 2020). The resolutions of land surface and numerical weather prediction models have increased as they seek to better represent large scale meteorology, leading to more grid spaces covering urban areas at finer detail. Improvements in computing have allowed for the integration of more processes. Despite this, the contributions of anthropogenic heat emissions are still not adequately realised, leading to uncertainties in urban weather modelling (Best and Grimmond, 2016; Hertwig et al., 2020). Monthly prescribed values are often used, ignoring temperature sensitivity and spatial differences in emission source. Existing modelling techniques provide reasonable estimates of anthropogenic heat flux (Q_F), with a range of approaches which vary in their scale of source and output (Sailor, 2011). However, no existing approaches are able to model interactions of the many fine-resolution behavioural aspects that govern anthropogenic heat across a large scale, or able to model the secondary effects of any adaptations that may occur and affect Q_F.

The behaviours influencing anthropogenic heat occur over a variety of scales. Seasonal and latitudinal variations in Q_F exhibit a dependence on meteorology and local climate (e.g. temperature), whilst socio-economic, demographic, and behavioural characteristics of the area and the people in it are reflected in Q_F magnitude and temporal patterns (Sailor, 2001; Lindberg et al., 2013). These behaviours and dependencies that govern Q_F are reflected in its great variation across both spatial and temporal scales. For example, people's movement across a city and their resultant day to day energy use have diurnal and local effects, whilst longer-term, city or nationwide impacts could occur as populations evolve, climate changes, or new technologies, such as energy efficient appliances and new transport system configurations, are adopted. Modelling possible changes to these behaviours across a large scale allows for the investigation into a range of Q_F scenarios and any further impacts on urban meteorology, including any causal mechanisms. Inclusion of low-level behaviours would also be reflected in high spatial and temporal variability of resultant Q_F values. This provides an advantage over current modelling methods that are only able to investigate Q_F retrospectively or at much smaller scales.

1.2 Objectives

The aim of this thesis is to provide a method of modelling anthropogenic heat flux (Q_F) via the related human behaviours that influence it, incorporating social, technical and physical aspects in a such a way that captures city heterogeneity. This will be adapted to provide an alternative suitable for use within a numerical weather prediction (NWP) or urban land surface model (ULSM).

The objectives of this thesis are:

1) To develop and evaluate a model to estimate anthropogenic heat fluxes that is responsive to human behaviour, associated with building and transport (Chapter 3)
2) To utilise the developed model to determine parameters that capture human behaviour and can be used in a faster model that can be incorporated into NWP-ULSMs (Chapter 4)
3) To identify the physical and socio-technical behavioural processes that influence anthropogenic heat emissions, and provide the ability to explore future scenarios (Chapters 2, 3, 4)

1.3 Thesis structure

Chapter 2 reviews the background and current literature surrounding: Q_F and its interactions with other surface energy balance fluxes and urban meteorology; current Q_F modelling approaches; the spatial and temporal variation in Q_F as related to human behaviour; and alternative modelling approaches that may be used to incorporate behavioural variations in Q_F.

The central contribution of this research is a novel approach towards modelling Q_F. Dynamic Anthropogenic activitieS impacting Heat emissions (DASH), is introduced, developed and evaluated in Chapter 3, which is published as a standalone paper[1]. An agent-based structure is used to enable dynamic responses between heat emitting sources and the environment. DASH allows factors such as building stock, demographics and meteorological forcing to influence Q_F. A simple transport sub-model simulates patterns of movement and transport across a city, allowing for spatial variation in

[1] Capel-Timms, I., Smith, S. T., Sun, T. and Grimmond, S.: Dynamic Anthropogenic activitieS impacting Heat emissions (DASHv1.0): Development and evaluation, *Geoscientific Model Development*, 13(10), 4891–4924, doi:10.5194/gmd-13-4891-2020, 2020.

energy use. A simple building energy model allows the energy use in buildings to respond to meteorological conditions. The model is applied and evaluated in Greater London.

DASH is used to derive parameters for two computationally efficient Q_F methods more suitable for use in NWP-ULSMs (Chapter 4). Both methods estimate bulk Q_F in response to outdoor air temperature and population density, and are distinguished by the shape of their response. Some of the behavioural characteristics of DASH are still accounted for through parameter derivation. The efficient methods and DASH are coupled to an urban land surface model, allowing for temperature feedbacks to occur.

Chapter 5 concludes the work done throughout the thesis, exploring the broader implications. Recommendations for future work are made, including scenarios under which changes in Q_F could be explored.

Chapter 2 Background and literature review

This literature review intends to detail the meteorology, behaviours and processes relevant to understanding the anthropogenic heat flux, as well as the existing methods used to model anthropogenic heat emissions. Section 2.1 introduces Q_F in the context of the surface energy balance (SEB) and urban climate, and states interactions with other fluxes and local to city scale meteorology to provide understanding of how changes in Q_F have wider implications for weather and climate. This describes the role played by Q_F within urban meteorology and establishes the need for responsive modelling. In Section 2.2, existing modelling approaches and Q_F integration with larger scale models are reviewed. Section 2.3 discusses the behaviours and processes that govern Q_F, detailing the scales on which these behaviours exist and change. Section 2.4 discusses agent-based modelling as a possible approach for the inclusion of behaviours and Section 2.5 concludes the review in light of the thesis objectives.

2.1 Q_F as part of the surface energy balance and urban meteorology

2.1.1 Anthropogenic heat flux

The focus of this work is the anthropogenic heat flux (Q_F), the rate of thermal emission from human activity into the surrounding atmosphere. Q_F is the sum of three fundamental components (Grimmond, 1992):

$$Q_F = Q_{F,B} + Q_{F,M} + Q_{F,T} \qquad (\mathrm{W\ m^{-2}}) \qquad (2\text{-}1)$$

where $Q_{F,B}$ is the heat flux originating from the use of energy in buildings (use of appliances, space heating/cooling), $Q_{F,M}$ is the heat flux released by the metabolic activity of humans and animals, and $Q_{F,T}$ is the heat flux caused by fuel consumption in the transport sector. This energy is released to the urban boundary layer (UBL) as sensible or latent heat, with proportions of such varying by source sector. Hence, each source sector is directly controlled by multiple aspects of human behaviour and practice (Sailor, 2011).

2.1.2 The surface energy balance

Q_F is unique to the urban SEB. The SEB describes the energy exchanges between the ground surface and the atmosphere and is critical to understanding and modelling urban microclimates (Oke, 1988). Variations in the SEB impact the diurnal growth and stability of the atmospheric boundary layer (Oke, 1988; Christen and Vogt, 2004). In an urban area the SEB also includes the storage heat flux (ΔQ_S) and the advective heat flux (ΔQ_A) (Figure 2-1; Oke, 1988):

$$Q^* + Q_F = Q_H + Q_E + \Delta Q_S + \Delta Q_A \qquad (\mathrm{W\ m^{-2}}) \qquad (2\text{-}2)$$

The net all wave radiation Q^* is the balance between the net short-wave and net long-wave radiation exchanges. The turbulent sensible heat flux density, Q_H, is the transport of heat by convection in the atmosphere, warming/cooling the atmosphere. Q_H is governed by the temperature gradient between the surface and the atmosphere. The turbulent latent heat flux density, Q_E, is the energy required to transport moisture away/to the surface by convection. This term directly links to the water balance as it is the energy equivalent to the mass term of evaporation. The storage heat flux ΔQ_S represents the exchange of heat stored in the urban fabric (i.e. building materials, ground). ΔQ_A is the flow of energy carried by the wind across the urban surface. For a widespread, homogeneous surface this is assumed to have a net value of zero (Oke et al., 2017b), and as such is ignored in most studies.

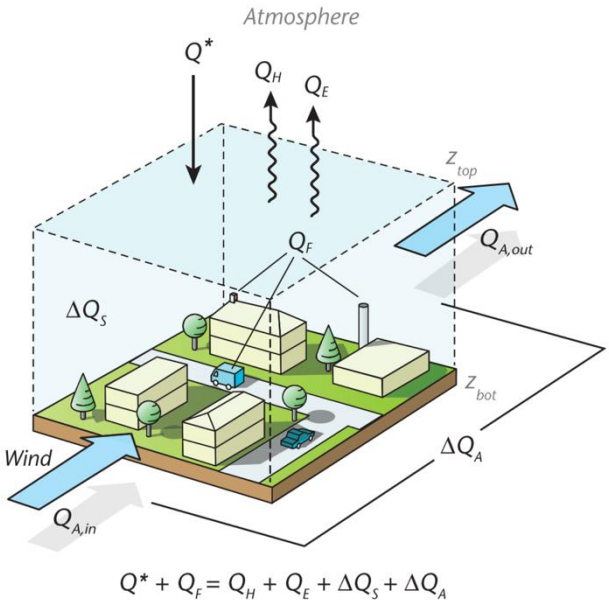

Figure 2-1: Schematic of the fluxes in the SEB of an urban building-soil-air volume. The volume that extends from the top of the RSL (z_{top}) down to a depth where there is no net conduction over the period of interest (z_{bot}). Arrows are drawn in the direction the corresponding flux is considered positive. For ΔQ_S and ΔQ_A, they are positive if the internal energy of the volume increases. (Modified after: Oke, 1987) (Oke et al., 2017b).

2.1.3 Q_F and urban meteorology

Interactions and feedbacks exist between Q_F and local environmental conditions, with impacts on wider aspects of urban meteorology varying seasonally, diurnally and spatially. Upon release to the outdoor environment, either directly or through the building fabric, Q_F contributes to turbulent heat fluxes or longwave radiation (Grimmond, 1992; Christen and Vogt, 2004; Bohnenstengel et al., 2014).

This has implications for the meteorology of the urban surface, from surface-level temperatures to the structure of the UBL. Studies and weather prediction rely on accurate modelling of these meteorological variables that are affected by Q_F, so it is crucial that anthropogenic heat is correctly accounted for. This is particularly important for studies focusing on the effects of urban meteorology on city inhabitants, for example with regard to health and energy demand. Understanding of the various impacts Q_F has on the urban environment, and more specifically the other elements of the SEB, is key to knowing the benefits that the inclusion of detailed Q_F will provide to urban land surface studies and forecasting.

2.1.3.1 Contributions to the turbulent and storage heat fluxes

As part of the available energy ($Q^* + Q_F - \Delta Q_S$; Oke et al., 2017) to the SEB, Q_F contributes to the turbulent heat fluxes (Grimmond, 1992; Christen and Vogt, 2004; Hertwig et al., 2020), affecting the depth and stability of the UBL (Fan and Sailor, 2005; Bohnenstengel et al., 2014). Misrepresentation of Q_F in urban land surface modelling or forecasts could therefore have consequences for skill when comparing forecasts to observations.

Q_F may be partitioned in to sensible (Q_H) and latent (Q_E) heat fractions, varying by source sector (Iamarino et al., 2012). Urban areas typically display an elevated Bowen ratio (Q_H / Q_E, $ß > 1$) compared to rural values, due to the lower availability of surface water and vegetation. Augmentation of Q_H from Q_F further increases this, contributing to warming of the surface layer. The proportions of Q_H and Q_E, and hence β, vary spatially. In a study undertaken from various sites in Basel, Switzerland, Christen and Vogt (2004) found elevated Q_E levels (and therefore a lower $ß$) during winter nights in the city centre, resulting in a $ß$ four times lower than the summer night-time values. This was likely due to the combustion of fuels from traffic or gas for indoor heating, as fuel combustion releases energy as both sensible and latent heat. Higher Q_E may also be found in central business districts (CBDs) due to the presence of evaporative cooling towers. Sailor et al. (2007), Moriwaki et al. (2008), Narumi et al. (2009) found that Q_F was partitioned equally between sensible and latent heat in the commercial areas of Houston, Tokyo and Osaka (resp.). This would have implications for local relative humidity. On the other hand, air-conditioning heat pumps enhance Q_H (Kondo and Kikegawa, 2003), and when used as heating systems extract heat from the outdoor environment (Ohashi et al., 2016). This highlights the importance of correctly representing the characteristics of an urban area in order to properly reflect its heterogeneity. Across an entire city the largest contribution is towards sensible heat, for example, 61% of total Q_F was released as sensible heat (23% as latent) in Osaka Prefecture (Narumi et al., 2009). This ratio is dependent on the climate and resultant energy behaviour of the city; Iamarino et al. (2012) found that 81% of Q_F emissions went to Q_H, whilst 7.3 % went to

latent heat across Greater London, where space cooling is less common. The remainder was lost to wastewater in both cases.

Any contribution of Q_F to the turbulent heat fluxes has the potential to change the stability of the UBL by changing the profile of the potential temperature gradient and through increased input of turbulent kinetic energy (TKE) to the thermal element (Ichinose et al., 1999; Martilli et al., 2002; Krpo et al., 2010; Best and Grimmond, 2016; Falasca et al., 2016). The greater the influence of thermal energy on the TKE, the greater the instability of the atmosphere. The height of the boundary layer would also be affected, as greater Q_H deepens the UBL through increased vertical air movement. When comparing the effect of multiple parameters on the UBL height via TKE production, Falasca et al. (2016) found that changes in Q_F increased the UBL height more than changes in albedo. Xie et al. (2016b) found that the UBL in Shanghai deepened by 140 m in January and 160 m in July, due to maximum contributions of Q_F to Q_H of 85 and 75 W m^{-2} respectively; depth increase is greater during the summer as the atmosphere is more unstable. They also found that relative changes in UBL height were greater during night-time for both months. During a study in Philadelphia investigating the impact of Q_F forcing using two UBL schemes, Fan and Sailor (2005) found that Q_F sources caused an otherwise stable UBL to become neutral during the morning transition in the summer case. Bohnenstengel et al. (2014) also demonstrated that Q_F caused instability in an otherwise stable boundary layer during winter nights, due to low Q_H from non-anthropogenic sources (e.g. solar radiation) and a shallow UBL. Hence, UBL stability is most likely to be affected by Q_F outside of a daytime unstable case (Barlow, 2014).

The addition of Q_F from inside buildings to the urban fabric causes an increase in the external building surface temperature, affecting the storage term ΔQ_S (Best and Grimmond, 2016). This energy is released into the UBL as additional longwave radiation and sensible heat - Bohnenstengel et al. (2014) found that one third of Q_F was emitted to the outdoor environment as longwave radiation and two thirds as sensible heat across Greater London. This creates a lag between anthropogenic emissions and changes in radiative flux. The magnitude and spread of this lag is controlled by factors such as the thermal properties of a building's materials (mainly heat capacity), its geometry and aspect ratios, and Q_F emitted within (Grimmond, 1992; Grimmond and Oke, 1999b; Offerle et al., 2005).

2.1.3.2 Q_F influence on air temperatures and the urban heat island

Multiple studies coupling Q_F estimation models to mesoscale or urban canopy models (UCM) show that local air temperatures are influenced by Q_F signals (e.g. Ichinose et al., 1999; Kondo and Kikegawa, 2003; Block et al., 2004; Fan and Sailor, 2005; Narumi et al., 2009; Krpo et al., 2010; Kikegawa et al., 2014; Salamanca et al., 2014; Xie et al., 2016a; Ohashi et al., 2016; Ginzburg and

Demchenko, 2017; Takane et al., 2019). Model runs that include Q_F are typically compared to control runs where Q_F is set to zero to show temperature variation across the city.

Ichinose et al. (1999) show an increase of 1.5 ℃ in summertime evening temperatures and 2.5 ℃ in wintertime evening temperatures in the CBD of Tokyo. Similarly, Ohashi et al. (2016) show that midday Q_F signals contributed 1 ℃ of warming in a commercial area of Osaka and up to 0.7 ℃ in residential areas. Seasonal variations also occurred: winter night-time residential values increased by up to 0.4 ℃, whilst no night-time temperature increase was seen during the summer. These winter values were attributed to space heating via ventilation or conduction through the urban fabric, highlighting the importance of including space temperature control that is responsive to outdoor temperatures in Q_F modelling. Conversely, they demonstrated that the use heat pumps resulted in a negative Q_F during the winter daytimes, causing a temperature decrease of -0.3 to -0.4 ℃. Fan and Sailor (2005) showed that Q_F contributed more to the winter night-time values (up to 2 - 3 ℃) than summer night-time (0.8 ℃) in a USA city. As with UBL height and stability, the Q_F signal is proportionally more important to changes in temperature in winter and at night-time. There are a few reasons for this: solar irradiance (and hence Q^*) is much lower, therefore contributing less energy (Kłysik, 1996); the use of space heating is more prominent, increasing Q_F values (Hinkel et al., 2003); and the UBL is shallower overnight, leaving a smaller total volume to be heated (De Munck et al., 2013; Takane et al., 2019).

Many of the studies mentioned in the previous paragraph explore the heat impacts of the positive feedback between space cooling and outdoor air temperature. During warm weather air conditioning units exhaust heat to the outdoor environment, further augmenting outdoor air temperature. This increased warming causes a higher energy demand for space cooling, leading to the expulsion of more waste heat (Salamanca et al., 2014). Takane et al. (2019) modelled the effects of this feedback on Q_F and outdoor air temperature for six climate change projection scenarios in Osaka, and was the first study to investigate the temperature difference due solely to this feedback. This additional warming induced by the feedback occurred at a rate of 1.18 ℃ $℃^{-1}$ of global warming. They also found a linear increase in air conditioning associated Q_F with increasing global warming trends of 1.76 (commercial areas) – 3.32 (residential areas) W m^{-2} K^{-1}. The study was undertaken in a city with widespread space cooling, but as global temperatures increase it may be necessary to study scenarios of space cooling adoption in cities with (at present) milder climates.

Hence, anthropogenic heat emissions contribute to the urban heat island (UHI), which occurs when urban air temperatures are greater than those of the rural surroundings. The UHI is caused by multiple factors: impervious surfaces which reduce opportunity for evaporative cooling (and increase sensible

heat fluxes), urban form (heat storage, radiation trapping in street canyons, reduction in wind speed), and anthropogenic heat (Oke, 1987). These factors may show interactions with one another (Ryu and Baik, 2012). Studies have explored the contributions of these factors, and most agree that the relative contribution of each can change seasonally and diurnally. Martilli (2002) found that night-time UHI intensity in the lower UBL is influenced more by thermal than mechanical (e.g. surface roughness) factors. The study did not fully acknowledge the diurnal patterns of Q_F, so anthropogenic sources were not quantified. More specifically, Ryu and Baik (2012) found that anthropogenic heat is the most contributing factor at night-time, and the second most during the daytime (after the effects of impervious surfaces). The increase in relative anthropogenic heat contribution during night-time can be attributed to weak convection (Ma et al., 2017). Seasonal patterns also occur. During summer daytime urban canopy effects are found to contribute the most to the UHI, whilst during winter nights anthropogenic heat accounts for up to 90% of the temperature increase (Bohnenstengel et al., 2014; Ma et al., 2017). Chen et al. (2014) found that during heatwaves, heat storage within the urban fabric and imperviousness of the surface were found to be the main cause of the UHI, though anthropogenic heat still contributed to 30% of 2 m air temperature increase. UHI patterns correspond to Q_F patterns in certain circumstances. As discussed, temperature increases are substantial during winter night-times. In a town in Alaska, Hinkel et al. (2003) found that the strength of the UHI increased with decreasing temperature, and found it corresponded to greater use of indoor heating. Although night-time UHI is more likely to be affected by Q_F, daytime values may also be substantially impacted. During winter daytimes in a low-density residential area of Melbourne, Australia, Q_F possibly contributed the most to the UHI, with a mean input of 30% to the sensible heat (Coutts et al., 2007).

2.1.3.3 Inclusion of Q_F in weather and climate modelling

Local interactions of Q_F with meteorology, described in Sections 2.1.3.1 and 2.1.3.2, have implications for the environment and human health. For example, Q_F has been shown to exacerbate the urban heat island during heatwaves (Chen et al., 2014), which has consequences for heat related mortality (Heaviside et al., 2016). This can operate on a local scale with socio-economic factors also accountable, for example, densely populated vulnerable groups are disproportionally affected (Koman et al., 2019). Jenkins et al. (2014) showed that by maintaining Q_F at present day levels on top of introducing other adaptive measures under a high emission climate change scenario, heat related mortality across Greater London in the 2050's could be reduced by up to one thousand deaths, as opposed to allowing urban land use and Q_F emissions to increase by 50%. As urban populations and energy consumption are increasing (Pérez-Lombard et al., 2008), Q_F adaptation measures need to be considered. This will involve modelling scenarios and reduction measures in order to influence urban

planning decisions (Chrysoulakis and Grimmond, 2016), and will require integration with land surface or numerical weather prediction models.

Q_F is also known to affect air quality in both urban areas and their rural surroundings. Both Yu et al. (2014) and Xie et al. (2016b) showed an increase in surface (shown via vertical profiles) ozone concentrations in urban areas due to the addition of Q_F. This is due to two causes. The reaction rate of ozone production is accelerated by increased temperature and increases in the height of the UBL lower NO_x concentrations at ground level, again increasing production. Additionally, Yu et al. (2014) found PM2.5 concentration increased in surrounding rural areas, as Q_F caused a decrease in rural precipitation.

Many studies and large-scale forecasting models typically use prescribed values of Q_F. For example, the JULES model uses monthly median values weighted by urban fraction per 1.5 km × 1.5 km grid square, ignoring any differences that may otherwise occur between the city centre and suburbs. Hertwig et al. (2020) found that JULES unscaled values compare more closely with Q_F values modelled for the suburban site than for a city centre site. MORUSES also uses monthly values (Hertwig et al., 2020), though previously it has used constant (Bohnenstengel et al., 2011) prescribed values. Even though Q_F can determine the stability and mixing height of the UBL (Fan and Sailor, 2005; Bohnenstengel et al., 2014; Falasca et al., 2016), which are fundamental factors for urban weather forecasting, the model neglects basic Q_F diurnal behaviours. As computing power increases, numerical weather prediction models are increasing their resolutions in order to better represent convection and provide more skilful forecasts, leading to more urban grids within a model. Hence, the inclusion of high-resolution Q_F to land surface models is becoming more important as resolutions increase, particularly as resolutions reach the urban grey zone (Hertwig et al., 2020). There is also call for global and regional climate models to more routinely include anthropogenic heat emissions (Flanner, 2009), though the need for fine resolution Q_F estimates has not been discussed at this scale. Studies investigating the addition of Q_F to models have been carried out, and while prescribed values based on monthly or seasonal means have been beneficial in reducing root mean square error (RMSE) and mean bias error (MBE) between modelled and observed fluxes (Best and Grimmond, 2016), it is noted that improvements may be gained in providing meteorologically and behaviourally responsive Q_F. For example, Barlow (2014) states that changes in anthropogenic heat (e.g. due to changes in climate or practice) could create unforeseen impacts on the urban environment due to unknown sensitivities and interactions. Higher resolution modelling of Q_F coupled with an urban land surface or mesoscale model would allow for studies into the mitigation of these effects (Barlow, 2014) through scenario modelling (Martilli, 2007). It may also be necessary for better performance of urban land surface models (ULSM) in general (Best and Grimmond, 2016; Hertwig et al., 2020). Some of the

studies discussed already in this section take advantage of a range of methods for modelling fine resolution Q_F. These are discussed in the following section.

2.2 Q_F modelling approaches

There are multiple existing Q_F modelling approaches (Sailor, 2011): top-down inventory (TDI), bottom-up simulation (BUS), statistical relations with meteorology (SR), energy balance closure (EBC) methods, and combination approaches (Q_F cannot be observed). The typical features of each of these approaches are detailed in Table 2-1, with examples of studies using or exploring the approaches given. Not included in Table 2-1 is satellite observation as this is not a modelling approach, but may be used to identify hotspots, though uncertainties may cause underestimations (Zhang et al., 2013; Chrysoulakis et al., 2018). All modelling approaches in Table 2-1 are reviewed in the following sub-sections.

2.2.1 Energy balance closure

EBC is briefly reviewed as it depends on SEB observations and therefore is not a modelling approach. In EBC Q_F is considered as the residual of the energy balance observations, with ΔQ_S often modelled. This means that any errors in observing the turbulent heat and net radiation fluxes or modelling ΔQ_S accumulate in these terms, which can lead to lower values compared to TDI studies (Pigeon et al., 2007) or even negative Q_F (Offerle et al., 2005). The approach is spatially restricted by the eddy covariance footprint of the observation tower, which depends on instrument capabilities and wind direction. Observation tower expense and land use restrictions determine where and for how long observations may continue.

Table 2-1**:** Characteristics of Q_F modelling approaches (TDI: top-down inventory; BUS: bottom-up simulation; SR: statistical relations with meteorology; EBC: energy balance closure) and their typical features (× no, ✓yes, ~ sometimes). *via observations, not modelled.

	TDI	**BUS**	**SR**	**EBC***
Able to show response of Q_F to temperature?	Implicit in data or combination approach	✓	✓	×
Ability to predict future states of Q_F within scope of model?	~	✓	✓	×
Capable of diagnosing causes of change in aggregate Q_F?	~	✓	×	×
Focus on changes in human behaviour?	×	✓	×	×
Components of Q_F (eq. 2-1)	$Q_{F,B}$, $Q_{F,M}$ and $Q_{F,T}$	$Q_{F,B}$, $Q_{F,M}$ or $Q_{F,T}$ (separately)	Typically only bulk Q_F or $Q_{F,B}$/energy consumption	Bulk
Spatial coverage	Constrained by data source, resolution sub-city	Building level only, fine resolution. Single sector. Limited by data collection constraints.	City level, possibly adaptable given similar behaviours and climates	Footprint of flux observations
Temporal coverage	Hourly to annual, constrained by data	Sub-hourly and above ($Q_{F,B}$)	Hourly to annual	Tower installation, instrument specification
Data needs	Energy consumption, traffic and population data (depends on model)	Energy consumption data, building structure, occupancy	Meteorological and energy consumption data, or Q_F data from another study	Flux observations
Limitations/errors	Depends on quality & provision of data and consistent scale allocation	Computationally expensive at city-scale, or representative building energy profiles used across extent	Output reliability depends on scales of input training data	Errors from other fluxes accumulate in Q_F, ΔQ_S terms. Q_F can be negative.
Examples	Kłysik (1996), Ichinose et al. (1999), Sailor and Lu, (2004), Sailor and Hart (2006), Pigeon et al. (2007), Lee et al. (2009), Allen et al. (2011), Ferreira et al. (2011), Iamarino et al. (2012), Lindberg et al. (2013), Lu et al. (2016), Dong et al. (2017)	$Q_{F,B}$: Kikegawa et al. (2003), Krpo et al. (2010), Salamanca et al. (2010), Bueno et al. (2012), Nie et al. (2014) $Q_{F,T}$: Grimmond (1992), Smith et al. (2009) $Q_{F,M}$: Thorsson et al. (2014) *All*: Quah and Roth (2012)	Q_F: (Sailor and Vasireddy, 2006; Ao et al., 2018) *Energy consumption*: Taylor and Buizza (quadratic) (2003), Hor et al. (2005), Ihara et al. (2008), Psiloglou et al. (2009)	Kato and Yamaguchi (2005), Offerle et al. (2005), Pigeon et al. (2007), Park et al. (2016), Crawford et al. (2017)

2.2.2 Top-down inventory

Top-down inventory (TDI) is the most common approach used for representing all Q_F sectors (eq. 2-1) across large spatial and temporal extents. Models have been created at fine scales for city blocks (Ichinose et al., 1999), individual (Ferreira et al., 2011; Iamarino et al., 2012) or multiple (Sailor and Lu, 2004; Sailor and Hart, 2006) cities, regional areas (Lee et al., 2009), entire countries (Lu et al., 2016), continents (Lindberg et al., 2013), up to covering the entire globe (Allen et al., 2011; Dong et al., 2017; Jin et al., 2020). As spatial extents increase, resolution tends to decrease. The highest resolutions are represented by administrative blocks, and regional, continental or global models may use arc-seconds/minutes or latitude/longitude ranges to create grids. TDI is useful for identifying emission hotspots but relies heavily on the use of past energy data and assumptions made at much larger scales. Such models typically require electricity and/or gas consumption ($Q_{F,B}$) and traffic ($Q_{F,T}$)

data which are supplied by governments or energy companies at low resolution (for data storage, privacy reasons etc.).

Annual or monthly energy consumption or traffic flow statistics can be rescaled to a finer temporal resolution using seasonal, monthly or daily trends. Temperature sensitivity is typically intrinsic to the data used, but further analyses can be used to give an impression of sensitivity to meteorological variables. For example, Iamarino et al. (2012) use daily gas data to create fractions that rescale the initial annual electric and gas consumption statistics and show daily variability. Allen et al. (2011) scale $Q_{F,B}$ based on a temperature balance point determined from thermal comfort studies and using weather data at the output resolution. Dong et al. (2017) employ techniques seen in SR Q_F studies to rescale, using results from regression analyses above and below a universal balance temperature of 20 °C, with constant values at hot and cold limits. City-scale correlations were considered and generalised globally with relations to annual mean temperature. In studies that do not rescale temporally, temperature sensitivity is solely implicit in the data used.

Sub-daily (usually hourly) diurnal profiles of energy use are typically used to allow models to operate at these resolutions, usually for different day types (i.e. weekday, weekend day). These may be obtained through separate sources to the energy consumption data or through analysis of further data. Iamarino et al. (2012) use profiles from other sources that provide national-scale diurnal profiles for each season and $Q_{F,B}$ sub-sector, whilst Sailor and Lu (2004) and Ferreira et al. (2011) find the mean diurnal profiles for each month. Although they are able to provide sub-daily estimations, these profiles are aggregate and again do not account for any sensitivities that may occur at sub-daily scales. Whilst aggregate behaviour would be accounted for, the resultant patterns may not be suitable when coupled with other fluxes in the surface energy balance due to the neglect of spatial variation, e.g. in land use or demographics. Traffic count data can be provided to disaggregate $Q_{F,T}$ to sub-daily scales, even for different modes when data are available (e.g. Iamarino et al., 2012).

Values tend to be spatially disaggregated using a spatial surrogate which suitably describes the spatial variation in Q_F and can be found at a desired resolution higher than the input energy data. Most fine resolution studies use a variety of spatial surrogates attributed to different source sectors. $Q_{F,B}$ (or building energy consumption) is usually disaggregated by population, as these data can be attributed to active energy use and are typically available from census collections at local scale. $Q_{F,B}$ sub-sectors may also use different types of population data. For example, residential population can be used to disaggregate domestic energy, and workplace population used for non-domestic energy. Land or building use types (dominant or proportional) are also suitable (Ichinose et al., 1999; Lee et al., 2009). Road length is used to disaggregate $Q_{F,T}$ as this directly indicates the presence of transport (Ichinose et

al., 1999; Lee et al., 2009; Iamarino et al., 2012). Sailor and Lu (2004), Sailor and Hart (2006) and Ferreira et al. (2011) operate at a city-scale or extent yet only use residential population density across all sectors, which may lead to a loss of detail (Gabey et al., 2019), especially with respect to movement between cities.

Alternatives also exist. Lu et al. (2016) used gross domestic product to disaggregate industrial, commercial and transport energy across mainland China. Low-resolution models with a global spatial extent use population density to disaggregate all Q_F sectors (Allen et al., 2011; Dong et al., 2017). Population is often the only consistent data available in a single dataset for the global extent, and whilst there may be some exceptions, the resolution at which the models operate will be low enough such that more detailed sector disaggregation is unnecessary.

The patterns of daily activities may also be used to reflect population movement patterns through sub-daily ratios of energy use at different $Q_{F,B}$ sub-sectors (e.g. using transitions between domestic and daytime populations), or $Q_{F,M}$ patterns (awake, sleeping). These patterns, or activity transitions, tend to be determined subjectively and are used across the entire spatial extent (Sailor and Lu, 2004). Whilst this is the most suitable approach given the scarcity of data, it fails to capture finer details that may arise due to non-typical patterns (e.g. work shifts, commutes). Large scale models may assume that there is no movement of populations between grid spaces and as such only use residential population data (e.g. Allen et al., 2011). This may be reasonable in most cases but could miss details when grid spaces cover, for example the centres of large cities.

Gabey, Grimmond and Capel-Timms (2019) demonstrate the importance of using a variety of spatial surrogates when disaggregating energy consumption. The aim of the study was to judge if the coarser resolution TDI model LQF (Allen et al., 2011; Lindberg et al., 2013) could skilfully reproduce the spatial patterns seen in the finer resolution (administrative area) GQF (Iamarino et al., 2012). City hotspots were found to be absent in LQF, which missed details in the city centre and near motorways where a large proportion of Q_F was produced in GQF. Skill improved towards the city's outskirts, and as resolutions became coarser. This was because GQF used residential and work populations, road length and local energy data to disaggregate Q_F sectors and subsectors, whilst LQF only used residential population. Spatial patterns for non-domestic $Q_{F,B}$ and $Q_{F,T}$ were therefore misrepresented in LQF. The two models also used different metabolic activity profiles, resulting in errors related to the transitions of residential and workplace populations.

Top-down inventory models supply reasonable estimates across large spatial and temporal extents, informing understanding of spatial (global, city, intra-city) and temporal (seasonal, monthly, diurnal)

Q_F patterns. However, they are typically constrained to the periods and areas (and their resolutions) of their input data, putting spatial and temporal limits on their capabilities for simulating Q_F. Whilst future predictions can be made given projected energy consumption and traffic data (e.g. Iamarino et al., 2012), they are not able to model any changes that may occur as a result of behaviours, especially with regards to any interdependencies that may occur. This is because individual and weather sensitivities are constant across the spatial resolution of the input data, for example building characteristics, working hour patterns, travel times and energy end-uses.

Such sensitivities are lost due to the aggregate nature of input data. Whilst such aggregate features are useful and can be disaggregated to finer resolutions, they are still dependent on assumptions made during development. As discussed, with the choice of sub-daily profiles and spatial surrogates,

2.2.3 Bottom-up simulation

Models using the bottom-up approach typically only model a single Q_F sector, but in great detail. By its nature, the bottom-up approach allows for fine processes to interact and be represented in output. For more complex studies, this can be used to reveal emergent behaviours, investigate scenarios through altering low-level variables and can allow for feedbacks to occur when coupled with another model or process. As such they require fine resolution data according to the needs of the study, which may not be available across large extents. BUS can also complement other approaches.

The most commonly represented sector is building heat emission, using detailed building energy models. A wide range of studies exist within the fields of construction, building energy and the built environment (Foucquier et al., 2013), but for brevity this section will focus only on a selection of studies specifically investigating Q_F or coupled with climate models.

Building energy models are designed to account for the physical attributes of individual buildings (e.g. Schoetter et al., 2017) or groups of buildings across a city-block/neighbourhood or use type (e.g. Kikegawa et al., 2003a; Salamanca et al., 2010; Nie et al., 2014). This involves representation of physical attributes (e.g. thermal properties of building components), the heat exchanges (radiative, conductive, convective) between the indoor and outdoor environments, and variations of energy-consuming activities within (e.g. temperature independent activity loads, metabolism). This allows for response to meteorological variables and human behaviour. Representative buildings/dwellings can be scaled for a wider area, such as a city (Heiple and Sailor, 2008; Bueno et al., 2012) or across an institution (Nie et al., 2014).

Building energy models allow for dynamic studies to be carried out. Kikegawa et al. (2003) coupled a building energy model (BEM) to a UCM for two city blocks, with mesoscale models providing single connections to winds and initial and boundary conditions. Internal heat gains were provided by static profiles of occupancy levels ($Q_{F,M}$) and equipment power demand. $Q_{F,T}$ was supplied directly to the UCM. The inclusion of these features allowed for variations in meteorology and human behaviour to influence the cooling response, and coupling with a UCM-mesoscale model allowed the authors to investigate feedbacks with the outdoor environment through the use of air conditioning. Krpo et al. (2010), Salamanca et al. (2010), Bueno et al. (2012) and Nie et al. (2014) used similar approaches in their studies at a variety of scales.

Schoetter et al. (2017) highlighted a need for better representation of human behaviour (with regards to energy consumption and heating/cooling set points) in large-scale building energy models. BEM-TEB, which previously (Bueno et al., 2012) represented an entire grid with a single BEM and related behaviours, was modified to account for fractional building use with multiple BEMs and their individual behaviours which then aggregate to grid scale. Whilst this may be computationally expensive for a city scale, this demonstrated that multiple behaviours may be considered within a single grid and may therefore benefit estimation through the consideration of more behaviours.

In their city-scale study of hourly $Q_{F,B}$ (residential and commercial, 1.33 km × 1.33 km grid scale), Heiple and Sailor (2008) compared BUS to TDI. For BUS, energy use intensity was simulated for individual representative building prototypes and groups of building types that shared similar energy patterns and uses, then distributed across the city using building use and floor area data. Variations in building type density within the BUS run allowed for better representation of expected spatial patterns of Q_F, such as greater intensity in the city centre, than for the TDI approach. The use of representative buildings distributed across the city did account for changes in Q_F patterns due to variation in building or land use, but there was no variation between the diurnal patterns within each building prototype.

At the finest detail, Quah and Roth (2012) used both top-down and bottom-up approaches for $Q_{F,B}$. Hourly consumption was determined for each building and summed to give total energy consumption across the study area. Whilst this is likely to give accurate results, it is very data intensive and therefore not feasible for the whole urban extent.

The BUS approach presents some advantages over TDI (Sailor, 2011). Firstly, inputs such as occupancy profiles and building component parameters can be altered to determine the effect that they might have on output emissions, allowing for a range of investigations into the effects. Secondly, the contribution of different energy end uses on overall heat emissions can be quantified. In TDI, this is

very dependent on the consumption data available, and is unlikely to go into detail beyond sub-sector (domestic, non-domestic) or energy type (electricity, gas). With BUS, the impacts of end-uses such as appliances, heating, cooling and hot water can be seen. Thirdly, the lag between energy use and its emission to the outdoor environment can be evaluated due to the inclusion of heat transfer though the building fabric, which is generally unaccounted for in TDI approaches (Sailor, 2011). Though employing an urban canopy model instead of a BEM, Bohnenstengel et al. (2014) show that a time lag due to inclusion of the urban fabric causes Q_H to persist later into the evening, hence there are consequences for the urban SEB that could be included by using building energy models.

There are also some disadvantages of BUS compared to TDI that should be taken into account when choosing an approach. The number of processes involved in a BEM make the method computationally expensive when used at the scale of an entire city, unless the method rescales representative building energy profiles. The drawback of this is that the behaviours and heat exchanges within each building type are homogeneous across the city and again, like TDI, does not capture the finer interactions across the city that may arise due to behavioural differences. The method is also data intensive as values must be found for each component of the BEM, as well as energy profiles.

BUS can also be used to simulate $Q_{F,T}$ and $Q_{F,M}$. Smith et al. (2009) use a bottom-up method to estimate transport across a region for each mode present, using vehicle kilometres, road length, speed and emissions data.

2.2.4 Statistical relations with meteorology

The third Q_F estimation method, statistical relations with meteorology (SR), relies on correlations between outdoor air temperature and energy consumption. The approach is most commonly used for energy demand forecasting or estimation (Taylor and Buizza, 2003; Hor et al., 2005; Ihara et al., 2008; Psiloglou et al., 2009), but is also used for Q_F estimation (Sailor and Vasireddy, 2006; Dong et al., 2017; Ao et al., 2018). Most of these methods simply use the linear responses of energy consumption to outdoor forcing temperature (usually daily mean). Taylor and Buizza (2003) use weather ensembles across multiple variables (temperature, wind cooling, illumination) to arrive at a non-linear function for forecasting purposes. Ihara et al. (2008) also consider the effect of relative humidity on the efficiency of cooling equipment, with relations for separate temperatures.

The most common SR approach is to consider a V-shaped relation, with each “arm” representing either a heating or cooling response (Sailor and Vasireddy, 2006). A single balance point T_b defines the temperature at which energy consumption is assumed to be temperature-independent (i.e. base

energy consumption). Below (above) T_b, space heating (cooling) is used, with energy use intensity linearly increasing with greater difference in outdoor temperature and T_b. This is normally measured in heating or cooling degree days (HDD/CDD), using T_b as base temperature. Linear regression is used on training data to find coefficients for HDD and CDD at the location of study/forecast. When either heating or cooling are not widely used at a location, the corresponding coefficient may be set to zero. Population density may also be accounted for using population weighted energy consumption data.

T_b is determined in a variety of ways. Sailor and Vasireddy (2006) use a single value to calculate degree days for energy modelling studies but note that this may change across locations. This change may occur due to differences in human temperature resilience, space temperature adjustment practices or by financial restrictions such as expense of cooling equipment (e.g. Lindberg et al., 2013). This same T_b value is used in other studies employing the same method in other locations (e.g. Ward and Grimmond, 2017). Hor et al. (2005) choose a T_b value for the sake of it being between heating and cooling base temperatures, despite identifying a range below the chosen temperature where there appears to be no temperature response in the analysed relation. No justification is provided beyond this. For the least validated method, Psiloglou et al. (2009) found T_b values through approximation by sight. An ideal method of finding T_b would be through statistical analysis of the relation at the location being studied.

Ihara et al. (2008) and Ao et al. (2018) identified a U-shaped relation between forcing temperature and energy consumption. This involves a range of temperatures for which thermal comfort is generally achieved, i.e. neither heating nor cooling are used and only temperature-independent energy exists. Furthermore, Ao et al. (2018) classifies plateaus at extreme temperatures in the relation when heating and cooling systems reach maximum capacity. Hor et al. (2005) recognised these features but still used the V-shape relation. Dong et al. (2017) identified the plateaus but did not use the thermal comfort range (i.e. otherwise used V-shape). The U-shaped approach is possibly more reflective of energy consumption in areas where both heating and cooling are widely used as it considers a range of temperatures where neither are in operation, though it has not been compared to the V-shaped approach.

The SR functions found for each of these studies give per capita energy consumption and hence can be used for any area, but current applications consider the city characteristics and behaviours involved to be aggregate across the area of the input analysis data. Hence the method is unsuitable for use at finer resolutions than the input data. Sailor and Vasireddy (2006) attempt to disaggregate but note that using functions at finer resolutions than they were created at may result in "significant errors". So, like TDI, SR is most suitable for the scale at which data is provided, but unlike TDI can be used in different

areas and periods, given city practices and thermal behaviours (such as energy intensity per capita and thermal comfort ranges) are similar. This method is also very efficient and requires only spatial surrogate (e.g. population) data once parameters are derived.

2.3 Patterns of Q_F and relations with human behaviour

Each Q_F source sector is directly controlled by multiple aspects of human behaviour which occur across a range of scales (Sailor, 2011). This section explores the physical processes and human behaviours that control Q_F, and the resultant patterns. General Q_F patterns are discussed first in Section 2.3.1. Section 2.3.2 addresses the patterns of Q_F that arise due to physical causes, such as climate and latitude. The social factors of Q_F patterns are discussed in Section 2.3.3, across multiple levels of human behaviour.

2.3.1 Typical patterns of Q_F

Table 2-2 shows the Q_F characteristics across multiple studies. Studies for this table were chosen based on a few criteria. These criteria were fairly flexible, as of course there is no standard across publications for method structure nor Q_F result presentation. Q_F must be the primary attention of the study, or at least form a considerable part of the research aim; articles including Q_F as an ancillary feature were found to not give sufficient detail in Q_F results. The studies must focus on an entire city or urban area agglomeration (such as a district), or a single or multiple distinct urban land uses (as in the cases of C07, QR12, A18), at a local grid scale for ease of comparison. For the studies shown in the current iteration, annual and/or seasonal averages of Q_F were already presented by the authors or easily calculated/interpreted from given data or figures. Most studies chosen were conducted later than 2000, with the exception of K96 which gave rich data across multiple land uses. The study that fulfils these criteria the least is A18, which was included for its links to Section 2.2.4 and Chapter 4.

High total Q_F intensity is typically seen in city centres and CBDs, where workday populations can be in the order of 100,000+ people km^{-2} (e.g. Iamarino et al., 2012) and building density is much greater than typical residential areas (Stewart and Oke, 2012). As in the cases of K96, P07, QR12 and ZW17 (Table 2-2), high density residential areas follow commercial or industrial districts in order of intensity, and suburbs or low-density residential areas show the lowest intensity. As mentioned in Section 2.3.1, winter values tend to be greater than summer values due typically to the increased use of space heating, (Table 2-2: K96, P07, I12) except in the case of Shanghai (A18). Ao et al. (2018) demonstrate that the response in energy consumption to air temperature is much steeper at higher temperatures, i.e. space cooling is used more widely and frequently than space heating. These high Q_F

values may be enhanced by feedback stresses on cooling (Section 2.1.3.2). Along with building density, this feedback creates more of a discrepancy in energy use between commercial and residential areas (Quah and Roth, 2012).

Building energy ($Q_{F,B}$) is the dominant Q_F source sector in most of the studies in Table 2-2, followed by vehicular sources ($Q_{F,T}$). Allen et al. (2011) report that $Q_{F,B}$ has a global contribution of 89 - 96%, but note that $Q_{F,T}$ might be underestimated by LUCY. The exception in this selection of studies is F11 where $Q_{F,T}$ takes the greatest share. Ferreira et al. (2011) note that there are more cars in São Paulo than most other cities where Q_F studies have been undertaken. Additionally, they state that heating is not commonplace across the city as it has a sub-tropical climate, leading to a lower contribution from $Q_{F,B}$. No mention is made about the distribution of cooling use, but the remarkably low seasonal variation in Q_F would suggest that either it is not widespread, or the climate also does not vary much seasonally. In some studies, arterial roads can be seen in the city-wide distribution of Q_F. This may be more pronounced when $Q_{F,B}$ is lower, such as during summer in mid-latitude cities (Pigeon et al., 2007). This is highly dependent on population density and hence varies across the day. $Q_{F,M}$ provides a minor contribution in all cases.

Table 2-2**:** Summary of Q_F across multiple studies. For the columns under Source sector (%), dominant sectors are emphasised in bold. Studies are: K96-Kłysik (1996), P07-Pigeon et al. (2007), C07-Coutts et al. (2007) (digitised and corrected by M. J. Lipson), S09-Smith et al. (2009), F11-Ferreira et al. (2011), QR12-Quah and Roth (2012), I12-Iamarino et al. (2012), ZW17-Zheng and Weng (2017), A18-Ao et al. (2018); abbreviations: med.-medium, dens.-density, res.-residential, wd-weekday, av.-average, spat-spatial, CBD-central business district.

Study	*City, grid resolution*	*Total extent / grid resolution*	*City area*	*Annual Q_F* ($W\ m^{-2}$)	*Summer Q_F* ($W\ m^{-2}$)	*Winter Q_F* ($W\ m^{-2}$)	*Source sector* (%)		
							$Q_{F,B}$	$Q_{F,T}$	$Q_{F,M}$
K96	Łódź, Poland		suburbs	4	2	8	-	-	-
			high dens. res.	34	14	73	-	-	-
			industrial	41	16	66	-	-	-
		80 km^2 / -	total	28.5	12	54.2	-	-	-
P07	Toulouse district, France		centre (dense)	-	25	100	-	-	-
			suburbs	-	5	5 - 25	-	-	-
		~154 km^2 / 100 m	total	-	7.7	17.3	-	-	-
C07	Melbourne, Australia		high dens. res.	11.3	10.1	12.9	-	-	-
		Flux tower footprint	med. dens. res.	10.5	9.3	11.9	-	-	-
			low dens. res.	9.8	8.8	11.2	-	-	-
S09	Greater Manchester, UK		city centres	peak: 50 - 75 spat. av.: 23	-	-	-	-	-
			non-central	10	-	-	-	-	-
		1276 km^2 / 200 m	total	6.12	-	-	**60**	32	8
F11	São Paulo, Brazil	854 km^2 / -	total (2007)	~12.5	-	-	42.0	**47.5**	10.5
QR12	Singapore,	0.785 km^2 / -	res.	11*	-	-	**54**	37 - 41	5 - 9
	*Oct. 08 - March 09	0.785 km^2 / -	high dens. res.	13*	-	-	**49**	30 - 38	13 - 21
		0.785 km^2 / -	commercial	85*	-	-	**83**	8 - 12	5 - 9
I12	Greater London, UK	3.2 km^2 / 200 m	CBD	140	-	-	-	-	-
		1596 km^2 / 200 m	total	10.9	min. av. ~8	max. av. ~14	**80**	15	5
ZW17	Los Angeles County, USA	- / 120 m	low dens. res.		< 20[‡]		-	-	-
	[‡]1700 h summer wd	- / 120 m	high dens. res.		20 - 100[‡]		-	-	-
	[‡‡] 0900 - 1700 h wd	- / 120 m	Downtown		max. ~100[‡]		**69.5**[‡‡]	22.1[‡‡]	8.4[‡‡]
A18	Shanghai, China	0.785 km^2 / -	dense urban	-	max. av. 236	max. av. 190	~**95**	~2	~3

The fundamental features of average city-wide Q_F diurnal patterns are common between studies (Sailor, 2011). Overnight Q_F is low, as most people are sleeping instead of actively using energy. Q_F increases rapidly as morning continues due to energy use in buildings, increase in vehicle use and changes in metabolic activity. End of morning Q_F levels generally continue until late afternoon/early evening, when another brief peak may appear (largely depending on traffic and space heating/cooling needs). After this, Q_F decreases steadily until midnight, reaching a nadir in the early hours of the morning. The weekday daytime profile tends to have a greater magnitude than weekend days (Sailor, 2011), though night-time values are likely to be similar as these are less dependent on active energy consumption. However, this has been shown to vary by land use type. Quah and Roth (2012) showed that weekday Q_F in a commercial area was on average 5% higher than on the weekend, but for residential areas weekday Q_F was 2 - 9% lower than at weekends. This is likely due to weekend daytime population being greater than during weekday daytime, hence more people are at home consuming energy. This demonstrates the necessity of including different Q_F profiles by land use and day type.

2.3.2 Physical drivers of Q_F variation

2.3.2.1 Seasonal and latitudinal variations

Various studies state that global differences in energy consumption (and therefore Q_F) are largely influenced by latitude and local climate (Oke, 1988; Sailor and Hart, 2006; Allen et al., 2011; Ferreira et al., 2011; Lindberg et al., 2013; Dong et al., 2017). This is mostly due to temperature sensitive Q_F sources; warmer climates will encourage greater use of air conditioning systems (Sailor and Lu, 2004) whilst space heating is more prevalent in cities with colder climates. This was discussed briefly in Section 2.1.3 and Section 2.3.1.

Buildings in cities with extreme summers and winters may require both space heating and cooling, which would be reflected in the response of the city's energy consumption (and hence Q_F) to outdoor air temperature (Section 2.2.4). Allen et al. (2011), Ferreira et al. (2011) and Dong et al. (2017) found notably lower seasonal/monthly variation in mean Q_F intensity in lower-latitude cities, implying that these cities experience less temperature variation throughout the year. This is often the case at sub-tropical latitudes and below due to a more constant need for space cooling. Conversely, cities in the higher latitudes, especially the northern mid-latitudes, generally show greater seasonal variation due to a high saturation of both heating and cooling equipment (Dong et al., 2017). This would be needed to maintain thermal comfort in such cities throughout the year. Patterns of indoor thermal control in mid- to high-latitude cities are reflected in the annual cycle of Q_F, which is dominated by values in the winter months (Grimmond, 1992; Kłysik, 1996), suggesting that air conditioning is seldom used, if at

all. For example, estimations from a study in Toulouse, France, displayed greater Q_F intensity during the winter from electricity and gas sources (Pigeon et al., 2007). There are however exceptions to the rule of latitude influence, and local climates must be considered. For example, Sailor (2001) found neighbouring USA states had opposing responses to increases in temperature. There were multiple reasons given for this, including other meteorological factors (such as changes in humidity influencing the use of air-conditioning) and socio-economic factors, which will be discussed later in this chapter.

Climate change will hence bring about adjustments to Q_F seasonal patterns and intensities due to the adaptations that will be made to heating and cooling needs (Li et al., 2012; Takane et al., 2019). Effects on city energy demand depend on the current and future states of the local climate. For example, Sailor (2001) estimate that electricity demand across seven of eight USA states analysed would increase by 5 - 15% per capita should CO_2 emissions double, due to a decrease in HDD (by as much as 50%) but an increase in CDD (by up to 125% in one case). On the other hand, Klimenko et al. (2016) also noted a decrease in HDD and increase in CDD in Moscow (and other Russian cities) across past decades and projected values, which caused a decrease in heating demand by 10% from 1950 - 2015. They also note that future increases in energy demand in CDD would be constrained by economy with regards to the installation and use of space cooling units.

$Q_{F,T}$ and $Q_{F,M}$ are generally considered to show little seasonal variation with regards to climate (Sailor and Lu, 2004).

2.3.2.2 Land use and building density

Other factors affecting Q_F include urban land cover and use. These factors tend to vary across local or neighbourhood scales and are heavily interconnected with other elements of the urban SEB and climate. The source sector of Q_F changes with land cover type. For example, paved land cover generally implies presence of vehicles and therefore $Q_{F,T}$. $Q_{F,B}$ is by its nature connected with building land cover, and is responsive to changes in building stock, morphology and use. $Q_{F,M}$ may exist at any land cover, but is mostly associated with built-up and paved areas.

Building density affects Q_F through the response of heating and cooling needs to outdoor air temperature. Coutts et al. (2007) investigated the differences in urban surface characteristics at three sites in Melbourne, Australia, with varying building density (C07, Table 2-2). The characteristics analysed included urban canopy height-to-width ratio (H:W), surface albedo and vegetation cover. Q_F estimation was included as input but feedbacks with temperature were not, hence the influences cannot be quantified, but may be inferred. They found that the heat storage term increased with building density, which would cause higher temperatures at later times of the day and possible changes in

heating and cooling needs (though this interaction was not specifically investigated). This was due to increased radiation trapping in the urban canopy, which has a lower H:W ratio as building density increases. Lower H:W ratio and greater building density will also cause a skimming wind regime, with less air advected from the urban canyon (Grimmond and Oke, 1999a). The contribution of urban canyon effects to the heat storage cancelled out the mitigating properties of a higher roof top albedo in the densest study area. This relation between building density in the heat storage intensity and profile would cause changes in temperature-sensitive $Q_{F,B}$.

2.3.2.3 Building stock

Another building characteristic affecting both Q_F and heat storage is the thermal properties of buildings themselves. Building stock refers to the distribution of buildings and their properties and morphologies across an urban area. Heat exchanges between a building and the outdoor environment, and therefore temperature sensitive Q_F, are influenced by building stock characteristics, such as thermal properties of materials and archetypes (Wright, 2008; Mavrogianni et al., 2012; Oikonomou et al., 2012; Evins et al., 2015). Building stock is influenced by policies surrounding building thermal efficiency, which may be involve replenishment or retrofitting in countries seeking to reduce carbon emissions (Clarke et al., 2009; Coffey et al., 2009; Kelly, 2009), with consequences for heating/cooling demand (Wang et al., 2019).

Changes in building stock present long term temporal trends, for example the UK building stock changes at a rate of 1 - 2% per year, with expansion occurring at 0.8% (Ravetz, 2008), and are driven by policy or housing demand. Spatial variation occurs at local or neighbourhood scale, and is important to consider in modelling, as characteristics such as a building's shape, internal space, and materials are central to its thermal efficiency (Wright, 2008). In a study of over 900 households in England, Huebner et al. (2015) attributed 39% of total energy consumption to building variables such as age, dwelling type, floor area and window type. Similarly, Guerra Santin et al. (2009) stated that 42% of heating energy use variation can be explained by building characteristics, adding that wall insulation levels are strongly linked to energy demand in all dwelling types. They also found that greater area of exposed wall per dwelling increased energy required for heating, i.e. detached dwellings consumed more energy whilst flats/maisonettes consumed the least.

Advances in construction materials and the influence of government policy (particularly with regards to carbon targets, e.g. Kelly, 2009) mean that thermal efficiency is highly linked to the age of the building (Oikonomou et al., 2012). Hence, heating and cooling demand trends are partly dependent on the rates of change in building thermal efficiency. These evolutions are not normally included in Q_F

studies as they tend to act over large time scales. TDI studies would include these effects inherently within the aggregate results, and as such would not be detectable at the local scale at which building stock change occurs. BUS studies that use reference buildings would need to determine the level of detail required for a city-wide study. As $Q_{F,B}$ is the dominant source sector of Q_F in most cases (Table 2-2) and building characteristics play such a large role in building energy variation, a city's building stock should be represented in a Q_F model. The best approach to use in this case would be BUS representing a range of building archetypes, though analysis should be carried out to determine the level of detail in building stock necessary. The change in building stock may not be necessary for short term studies of only a few years, but should certainly be considered in some capacity if studying future scenarios.

2.3.3 Social drivers of Q_F variation

The social behaviours and dependencies that govern Q_F are reflected in its great variation across both spatial and temporal scales. For example, people's movement across a city and their resultant day to day energy use could have diurnal and local effects, whilst longer-term, city- or nationwide impacts could occur as populations evolve, climate changes or new technologies are adopted. In this section human behaviour is separated into "practices" and "actions" which operate on different spatial and temporal scales: practices refer to the large-scale behaviours shared by a society or culture, whilst actions are small-scale, individual behaviours (Calhoun, 2002). These actions may be influenced by societal norms, i.e. practices.

2.3.3.1 Vehicle use

Traffic flow is defined by the movement of people across the city, with high $Q_{F,T}$ occurring during rush-hours as citizens travel between their homes and workplaces (Grimmond, 1992; Sailor and Lu, 2004; Smith et al., 2009; Ferreira et al., 2011; Iamarino et al., 2012), but $Q_{F,T}$ can also experience long-term changes. Changes in vehicle fleet distribution may occur due to factors such as policy (e.g. emission standards) or availability of public transport, which could then change $Q_{F,T}$. These influence the practices and actions of urban dwellers, for example people may choose to use public transport if it is more accessible, or may be encouraged by government schemes and social influence to switch to driving electric vehicles (as modelled by Hattam and Greetham, 2017). For example, Ellison et al. (2013) demonstrated that diesel vehicles that did not conform to government-mandated emission standards were less present in the low emission zone covering most of Greater London after such zones were introduced. The study focussed on particulate matter, but as different vehicles and emission classes show variation in fuel consumption (Smith et al., 2009), this would be analogous to

$Q_{F,T}$. Vehicular heat emissions will also be affected by imposed speed limits, as fuel consumption is dependent on speed (Smith et al., 2009). Vehicle speeds could also be affected by safety initiatives (such as speed cameras) affecting driving practices (Schechtman et al., 2016). Additionally, weather and climate change has been shown to alter day-to-day mode choice for particular journeys (Böcker et al., 2013). The heat-related advantages of electric vehicles were discussed by Li et al. (2015), who modelled that the replacement of the entire stock of conventional vehicles with electric vehicles (which produce a fifth of the heat emissions) reduced the UHI intensity by almost 1 °C, with the added bonus of reducing annual air conditioning energy demand by 14.4 GW h.

2.3.3.2 Population density across building uses

Population density is a significant driver of Q_F intensity (Oke, 1988; Grimmond, 1992; Ichinose et al., 1999; Allen et al., 2011; Dong et al., 2017), as the majority of energy is actively consumed by humans within a space. This is the case at all scales. When comparing London and Paris, cities with similar areas, population sizes and climate classifications, Lindberg et al. (2013) found that higher population density in the centre of Paris was the main reason for greater Q_F values. Iamarino et al., (2012) found direct correlations in $Q_{F,B}$ and population density across both domestic and industrial sub-sectors at sub-city spatial resolutions. They also found increased Q_F when studying projections related to population change.

Population is however not a direct indicator of energy consumption on a large scale. Factors such as wealth can also play a part, changing the per capita energy consumption and practices at national scales. Lindberg et al. (2013) demonstrated that countries with a greater income have a greater energy consumption per capita, despite similarities in the sum of HDD and CDD between nations. At the scale of a single city, Iamarino et al. (2012) used historical data to show a decrease in energy consumption after 2002 which they related to increased fuel prices and slower economic growth. As mentioned in Section 2.3.2, Sailor (2001) stated economic disparities as a possible contributing factor in the differences of heat-related energy consumption between neighbouring states.

Studies often consider static populations when estimating Q_F (Section 2.2.2), which may be appropriate at low-resolutions (Gabey et al., 2019) but is restrictive in fully representing the dynamics of local-scale areas, especially if the movement of people extends beyond the “static” population density resolutions. For example, city-wide shifts in population density may also occur due to cultural practices, such as national holidays. An example of this is Chinese New Year, which sees an estimated population outflow of nine million people in Beijing (almost half of the city’s population). Zhang and Wu (2017) studied the differences in UHI strength between Chinese New Year and a background

period surrounding the holiday across a decade. The only differences would be the lower city populations as urban surface properties remained the same. Average mean difference in UHI anomaly showed a cooling of 0.36 ℃ during New Year across the ten-year period, whilst minimum night-time values cooled more at 0.55 ℃. In a less extreme scenario, Pigeon et al. (2007) note that summertime $Q_{F,T}$ in Toulouse, France may be lower than during the rest of the year because of the vacation season.

The populations within different building uses (i.e. building occupancy levels) vary diurnally and weekly, and this is reflected in Q_F patterns at all spatial scales. The greater Q_F values in commercial areas (Section 2.3.2) are mostly seen in the daytime during typical working hours. In the morning and evenings, energy demand is greater across predominantly residential areas when people are at home using energy for indoor temperature control and activities such as cooking and leisure. Values in both residential and commercial areas are lowest during the night when occupants are either absent (commercial) or asleep (residential) and therefore not using energy. This influence of movement and behaviour between residential and workday populations is also seen at a weekly time scale, as a city's Q_F values will typically be lower during the weekends when fewer people are working (Pigeon et al., 2007; Sailor, 2011; Iamarino et al., 2012).

These city-wide diurnal population patterns occur as a result of the working week practice, and tend to be modelled in TDI Q_F studies by attributing diurnal population transitions and aggregate load profiles of building energy sub-sectors to corresponding populations (e.g. domestic and non-domestic) (Section 2.2.2). For example, Sailor and Lu (2004) demonstrate that the population moves towards the centre in the daytime in San Francisco, USA, but this was based on the assumption that people work between the same hours. This working pattern may be most common in aggregate but is biased towards the typical full-time work pattern and ignores different shift patterns. Also, other variations may occur based on commute travel time. For example, people who live further from their workplace or use certain modes of transport may leave their houses earlier to get to work and return later, which could affect the aggregate domestic occupancy levels in the city outskirts.

2.3.3.3 Behavioural characteristics of building energy use

Building occupants and their actions are major influences on building energy consumption (Hoes et al., 2009; Yan et al., 2015), as people present will use energy for instant activities (e.g. using appliances) and in response to their thermal environment (heating, cooling and ventilation). The behaviours prompting energy consumption, and therefore $Q_{F,B}$, vary across each building use sector (e.g. commercial, industrial and domestic). Energy intensity across the non-domestic sector varies greatly across sub-sector types (e.g. shops, schools, offices, manufacturing), as each have different energy needs and factors governing energy change (Bruhns and Wyatt, 2011; Evans et al., 2019;

Ward, 2008). This is particularly important in CBDs, where the distribution of commercial business types can be highly mixed (Evans et al., 2019). As well as different energy consuming equipment existing across sub-sectors, these building uses will have different heating needs driven by their functionality (e.g. warehouses may not require as much heating as office spaces). Despite this there is currently poor modelling of building use across city extents, particularly with respect to mixed use buildings (Evans et al., 2019). This is more meaningful towards city centres where there is a greater variety of building use (Kunze and Hecht, 2015) and greater Q_F intensity. In turn this presents difficulties in modelling the energy use across the non-domestic sector. A possible solution would be to consider different building uses within fractional building BUS (e.g. Schoetter et al., 2017). Each building use type would require its own input variables, such as floor area, diurnal patterns in occupancy, and average power demand. Physical building characteristics could be grouped by factors such as archetype or dominant construction material type, but individual BEMs would need unique occupancy and power demand profiles in order to represent the behaviours within as a function of building use and location.

Multiple studies (Wood and Newborough, 2003; Firth et al., 2008; Page et al., 2008; Widén et al., 2009b; Richardson et al., 2010; Andersen et al., 2014; Delzendeh et al., 2017; Kim and Srebric, 2017) have identified the number of active (awake and present) occupants in domestic or commercial buildings at a given time as an important factor when simulating energy demand at a one minute (Richardson et al., 2010) to one hour (Widén et al., 2009b) time resolution. The energy use (and subsequent $Q_{F,B}$) is influenced by the occupancy and the activity. Occupant interactions with the indoor building include electrical plug loads (appliances), heating/cooling use, ventilation (inc. windows) and hot water (Delzendeh et al., 2017). Passive influences occur in the form of metabolic heat of occupants ($Q_{F,M}$) contributing to a building's internal heat gains (Page et al., 2008). For commercial buildings there is a high correlation between energy consumption and occupancy levels (Kim and Srebric, 2017) (highest 1 kW/person), whilst occupancy is essential for reproducing domestic load patterns (Widén and Wäckelgård, 2010). Occupants use appliances when carrying out activities (Richardson et al., 2010) and adjust the heat of the building for thermal comfort, altering the internal thermal environment. Accurate representation of occupant behaviour is therefore key to understanding and calculating the release of anthropogenic heat into the atmosphere. In modelling, the oversimplification of occupant presence and their activities in buildings, typically due to the use of aggregate input data, leads to discrepancies in modelling results (Azar and Menassa, 2012; Chen et al., 2017; Dziedzic et al., 2020). As such, some studies argue that building occupancy should be included in every model of building energy or performance, at the highest resolution possible (Dziedzic et al., 2020). Proper representation should therefore be carefully considered for the scales modelled.

Domestic energy is influenced by a lot of factors, both physical (Section 2.3.2) and socio-economic (Guerra Santin et al., 2009). Huebner et al. (2015) found that almost one quarter of domestic energy demand variability can be associated with socio-economic characteristics such as income, age and tenure, but stated that household size (number of people living in a dwelling) was the most substantial factor. This is relevant to future trends in energy demand (and hence $Q_{F,B}$) as populations continue to grow and housing demand increases. It is widely recognised that dwelling floor plan area is also a considerable factor, as this affects the amount of space requiring thermal control and can be linked to the number of appliances within (Yohanis et al., 2008; Karatasou and Santamouris, 2019). Despite this growth in population, the average UK household size is decreasing by 1.2% per year (Ravetz, 2008), also driving up housing demand. This would have implications for Q_F as energy demand evolves with these changes.

The demographics of occupants, including age, income, household size and choice of appliances, can also be a source of great variation in energy consumption, particularly for appliance use in the domestic sector (Yohanis et al., 2008; Huebner et al., 2015; Jones et al., 2015; Karatasou and Santamouris, 2019). Druckman and Jackson (2008) also quantify the influence of these factors, and state that trends within them could be investigated in order to provide information to guide policy or scenario development. With the focus being on energy demand in these studies, such trends could also be used to investigate changes in Q_F, either with regards to spatial variation in Q_F at local scales across the city extent, or in terms of changes of the population as it evolves.

Appliance ownership is also highlighted by Jones et al. (2015) as a factor influencing energy consumption. For example, Karatasou and Santamouris (2019) found this to be the second greatest influence on domestic energy consumption, after heating, with socio-economic status being a strong causal factor in appliance ownership (socio-economic factors were also seen in Mansouri et al., 1996). This relates to human behaviour in that the actions undertaken by building occupants involving the use of appliances are attributed to energy demand and resultant $Q_{F,B}$. Torriti (2017) discusses how each of these actions may be time-dependent, in that actions at the level of social practice can be represented by diurnal, weekly or seasonal patterns. For example, it was found that peaks in food preparation occur at morning, noon and evening, whilst washing tends to happen in the mornings and evenings and watching television most commonly happens in the late evening. Some activities were shown to be less time dependent. Such activity profiles have been included in many studies of building energy demand at the building or local scale (Richardson et al., 2009, 2010; Widén et al., 2009b, 2012; Liddiard, 2013; Gaetani et al., 2015). Whilst HVAC needs account for the largest proportion of domestic energy end use (e.g. Eurostat, 2019), the energy consumption of appliances can dominate $Q_{F,B}$ in scenarios where the need for HVAC is low (e.g. during mild weather). It is therefore important

to consider the influences on appliance demand profiles, particularly when simulating the effects of changes to any behavioural factors.

Detail can also be included by considering the relations between various activities and metabolic response ($Q_{F,M}$). For example, Quah and Roth (2012) attributed metabolic heat production values to various activities that may be regularly undertaken in the study areas, with the highest values given to domestic work. In aggregate across a spatial extent, such as a residential neighbourhood or an entire city, these actions and their resultant energy consumption will also be reflected in the diurnal and weekly patterns of $Q_{F,B}$.

2.4 Modelling physical and social aspects of Q_F and energy demand

Modelling a city from the top down treats the system as pre-determined and assumes that heterogeneity occurs only through very simple parameters that represent aggregate behaviour or characteristics (Batty, 2005). For example, using residential population as a proxy for disaggregating large-scale energy consumption ignores the smaller scale properties of demographic (e.g. age, gender) and energy use type (heating, ventilation and air-conditioning – HVAC; temperature independent). Crooks et al. (2008) state that as cities and their functions are highly heterogeneous, the use of aggregate data at city scale makes it difficult to separate city and local scale phenomena. As Q_F is fundamentally a result of human activity, simulated Q_F should be responsive to the behavioural/demographic characteristics of a city's inhabitants. This could include low-level actions, such as activities within buildings, as well as the practices that act and interact across city geographies, such as transport networks, infrastructures and building stock (Section 2.3.3.3). Hence, effects on Q_F would be permitted to occur should the practices or actions within these behaviours or geographies change at any level. This would allow for the dynamic investigations into the present and future Q_F scenarios that impact urban meteorology. Response could be triggered at a variety of scales. This could be included by using a bottom-up simulation structure (possibly hierarchical) that involves all Q_F source sectors and operates throughout the spatial and temporal scales at which Q_F operates (Section 2.3). The movement and flow of different populations across a city is key to providing the connections between spatial scales and systems (Section 2.3.3.2), yet including detail at the level of individuals or groups (e.g. age groups) across an entire city is not typically seen in Q_F studies. The resolution of model time steps must also fully represent temporally changing behaviours.

The influences on Q_F presented in Section 2.3 exist across a variety of scales and systems (i.e. the source sectors). Simulation of each system could be achieved separately across the necessary scales and imposed trends could be instigated, for example by accumulating the output of multiple BUS models for each behaviour. However, this would ignore the connectivity and interdependencies

between systems, providing little or no improvement upon the drawbacks seen in the fundamental structures of current approaches.

2.4.1 Agent-based modelling

Sufficient modelling of interdependent behaviours would require a method that allows for connectedness between systems. Agent-based models (ABMs, also as "agent-based modelling") are used for modelling complex systems that comprise multiple components (agents), each of which may share a common fundamental design but have their own characteristics, attributes and behaviours, therefore displaying heterogeneity. These agents are able to interact with one another by sharing or competing for information or resources. They may also interact with the environment in which they are based. Rules and behaviours govern how the agents may interact with each other and the environment (Macal and North, 2010; Crooks and Heppenstall, 2012; O'Sullivan et al., 2012). A state change occurs within the agents in consequence to any interactions, prompting the agent to independently react according to another set of behavioural reaction rules (O'Sullivan and Haklay, 2000; Crooks and Heppenstall, 2012). This results in further heterogeneity between agents, not only within their attributes but also in their reactions and state. The attributes that an agent may possess can be static or dynamic, and include resources, capacities, definitions of its surroundings (for example, neighbouring agents), and, in some cases, memory of previous states (Macal and North, 2010). In terms of behaviour, agents can either share a set of rules or each have their own unique rules (Crooks and Heppenstall, 2012).

Agent-based modelling has not previously been used in relation to Q_F, but elements of Q_F and its causational factors have been modelled. For example, ABM has been employed to address the discrepancies of building energy model outputs caused by oversimplifying the interactions of occupants (Section 2.3.3.3). As occupancy levels and energy needs differ by building use type (Section 2.3.2), studies exist for both commercial and residential buildings. The method allows for the inclusion of occupant-occupant (e.g. social influence of energy saving schemes) and occupant-building (agent interaction with environment, e.g. thermal comfort, adaptation of technologies) interactions using high resolution input data (e.g. Azar and Menassa, 2012; Chen et al., 2017; Ding et al., 2019; Dziedzic et al., 2020). Agents can be used to represent just the individual occupants (Azar and Menassa, 2012), as well as building components, appliances, and HVAC (e.g. Chen et al., 2017; Ding et al., 2019). As occupants move around a building, energy use can be modelled at a variety of scales (room, building floor, whole building). Occupant agents can be given stochastically generated schedules of activity to allow for random behaviour (Luo et al., 2017), building on the stochastic activity profiles used in traditional building energy demand models (Section 2.3.3.3). Such studies

found that the inclusion of these interactions and activity profiles could be used to improve output accuracy of building energy models (Azar and Menassa, 2012; Luo et al., 2017; Dziedzic et al., 2020).

If a system is able to be suitably represented by an ABM structure, i.e. it displays interactions between multiple (heterogeneous) components and an environment, its spatial scale (at both agent and environment level) is defined based on the needs of that system (Crooks and Heppenstall, 2012). As such, the scalability of ABM also allows for energy demand processes to be represented at larger scales. Bustos-Turu et al. (2016) present an ABM of residential energy demand based on domestic user-behaviour and prevalence of electric vehicles at sub-regional scale (boroughs of Greater London), with land-use and infrastructure considered within the system. Electricity, heating and vehicle charging demands are modelled at point of use. Basic interdependence between the domestic activity and transport patterns is shown, as agents (individual people) are each given generated activity schedules and travel patterns based on their characteristics. The model does however neglect low-level interactions, as it is not clear how the activity schedules are generated. Energy demand is simulated using basic functions that appear to allow for heterogeneity in a similar way to BUS and SR techniques.

The temporal scale of an ABM is governed by what drives the agents (O'Sullivan et al., 2012; Heppenstall et al., 2016), whilst separate processes can evolve over different time scales (Liu and Andersson, 2004; Batty, 2005). The evolution of energy consumption due to new technologies or policies can be modelled across a variety of scales. Azar and Menassa (2012) modelled the efficacy of energy efficiency policy within an office building, using social influence between workers. Hattam and Greetham (2017) modelled the spread of electric vehicles and photovoltaics across neighbourhoods, seeded by certain demographics and house size, and proliferated by neighbour influence. The uptake of district heating has also been modelled at city scale, involving agents that represent policy organisations and local scale spatial units (Busch et al., 2017). Nägeli et al. (2020) use ABM to model changes in energy consumption and emissions due to changes in building stock dynamics (Section 2.3.2), such as retrofitting and replenishment through policy and economical influences. Again, Q_F studies do not tend to represent such long-term trends, but may be worth including in studies that cover a long time period (e.g. decades). Some top-down studies do include changes in factors such as energy consumption, climate change and traffic flow via deliberate, informed alteration of factors (e.g. from projections) (Iamarino et al., 2012; Lindberg et al., 2013), but not as an un-predetermined evolution of behaviour.

The ability for a set of agents to interact is defined by a connectedness between agents (Macal and North, 2010), which could be spatial (e.g. neighbours) or due to agent characteristics (e.g. agents with

similar/different characteristics, available resources). It is often the case that agents are able to move about their surroundings (for example, people moving about a city), but agents can also have a fixed location whilst changing state (Crooks and Heppenstall, 2012). Though not employed at high detail in energy demand studies, the movement of individuals or cohorts of populations is commonly modelled in epidemiology studies. This is used to provide information on the spread of diseases via large-scale urban mobility. The aggregate flow of heterogenous movement of populations can be modelled using large-scale data (Heppenstall et al., 2016), such as travel card entry and exit points (Hasan et al., 2013), though factors such as the represented demographics are constrained by the data used. Perez and Dragicevic (2009) model the movement (and resultant infection rates) of individuals across a small city, combining the systems of population distribution, land use and transport networks. Movement is based on basic rules: a destination is decided by land use (home, work, school, leisure), and travel occurs through an idealised transport network without disruptions. Agents stay at their destinations and travel for set amounts of time and are not characterised by demographic features. Despite this, the authors find that the movement rules realistically capture urban mobility and varying population groups. Though the movement patterns were not specifically evaluated in the scope of the study, it does demonstrate how ABM can be used to model population flow between land or building uses and provide interactions between systems.

Phan and Varenne (2010) discuss the epistemological concepts of different modelling purposes. One such purpose is to solve a specific problem by developing the model around a single issue or context. If this is the sole purpose of a model then its functionality is limited outside of its context, and the model is largely only suitable for the goals behind its design. Additionally, models can also be used as a way to explore and evaluate hypotheses, sharing characteristics with experimentation. In terms of Q_F modelling, the TDI approach could be seen as a tool for estimating heat fluxes limited to the study area and period. As such they not suitable for investigating variability due to situations outside of the given data. BUS has a bit more flexibility in this regard. Scenarios could be explored by using different forcing variables (such as meteorology, activity patterns), and the results of changing building or land uses could be investigated when changing the distributions of representative buildings or road types. However, this still neglects modelling the primary and secondary effects of changing the structure of the city as a system. ABM is able to include such interactions of a complex system, and in doing so provides a controlled method of observing scenarios across multiple influences and effects, providing experimentation capabilities (e.g. scenarios) and the ability to explore concepts and hypotheses.

In modelling the actions of multiple, distinct agents, ABM can be seen as a method of modelling the relations between a system's parts and its behaviour as a whole, allowing emergent behaviours to

occur as an aggregate result of small-scale interactions (Castellani et al., 2019). It provides a method that moves away from the deterministic, top-down modelling techniques that may operate at coarse resolutions (Crooks and Heppenstall, 2012), instead providing the some of the benefits of BUS in that small scale processes are able to be modelled.

Agent-based modelling is however not without its challenges and cautions, as vulnerabilities and disproportionate sensitivities may occur when there are many highly detailed dependencies (Fu et al., 2014). For example, when linking human interactions to the environment, processes from both areas need to be included, increasing complexity (Sun et al., 2016). When modelling processes, it is tempting to include as much detail as possible, but as simulations become more realistic, complexity increases and testing becomes more difficult (Crooks et al., 2008). Abstraction of process representation may therefore be needed in order to mitigate this, but it would be important to find the balance between the realism of processes included and the feasibility of an agent-based model's operation. This involves considering the following elements: agent identity (types of agent, number of individual agents, agent attributes), interactions (inter-agent, with environment, direct or indirect), nature of decisions (stochastic, goal-oriented, adaptive), environment characteristics, and scheduling of responses (Sun et al., 2016).

2.5 Chapter summary

This literature review has identified the causes of spatial and temporal variation in Q_F with respect to social and physical aspects of the city. These include meteorological (climate, climate change, heatwaves, UHI), physical (increased urbanisation and building density, building stock), social (population change, city movement, demographics) and technical (heating/cooling systems) vehicle fleet distribution, appliances) characteristics. Many of these are recognized within current Q_F models, either in terms of model development or as possible causes of unexpected results or discrepancies. The importance of these factors is highlighted as they may continue or emerge as influences on present and future Q_F across its three source sectors.

Current Q_F modelling methods are able to provide reasonable results at high spatial resolutions, but neglect some of the dynamics required to represent changes to Q_F that may occur and cause trends in heat emissions. Little consideration is given towards the individual factors driving behaviourally responsive Q_F. This neglects the possibility of adequately modelling scenarios and macro- or local-scale consequences that may occur as a result of lower-level processes, such as many of the social drivers of Q_F variation.

The scales of variation in behaviour-based $Q_{F,B}$ cannot be adequately represented by top-down inventory approaches, which use aggregate values distributed by subjectively transitional static populations. The sensitivities of Q_F to factors such as energy behaviours across Q_F sub-sectors and high-resolution meteorology are lost due to the aggregate nature of input data. Whilst such aggregate data are useful and provide fast estimates of Q_F, their disaggregation to finer resolutions by use of sub-daily profiles and spatial surrogates is still dependent on assumptions made during development. Diurnal energy use profiles may not be representative of behavioural variation across the city or even the extent of the study area itself (e.g. Gabey et al., 2019), and frequently do not account for sensitivity to meteorological forcing. Sensitivity to local weather is particularly important when including Q_F in SEB studies, as it is known to affect stability of the boundary layer and response temperature (Section 2.1.3.1). Low-resolution energy consumption data can be spatially disaggregated using spatial surrogates, but again the daily patterns used to represent the transitions between different data (e.g. residential and workplace populations) are not necessarily indicative of true, fine-scale movement (Sailor and Lu, 2004). TDI models are also restricted by the spatial and temporal extents of the input data, limiting the capabilities of a model to those imposed by the input data. This makes TDI models unsuitable for investigating the factors that influence Q_F, and any changes that may occur in the future.

$Q_{F,B}$ bottom-up simulation methods are able to model interactions with the environment and reflect the heterogeneity of building energy use. Energy behaviours can be modelled at high detail, and interactions with the environment can be included, accounting for thermal properties of the urban fabric. Currently, BUS at the city scale is either computationally expensive or again uses aggregate results, e.g. representative buildings using the same characteristics and patterns of occupancy or energy use across the study area (e.g. Heiple and Sailor, 2008). However, the adaptive and responsive characteristics of BUS can be included in developing a model that considers the behaviours of a city as whole system, allowing the fine scale BUS behaviours and interactions to include primary and secondary responses to any changes that could occur across the study area as a whole.

Creating a model that can explore Q_F responses to changes in its physical and social drivers will allow for multiple Q_F scenarios to be considered in future studies, expanding the limits of what can be investigated with the model and providing experimental capabilities. This will address a need for the inclusion of high-resolution Q_F in scenario modelling (Martilli, 2007; Barlow, 2014), leading to more investigations into changes to the SEB. This could have impacts and uses in a range of fields, including forecasting and urban health (particularly heat stress and pollution).

Chapter 3 Dynamic Anthropogenic activitieS impacting Heat emissions (DASH v1.0): Development and evaluation[2]

This chapter presents the paper *Dynamic Anthropogenic activitieS impacting Heat emissions (DASH v1.0): Development and evaluation* by Capel-Timms et al. (2020b). The paper presents the development and evaluation of a novel, agent-based Q_F estimation model that aims to provide a method of modelling scenarios under which Q_F may change in response to alterations in the behaviour of a city as a system. Text and figures that were not included in the published paper are indicated by footnotes or in the figure caption. Code and data for this model is available at https://doi.org/10.5281/zenodo.3936025 (DASH v.1.0; Capel-Timms et al., 2020a).

Abstract

Thermal emissions - or anthropogenic heat fluxes (Q_F) - from human activities impact urban climates at local and larger scale. DASH considers both urban form and function in simulating Q_F through the use of an agent-based structure that includes behavioural characteristics of urban residents. This allows human activities to drive the calculation of Q_F, incorporating dynamic responses to environmental conditions. The spatial resolution of simulations depends on data availability. DASH has simple transport and building energy models to allow simulation of dynamic vehicle use, occupancy and heating/cooling demand, and release of energy to the outdoor environment through the building fabric. Building stock variations are captured using archetypes. Evaluation of DASH in Greater London for periods in 2015 uses a top-down inventory model (GQF) and national energy consumption statistics. DASH reproduces the expected spatial and temporal patterns of Q_F, but the annual average is smaller than published energy data. Overall, the model generally performs well, including for domestic appliance energy use. DASH could be coupled to an urban land surface model and/or used offline for developing coefficients for simpler/faster models.

Keywords: Anthropogenic heat emission; dynamic model; energy; urban climate; London

[2] Capel-Timms, I., Smith, S. T., Sun, T. and Grimmond, S.: Dynamic Anthropogenic activitieS impacting Heat emissions (DASHv1.0): Development and evaluation, *Geoscientific Model Development*, 13(10), 4891–4924, doi:10.5194/gmd-13-4891-2020, 2020.

3.1 Introduction

The anthropogenic heat flux, Q_F, the thermal emissions arising from metabolic, chemical and electrical energy use, is an additional energy source in the urban surface energy balance. Q_F varies with human activity across a range of spatial and temporal scales, impacting weather and climate at micro, local and city scales. Heating of buildings in cold climates can be an important influence on the urban heat island (UHI) (Hinkel et al., 2003; Bohnenstengel et al., 2014), whilst in summer the additional heat release from air conditioning (De Munck et al., 2013; Salamanca et al., 2014) can elevate air temperatures. The impacts of additional heat may exacerbate heat-related mortality rates during heatwaves in urban areas (Heaviside et al., 2016) and increase electricity consumption in warmer weather (Santamouris et al., 2001). Although there are multiple methods to estimate anthropogenic heat emissions, and it can be a significant term, it has often been ignored in urban climate studies (Sailor, 2011).

The impact of Q_F on other surface energy balance fluxes can be important (Bueno et al., 2012; Best and Grimmond, 2016). The surface energy balance for an urban volume can be written (Oke, 1988):

$$Q^* + Q_F = Q_H + Q_E + \Delta Q_S + \Delta Q_A \qquad (\mathrm{W\ m^{-2}}) \qquad (3\text{-}1)$$

where Q^* is the net all-wave radiation, Q_F the anthropogenic heat flux, ΔQ_S the net storage heat flux, Q_H the turbulent sensible and Q_E turbulent latent heat fluxes, and ΔQ_A the net energy transported by advection. These fluxes influence the transfer of heat, mass and momentum (Oke, 1988) and the stability of the urban boundary layer. The three major source terms of Q_F (Grimmond, 1992):

$$Q_F = Q_{F,B} + Q_{F,M} + Q_{F,T} \qquad (\mathrm{W\ m^{-2}}) \qquad (3\text{-}2)$$

relate to buildings ($Q_{F,B}$), metabolic (people, animals) activity ($Q_{F,M}$), and transport ($Q_{F,T}$). As a result, Q_F is highly variable spatially and temporally. The daily movement of people through a city will have a local, short term effect, whilst the widespread uptake of new technologies (e.g. energy efficient appliances) could have a city-wide, long term consequences.

There are multiple approaches to estimate Q_F (Sailor, 2011). Using population data, top-down methods disaggregate energy consumption and traffic data to produce diurnal profiles of Q_F (Sailor and Lu, 2004; Lee et al., 2009; Allen et al., 2011; Ferreira et al., 2011; Iamarino et al., 2012; Lindberg et al., 2013; Lu et al., 2016) Although constrained by data availability, such approaches can be updated quickly to provide representative values of past states for large areas (Gabey et al., 2019). However, these methods generate little variations between days, as the models tend to use static diurnal profiles. For example, the flow of people between residential and work areas does not respond to potential events that cause actual changes (e.g. blocked roads from an accident or from flooding)

and is assumed to be homogeneous across a city (Iamarino et al., 2012). Furthermore, energy is often assumed to be released directly to the outdoor environment (Sailor, 2011) rather than indoors. Whilst aggregate behaviour may be captured, the heterogeneity in processes (e.g. attributable to appliance use, technology uptake, changing work practices) are missed despite components (of eq. 3-2) being determined. Top-down approaches do though provide a basis to assess other approaches as their aggregate output is based on metered data.

Bottom-up models exist for the different types of heat emissions (of eq. 3-2) from buildings (e.g. Kikegawa et al., 2003; Bueno et al., 2012; Schoetter et al., 2017), transport (e.g. Smith et al., 2009), and metabolism (e.g. Thorsson et al., 2014). Individually, they provide information about behavioural and system change impacts on energy use and heat emissions. For example, building heat releases to the outdoor environment can be modified by building design (e.g. material conduction) and occupancy behaviours (e.g. ventilation, heating systems); and metabolic models capture activity and metabolic types (e.g. adults, children, animals). Other methods to estimate Q_F include assuming energy balance closure (Offerle et al., 2005; Pigeon et al., 2007; Crawford et al., 2017; Chrysoulakis et al., 2018) in eq. 3-1 with all other terms measured or estimated, and measurements of component fluxes (e.g. Kotthaus and Grimmond, 2012).

Whilst existing models of Q_F give plausible estimates, they typically do not capture changes resulting from human behaviour in small areas as city-wide assumptions are used when finer spatial resolutions are unavailable. This means Q_F hotspots (Gabey et al., 2019) cannot be identified. Moreover, they do not allow changes in anthropogenic energy use to be modelled dynamically, so the nature of Q_F and implications of disruption to social practices cannot be investigated. Capturing the interplay between energy related behaviours and meteorological conditions is important to explore system feedbacks and resulting effects on urban climates and city activities.

The terms of eq. 3-2 vary with land use and activity within an area resulting in spatial and temporal heterogeneity of Q_F. In turn, this impacts the urban surface energy balance (eq. 3-1). Models that can respond to influencing factors allow changes to be understood and potentially managed or mitigated. Changes may occur at different spatial and temporal scales, for example: (i) city-wide building stock (e.g. type, dimension, materials) changes at decadal time-scales impact heating and cooling needs (i.e. modifying $Q_{F,B}$); (ii) individuals' many activities and travel decisions each day impact all three components at the microscale; (iii) social-cultural practices play out across large spatial and temporal extents; (iv) transport dynamics can be modified over small spatio-temporal scales (e.g. road closures) or large spatial and temporal extents through changes in technology (e.g. fuel, transport) and policy/planning (e.g. speed limits in neighbourhoods; planning legislation).

Human behaviour and regional climate can impact each source term of Q_F. High- to mid-latitude cities with colder climates use winter space heating, whereas in hotter climates air-conditioning in summer (Sailor and Lu, 2004) is increasingly used. Work schedules and other culturally informed practices (e.g. social eating, religious worship) alter the time of day, day of week, and time of year (i.e. national holidays) that energy demand occurs (Allen et al., 2011). These influences are not addressed by many static models (Allen et al., 2011; Dong et al., 2017) and associated dynamics are neglected despite having important impacts on emissions (e.g. Björkegren and Grimmond, 2018).

Here we present a new bottom-up model for Q_F (DASH, ***D****ynamic* ***A****nthropogenic activitie****S*** *impacting* ***H****eat emissions*) that captures city features (i.e. place), variations in building-type (e.g. thermal properties), peoples' activities and the variability of these with demographics, and transport energy use and heat release. The DASH model allows the impacts of activities and their interactions across a wide range of spatial and temporal scales to be explored by taking an agent-based approach. With both the heterogeneity of city energy use and dynamics of the whole city captured by DASH, comparisons to top-down inventories or other data with coarser spatial and temporal scale resolutions are possible. These patterns can be analysed to diagnose the sensitivity of the steady-state to events that cause perturbations by human behaviour. The general model structure and functionality are described (Section 3.2). DASH is applied (Section 3.3) and evaluated (Section 3.4) in Greater London using inventory-based results (Gabey et al., 2019).

3.2 Model development

Given DASH takes an agent-based approach, all processes have either an interaction or reaction of agents (Macal and North, 2010). The agents represent the decisions for movement and activities of people (e.g. cooking) that impact energy use and therefore Q_F. The dynamics result from agent activity across multiple processes in each Q_F source term (Figure 3-1a) but share outputs (Figure 3-1b). For each spatially scalable agent (Section 3.2.1) there is (Figure 3-1a):

1) *An agent-based model (ABM) scheduler*: to capture the evolutionary dynamics (Section 3.2.2) of the spatially discrete agents A_N (Figure 3-3a).
2) *Three source-specific Q_F estimators*: use movement and activity from the ABM scheduler to model metabolic ($Q_{F,M}$, Section 3.2.4.1) and transport-related ($Q_{F,T}$, Section 3.2.4.2) anthropogenic heat. Given the dominant role of building energy use to urban anthropogenic heat (Sailor and Lu, 2004; Pigeon et al., 2007; Allen et al., 2011; Sailor, 2011; Nie et al., 2014; Zheng and Weng, 2017; Gabey et al., 2019), a building energy model (Section 3.2.4.3 and Appendix B) is integrated within DASH to estimate $Q_{F,B}$ - this accounts for behaviour of occupants that impacts both appliance energy use and any indoor environmental conditioning (Figure 3-3b).

The main DASH workflow is driven by agent-agent interactions with a three-stage process determining Q_F per time step (Figure 3-1b, 3-2):

Stage 1: Agent-agent interaction occurs through occupant (O_C) exchange processes (blue, Figure 3-1b, 3-3a) that are modified by demographics as well as type and time of day.

Stage 2: Occupancy levels associated with an agent (yellow, Figure 3-1b) modify appliance energy use ($P_{\alpha,}$ Figure 3-1), building heating and cooling control (via the building energy model, STEBBS - **S**implified **T**hermal **E**nergy **B**alance for **B**uilding **S**cheme[3]), and volume of vehicles on the transport network (green, Figure 3-1, 3-3a).

Stage 3: Source-specific $Q_{F,B}$, $Q_{F,T}$ and $Q_{F,M}$ terms are calculated for each agent and combined to give Q_F for each agent's geographical region (Figure 3-3b).

All processes operate at the same spatial unit (rather than area) and time step. These are both defined by the data used to inform the ABM scheduler. Rules that govern the processes may be informed by data and actions at coarser scales.

3.2.1 Spatial granularity

Agent-based model design allows flexibility as to what "agents" represent; for example, individuals, households, specified areas, or businesses (Crooks and Heppenstall, 2012; O'Sullivan et al., 2012). However, the chosen units should be able to interact with each other and respond. The constraints on selecting the most suitable entity for an agent include the purpose of the simulation, data availability and computer resources. In DASH, agents represent spatial units that interact by exchange of occupants - the number, activity and type of which informs the calculations of Q_F (Figure 3-1).

The Q_F of a spatial unit depends on the number occupants and their characteristics and activities. For example, in residential areas $Q_{F,B}$ increases as occupants wake up and start to use appliances or heating/cooling. As they leave home, $Q_{F,T}$ increases as fuel is used for transport and as the O_C are passed between agents the changing activity and occupancy numbers impact on each agent's Q_F. By using spatial units as agents (with O_C as an agent property), agents can be scaled according to behavioural data and computational constraints. The relationship of agents to occupants can be from many-to-one and many-to-many. Here, a many-to-many relationship is used given computational and data constraints.

[3] The STEBBS building energy model was developed by co-author Stefán Smith for Capel-Timms et al., 2020b

The agents interact by exchanging O_C based on rules associated with the number, type, and activities of occupants. These are also used in calculation of the energy use of an agent, i.e. the agents' response. Agent representation is designed to be data-driven (analysed) and so behaviour is constrained by data availability. For individual cities, the context (social, physical) provides the agents probable ('exact') characteristics, while administrative boundaries from national census (or other large survey data) will typically constrain DASH.

The agent (A_N) based spatial unit (as determined by data availability) contains subareas (a_S^N) of activity (not spatial units) to which the O_C are assigned. Hence, population statistics are needed to characterise subareas. The subarea notation identifies the agent (superscript) and activity area (subscript). In this version of the model, there are six subareas: (i) domestic (a_D^N), (ii) workplace (a_W^N), (iii) primary school (a_E^N), (iv) secondary school (a_H^N), (v) shop (a_R^N), and/or (vi) other (a_O^N). There is a minimum of one subarea in each A_N, with the total number and type in each A_N to be determined according to available data and city context (e.g. a commercial district may only consist of a_W^N). Despite the A_N location being static their properties are dynamic.

As A_N have the decision-making capability for exchanging O_C, they interact by 'releasing' or 'accepting' occupants. Spatial variation in O_C exchange is provided by the characteristics of the a_S^N, for example a_W^N with higher workday populations being more likely to accept occupants during workday hours than other a_W^N with smaller workday populations. Temporal variability is governed by aspects of human behaviour, with granularity provided by different categories of O_C identified within the data used to inform *the ABM scheduler*. The model can, therefore, capture differences associated with time of day, day of week, type of day (e.g. holiday or not) and time of year within (and across) different O_C categories. Thus, this design results in the spatiotemporal dynamics of Q_F.

Each A_N is located within larger spatial units (B) to allow coarser resolution spatial data to inform model behaviour (e.g. traffic speed limits, school districts), as well as enabling different spatial representation of Q_F in analysis. Note that there can be multiple levels of directly nested spatial units. This permits different level of data availability and governance structure (e.g. impacting decision making/options) to be appropriately captured. Hence, impacts from changes in small areas on the surroundings can be explored.

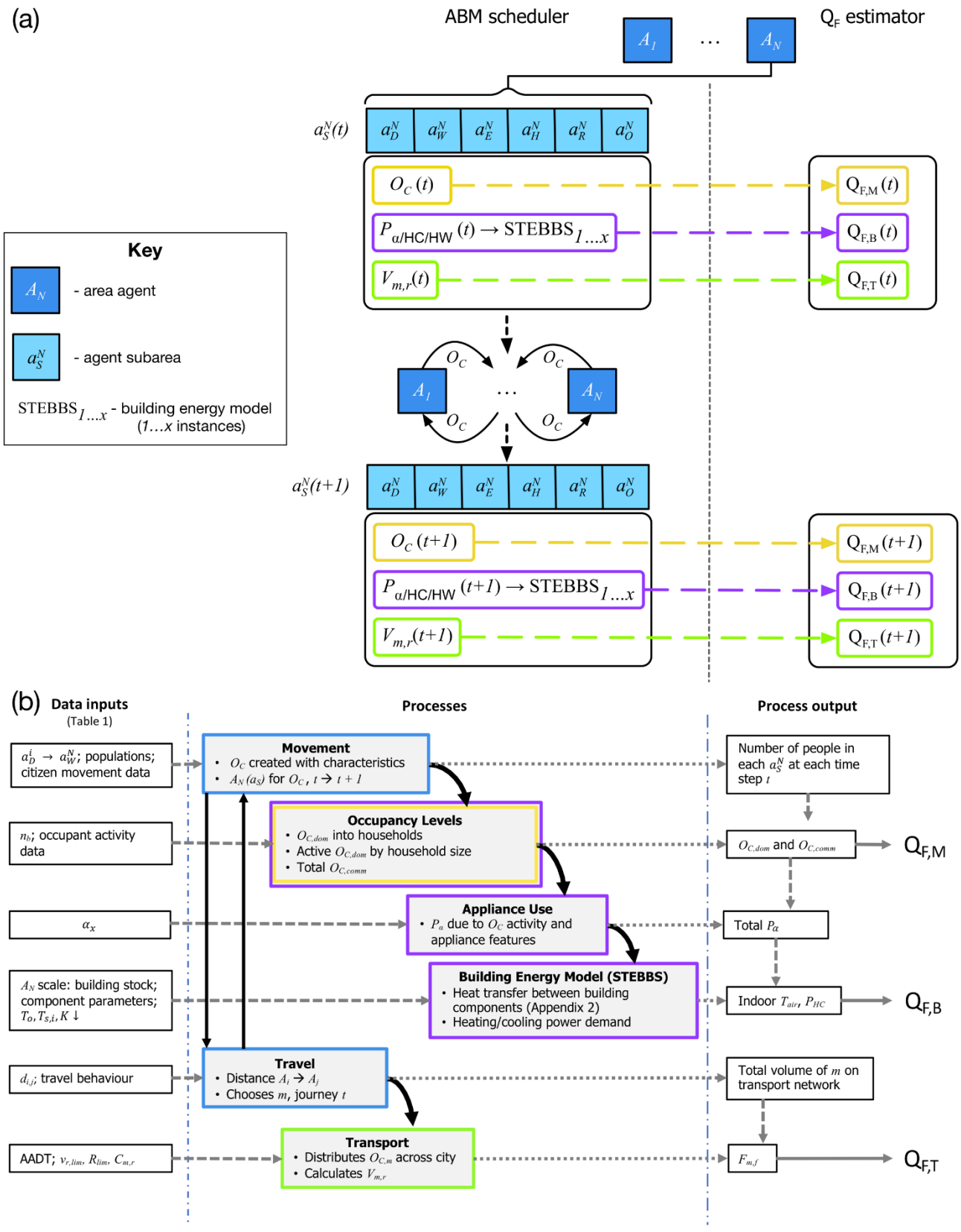

Figure 3-1: Overview of DASH agent reaction and interaction with environment ($Q_{F,B}$: purple, $Q_{F,M}$: yellow, $Q_{F,T}$: green boxes), inputs (dashed lines), process outputs (dotted lines) and their interactions (thick lines), and Q_F outputs (solid grey lines). Notation list gives definitions.

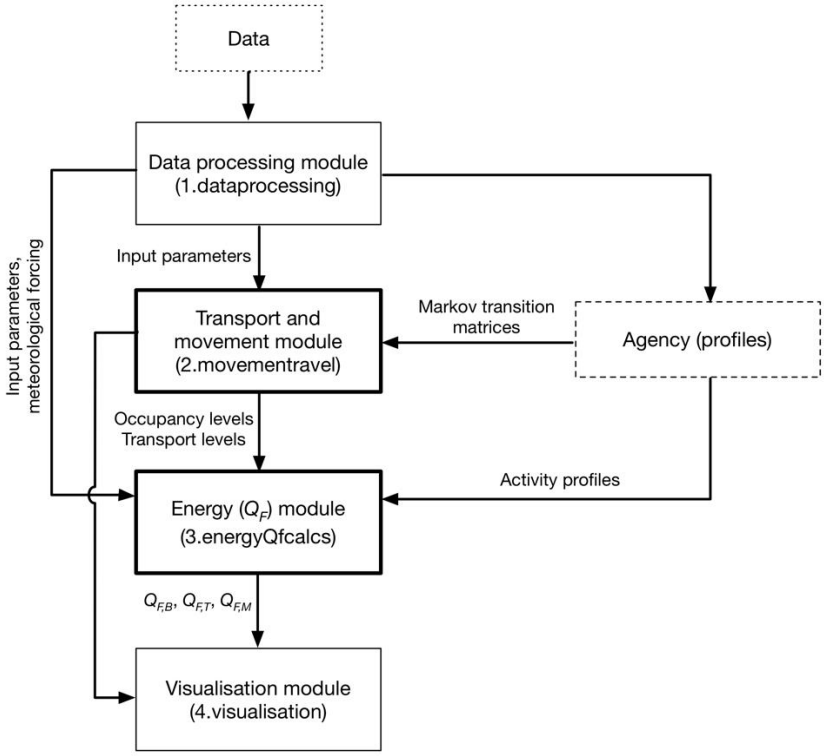

Figure 3-2: Overview of the entire model run across the four components including: model running components (thick lined boxes), pre- and post-processing components (thin-lined boxes), raw input data (dotted box) and demonstration of where and when agency occurs within the model running components (dashed box, not its own component). This figure is not included in the published paper.

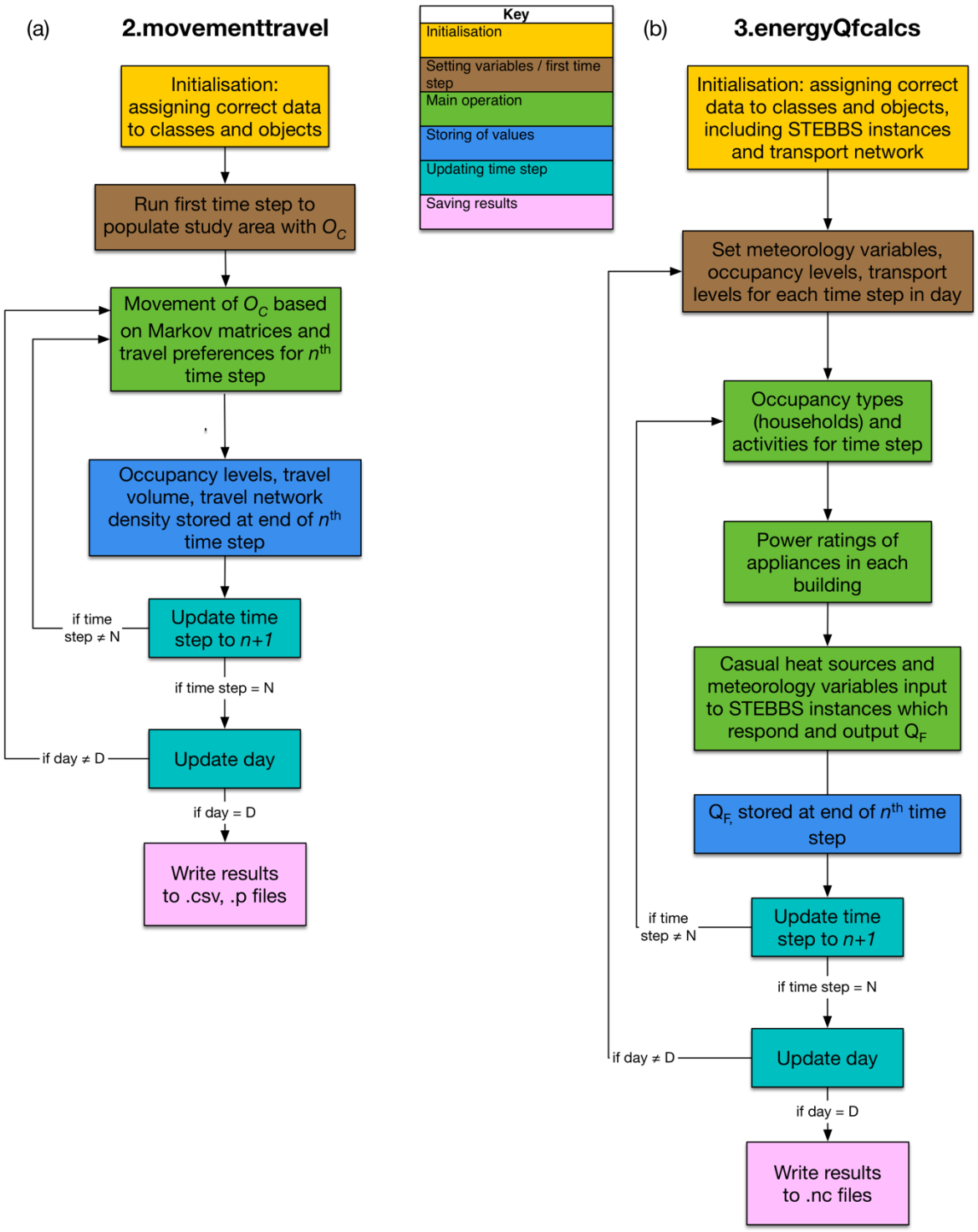

Figure 3-3: Flow diagrams of the basic processes within a total run of (**a**) the agent interaction component 2.movementtravel and (**b**) the agent reaction component 3.energyQfcalcs through N time steps and D days (DASH v1.0; Capel-Timms et al., 2020a). Each process step is colour-coded by process type. This figure is not included in the published paper.

3.2.2 Rules of A_N interaction

O_C are generated and assigned to categories used to inform energy demand behaviour and movement (e.g. age, work). To enable movement of O_C, they are each associated with subarea types a_S^N corresponding to different activities. The a_S^N may be located both within one A_N or across as many A_N as there are a_S^N. A minimum of one 'anchor' subarea is required per O_C to identify a place of residence, a_D^N. For other activities (e.g. work or formal education) to be captured further a_S^N are needed. Data driven assignment of occupants to subareas enables the exchange of O_C by A_N (Section 3.3.1). The 'anchor' a_S^N are relatively static (i.e. changing infrequently) as for example, workplace remains constant for long periods.

If data do not allow direct matching of multiple 'anchor' a_S^N for O_C, then a_D^N is assigned randomly (SciPy, 2019) but in proportion to the available choices. The choice can be informed by rules, such as imposed by local governing structures (e.g. school choice). For O_C trips to non-anchor subareas (e.g. leisure activity, shopping), assignment is stochastic. Gravity weightings (Γ) for all potential trips between origin *i* and destination *j* locations (*B*, for coarser resolution than A_N) of distance $d_{i,j}$ are pre-calculated and stored in a matrix (Casey, 1955):

$$\Gamma_{i,j} = \frac{B_i B_j}{{d_{ij}}^2} \tag{3-3}$$

where weights $\Gamma_{i,j}$ are derived by an attractor (e.g. total number of shops) within *B* and the distance (*d*) between locations. The destination is randomly selected using gravity weightings (eq. 3-3), accepting amenity attraction rules (Reilly, 1953). The process is nested to allow for spatial nesting of agents and account for spatial resolution of data on amenities.

Within an A_N, further rules, associated with movement, can be assigned to O_C to represent structural and personal factors that impact timing and ability to move between a_S^N. For example, associated dependants (e.g. children) impact on timing of movement of an O_C due to caring responsibilities.

3.2.3 Evolutionary dynamics

At each time step, the decision for an A_N to release O_C applies a Markovian approach (Appendix A). This stochastic state determination process decides the nature of an object's (e.g. O_C) next state (e.g. a_S^N) using knowledge of its previous states (Blitzstein and Hwang, 2019). The subsequent time at which an O_C is accepted by the destination A_N is influenced by factors such as distance and time of travel. This allows random variability in human behaviour to be simulated such as presence and activities of occupants in a single building (Page et al., 2008; Richardson et al., 2008; Widén et al.,

2009a) for long periods (Page et al., 2008) whilst aggregate behaviour (informed social structure) will still be apparent. This requires knowledge (data) based on movement and location associated with time and allows decision making to be identified with individual O_C as well as populations.

The movement and location data are used to create the Markov matrices' stationary distributions (eq. A-1) for the exchange of occupants at each time step (t). The Markov matrices are created prior to a model run but could be recalculated between each timestep of the model run in order to capture potential response (in movement and activity) to disruptions.

3.2.4 Calculation of Q_F

Heat sources (eq. 3-2) from people, buildings (with appliance load breakdown), and transport are determined using the O_C count and associated activity in each of the a_S^N of all A_N.

3.2.4.1 Metabolism $Q_{F,M}$

Metabolism ($Q_{F,M}$) of each O_C uses an individual metabolic rate (M):

$$Q_{F,M,i} = M \cdot O_C \tag{3-4}$$

with the sensible (H) and latent (E) components, using the Bowen ratio β (sensible to latent heat) as (for one O_C):

$$Q_{F,M(E),i} = \frac{Q_{F,M,i}}{1 + \beta} \tag{3-5}$$

$$Q_{F,M(H),i} = \frac{Q_{F,M,i} \cdot \beta}{1+\beta} \tag{3-6}$$

Both β and M can vary with activity (e.g. office work/sitting, walking, sleeping) and demographics (e.g. age, gender). Occupants are assumed to be indoors when present in an a_S^N. When occupants travel and are outside, contributions are made to $Q_{F,M(T)}$.

3.2.4.2 Transport $Q_{F,T}$

If an A_N releases an O_C, the journey time, route and mode of transport are needed to determine $Q_{F,T}$. These allow travel dynamics to influence the time and nature of energy use at the associated spatial unit through a simple traffic model. $Q_{F,T}$ is calculated at each timestep for the spatial units for each mode type m (e.g. car, truck, train, walk) and route type r (e.g. minor- or major-road, over-ground- or below-ground-rail), with speed v (m s^{-1}) and heat emission F (W m^{-1}) for all travelling O_C. The journey time is tracked to enable release of O_C at appropriate (e.g. timely, delayed) periods at their destination

A_N by using a mode and journey specific time bin (t_b). The journey time t_b is updated at each time step. The notional duration is found from the mode's distance/time relation using LOWESS analysis (Cleveland, 1988) on travel data for distance travelled.

The total number of travelling O_C in each spatial unit is the sum of O_C in all t_b for all m. The number of O_C in a t_b changes at each timestep as, and when, new journeys begin. When the t_b time is zero, the held O_C are released to the next spatial unit of their journey which may be a destination or an intermediate location (e.g. mode transfer from walking to bus).

The choice of m is informed by data that associates probability of m to origin-destination pairings. If journey combinations data are unavailable, weighting by distance $d_{i,j}$ is used, informed by other sources (e.g. travel surveys). The journey route (through different spatial units that calculate local $Q_{F,T}$) is determined from geographical information system (GIS) data (e.g. OpenStreetMap, 2017), mapping application programming interfaces (APIs, e.g. Google, 2019) or straight line distances between centroids (in the absence of data). For the latter, spatial nesting can be used between A_N and B. Routing options between spatial units can be one (most basic) or many (data dependent).

Route (r) parameters have a capacity limit (R_{lim}) assigned by r-related spatial (B, A_N) capacity constraints (e.g. size and possible number of occupants of a bus or a railway carriage that operate in that area, road congestion limits). However, these may be modified if a disruption impacts part of the transport network (e.g. power failure, intense flooding). The current occupancy is constrained by a mode-appropriate ratio ($C_{m,r}$) such as number of occupants ($n_{o,m,r}$) per unit vehicle. For road related transport, unit vehicle length (L_m) is required as, for example, buses hold more people than a car but require more space on the road. These constraints are informed by local data.

A total vehicle count for each m, r (as $V_{m,r}$) is used to determine if O_C in travel can be moved between spatial units. When both

$$V_{m,r} \leq \frac{n_{o,m,r}}{C_{m,r}} \quad \text{and} \quad \left(\left(\sum_{m=1}^{lim} V_{m,r} \,.\, L_m\right) + \Delta_{V_{m,r}}\right) \leq R_{lim} \tag{3-7}$$

then $V_{m,r,}$ is incremented by $\Delta_{V_{m,r}}$ (i.e. $V_{m,r} + \Delta_{V_{m,r}}$) where $\Delta_{V_{m,r}} = \frac{O_C}{C_{m,r}}$. If R_{lim} (e.g. total road-type length in a spatial unit) is exceeded, O_C will not be passed to the next spatial unit: time associated (t_b) in neighbouring spatial units will be lengthened. When

$$V_{m.r} > \frac{n_{o,m,r}}{C_{m,r}} \tag{3-8}$$

then $V_{m,r,}$ becomes $V_{m,r}$ - $\Delta_{V_{m,r}}$.

Where transport is considered at the spatial resolution of *B*, $V_{m,r}$ are distributed to child spatial units based on the ratio of nested spatial unit capacity to the parent spatial unit's capacity (e.g. $L_{m,A_N}/L_{m,B}$ for cars).

The anthropogenic heat flux from transport, $Q_{F,T}$ for an A_N of area A, at time *t* is (Grimmond, 1992):

$$Q_{F,T} = \frac{\sum_{r=1}^{nr}\sum_{m=1}^{nm} V_{\mathrm{m,r}} \cdot F_{m,f} \cdot L_{r,\mathrm{t}}}{A} \qquad (\mathrm{W\ m^{-2}}) \tag{3-9}$$

where $L_{r,t}$ is the distance travelled in a time-step. Heat emission ($F_{m,f}$; W m^{-1}) varies with fuel type (*f*), *m*, *r* and vehicle speed ($v_{m,r}$; m s^{-1}). For the case of road traffic, speed can be represented as a function of permitted, or average speed limit ($v_{r,lim}$). This is linked to traffic density (i.e. vehicles per unit length, e.g. Salter, 1989) which we relate to a ratio of total on-road vehicle length to total route length (equates to R_{lim}) as:

$$D = \frac{\sum_{m=1}^{lim} V_{m,r} \cdot \mathrm{L}_m}{R_{lim}} \tag{3-10}$$

Hence, speed-density function changes with time (e.g. Greenshields et al., 1935; Wu, 2000):

$$v_r(t) = v_{r,lim} - \mathrm{D(t)} \cdot v_{r,lim} \qquad (\mathrm{m\ s^{-1}}) \tag{3-11}$$

The relation of v_r(t) to $F_{m,f}$ is dependent on local fuels types (e.g. Grimmond, 1992; Smith et al., 2009) and is part of the model parameters specification (e.g. Section 3.3).

3.2.4.3 Building energy ($Q_{F,B}$)

$Q_{F,B}$ accounts for appliance usage ($Q_{F,B}^{\alpha}$), lighting ($Q_{F,B}^{l}$), heating and cooling demands ($Q_{F,B}^{HC}$) and hot water demand ($Q_{F,B}^{HW}$):

$$Q_{F,B} = Q_{F,B}^{\alpha} + Q_{F,B}^{l} + Q_{F,B}^{HC} + Q_{F,B}^{HW} \qquad (\mathrm{W\ m^{-2}}) \tag{3-12}$$

These vary by A_N as O_C composition changes activities a_S^N, and the local building form, construction (materials and dimensions), and control systems (heating, cooling, lighting) change (e.g. as neighbourhood age or construction period varies). A_N release (acceptance) of O_C to (from) the movement and travel module leads to a change in occupancy levels in associated building types. Activity of O_C informs appliance (α), hot water (HW) and lighting (*l*) energy use as well as heating and cooling (HC) set-points for building environmental control.

$Q_{F,B}$ is determined through use of STEBBS, that calculates heat transfer through building fabric and ventilation using an adjustable time resolution. $Q_{F,M}$, α, HW, and *l* provide internal gains to the building volume and fabric (Appendix B). The dynamic 1-D energy model enables both simple representation of individual buildings (Klein et al., 2017), as well as scaling to represent groups of building within an A_N. By using building archetypes, STEBBS provides a computationally efficient

representation of buildings across a city (Heiple and Sailor, 2008; Bueno et al., 2012; Kikegawa et al., 2014) and permit multiple types within an A_N.

For each archetype with an A_N, STEBBS requires the building dimensions (width, depth, height), window-wall ratio, and thermo-physical properties for the building components (i.e. window, wall, roof, floor, internal mass). Thermal inertia of appliances and lighting is assumed to be negligible (i.e. no regulating thermal mass) and so the heat resulting from their use (i.e. total power demand P_a) is exchanged directly with the indoor air.

Domestic hot water (DHW, following building services convention this includes both domestic and commercial buildings) heating and air heating/cooling are a response to internal conditions, controlled by a setpoint temperature (T_{set}; K). The energy use (q) depends on the system efficiency (κ) and maximum power rating (P_{max}) for heating using an exponential control to avoid heating overshoot:

$$q_H = \kappa\left(P_{max} - \frac{P_{max}}{exp^{(T_{set} - T_i)}}\right) \quad \text{(W)} \tag{3-13}$$

and for cooling:

$$q_C = \kappa\left(P_{max} - \frac{P_{max}}{exp^{(T_i - T_{set})}}\right) \quad \text{(W)} \tag{3-14}$$

where T_i is the internal water/air temperature (K). Efficiency losses of the heating system and all cooling energy are calculated as direct heat ejection to the outdoor environment. The heating of the building fabric modifies the storage heat flux of the urban energy balance (Grimmond et al., 1991; Grimmond and Oke, 1999b). Thus this term is tracked and removed from $Q_{F,B}$. Setpoint temperatures are controlled (between minimum and maximum) in relation to occupancy recognising the one-to-many representation of buildings in the model. Domestic instances vary based on proportion of active occupants to total residential population, whilst non-domestic instances may have setpoint temperatures based on occupancy thresholds.

Ventilation loss/gain (q_{vent}) is given as (Spitler, 2011):

$$q_{vent} = V_R\, \rho_a\, c_p (T_o - T_i) \quad \text{(W)} \tag{3-15}$$

where V_R is the ventilation rate ($m^3\ s^{-1}$), ρ_a is the air density ($kg\ m^{-3}$), c_p is the specific heat capacity of air at constant pressure ($J\ kg^{-1}\ K^{-1}$), and T_o the outdoor air temperature (K). In the standalone version of this model no spatial variations of these are considered. If coupled to a meteorological model these outdoor variables can be spatially dynamic and respond to Q_F emissions locally (Sun and Grimmond, 2019).

DHW is considered as a sensible heat gain only (no latent) with hot water to drains unaccounted for in $Q_{F,B}$. Heat exchange between DHW in storage (tank and water pipes) and building volume is accounted for. Volumetric flow rates (V_{FR}, $m^3\ s^{-1}$) of DHW use and to-drain can be set to control volume of DHW in-use. The internal heat gain from this varies with O_C level and activity.

The combined internal gains based on internal building activities are passed to STEBBS. The number of active (i.e. present and awake) O_C in a building (e.g. domestic, work) influences total energy use (Druckman and Jackson, 2008; Yohanis et al., 2008) and the energy demand profiles at timescales from seconds (Richardson et al., 2010) to hours (Widén et al., 2009b). Hence, occupancy levels are essential to reproducing commercial (Kim and Srebric, 2017) and domestic load patterns (Widén and Wäckelgård, 2010).

Hence, each building archetype within an A_N is impacted by its O_C level and their activities (i.e. a_S^N). As O_C categories (e.g. age related) participate in different activities (e.g. infant differs from adult), local census (or other) data both constrain and spatially inform O_C characteristics.

Lighting and appliance gains are associated with activity, appliance type α (Firth et al., 2008) set efficiency and power usage (P_α) associated with different building types (e.g. commercial, domestic). We distinguish three energy consumption classes:

(i) *active only (AO)* - only occurs with user activity (e.g. oven, iron)
(ii) *continuous (C)* - always consuming energy (e.g. cold appliances: fridge, freezer; small appliances: telephone, clock, burglar alarm). As these may cycle power (e.g. cold appliances) the power rating accounts for the fraction of time the appliance draws power during a single complete cycle and the mean power consumed whilst operating.
(iii) *active/standby (AS)* – two modes which depend on user activities (e.g. television, computer): (1) as *AO*, (2) less when not actively used.

Each appliance (α) type (j) is assigned to either *AO*, *C*, or *AS* with an active power rating α_p and additionally for *AS* appliances a standby rating α_s. The number of appliances of type j in A_N (α_{j,A_N}) is determined by domestic/non-domestic appliance market permeation ($\alpha_{j,k}$) as:

$$\alpha_{j,A_N} = \alpha_{j,k} \cdot n_b \tag{3-16}$$

where n_b is number of households (domestic), number of work-desks (non-domestic, commercial), or floor area (non-domestic, other) in an A_N. α_{j,A_N} acts as the limit of appliance use at any time. If no distinction between j use profiles can be given (data dependent) all appliance demand is combined as one type.

For domestic use, households are categorised by total number of residents such that proportion of α_{j,A_N} (by *AO*, *C*, or *AS*) in use at a given time *t* is:

$$\alpha_{j,u}(t) = \sum_{x=1}^{lim} f_{x,\alpha_j}(t) \cdot \frac{n_{b,x}(t)}{n_b} \cdot \alpha_{j,A_N} \quad (3\text{-}17)$$

with $f_{x,\alpha_j}(t)$ the fraction of households with *x* active occupants using α_j at *t* (based on occupant activity scheduling) and $n_{b,x}(t)$ the number of households with *x* active occupants at *t*. For non-domestic buildings, appliance use is proportional to occupancy level and lighting is considered part of this load.

The power demand P_α (W) of all appliances in use is:

$$P_\alpha = \underbrace{\sum_{j=1}^{n_{AO}}(\alpha_{j,u}(t) \cdot P_{\alpha_j}) + \sum_{j=1}^{n_{AS(1)}}(\alpha_{j,u}(t) \cdot P_{\alpha_j})}_{P_{\alpha(active)}} + \underbrace{\sum_{j=1}^{n_{AS(2)}}[\left(\alpha_{j,A_N} - \alpha_{j,u}(t)\right) \cdot P_{\alpha_j}]}_{P_{\alpha(standby)}} + \underbrace{\sum_{j=1}^{n_C}(P_{\alpha_j} \cdot \alpha_{j,A_N})}_{P_{\alpha(continuous)}} \quad (3\text{-}18)$$

and is the heat gain passed to each STEBBS instance (i.e. each building archetype per A_N). Appliance characteristics are currently uniform throughout A_N but could be variable (e.g. by socio-economic structure).

Domestic lighting is considered as a separate load impacted by an outdoor downwelling shortwave radiation threshold ($K_{\downarrow lim}$), number of households with active (awake) occupants $n_{b,x}$; and a base/min/max illuminance, $l_{base/min/max}$ (lm m^{-2}), per household for scaling lighting requirement (Widén et al., 2009a):

$$K_\downarrow(t) < K_{\downarrow_{lim}}: P_{light} = P_l \cdot n_{b,x} \cdot \left[l_{base} + \left(l_{min} \cdot \frac{K_\downarrow(t)}{K_{\downarrow_{lim}}} + l_{max} \cdot \left(1 - \frac{K_\downarrow(t)}{K_{\downarrow_{lim}}}\right)\right)\right] \quad \text{(W)} \quad (3\text{-}19)$$

Luminous intensity is converted to total power (P_{light}) using a per light power rating (P_l). This is passed to STEBBS as part of the appliance load P_α.

3.3 Evaluation of DASH in Greater London

3.3.1 DASH setup and data sources

We evaluate DASH in Greater London (GL). In the United Kingdom (UK), the output area (OA) is the smallest spatial unit for census data. We adopt the OA as the agent spatial unit (i.e. A_N) in the model runs, with A_N nested within four coarser spatial units (*B*): lower-layer super output area (LSOA); middle layer super output area (MSOA); Local Authority (LA); and City/Region as data (from various

agencies) are aligned to one or more of these spatial units. The LA have several governance roles (e.g. traffic speed, school districts, planning decisions, etc.) that will impact energy use (LGA, 2019). Similar structures are used in other countries but with varying levels creating the complete city (e-Stat Statistics of Japan, 2017; National Bureau of Statistics of China, 2017; Statistics Canada, 2017; US Census Bureau, 2019). In London there are 25,053 OA (determined by residential population and social homogeneity, Office for National Statistics, 2017) that vary in size from $1.56 \cdot 10^{-4}$ to 12.3 km^2, 4,835 LSOA, 983 MSOA, and 33 LA within one Greater London Authority Region (Table 3-1).

The UK Time Use Survey (TUS) 2014 – 2015 (Gershuny and Sullivan, 2017) provides a structured source of data for simulating population movement and human activity (Iamarino et al., 2012; McKenna et al., 2015; Baetens and Saelens, 2016). Such surveys are carried out in many countries by governments or research institutes (Fisher and Gershuny, 2013), allowing DASH to be applied elsewhere with appropriate cultural practises accounted for. In the UK TUS, residents record their activities and location for one weekday and one weekend day, normally creating profiles of individuals with income, age, sex and household type meta-data. The data samples are sufficient to allow analysis at national to regional (e.g. GL) scale in many cases. The 10 min time-step resolution of TUS data (Gershuny and Sullivan, 2017) is the basis for the model timestep.

The TUS data are used to construct Markov chains (Appendix A) that govern the exchange of occupants in DASH (Figure 3-1a) and the levels and type of activities undertaken by different groups of O_c across the day (Section 3.2.3, Table 3-2). Age cohorts (Table 3-2) are used as the group identifier. Appliances attributed to TUS activities (Table 3-2) have different power ratings and market permeation (Table 3-2, Table C-1). Non-domestic activity varies by workplace appliance types according to the land use (e.g. industrial, office) of the A_N (BEIS, 2017a; OpenStreetMap, 2017) with appliances (Table D-1iii) having greater energy consumption in industrial than commercial areas.

The application is undertaken for 2015 to coincide with the TUS data, when GL had a population of 8.539 million (census data updated annually, Table 3-2). The remaining data needed are obtained for the closest year. Throughout we endeavour to use open-source, freely available data. A variety of data types are used, at a range of spatial resolutions (Table 3-1) with more detail given subsequently (Table 3-2 to 3-5).

Movement of occupants is informed by the (Department for Transport, 2017) and census data on commute patterns ($\S_{8,10}$, Table 3-4), to determine choice of mode by distance or type of journey providing the travel attributes (Table 3-4). In this evaluation, nine modes of transport (m) exist: cars, motorcycles, vans, taxis, buses, surface rail, underground rail, cycling and walking. Other

deployments could include freight and boat related modes. Exclusion of freight vehicles does not directly affect the travel dynamics, but will result in an underestimation of $Q_{F,T}$. Route types (r) considered, include four road types (residential, minor (so called B-roads in the UK), major (UK's A-roads) and motorways (highways)); and two rail types (underground and surface). In the model runs, journey distances for all routes that move between LAs are determined at LA scale based on GIS shapefile LA centroids. This is the coarsest implementation of the transport component of the model.

STEBBS is used with different parameters for domestic and non-domestic buildings (Field, 2008). We simplify to the three most common domestic building (houses, bungalows, and flats) archetypes in GL, varied by presence at LSOA level (Table 3-3; Mavrogianni et al., 2012; Valuation Office Agency, 2015). Despite advances in non-domestic buildings characterisation for GL (Evans et al., 2019), the heterogeneity in form and use limits use of a range of archetypes (Steadman et al., 2000). Again, for simplicity in this evaluation, we use a single STEBBS characterization based on the most common domestic archetype parameters for non-domestic (e.g. shops, hospitals, offices). Hence, a maximum of four STEBBS instances per A_N with the appropriate building fabric thermo-physical properties assigned from one of two building age groups (pre- or post-1965, Table 3-3 and Table C-2). Building dimensions are informed by total A_N building footprint and height (Table 3-3) for each archetype by age category. The limited consideration of building material thermophysical properties and dimensions is expected to reduce the spatial variance in heating and cooling contributions to Q_F in DASH. DASH can use more building features given suitable input data.

Meteorological data to force the model are from the KSSW site in central London (Table 3-5, Kotthaus and Grimmond, 2014). Means (1 and 5-min) are used to obtain 10-min means (model time step). Outgoing longwave radiation observed with a Kipp and Zonen CNR4 radiometer (Table 3-5) is used assuming an emissivity of 0.9 (Butcher and Craig, 2016) and Stefan-Boltzmann equation (Oke, 1988) to obtain surface temperature. Soil temperature (at 5 m depth) is assigned assuming it is equivalent to the mean annual (2014-2015) air temperature (Sellers, 1972; Busby, 2015) of 11.9 °C.

As the model requires continuous atmospheric data, gaps are filled in consecutive order: (a) linear interpolation when less than 4 h; (b) median for same time in the surrounding $\pm$ 48 h for gaps of 4 – 24 h; and (c) similarly for gaps greater than 24 h, using the median $\pm$ 72 h. The various model runs (Table 3-6) have a spin-up period of 24 h (144 timesteps) for the STEBBS model to become stable.

Table 3-1: Sources of data used by DASH and the highest spatial resolution (columns) used in Greater London. Details are given in the other Tables (Tab) and Appendices (App) indicated. Notation defined in text.

Data Category	Spatial Scale	A_N	B				
		OA	LSOA	MSOA	LA	City	London/National
Population		Tab 3-2					
Activities						App. A	
Appliance						Tab C-1	
Building	Size	Tab 3-3					
	Types					Tab 3-3	
	Properties					Tab 3-3	Tab C-2
Trans-port	Mode Attributes						Tab 3-4
	Route speed limits				Tab 3-4		
	Mode & route capacity	Tab 3-4					
Environmental conditions						Tab 3-5	

Table 3-2: Spatial, temporal, and demographic data used to inform activity in Greater London. Data sources: Greater London Authority (GLA), Office for National Statistics (ONS), Chartered Institution of Building Service Engineers (CIBSE), Ordnance Survey (OS), Valuation Office Agency (VOA). See also Table D-1.

Data Category	**Model Application**	**Data Source**
Area Codes	All B – LSOA, MSOA, LA All A_N – OA	GLA (2011)
Centroid	All B, A_N	GLA (2011)
Area	A_N - OA	
Population	Domestic (a_D^N) - # by age cohort [all]	ONS (2015)
	Workplace (a_W^N) - # by age cohort [Teen/Adult/Senior]	ONS (2014)
	Primary school (a_E^N) - # registered [Child]	GLA (2014)
	Secondary School (a_H^N) - # registered [Teen]	
	Shops (a_R^N) - # of shops	OpenStreetMap (2017)
	Other (a_O^N) - # of businesses	
Household	Domestic (a_D^N) – distribution by # of O_C per house	ONS, (2011)
Age cohort	Infant [0-4 years] - # in a_D^N	ONS (2015)
	Child [5-11 years] - # in a_D^N, a_E^N	
	Teen [12-18 years] - # in a_D^N, a_H^N, a_W^N	
	Adult [19-64 years] - # in a_D^N, a_W^N	
	Seniors [65+ years] - # in a_D^N, a_W^N	
Anchor locations	A_N - # of residents/workers/students as function of age	-
Day Types (to inform activity profiling)	School weekday [by age cohorts: Child/Teen/Adult]	Gershuny and Sullivan (2017)
	Weekend [by all age cohorts]	
	Public holiday [by all age cohorts – as weekend]	
	Non-school weekday [by age cohorts: Child/Teen/Adult and # of dependent children in different households]	ONS (2017), Gershuny and Sullivan (2017)
Initiation of travel	Clock time of start of journeys within city and subareas	Gershuny and Sullivan (2017)
Building Archetypes assigned Areas	Typical height (m), depth (m) and total floor area (m) of identified types. Height: depth ratios: House 9:12.5, Bungalow 5.5:12.5, Low-rise flats: 6.1:20. Width calculated to maintain ratio and total building volume.	VOA (2015), Butcher and Craig (2016), Mavrogianni et al. (2012)
	Floor Plan Area (m^2) and average height (m) to give volume.	(OS, 2014)

Table 3-3: Data sources for physical building characteristics applied to building archetypes. Symbols in notation table. Symbols used are: $\boldsymbol{L}$ wall thickness (m), $\boldsymbol{\rho}$ building material density (kg m^{-3})**,** $\boldsymbol{k_e}$ wall effective thermal conductivity (W m^{-1} K^{-1})**,** $\boldsymbol{\varepsilon}$ emissivity, $\boldsymbol{h}$ convection coefficient (W m^{-2} K^{-1}), $\boldsymbol{V_T}$ (m^3) volume of tank (dependent on number of persons per household), **ToU** time of use. **Data Sources:** §1 – British Council for Offices (BCO, 2009), §2 - Richardson et al. (2010), §3 - DECC and BRE (2016), §4 - Hawkins (2011), §5 - DECC (2015), §6 - HCA (2010), §7 - Butcher (2004). §2 used for cycling patterns of continuously on appliances (i.e. fridge/freezer). See also Table D-1.

Characteristic			**Domestic**	**Non-Domestic**
Building dimension		Height / Floor Plan	Mavrogianni et al. (2012), OS (2014)	
		WWR	Butcher (2012)	
Thermophysical properties (Table C-2)	Building	L, ρ, k_e	Butcher and Craig (2016)	
		ε,c_p	Stewart et al. (2014), Butcher and Craig (2016)	
		V_R	Butcher (2014)	
		Internal h	Butcher and Craig (2016)	
		External h	Cole and Sturrock (1977)	
	External	k_{ground}	Butcher and Craig (2016)	
DHW Services (Tank/Pipes)		L	Flamco (2017)	
		ε, c_p, k_e	Butcher and Craig (2016), Flamco (2017)	
		ρ	Butcher and Craig (2016), Flamco (2017)	
		h	Butcher and Craig (2016), Knudsen (2002)	
		V_T	MWS (2019)	IOP (2002)
Power Ratings (W) (*see Table C-1)		Heating/ Cooling	Butcher and Craig (2016), Palmer (2016)	
		DHW	Flamco (2017),	
		Appliance*	§1 §2 §3 §7	§4 §5 §6
Activity		Appliance $\alpha_{j,k}$	§7 , §1, §3	
		DHW V_{FR}	BSI (1997), Butcher (2014)	
		ToU	Gershuny and Sullivan (2017)	

Table 3-4: Transport data and sources for (**a**) modes and (**b**) route. Variations used from actual data, include: Buses: 85% diesel of fleet (in 2015) and rest mostly hybrid; Electric (EV) and low-emission vehicles: EV cars 0.2% of GL registered vehicles (2015) (DfT and DVLA, 2019). Data sources: §8 - ONS (2014b); §9 - ONS (2018); §10 - DfT (2017); §11 - DfT (2014a, 2014b); §12 - London Datastore (2014); §13 - OS (2016); §14 - Smith et al. (2009); §15 - Highways Agency (2017); §16 - TfL (2018); §17 - TfL (2019); §18 - OS (2015); §19 - TfL Train and Underground Rolling Stock Information Sheets from §10; §20 - TfL working timetables from §10; §21 - Iamarino et al. (2012). [Δ]Not applied in evaluation

(a) Mode m	People vehicle^{-1} §10, §15	$Q_{F,M}$ person^{-1} (W m^{-2}) §21	Fuel Use Ratio §10, §17	
			Petrol	Diesel
Car	1.4	70	0.84	0.16
Van	1.4	70	0.1	0.9
Taxi	2.5	70	0	1
Motorcycle	1	70	1	0
Bus	17.3	55	0	1
UG rail	--	62[Δ]	--	--
Surface rail	--	55 [Δ]	--	--
Bicycle	1	230	--	--
Walking	1	140	--	--

(b) Route (data vary)	*Source*
AADT (road vehicles)	§12
$v_{r,lim}$ (road vehicles)	§18
$F_{m,f}$ by speed & fuel for road vehicles (electric not considered in this evaluation)	§9, §14
Commute mode choice ($a_D^i \rightarrow a_W^j$)	§8
Journey Time	§10
$C_{m,r}$, R_{lim}	§11, §19 [Δ], §20 [Δ]
Route (r) dimensions (e.g. length, no. of lanes, no. of tracks)	§12, §13, §16, §19 [Δ]

Table 3-5: Observed meteorological variables at King's College London KSSW site, 50.3 m above ground level (Kotthaus and Grimmond 2014, Ward et al. 2016). See Figure 1a in Kotthaus and Grimmond (2014) for site location. From these other variables are derived.

Meteorological Variable		Sensor
T_o	Outdoor air temperature (°C)	Vaisala WXT 520
ws	Wind speed (m s^{-1})	
$K_{\downarrow}$	Incoming shortwave radiation (W m^{-2})	Kipp & Zonen CNR4 Net Radiometer
$Q_{L\uparrow}$	Outgoing longwave radiation (W m^{-2})	

3.3.2 Evaluation methodology

Ideally a model is evaluated with observations of the simulated variables (Table 3-6). However, direct observations of Q_F are extremely limited or are indirect with a series of assumptions within them. At the neighbourhood scale, combining radiation and eddy covariance observations while assuming energy balance closure has been used to assess monthly and daily values (e.g. Offerle et al., 2005;

Pigeon et al., 2007). Using satellite earth observation, a much larger spatial extent (e.g. city wide) is observed but with a bias to clear sky conditions. The snapshot values at the time of the satellite overpass require a very large number of assumptions in addition to energy balance closure (e.g. Chrysoulakis et al., 2018). The closest to "direct" measurements of Q_F are micro-scale emissions from building vents (i.e. part of $Q_{F,B}$) using eddy covariance sensors (Kotthaus and Grimmond, 2012) but there are extremely limited data available. Thus, the spatial and temporal scales that DASH is capable of simulating cannot be directly compared to measured Q_F. We therefore use a series of different sources of public data and another model to evaluate various aspects of DASH.

The reference model used, GQF (Iamarino et al., 2012; Gabey et al., 2019), is a top-down inventory Q_F model developed for London. This is selected as it is amongst the most (spatially and temporally) detailed models for London currently available (Gabey et al., 2019). We apply it to 2014 – 2015 to align with metered data used in the evaluation. The model uses energy consumption, traffic, and workday population data to provide half-hourly estimates of Q_F at city, LA, and OA resolutions. Hence, Q_F estimates for both models are at city scale with OA resolution.

There are several GQF features that restrict DASH being evaluated at higher detail. These are: (i) GQF uses data from a range of scales (up to national) to determine OA results with population weighted disaggregation; (ii) diurnal patterns are prescribed based on either assumptions or coarse spatial data, with variation by day type (weekday, weekend) and season – meaning variability at smaller scales are not captured; (iii) GQF assumes the same diurnal profile for both gas and electricity usage; and (iv) effects of temperature in GQF are the net seasonal diurnal energy use profiles rather than reproducing the day-to-day conditions in London. Hence, individual DASH diurnal patterns cannot be evaluated against GQF with fine temporal or spatial resolution as differences are expected.

To evaluate DASH, appliance (including cooking) power demand is equated to GQF electricity demand and DASH heating and cooling demand to GQF gas demand. This will lead to discrepancies as the demand profiles used in GQF are not energy carrier or vector specific. The calculation and evaluation of $Q_{F,T}$ is undertaken at A_N scale rather than individual routes. In both models, many of the minor residential roads in A_N are unaccounted for.

DASH evaluations (Table 3-6) use annual (1 Oct 2014 to 30 Sept 2015) publicly available gas and electricity consumption data (GWh) for domestic and non-domestic (commercial + industrial) use (BEIS, 2017a,b) and national gas transmission operational data for the same period (NG, 2015). DASH, run with the appropriate meteorology (Table 3-5), OA results are aggregated for assessment to the LSOA (domestic) and MSOA (non-domestic) scales. These evaluation data have some issues: (i)

some non-domestic meter data are undisclosed at MSOA level but appear at LA level (without a MSOA) (BEIS 2018); (ii) meters with insufficient address metadata cause underreported consumption statistics for some areas; (iii) some gas consumption statistics may be wrongly classified (domestic/non-domestic) as this is done based on annual consumption (threshold =73200 kW h year^{-1}) (BEIS, 2018); and (iv) spatial misallocation of metered commercial gas consumption to the billing address rather than actual building/location of use (BEIS 2018).

Basic metrics assessed include the median (50%), interquartile range (IQR), and standard deviation (SD). To evaluate the modelled ($X_{M,i}$) and observed (or reference) ($X_{O,i}$) time and/or spatial data series both the difference:

$$\Delta_i = X_{M,i} - X_{O,i} \quad (3\text{-}20a)$$

and the absolute errors

$$AE_i = |\Delta_i| \quad (3\text{-}20b)$$

are determined, from these:

(1) Cumulative distribution of AE_i is obtained all values (e.g. across all 25,053 OA, Figure 3-11)

(2) Normalised by maximum: $nMax = \frac{X_i}{\max(X_i)}$ (e.g. Figure 3-12)

(3) Normalised errors (%): $nE_i = (\Delta_i / X_{O,i})100$ (e.g. Figure 3-13a,b; ideal value would be 0).

(4) Absolute normalised error: $AnE_i = \left| \frac{X_{M,i}}{\max(X_{M,i}) - \min(X_{M,i})} - \frac{X_{O,i}}{\max(X_{O,i}) - \min(X_{O,i})} \right|$ (e.g. Figure 3-13c, d; ideal value would be 0).

Table 3-6: DASH model runs (R) setup. Runs are characterised by period (dates, and day types: WD weekdays), areal extent (Table 3-1, dom: domestic, n-dom: non-domestic). Data sources: §$_{22}$ GLA (2014), §$_{23}$ ONS (2015), §$_{24}$ ONS (2014a), §$_{25}$ National Grid (NG, 2015), §$_{26}$ BEIS, (2017c). Other details are given in Appendix D and Section 3.2.

R	*Period*	*Extent run*	*Area Analysed*	*Spatial Scale*	*Spin-up (days)*	*Evaluation Data*	*Temporal Scale*	*Fig.*
1	12 – 17 Feb 2015	GL	Camden	a_N^x	-	-	10 min	2
2	12 Feb 2015	GL	GL	A_N	-	§$_{22}$, §$_{23}$, §$_{24}$	10 min	3
3	13 – 14 Feb 2015	GL	E00023911, E00015661, E00008490	A_N	-	-	10 min	4
4	First 44 WD of 2015 preceded by WD 6-9, 13-16, 20-23, 27-30 Jan, 3-6, 10-13, 24-27 Feb, 3-6, 10-13, 17-20, 24-27 Mar 2015	GL	GL	LA	-	-	10 min	5
5	19 June 2015	GL	GL	GL, LA	1	-	10 min	6
6	18 June 2015, 27 Jan 2015	GL	GL	OA (A_N)	1	GQF	30 min	8, 9
7	1 Oct 2014 – 30 Sept 2015	GL	GL	GL	1	§$_{25}$	Annual	10
8	1 Oct 2014 – 30 Sept 2015	GL	GL	LSOA - dom, MSOA - n-dom	1	§$_{26}$	Annual	11

3.4 Analysis of model dynamics

As behaviour, demographics, and travel choices influence the temporal and spatial variation in movement and activity profiles in DASH Q_F estimates, we examine these first. A critical control on Q_F is the number of occupants within an area. The area itself may be static (e.g. where buildings are located) or moving (e.g. transport area). The occupancy level will change as people travel to different locations (Figure 3-4).

In model run R1 (Table 3-6), the results for one *B* spatial unit (LA Camden, London) are used to demonstrate the O_C movement and travel through time (six consecutive days) within each a_S^N for each age group for three day types (weekday (school/non-school), weekend) as a result of A_N occupant exchange (Section 3.2.2). The occupancy levels vary by day type and between age groups, whilst having general consistency within day-type by age cohort. Note, people travel outside (and into) this B during the period, but no perturbation is undertaken (e.g. changing transport availability or road construction).

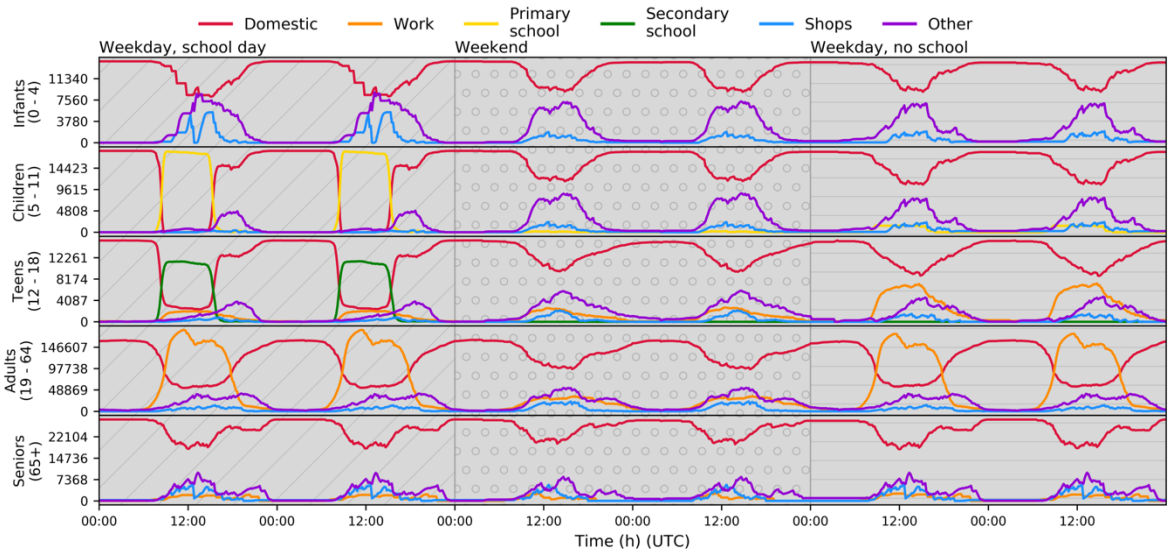

Figure 3-4: Total occupancy of each a_S^N in one LA for five age groups across six consecutive days of three types (textured background): SW (diagonal lines); WE (dotted); NS (horizontal lines); (R1, Table 3-6).

During school weekdays most children and teenagers are in school (a_E^N, a_H^N). Adults, some teenagers, and some seniors work during all day types, and during all times of day. Adult a_W^N occupancy at work (increase at home) is slightly lower on non-school (NS) weekdays than school/work (SW) days as a result of childcare - a small dip observed during noon on NS and SW days that reflects lunchtime

activity. a_D^N, a_R^N and a_O^N occupancy levels increase after peak school and work times, with a_D^N occupancy returning to similar levels each night.

The occupancy levels of each a_D^N, a_W^N, a_E^N, a_H^N are partly informed by population data, so it is important realistic values occur from the movement processes. This is assessed by comparison of the median and IQR of the total occupancy across each a_S^N in the city to the static populations of each A_N and subarea (i.e. residential, workday, school populations) for one weekday (Figure 3-5). Hence, a value of 1 indicates the total population is present. a_W^N occupancy levels have a median peak just over 0.6 of the workday population. A_N interaction in DASH allows for different types of work, such as full/part-time and shift work, as it is inherent to the movement data (in this case the TUS, Table 3-2). Whilst this might not reflect the accurate behaviour of a particular a_W^N (e.g. an a_W^N comprising entirely office work may in reality only be occupied 09:00-17:00 local time), the total variability over a group of a_W^N may be more realistic, given varying work times between commercial sectors.

For R2 (Table 3-6) both a_E^N and a_H^N IQR occupancy levels are less than some A_N school populations (Figure 3-5), but for morning to noon a_H^N the population is exceeded in some areas. Both the deficit and surplus may relate to the method of assigning school anchors to child and teenager O_C (Section 3.2.2). If the age group residential population is lower (higher) than the school population in a LA, there will be too few (many) students occupying this LA schools during the day. As students are assumed not to cross LA boundaries, given state school catchment area restrictions. In Greater London 89% of pupils are in state schools (DfE, 2019).

a_D^N occupancy levels are always below 1. The highest values occur overnight when most people are expected to be at home. The narrow IQR indicates there is little variation in total occupancy levels between areas. Variations are expected with active occupancy (e.g. household sizes, Section 3.2.4.3) and in a_D^N with large differences in resident age groups.

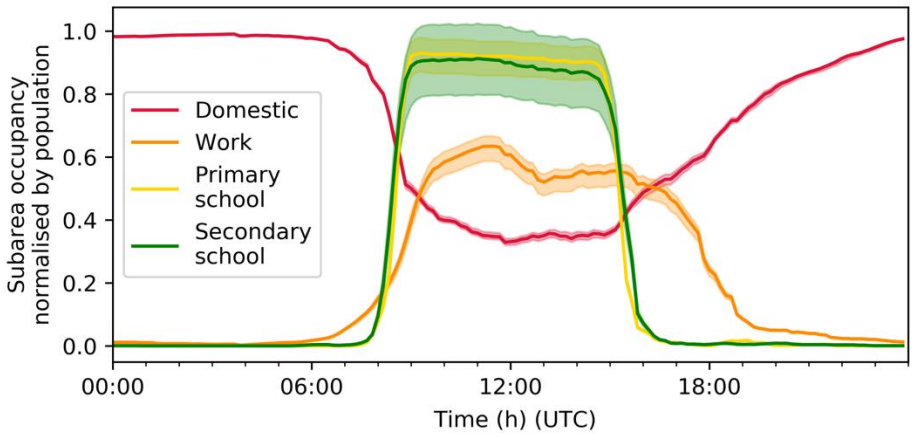

Figure 3-5: Median (line) and IQR (shading) of total occupancy of each a_S^N in Greater London for one weekday (R2, Table 3-6), individually normalised by actual static population for each a_S^N (Table 3-2).

Total occupancy varies with behaviour of different age groups and will affect the power demand within the neighbourhood. To demonstrate the impact of demographics on daily profiles of O_C in the a_D^N, three A_N (neighbourhood, OA, scale) with similar residential populations but different dominant age-cohort are compared in Figure 3-6 (R3, Table 3-6). The a_D^N of each of the three A_N have distinct dominant age groups as: a_D^{senior} 78% (291) residents are seniors; $a_D^{working}$ 92% (297) residents are adults; and a_D^{young} 47% (300) residents are infants, children or teenagers. In a_D^{senior} (Figure 3-6a), daytime O_C remains proportionally higher (Figure 3-6d) than $a_D^{working}$ (Figure 3-6b) and a_D^{young} (Figure 3-6c). a_D^{young} has a steeper morning decrease in O_C and earlier inflection point in the afternoon than $a_D^{working}$, likely due to formal school day lengths (Figure 3-4). On the weekend day, all age groups, apart from teenagers, follow similar patterns, with about 60 – 70% remaining in the A_N (Figure 3-6d).

The diurnal pattern of occupancy levels by day type is consistent between days and boroughs (R4, Table 3-6). The variability of borough occupancy levels for a_D^N (Figure 3-7a) and a_W^N (Figure 3-7b) is greater in the daytime when movement is more likely. Although, these standard deviations are quite small compared to the actual LA-level residential (8,760 - 379,691 residents) and workday (58,444 – 356,706 workers) populations (ONS, 2014a, 2015). This demonstrates that the occupancy exchange method (Section 3.2.2) produces variation in occupancy levels on a daily basis when the same parameters are used for each day.

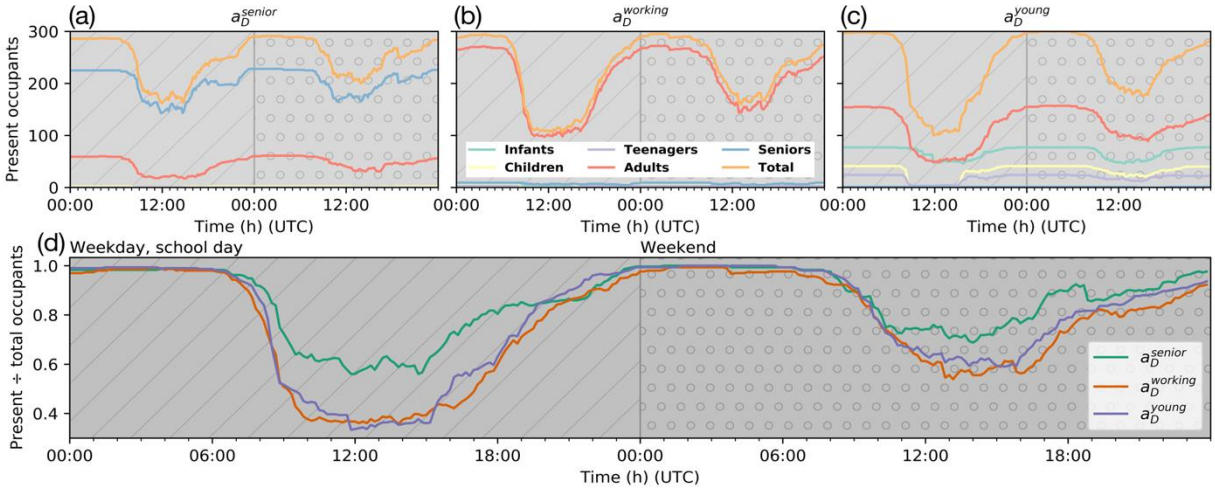

Figure 3-6: Present occupancy levels (R3, Table 3-6) in three a_D^N by day type (textured background) (**a**) a_D^{senior} (number of people per age group living in the area: 0 infants, 2 children, 0 teenagers, 61 adults, 228 seniors); (**b**) $a_D^{working}$ (5 infants, 6 children, 3 teenagers, 274 adults, 9 seniors); (**c**) a_D^{young} (77 infants, 41 children, 24 teenagers, 157 adults, 1 senior). (**d**) Normalised total occupancy levels for the three a_D^N.

In this road vehicle evaluation (R5, Table 3-6), routing is at LA scale with inter-LA routes determined using Google Directions (Google, 2019). The volumes of vehicles in use by mode (Figure 3-8) predicted by the movement component (Figure 3-1, Section 3.2.3) peaks in the morning (07:30-09:30). Slight increases are present around noon and early evening. Low values (00:00-06:00) occur when movement is low (Figure 3-4). The increase at 04:00 is due to both low sampling and the temporal boundary of the TUS, which considers a day's worth of entries to occur 04:00-04:00. The volume of buses is constant over the period 08:00 – 20:00 due to an imposed condition on capacity that represents an increase in $C_{bus,r}$ (Section 3.2.4.2) instead of increasing $V_{bus,r}$. With only one route option given per LA origin-destination pair, road traffic is distributed between A_N in proportion to LA total road area. Routing options at A_N scale have not been implemented.

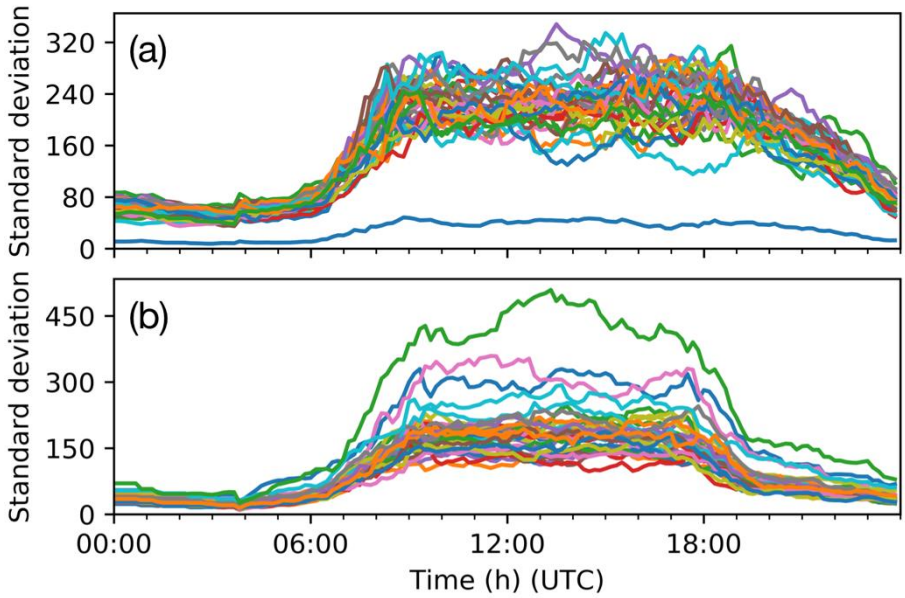

Figure 3-7: Standard deviation of LA (all boroughs of London, colours; for 44 weekdays preceded by weekdays) active occupancy levels (R4, Table 3-6) for: (**a**) a_D^N and (**b**) a_W^N.

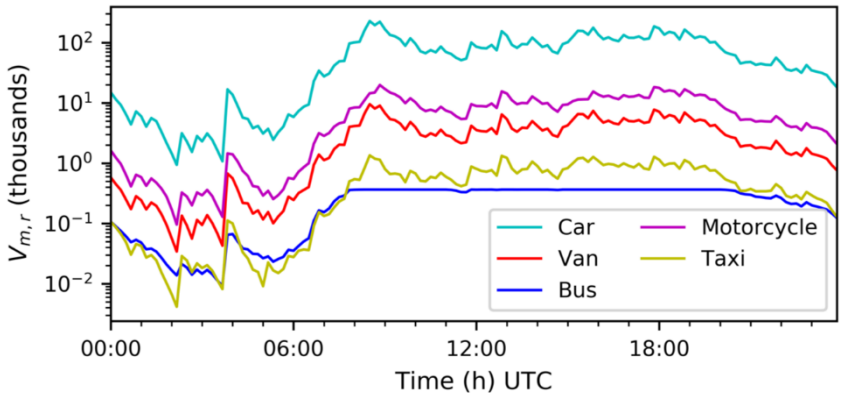

Figure 3-8: Simulated volume of vehicles across Greater London for 19 June 2015 (R5, Table 3-6).

3.5 Evaluation of DASH with GQF

The evaluation of DASH assumes average or typical conditions (i.e. no disruptions are imposed to modify movement and/or timing of activity). As a result the contribution of appliance use to $Q_{F,B}$ is expected to be similar for all days of each type (e.g. weekday, weekend) throughout the year for both domestic and commercial settings (seasonality in appliance-based activity is not considered). In a non-perturbed state, variation within day types across a year is expected to come from heating (space and water) and cooling use as these demands respond to immediate environmental forcing within DASH. As GQF (Section 3.3.2) only varies electricity demand with day type and season and gas with season, we compare the DASH diurnal pattern and magnitude of $Q_{F,B}$ components for two school weekdays

(SW) in different seasons (summer: 18 June 2015, winter: 27 January 2015). The mean air temperature is warmer in summer (17.0°C) than winter (7.0°C) and has more total radiation (Figure 3-9).

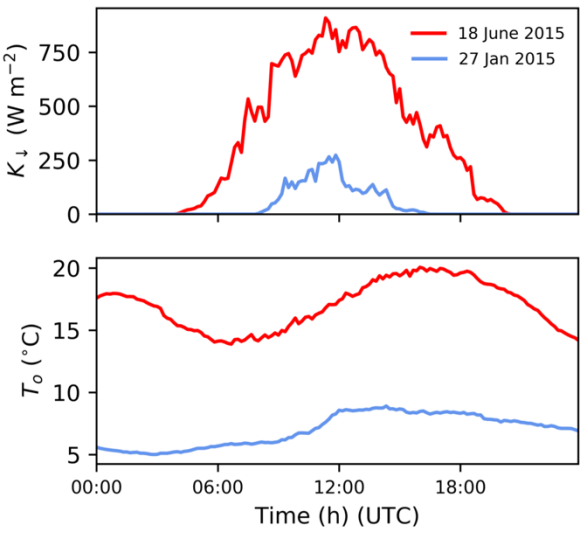

Figure 3-9: Incoming shortwave radiation ($K\downarrow$, W m^{-2}) and outdoor air temperature (T_o, °C) for two SW days. Observations (Table 3-5) are assumed to be constant across the domain in all runs (Table 3-6).

To evaluate heat emissions from buildings ($Q_{F,B}$) the city-wide emissions of domestic (dom) and commercial/non-domestic buildings (n-dom) are considered separately (R6, Table 3-6). As DASH and GQF have the same spatial resolution, comparison is made of spatial inter-quartile ranges (IQR) at the GQF 30-min temporal resolution (i.e. 30-min means (time-ending) are calculated from the DASH 10-min values). DASH appliance emissions ($Q_{F,B}^{\alpha}$) are compared to GQF electricity demand ($Q_{F,B}^{elec}$) whilst combined heating (space and water) and cooling ($Q_{F,B}^{HC} + Q_{F,B}^{HW}$) in DASH are equated to GQF gas demand ($Q_{F,B}^{gas}$). Discrepancies between values are expected, for example in some areas heating may be powered by electricity.

For the summer weekday, DASH domestic $Q_{F,B}$ has similar characteristics to GQF with consistent morning and evening peaks. The mean and IQR are similar from midnight to 5 am, but consistently lower (difference in medians of 2 – 2.5 W m^{-2}) in DASH from the morning to end of evening peak (Figure 3-10ai). Across spatial A_N more than 60% have an absolute error (AE, eq. 3-20b) of ≤ 2 W m^{-2} for all times sampled, and for ~90% the AE ≤ 5 W m^{-2} (Figure 3-11a).

Domestic $Q_{F,B}^{\alpha}$ closely follows $Q_{F,B}^{elec}$ in both pattern and magnitude on the summer day. DASH has three distinct appliance demand peaks: morning, midday, and a larger more sustained evening peak. The magnitude and timing of $Q_{F,B}^{\alpha}$ and $Q_{F,B}^{elec}$ peaks are similar between DASH and GQF, although the

morning peak in GQF is maintained with less variability throughout the day (Figure 3-10a.ii). The domestic summer day gas (GQF) and heating/cooling (DASH) $Q_{F,B}$ profile (Figure 3-10a.iii) have the largest discrepancy in daily profile and magnitude. Under summer conditions, DASH heating/cooling is largely driven by hot water demand as indoor temperatures in all instances of STEBBS are passively maintained between heating and cooling setpoints.

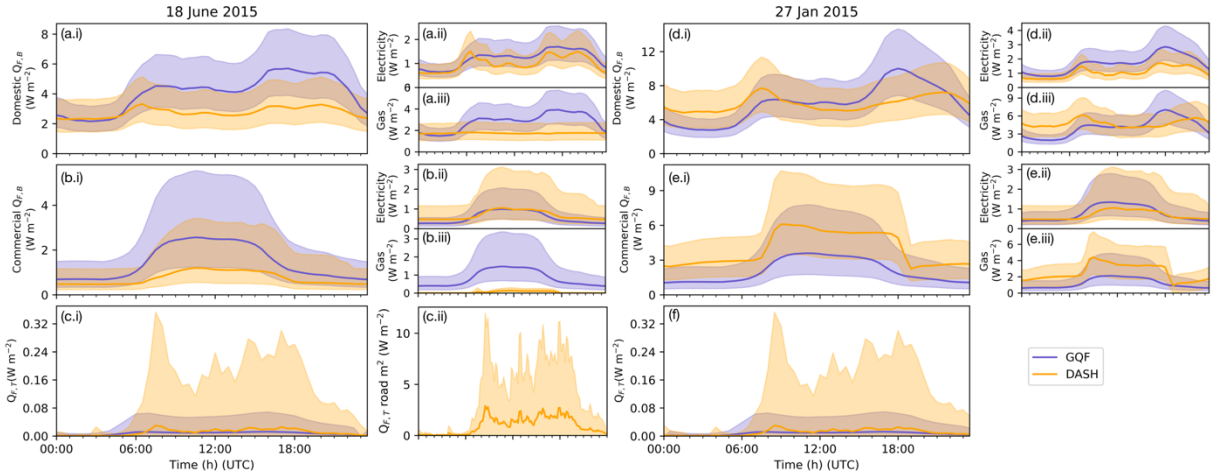

Figure 3-10: Analysis of Q_F (R6, Table 3-6) median (line) and IQR (shading) in 2015 for (**a, b, c**) 18 June and (**d, e, f**) 27 January; showing total $Q_{F,B}$ for (**a.i, d.i**) domestic, (**b.i, e.i**) commercial; with the following: (**a.ii, d.ii**) domestic electricity (GQF) or appliance power demand (DASH); (**a.iii, d.iii**) domestic gas (GQF) or heating + cooling + hot water demand (DASH); (**b.ii, e.ii**) commercial electricity (GQF) or appliance power demand (DASH); (**b.iii, e.iii**) commercial gas (GQF) or heating + cooling + hot water demand (DASH); and (**c.i, f**) $Q_{F,T}$ at A_N scale; and (**c.ii**) $Q_{F,T}$ for road area only. Figure 3-9 shows weather conditions. Figure 3-11 shows absolute errors between the two models.

DASH domestic $Q_{F,B}$ has a more distinct morning peak in winter (Figure 3-10), and from midnight to the morning peak DASH values are 1 – 4 W m^{-2} greater than GQF. This is caused by greater $Q_{F,B}^{HC+HW}$, and may relate to greater sensitivity to temperature for DASH and low outdoor air temperatures. The evening peak is less pronounced and shifted to later evening, with roughly 70% of the A_N having AE ≤ 5 W m^{-2} at 18:00 (Figure 3-11b). All other times analysed more in agreement with GQF. $Q_{F,B}^{elec}$ (Figure 3-10d.ii), but follows a similar pattern throughout the day. This discrepancy is likely due to electric

heating use, which $Q_{F,B}^{elec}$ would include on both a small (e.g. space heaters) and large (e.g. 'district' electric heating in high-rise flats) scale.

Figure 3-11: Ranked cumulative frequency of spatial AE_i (eq. 3-20b) with 2, 5 W m^{-2} (vertical lines) and maximum (key, W m^{-2}) indicated at six times (colour) for R6 (Table 3-6, Figure 3-10) in 2015: (**a, c, e**) 18 June 2015, (**b, d, f**) 27 January 2015, for (**a, b**) total domestic $Q_{F,B,}$ (**c, d**) total

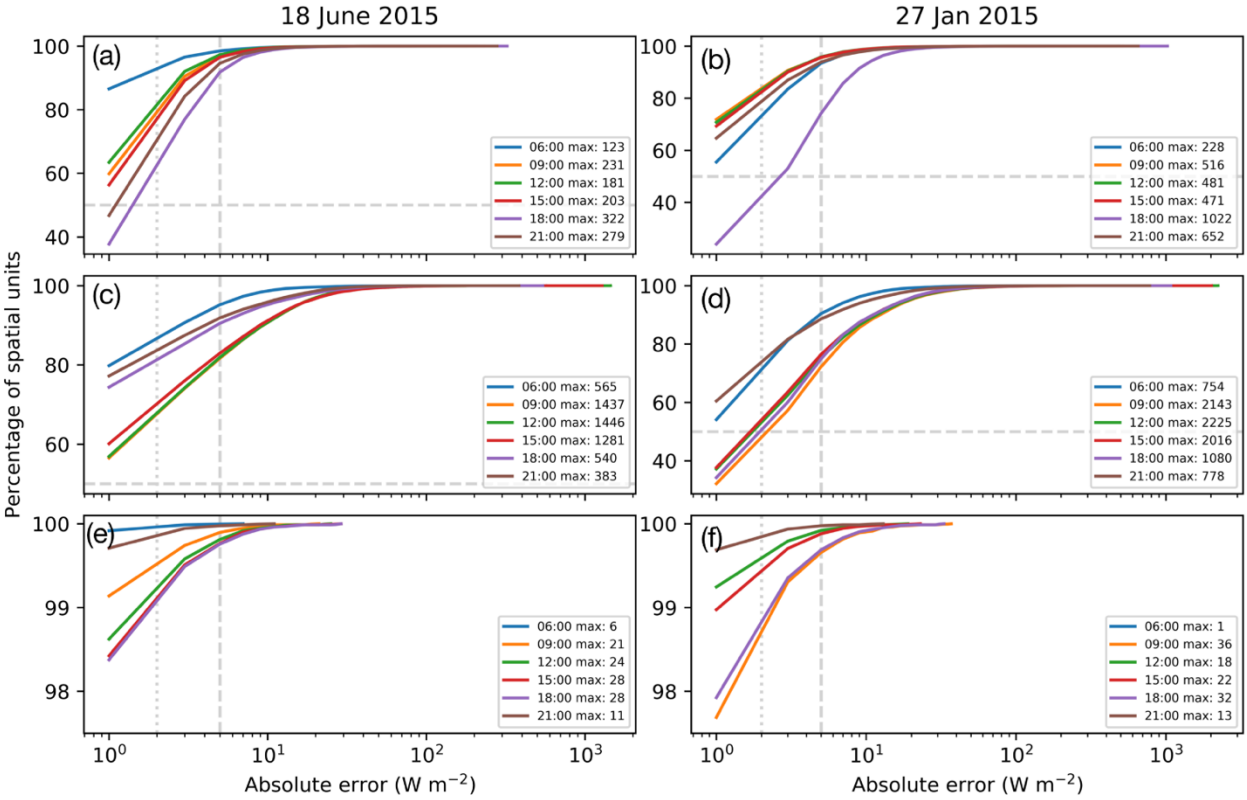

commercial $Q_{F,B}$, and (**e, f**) total transport $Q_{F,T}$. Note y-axes are different between rows (50 % of spatial units shown by horizontal dashed line if applicable) and x-axes are $\log_{10}$.

Summer commercial $Q_{F,B}$ is consistently lower in DASH (median ~1.5 W m^{-2} less) than GQF in the middle of the day (Figure 3-10b.i) with morning and evening medians more similar. The evening IQR increases for DASH and is reflected in $Q_{F,B}^{\alpha}$, likely associated with energy demand from commercial properties that remain open later in the evening (e.g. leisure facilities). There is close agreement between $Q_{F,B}^{\alpha}$ and $Q_{F,B}^{elec}$ medians (Figure 3-10b.ii). At least 60% of A_N agree within 2 W m^{-2} for all sampled time steps (Figure 3-11c).

The winter diurnal patterns for commercial $Q_{F,B}$ are similar for DASH and GQF (Figure 3-10e.i) but DASH has a steeper morning (evening) increase (decrease) as well as consistently higher values (median 2 - 3 W m^{-2} in the daytime). The evening decrease starts ~ 2 h later in DASH. These higher values are due to $Q_{F,B}^{HC+HW}$ (Figure 3-10e.iii), which dominates the total pattern. The median $Q_{F,B}^{\alpha}$ and

$Q_{F,B}^{elec}$ profiles (Figure 3-10e.ii) are in good agreement, with slightly broader IQR for DASH. More than 50% of A_N have a MAE of ≤ 2 W m^{-2} for all times except 09:00, which is slightly below 50% (Figure 3-11d).

For both domestic and commercial use, summer $Q_{F,B}^{HC+HW}$ have the largest discrepancy in profile and magnitude compared to $Q_{F,B}^{gas}$(Figs. Figure 3-10a.iii, Figure 3-10b.iii). In summer for DASH, $Q_{F,B}^{HW}$ is expected to dominate as indoor temperatures in all instances of STEBBS are passively maintained between heating and cooling setpoints. City-wide domestic $Q_{F,B}$ is greater than commercial $Q_{F,B}$ in both DASH and GQF.

The median $Q_{F,T}$ values are fairly similar between both models but GQF has less temporal variability (Figure 3-10c.i, f) with IQR_{DASH} ~ 4 x IQR_{GQF}. As DASH responds to variations in travel demand, and exchanges occupants across the city more temporal variation occur between A_N. Figure 3-11e, f, show small MAEs between the two models, with more than 98.5% of A_N within 2 W m^{-2}. When considered for road area only, DASH $Q_{F,T}$ median values reach 2.9 W m^{-2}, with diurnal mean of 3.25 W m^{-2} (Figure 3-10c.ii). Summer (Figure 3-10c.i) and winter (Figure 3-10f) values differ because of the behavioural change caused by daylight savings time. But no other seasonal changes are expected or occur.

Here the mean GQF values are based on key day types appropriately weighted for the year, whereas DASH is run for the year. The GL annual average $Q_{F,M}$ for DASH is 0.663 W m^{-2}, for GQF it is 0.717 W m^{-2}, whereas assuming one mean metabolic flux for all that live in GL gives 0.386 W m^{-2}. The GL annual average $Q_{F,T}$ from DASH (0.24 W m^{-2}) is larger than for GQF (0.0303 W m^{-2}) as GQF uses a smaller road network (OS (2016) vs. AADT, respectively). The GL annual average $Q_{F,B}$ for DASH (5.53 W m^{-2}) is slightly smaller than the 2015 average meter data (7.22 W m^{-2}, Section 3.6). The GL annual total Q_F for DASH (5.79 W m^{-2}) is smaller than for GQF (7.97 W m^{-2}). The Iamarino et al. (2012) (earlier version of) GQF annual average (10.9 W m^{-2}) for 2005 to 2008 is larger, which is consistent with the decrease in published values seen for London (e.g. Ward et al., 2016; Ward and Grimmond, 2017).

3.6 Evaluation of DASH with annual gas and electricity consumption data

To assess the annual DASH city-wide hot water, heating and cooling energy demand (R7, Table 3-6) results are compared to normalised national gas demand. The seasonal pattern (winter peak, summer minimum) is evident in both (national, DASH) heating data, with short and long period responses to temperature also evident (Figure 3-12). The DASH response to the higher frequency variations is similar to the demand data but the amplitude of normalised demand differs. DASH is seemingly more sensitive to temperature changes but as the national demand profile has net local responses to weather (*etc.*) variations across the country these may be smoother than if only London responses were observed.

In June to August, DASH heating/cooling demand is solely attributed to DHW demand for both domestic and commercial buildings. The consistency in DASH daily-behaviour (i.e. R7 without imposed perturbations) results in a steady-state summer load, with a baseline demand that is less dependent on environmental variability. The normalised national data have both greater magnitude and amplitude of fluctuation in summer (cf. DASH). The national data includes appliance (e.g. cooking) and industrial gas demands whereas DASH accounts for these in appliances (omitted in Figure 3-12). The heating season dominates the DASH results (Figure 3-12). The DASH pattern is less variable with the cooking and industrial baseline demands included (not shown).

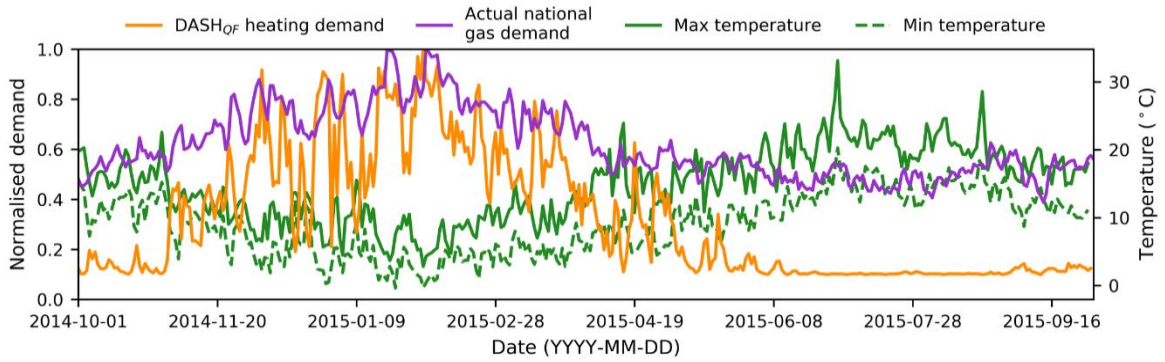

Figure 3-12: Daily (1 October 2014 - 30 September 2015) DASH normalised total HC and DHW energy demand (R7, Table 3-6) for Greater London, minimum and maximum London outdoor air temperature (°C) (Table 3-5) and normalised national gas demand (NG, 2015). See Section 3.3.2 for normalisation.

Evaluation of DASH[4] (R7, Table 3-6) at LSOA scale (Table 3-1) suggests the DASH total domestic energy consumption is less than metered values (Figure 3-13a.i). The DASH IQR is 46 to 29 % lower (Figure 3-13a.ii). Although the LSOA domestic consumption in the central business district (CBD – City of London) has the largest discrepancy (-82.56%), this may in part be caused by misallocation in the published data (e.g. some dwellings classified as commercial because of a large shared meter). There is no evidence of a relation between percentage difference and population density.

The percentage difference between commercial DASH and non-domestic energy consumption is skewed to overestimation by DASH in most MSOAs (Figure 3-13b.ii). The CBD underestimation (-53.2%, Figure 3-13b.i) is likely caused by a large misallocation of commercial gas consumption in this area (Section 3.3.2). One spatial unit (East London) overestimates by more than 1000% (maximum being 1184%, 24.2 GW h). Some OAs (i.e. A_N scale) with large retail buildings have potential uncertainty in both the energy consumption data (e.g. undisclosed data, Section 3.3.2) and DASH simulations.

At MSOA scale, DASH simulates 38% of the areas to within ±100% of published values. The MSOAs that DASH most overestimates (as percentage differences) have fairly small actual magnitude differences and low workplace populations. The mean difference in magnitude across the top 5th percentile is 28.7 GW h, however 77% of these (mean difference 18.1 GW h) have workday populations of fewer than 2,000 people in the MSOA, with most businesses in these MSOA having fewer than 50 employees. Whilst the proportion of these small businesses is fairly high (89% on average) across Greater London (ONS, 2019), it is not the main cause of the uncertainty, as this arises from misclassification of small businesses as domestic within published data. Some overestimation occurs in areas with buildings that are not typically temperature controlled (e.g. warehouses, factories) as DASH assumes all commercial spaces are temperature controlled.

Although the percentage differences in commercial annual energy consumption are larger than for domestic (Figure 3-13a.ii, b.ii), the actual commercial values (Figure 3-13d) are more spatially similar across the city than domestic values (Figure 3-13c). The most spatially disparate commercial area,

[4] Asides from the reasons mentioned in the text (i.e. single source of meteorological forcing, misallocation of metered data), uncertainty could also be due to the assumptions made around the distribution of building use types across and within sectors, and the variety of building thermal properties across the city. The size of discrepancies, and therefore the skill of DASH as a model, relies heavily on the quality and detail of input data. This footnote is not included in the published paper.

containing Heathrow airport (west GL, Figure 3-13d), likely has undisclosed data, hence the large difference (394.7%) of 726.8 GWh. Domestic values are more spatially similar in the less densely populated suburbs, whereas areas east of the CBD are more densely populated and more spatially variable.

The annual LA (Table 3-1) energy fluxes have fewer data inconsistencies when the domestic and non-domestic/commercial energy consumption are combined, allowing meter classification to be ignored. DASH Q_F estimates for Greater London (5.53 W m^{-2}) are lower than those found using the published meter data (7.22 W m^{-2}), with the greatest difference in the smallest LA, City of London (DASH gives 57.53 W m^{-2} and published data gives 123.48 W m^{-2}). The overall spatial patterns are similar, with greater values towards the city centre and more consistent values in the surrounding suburbs.

Although address misallocation (Section 3.3.2) is expected to cause the observed discrepancies (i.e. apparent DASH underestimation for aggregate annual values) found in the CBD, it is not possible to quantify this uncertainty. Similarly, an underestimation is expected from DASH as the meteorological input used is for one central site (Table 3-5) so variations (e.g. cooler temperatures or wind effects) are unaccounted for. This could be improved by coupling DASH with a meteorological model accounting for spatial heterogeneity.

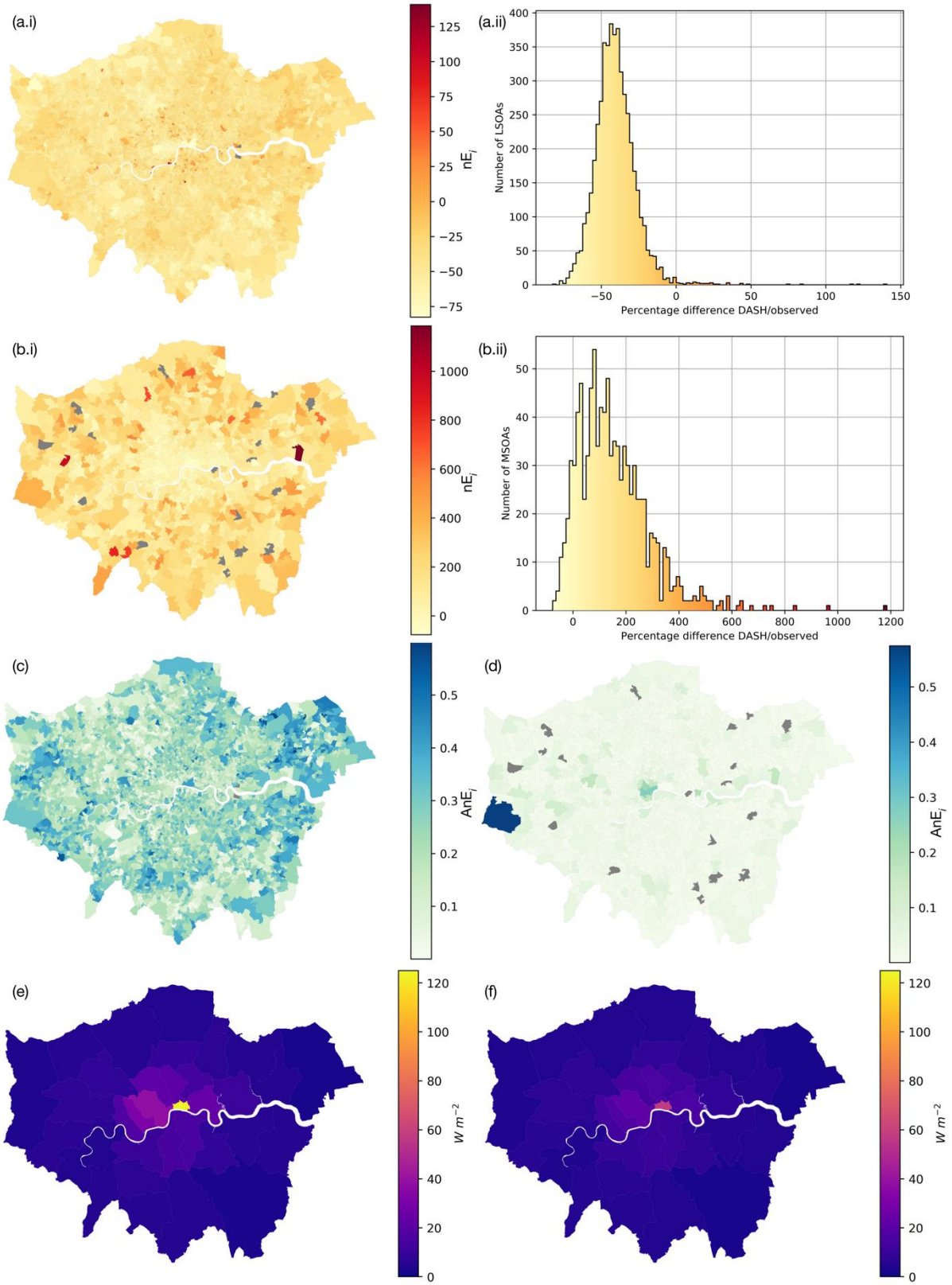

Figure 3-13: DASH (R8, Table 3-6) nE_i of total energy consumption represented by (**i**) choropleth and (**ii**) histogram for (**a**) LSOA scale domestic use and (**b**) MSOA scale commercial use. AnE_i of total energy consumption for (**c**) LSOA scale domestic and (**d**) MSOA scale commercial. Annual average energy flux at LA scale for (**e**) reference data and (**f**) DASH.

3.7 Conclusions

DASH allows anthropogenic heat fluxes to be simulated accounting for both urban form and function, using an agent-based structure. The impact of people's behaviours at the neighbourhood scale is captured as occupants move (10 min time step), varying by day type (e.g. week day, weekend), demographics (e.g. age), location (e.g. residential, work, school), activity (e.g. cooking, recreation, travelling to school or work), socio-economic factors (e.g. appliance availability) and in response to environmental conditions (e.g. temperature related heating use). DASH includes simple transport and building energy models to allow simulation of dynamic vehicle use, occupancy, and heating/cooling demand with subsequent release of energy to the outdoor environment through the building fabric or ventilation.

Evaluation of DASH in Greater London for periods in 2015 uses a top-down inventory model (GQF) and national energy consumption statistics (as cited in Table 3-6, R8). Overall, the model performs well. Some of the spatial and temporal differences may be explained by data inconsistencies in the official data (e.g. privacy related, allocation of use to office headquarters rather than place of use). Analyses with DASH allow high spatial and temporal resolution for a wide range of time periods (demonstrated here from 10 minutes to 1 year) and large spatial extent (demonstrated from output area to mega-city). The model performance evaluation addresses a wide range of these scales (e.g. 30 min spatial patterns at OA, annual at LA scale).

The expected temporal and spatial patterns of Q_F are obtained (e.g. two diurnal peaks and larger fluxes in the city centre). Given DASH's capabilities these can be explored and explained. For example, domestic building $Q_{F,B}$ is more intense towards the city centre than in outer suburbs, following residential population density. The morning and evening peaks are linked to active occupancy and appliance power demand.

As DASH is demonstrated to be able to reproduce conditions generally, future work will investigate dynamic feedbacks within a city that result from changes in urban form and function. DASH is designed to allow parameters to be altered spatially, thus impacts on Q_F emissions can be assessed. Changes may be both slow (i.e. over years) such as from an aging population, uptake of new technology (e.g. change of vehicle fuels and efficiency), or governance (e.g. national energy or carbon goals) and short-term (i.e. hours, days to months), resulting from traffic restrictions (e.g. roadworks, flooding) changing flows. The model performance suggests that other capabilities (e.g. additional transport types) and feedback on other variables (e.g. CO_2) emissions are warranted in the future. With DASH coupled to an urban land surface model, impacts can be assessed both on Q_F itself (e.g. a traffic

disruption at one point in terms of the impact on $Q_{F,B}$) and feedbacks on other surface energy balance terms and near-surface urban temperatures. Such model capability is critical in considering future urban climate scenarios and impacts of human behaviours and feedbacks.

DASH flow diagrams

Flow diagrams of DASH operation and functionality are shown in Appendix F. These are not included as part of the published paper

Acknowledgements

Dr Andy Gabey provided support in early development of DASH and adaptation of GQF for evaluation purposes. George Meachim carried out the gap filling for use of meteorological data. We acknowledge Ian Hamilton (UCL) for some building parameters.

Financial support

This work has been funded by EPSRC (University of Reading doctoral training grant), NERC APEx (NE/T001887/1), NERC Independent Research Fellowship (grant no. NE/P018637/1), Newton Fund/Met Office CSSP China for Sue Grimmond and Isabella Capel-Timms (grant no. AJYG-DX4P1V), and ERC urbisphere (grant no. 855005).

Chapter 4 Fast estimates of anthropogenic heat flux informed by the agent-based model DASH

4.1 Introduction

Chapter 2 addressed the implications of Q_F for the urban meteorology. Despite the consequences for outdoor air temperature response and atmospheric stability (Section 2.1.3), Q_F is underrepresented in NWP-ULSMs (Section 2.1.3.3). Current modelling approaches, along with their advantages and limitations, have also been reviewed (Section 2.2). Chapter 3 (Capel-Timms et al., 2020b) presented the development and evaluation of a novel agent-based Q_F estimation approach with dynamic interactions governed by aspects of human behaviour. This would be suitable for investigating scenarios under which Q_F may change, but its computational expense (Table F-1) makes it difficult to include in broader applications.

Current computationally fast methods using statistical relations (Section 2.2.4) take advantage of Q_F being highly sensitive to both temperature and population density (Oke, 1988; Grimmond, 1992; Sailor, 2001; Allen et al., 2011). Seasonal variations in Q_F are largely driven by the need to maintain thermal comfort within buildings, with some noted dependence on latitude, cultural behaviour (Allen et al., 2011; Dong et al., 2017), climate and socio-economic (i.e. residential, commercial: Kipping and Trømborg, 2017, and industrial: Elkhafif, 1996) make-up.

Statistical relations with meteorology (Section 2.2.4) provide a rapid method to estimate Q_F for urban land surface models. Previous applications of this approach (e.g. Sailor and Vasireddy, 2006; Ward and Grimmond, 2017; Ao et al., 2018) have used top-down inventory models to derive the necessary parameters for the relations, but these neglect some of the Q_F behavioural dynamics that more detailed models can provide. The objectives of this study are to:

i. use the detailed agent-based Q_F model DASH (Dynamic Anthropogenic activitieS impacting Heat emissions, Chapter 3) to obtain behaviourally representative parameters for two simpler Q_F models (Section 4.2, 4.4)
ii. assess the differences in Q_F output for two simpler schemes, in relation to DASH output (Section 4.4)
iii. assess the impact of the three approaches on other surface energy balance fluxes and meteorological variables across Greater London (Section 4.5)

In this study we use the Surface [Urban] Energy and Water balance Scheme (SUEWS, Section 4.3.2) (Järvi et al., 2011; Ward et al., 2016) coupled to the three anthropogenic heat flux models.

4.2 Anthropogenic heat flux models

Multiple Q_F estimation methods exist (Section 2.2, Sailor, 2011). In this study, we make use of two estimation approaches:

i. Agent-based
ii. Temperature dependent statistical relations

The two approaches differ in terms of both data and computational requirements (most: agent-based, least: temperature dependent).

Data-mining the outputs from DASH provides a way to integrate some of the feedbacks between social and environmental conditions into global and/or regional climate/weather models where rapid calculation is essential. These much simpler temperature response approaches differ between using a single critical temperature (e.g. Sailor and Vasireddy, 2006) creating a V-shape (purple, Figure 4-1a) and a slightly more nuanced set of temperatures (e.g. Ao et al., 2018) creating a U-shape (green, Figure 4-1a).

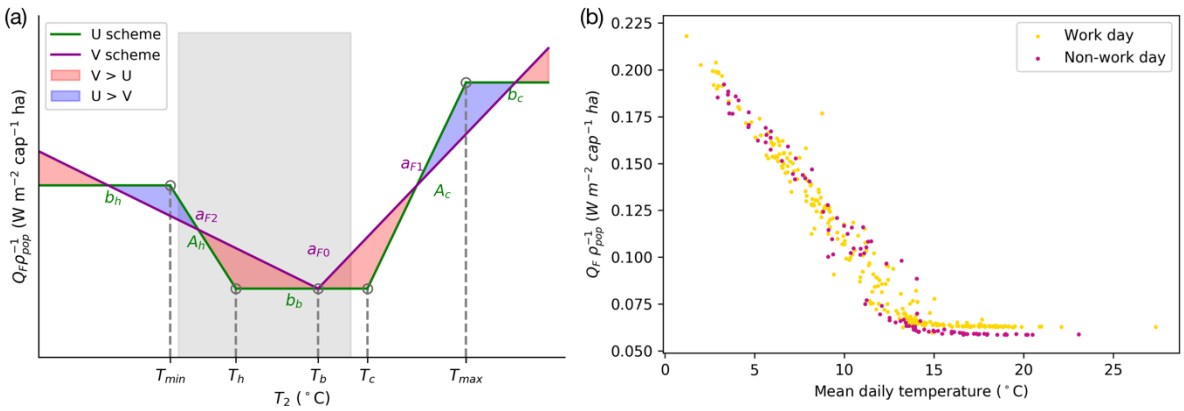

Figure 4-1: Anthropogenic heat flux Q_F normalised by population density ρ_{pop} (cap ha^{-1}) variation with temperature (**a**) U (eq. 4-3) and V (eq. 4-2) forms (shaded area covers likely temperature ranges for mid-latitude cities, e.g. Greater London, **b**), and (**b**) median modelled (D1, Table 4-1) output area (OA) scale fluxes for Greater London for 1 October 2014 – 30 September 2015 (N=365) for work and non-work days. Notation is defined in Section 4.2. **a** modified after Ao et al. (2018).

These two temperature dependent statistical relation methods (Section 2.2.4, stated here as U and V) that utilise daily mean temperature (T_{av}) and population density (ρ_{pop}) to inform daily spatial and temporal variations of Q_F (Figure 4-1) have been chosen as more efficient schemes for Q_F estimation. These both assume linear responses between temperature and Q_F. Q_F emission sectors (eq. 2-1) are here considered as a bulk characteristic, embedded in the shape-parameters that may vary by spatial

unit or day type. Q_F can be estimated at a finer temporal resolution through the inclusion of a diurnal profile E_d. E_d has a mean of 1 across all hourly time steps, such that mean daily (d) flux ($Q_{F,d}$) is preserved. E_d may be derived from energy statistics (e.g. Ao et al., 2018) or sub-daily Q_F estimations from other studies, and may vary spatially and temporally (e.g. seasonally).

The shape of response to temperature (Figure 4-1a), in particular the number and type of critical points, identifies the two schemes as U and V. For both, $Q_{F,d}$ is modified by ρ_{pop} and E_d to give the hourly (h) (or other time interval) flux $Q_{F,h}$:

$$Q_{F,h} = \rho_{pop} \times Q_{F,d} \times E_d(h) \quad (4\text{-}1)$$

For the V-shaped approach (Sailor and Vasireddy, 2006) the daily mean flux per capita ($Q_{F,d,V}$) is:

$$Q_{F,d,V} = a_{F0,\mathrm{w}} + a_{F1,\mathrm{w}} CDD + a_{F2,\mathrm{w}} HDD \quad (4\text{-}2)$$

where $a_{F0,w}$ is considered a base energy use that accounts, for example, for transport and appliances that are assumed not to vary with temperature but can vary with day of week (w) (i.e. work and non-workdays as in Ward and Grimmond, 2017). As $a_{F0,w}$ is a constant, it is assumed that seasonal variations in transport mode choices, appliance use, temporality, etc. are negligible or compensating (Sailor and Lu, 2004). The heating degree day (HDD) or cooling degree day (CDD) are calculated from T_{av} relative to a regional base temperature (T_b) (e.g. Europe: JRC and EEA, 2019; UK: Day, 2006; USA: Arguez et al., 2010; China: Beijing Construction Bureau, 2005). On an individual day either HDD or CDD may occur, hence the other is 0, so only one temperature dependent energy use response ($a_{F1,w}$ or $a_{F2,w}$) is used.

The V-scheme assumes a narrow thermal comfort range. It also allows unlimited heating or cooling with extreme temperatures, despite this being unlikely (Lindberg et al., 2013; Dong et al., 2017; Ao et al., 2018). T_b may be derived from outdoor human thermal comfort temperature (e.g. Järvi et al., 2011; Ward and Grimmond, 2017).

The U-form allows a wider thermal comfort range (T_h to T_c, Figure 4-1a) when no additional energy is used for heating or cooling in buildings (Ihara et al. 2008, Ao et al. 2018). In milder climates where air temperatures are most commonly between T_h and T_c, a better estimate might be found using the U-shaped scheme. The daily U-form is (Ao et al., 2018):

$$Q_{F,d,U} = b_{b,w} + l_{c1} A_{c,w} CDD + l_{h1} A_{h,w} \mathrm{HDD} + l_{h2} b_{h,w} + l_{c2} b_{c,w} \quad (4\text{-}3)$$

where $b_{b,w}$ is the energy consumption assumed independent of temperature. Logic parameters (l_{c1}, l_{h1}, set to 0 in a specified comfort temperature range) are used to activate heating or cooling as:

(i) a heating response (A_h) when $T_{min} < T_{av} < T_h$, driven by HDD = $|T_h - T_{av}|$ ($l_{h1} = 1$)

(ii) a cooling response (A_c) when $T_{max} > T_{av} > T_c$, driven by CDD = $|T_c - T_{av}|$ ($l_{c1} = 1$)

Logic parameters ($l_{c2,}$ l_{h2}) are 0 except when at extreme temperatures (Fig 1a) when the maximum capacity plateaus are reached:

(i) b_h for heating if $T_{av} < T_{min}$ then $l_{h2} = 1$ and HDD = 0

(ii) b_c for cooling if $T_{av} > T_{max,}$ then $l_{c2} = 1$ and CDD = 0.

Given different slopes and thresholds, the two schemes will provide different Q_F estimates at some temperatures (blue and red shading, Figure 4-1a). There are more coefficients and temperature thresholds needed (Ao et al., 2018) for the U-form (e.g. T_h, T_c, T_{min}, T_{max}) than the V-form (e.g. T_b). If the plateau limits of energy use (b_h and b_c) are not visible within the available range of temperature data, values could be limited at the minimum and maximum temperatures of the derivation data.

Some parameters values will vary spatially. For example, Ward and Grimmond (2017) derived a_{F0} and a_{F2} values for each of London's 33 boroughs or Local Authorities using data from GQF (Iamarino et al., 2012; Gabey et al., 2019). Following Zhang et al. (2013), in this study we use the total impervious land cover fraction ($\lambda_i = \lambda_{build} + \lambda_{paved}$, the proportion of plan area covered by building and paved surfaces relative to the total area) as a proxy for spatial variation of the thermal response coefficients (eq. 4-2, 4-3), as anthropogenic heat emissions are predominately associated with buildings ($Q_{F,B}$) and transport ($Q_{F,T}$). Deriving parameters by land characteristics allows them to be applied to regions with similar energy behaviours and for different spatial scales. Although emissions also occur above some pervious areas (e.g. agriculture over rural land use), they are typically small or negligible above urban pervious areas (e.g. metabolic heat from people and animals) (Stewart and Kennedy, 2017).

4.3 Methods

This section describes the methods used for the operation and analysis of this study. Firstly, Section 4.3.1 specifies the spatial and meteorological characteristics of the study area and period. Section 4.3.2 provides an overview of the individual runs for the three approaches and describes the urban land surface model SUEWS, to which the three models will be coupled. The DASH configurations and SUEWS-DASH coupling are explained in Section 4.3.3, and Section 4.3.4 details the methods used to obtain parameters for the U- and V-schemes. Section 4.3.5 gives an overview of the analysis.

4.3.1 Study area and period

The study area is Greater London, where DASH has been evaluated (Chapter 3, Capel-Timms et al., 2020b). DASH is applied at the highest resolution (Output Area, OA) for which the UK government publishes statistical data (Office for National Statistics (ONS), 2020). An OA has 40 to 125

households in an area of variable size (156 m^2 to 12,265,743 m^2, median: 33,528 m^2), hence differ in population density (residential median: 10,174.7 cap km^{-2}), land cover characteristics, and building stock. In Greater London, the 25,053 OA combine into 33 Local Authorities (LAs) (ONS, 2020).

Variations in land cover (Chrysoulakis et al., 2018; Lindberg et al., 2020) and population obtained at the OA scale (ONS, 2014, 2015) are used to characterise London (Figure 4-2). The relative land cover fraction with buildings ($\frac{\lambda_{bldg}}{\lambda_i /2}$) and paved ($\frac{\lambda_{paved}}{\lambda_i /2}$) areas relative to the total impervious land cover fraction (λ_i) varies across the city (Figure 4-2b). As λ_i increases, the residential population density decreases relative to the workplace population density (Figure 4-2b, c). Areas with the highest building land cover are frequently in the central business district (CBD) areas, where there are more commercial buildings.

To ensure that local-scale spatial units (Oke et al., 2017b) are modelled with SUEWS, small OA with large building land cover fraction need to be amalgamated to adjacent OA to create areas that are greater than 12000 m^2. As SUEWS is run offline (i.e. without flow between spatial units), areas with high population density have very large Q_F values. This impacts the turbulent heat fluxes and hence large near surface air temperatures occur, with the resulting feedback impacting the Q_F. To resolve this, spatial unit characteristics (paved and building land cover fractions, population density, mean building height) were equated as a mean of the adjacent spatial units. 1475 OA were amalgamated overall.

The one-year study period is defined to give complete winter and summer responses (2014/10/01 - 2015/09/30, the latest time-use survey data used to inform activity and movement in DASH). In this period the monthly mean maximum and minimum temperatures are similar to the 1981-2010 Normal, with a mean difference of ±0.2 °C across the year (Met Office, 2020) (Figure K-1). However, the ERA5 data (Hersbach et al., 2020), used as meteorological forcing for this study (Appendix H), shows lower rainfall than Normal in March, April and June (48 - 57%), whilst July and August were wetter (166% of Normal). All three variables are similar to Normal on an annual basis so we do not see the full extremes of temperature responses (Figure 4-1).

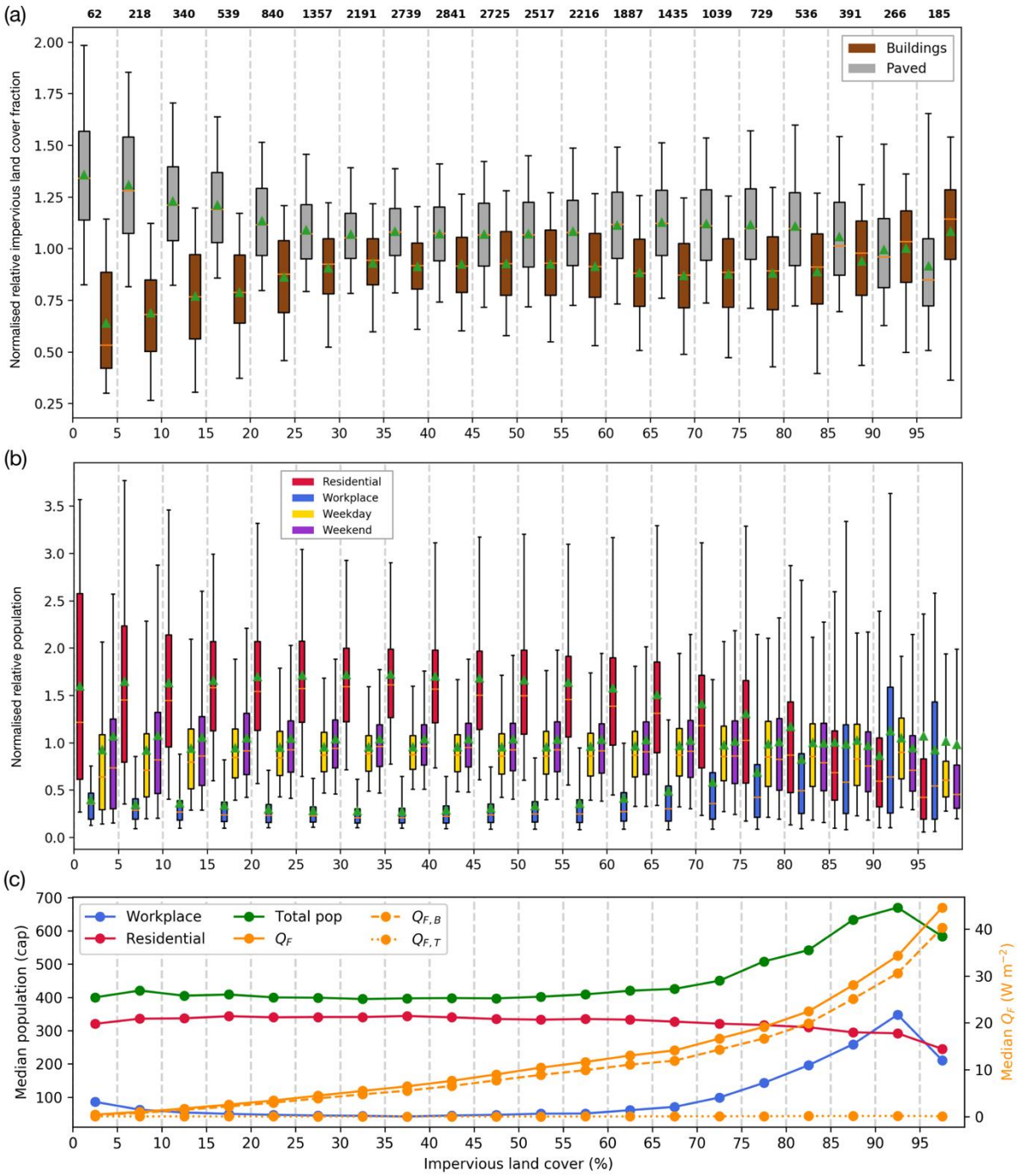

Figure 4-2: Characteristics of London's output areas stratified into 5% classes of impervious land cover (λ_i), including: **(a)** $\frac{\lambda_{bldg}}{\lambda_i/2}$ (brown) and $\frac{\lambda_{paved}}{\lambda_i/2}$ (grey) ; **(b)** residential (red) and workday (blue) census populations (normalised by mean of residential + workplace populations for each class) and DASH dynamic total occupancy level across workdays (yellow) and non-workdays (purple) (normalised by mean of workday and non-workday occupancy levels for each class); and (**c**) median residential, workplace and total populations (left y axis) and annual median daily Q_F (solid), $Q_{F,B}$ (dashed) and $Q_{F,T}$ (dotted) (W m^{-2}) (right y axis). Number of OA per class shown above (**a) (a,b)** Boxplots show the interquartile range, 5th and 95th percentiles (whiskers), median (orange line) and mean (green triangle). Data sources: see Section 4.3.

4.3.2 Model runs

Two DASH model runs are undertaken, hereafter referred to as D1 (DASH v1.0) and D2 (DASH v1.1) (Table 4-1). The only difference between the two DASH versions is that v1.1 includes a coupling with SUEWS (Section 4.3.3.2). D1 output is mined to calculate the values of coefficients for the U and V-schemes (Section 4.3.4). D1 is equivalent to model run 7 at the original OA resolution of in Capel-Timms et al. (2020b) (Table 3-6). D2 is used for the evaluation of the V- and U-schemes. ERA5 (Hersbach et al., 2020) meteorological data are adjusted by neighbourhood building morphology to force D2 (Appendix H), whereas D1 used meteorological observations from one central London site (KSSW) for all areas of Greater London (Table 4-1). The KSSW 5 min air temperatures, observed at 50.3 m above ground level, are gap filled prior to the daily means being determined (Section 3.3.1).

Runs V1 and U1 use the two computationally fast, temperature responsive V- (eq. 4-2) and U-schemes (eq. 4-3) (resp., Section 4.2). The two runs will be compared with both each other and D2 in Section 4.5. Comparison of the fast schemes allows for the differences in magnitude and diurnal profile to be observed, whilst comparison with D2 will show which method is best suited to estimating behavioural Q_F.

Table 4-1: Model runs undertaken use U, V (Section 4.2) and DASH coupled (C) to SUEWS (Section 4.3.2) or standalone (S), with different population density data and meteorological forcing (KSSW - central London observations (Kotthaus and Grimmond, 2014); ERA5 1 h, 0.125° x 0.125° reanalysis data (Hersbach et al., 2020) with 22 grids across Greater London (Appendix H), WG17 - Ward and Grimmond (2017), CT20 - Capel-Timms et al. (2020)

Run	U1	V1	D1	D2
Type	C	C	S	C
Meteorological	ERA5	ERA5	KSSW	ERA5
Q_F parameters	Section 4.3.4	Section 4.3.4	CT20	CT20
Population density	D1 daily mean	D1 daily mean	dynamic	dynamic
Diurnal profile	Section 4.3.4.2	WG17	dynamic	dynamic

4.3.2.1 SUEWS

For this study, DASH is coupled to SUEWS for run D2 (Table 4-1, Section 4.3.3.2) to enable DASH to be driven by spatially varying local meteorology and in turn impact the local meteorological and hydrological variables. Of the many land surface models to which the Q_F methods can be coupled (e.g. Grimmond et al., 2009; Best and Grimmond, 2015; Lipson et al., 2018; Salamanca et al., 2018), we use SUEWS (Järvi et al., 2011) (v2020b) via the python wrapper to SUEWS, SuPy v2020.8.9 (Sun and Grimmond, 2019). Meteorological forcing and land cover data are required to simulate energy and radiation balance fluxes. SUEWS can also simulate water and CO_2 exchanges (Järvi et al., 2019). In SUEWS, an area has some mix of seven land cover types: paved, building, evergreen and deciduous trees, grass, bare soil and water. Q_F can either be provided from an external model or calculated within a SUEWS option (Sun et al., 2020a).

The U-scheme has been added (alongside the existing V-scheme) directly into SUEWS as a further Q_F emissions method option for this study (Sun et al., 2020a). Previous users of the U-scheme with SUEWS (e.g. Ao et al. 2018) used the option to supply values with the meteorological input (Sun et al., 2020a).

For all the SUEWS coupled runs (C, Table 4-1) the model requires sufficient spin-up (one year before study period) to obtain the appropriate initial state of the environment (e.g. leaf area index, soil moisture deficit) for the run period. In this application, a complete spatial run is then done for the entire study period (one year, Section 4.3.1). All the SUEWS inputs (Sun et al., 2020b) are provided at OA scale (Section 4.3.1). All differences between the model runs are associated with the Q_F related parameters (Table 4-1). All other parameters are consistent between schemes. For the U- and V-schemes, the required daily mean T_{av} is calculated from the previous day. Hence, for these schemes Q_F alters all other variables at each time step but the change in current day outdoor temperature is altering the HDD and CDD that is used in the next day Q_F calculations. The diurnal pattern of the Q_F is for that actual day. Unlike for the SUEWS-DASH coupling (Section 4.3.3.2), no feedbacks occur between the U and V schemes. This may cause further differences between D2 and V1, U1 as the DASH and the faster schemes will respond to different temperatures (though using the same forcing data).

4.3.3 DASH

4.3.3.1 DASH model runs

The building thermal properties for both D1 and D2 differ based on building age (pre/post 1965) (Capel-Timms et al., 2020b). 1965 is when UK building regulations were introduced, including standards that governed thermal efficiency (UK Statutory Instruments, 1965). Buildings older than 1965 did not typically have wall cavities or insulation when built (Oikonomou et al., 2012, appendices). Wall insulation is a strong determinant of energy consumption for space thermal control (Guerra Santin et al., 2009; Mavrogianni et al., 2012; Hamilton et al., 2013), hence these properties have a critical influence on the spatial heterogeneity of heating requirements across London. This assumes no retrofitting has taken place; spatially resolved data of such changes were not available at the needed resolution and extent. The key properties that vary between building ages are the effective conductivity, density, specific heat capacity and thickness of construction component (walls, windows, ground floor, Table 3-3, Appendix G). Five population cohorts (by age: 0-4, 5-10, 11-18, 19-64 and 65+) are used to identify different profiles and choices (agency) in activities undertaken in time and space (e.g. work, home, school, recreation; Capel-Timms et al., 2020b, Section 3.4). Note in both the D1and D2 runs space cooling is not permitted.

4.3.3.2 SUEWS-DASH coupling

The building model STEBBS within DASH (Section 3.2.4.3) uses air temperature (T_{air}), wind speed (U), and downwelling shortwave radiation ($K_{\downarrow}$) to simulate heat exchanges between internal and external environments through the building fabric. For the D1 model run, observations above the urban canopy (KSSW, Table 4-1) are used. The ERA5 data are used to force SUEWS for the D2 model run. The SUEWS-DASH coupling passes the following meteorological forcing variables for each spatial unit:

(i) downwelling shortwave radiation ($K_{\downarrow}$): in this version neither sky view factor nor facet fraction are considered. Hence, these data are effectively passed directly through from their source.

(ii) air temperature and wind speed ($T_{0.5z_H}$, $U_{0.5z_H}$): using the SUEWS ability to model the atmospheric profile (Sun et al., 2020c) as described in Tang et al. (2020), we select the variables to pass to SUEWS from the SUEWS output at half mean building height ($0.5z_H$). The z_H and mean spacing parameters for each model spatial unit are passed SUEWS → DASH to ensure consistency upon initialisation. By using the meteorological variables at $0.5z_H$ to force DASH, variations with building types are possible but not as computationally intensive as complete profiles (Tang et al., 2021).

(iii) bulk surface temperature: using the SUEWS *Tsurf* output (Sun et al., 2020b) as described in Omidvar et al. (2020).

In the D2 run, the time steps for SUEWS (5 min) and DASH (10 min) differ (Figure 4-3). The DASH provided Q_F is used for the next two SUEWS time steps. SUEWS provides DASH with meteorological forcing at each DASH time step. This results in a feedback between DASH and SUEWS (Figure 4-3a). As a consequence, DASH Q_F is able to respond to Q_F-induced changes in the local meteorology (Section 2.1.3).

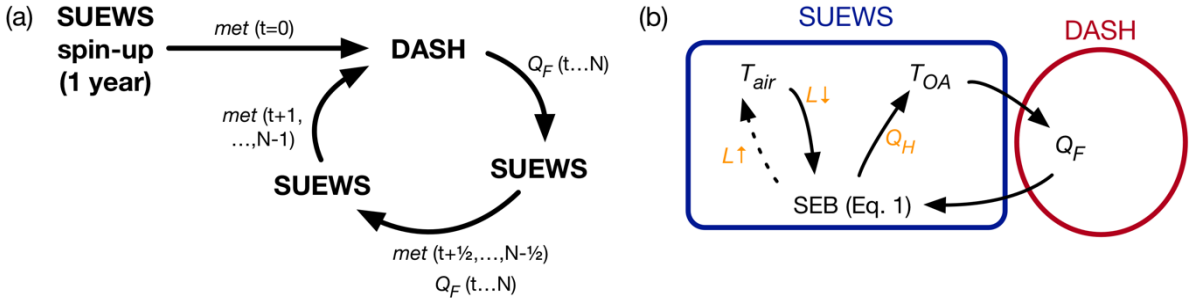

Figure 4-3: Coupling of DASH to SUEWS (**a**) Time step sequence (SUEWS operates at 5 min time steps, whilst DASH operates at 10 min time steps after one-year spin-up of SUEWS. SUEWS provides meteorological forcing variables (*met*) including: T_{OA} - air temperature at ½ the mean building height in OA (°C); T_{surf} - bulk surface temperature (°C); $K_{\downarrow}$ - downwelling shortwave radiation (W m^{-2}); *ws* - wind speed (m s^{-1}) (**b**) Forcing feedbacks (solid line: implemented, dashed line: not implemented) between DASH and SUEWS, where T_{OA} is air temperature (°C) at ½ the mean building height in OA

4.3.4 U- and V-scheme parameters

4.3.4.1 Thermal response parameters

Daily data from D1 (Table 4-1) are analysed to obtain the parameters applied to the U- and V-schemes (Section 4.2). Three day-types (non-school weekday, school weekday, weekends) inform the movement of the five age groups, resulting in the largest ρ_{pop} differences. Hence, the diurnal mean DASH calculated ρ_{pop} by day type are used to determine $Q_{F,d}\ \rho_{pop}^{-1}$ for each OA. Population density considers only the residential and workplace populations in both cases. It is assumed that energy users do not include people visiting a commercial area for retail or leisure, i.e. residents and workers are the only populations actively using energy, with energy use in retail and leisure attributed to workers only.

The coefficients for both schemes (V: $a_{F,0}$ and $a_{F,2}$, U: A_h and b_h) are each derived for workdays and non-workdays (non-school weekdays included as workdays and public holidays included as non-

workdays). Thus, for each day the coefficients are able to produce $Q_{F,d}\ \rho_{pop}^{-1}$ flux values per OA. The relation of thermal response parameters to λ_i was assessed in 1% bands (except for the lowest band $\lambda_i \leq 3\%$, ensuring 20 or more OA in each band) using linear regression with Python scikit-learn (v. 0.21.3, Pedregosa et al., 2011). As cooling was not permitted in the D1 (Section 4.3.3.1), cooling responses a_{F1} and A_c will not be found (Section 4.4.1). The heating responses are the linear regression slope coefficients:

- a_{F2} when $T_{av} < T_b$
- A_h when $T_{av} < T_h$

and the base values the intercept:

- a_{F0} when $T_{av} > T_b$
- b_b when $T_{av} > T_h$

The temperature balance points are found differently for the two methods. For the U-scheme, a single T_h value is used for setting parameter values (A_h, b_b) through a two-stage procedure. The first stage finds the optimum T_h value within a range of 12.5 - 15.5 °C around the observed temperature turning point (Figure 4-1b) for each λ_i and day type. Optimum T_h will minimise mean absolute error (MAE) between the regression lines and D1 $Q_{F,d}\ \rho_{pop}^{-1}$ values (i.e. across A_h and b_b arms, Figure 4-1) (Willmott et al., 2017). The second stage calculates the single city-wide T_h by taking the weighted average (by number of OA and day type frequency) of optimised T_h for each λ_i class. T_h is dependent on the setpoints used in STEBBS (Section 3.2.4.3). Setpoints are consistent between runs D1 and D2, so U1 and D2 are comparable.

Calculating T_b (and hence a_{F0}, a_{F2} V-scheme) using the same method would result in the same response coefficients in the case of no space cooling response (i.e. a_{F2}=A_h, a_{F0}=b_b). To challenge the assumptions made by the V-scheme, i.e. no thermal comfort range between heating and cooling, and quantify any improvements provided by the U-scheme, T_b is determined from similar studies undertaken in London. If space cooling were widespread in London, it is assumed that differences in the cooling responses of the two schemes would be similar to those seen during the heating response. That is, as T_b lies between T_h and T_c, V-scheme estimations would be greater than the U-scheme at higher temperatures (red regions, Figure 4-1a). It may also be assumed that similar differences occur between schemes at lower temperatures in cities that widely use both heating and cooling. The use of both heating and cooling is frequently seen in cities across the world, e.g. North America (Sailor and Vasireddy, 2006; Allen et al., 2011; Järvi et al., 2011; Lindberg et al., 2013; Dong et al., 2017) and East Asia (Ihara et al., 2008; Ao et al., 2018). a_{F1} will still be set to zero for the London case as cooling is negligible across Greater London and therefore not accounted for in D1.

There are a variety of methods for finding T_b (Section 2.2.4). Although no evidence of cooling in London was found for the study, Ward and Grimmond (2017) used a value of 18.2 ℃. This study also used the V-scheme coupled with SUEWS for Greater London but used a non-native T_b. The value was instead taken from a US-based study and sourced from energy modelling standards (Sailor and Vasireddy, 2006), assuming the presence of heating and cooling. Other studies using the V-scheme to estimate energy consumption in London or the UK have used T_b values of 20 ℃ (UK: Hor et al., 2005; London: Dong et al., 2017) and 16 ℃ (Psiloglou et al., 2009). CIBSE (Day, 2006) suggests a T_b of 15.5 ˚C, though this appears to be based on space heating only. The UK Met Office suggests base degree-day temperatures of 15.5 ℃ (HDD) and 22 ℃ (CDD) (Met Office, 2009 via Azevedo et al., 2015 - original source not found). As 18.2 ℃ lies between these values, the Ward and Grimmond (2017) value is deemed an appropriate benchmark for T_b. This *a priori* method of choosing the value of T_b will affect results when comparing the V scheme to either U or DASH, but is necessary for investigating the differences in response for the schemes, especially in a city with negligible cooling demand.

4.3.4.2 Diurnal Q_F profiles

A diurnal profile of Q_F (E_d, eq. 4-1) is required to obtain sub-daily (hourly resolution) Q_F estimates for each area. Different profiles are used for the two schemes (Section 4.4.3). The V-scheme uses diurnal profiles that vary by day type (workday, non-workday) only (Ward and Grimmond 2017). By restricting the V-scheme variability to day type, a comparison to using behaviourally responsive profiles (i.e. the U-scheme) can be given.

For the U-scheme, the DASH D1 data are analysed to capture the influence of both behavioural patterns (e.g. occupancy levels, habits of appliance use) and environmental factors (e.g. outdoor temperature influence on heating needs) on diurnal Q_F profiles. Initially, the data are split into two seasons based on daylight savings dates (UTC: 25th October 2014, UTC + 1: 29th March 2015) to capture the behavioural patterns that change with the British Summer Time hour change. Profiles of mean-normalised fluxes (eq. 4-4) derived from D1 data (i.e. all days, all OA) ($E_{w,OA}$) are stratified by five-day moving average temperature ($T_{av,5}$) and by five λ_i (20%) classes. This stratification allows the profiles to reflect the spatial variety in Q_F behaviours across the city (Section 2.3.2.2) and the seasonal pattern changes seen due to heating needs (Section 2.3.2.1). Using $T_{av,5}$ and broad λ_i groups mitigates the contribution of anomalous areas and temperature days. Temperature ranges are chosen using quartiles of $T_{av,5}$ to define the range boundaries for each of the two time zone seasons (T1 and T2, Figure K-3). Ranges are then collapsed between the time zones given similarities in shape and

magnitude. The profiles for each day type, land cover class, temperature range ($E_{w,\lambda_i,T_{av,5}}$) are the fluxes of all corresponding OA normalised by the mean (i.e. the resultant profile is relative to 1):

$$E_{w,\lambda_i,T_{av,5}} = \frac{\sum E_{w,OA}(\lambda_i,\ T_{av,5})}{\overline{\sum E_{w,OA}(\lambda_i,\ T_{av,5})}} \tag{4-4}$$

These profiles are smoothed using LOWESS regression (Seabold and Perktold, 2010) to create 10 min time interval E_d profiles, maintaining a mean of 1 across all time steps of the diurnal profile.

4.3.5 Analysis of results

The results are analysed in two sections that consider two different spatial extents of London. In Section 4.4, the U- and V-schemes parameters are derived using the D1 (Table 4-1) results across Greater London (Section 4.3.1) and analysed across λ_i rather than real areas.

In Section 4.5, analysis focuses on all of the OAs within two of the ERA5 0.125° × 0.125° grids located in (i) the centre (hereafter referred to as Central, midpoint 51°30' N 0°07.5' W) and (ii) west (West, midpoint 51°30' N 0°22.5' W) of London. Amalgamated areas are omitted from all results as D2 ρ_{pop} in these areas would be different to that used for U1 and V1.

The SUEWS (Section 4.3.3.2) coupled model runs (Table 4-1, C) use the different anthropogenic heat flux models (D2, U1 and V1). The results allow analysis of the SEB fluxes and feedbacks on the forcing meteorology. The effects on the turbulent heat fluxes are analysed for the midday (11:00 – 14:00 UTC) period using the median (MM). The variables analysed include the turbulent sensible ($Q_{H,MM}$) and latent ($Q_{E,MM}$) heat fluxes, and 2 m air temperature (T_{2m}). The Q_F forcing is dependent on the ERA5 data (Appendix H).

Firstly, the differences in $Q_{F,d}$ between D2, V1 and U1 are compared to assess if it is appropriate to derive coefficients for the fast schemes from DASH, and if so, which fast scheme performs best compared to DASH (Section 4.5.1). Secondly (Section 4.5.2), the D2, V1 and U1 runs are compared both between each other and relative to previous SUEWS observation based evaluation (Ward et al., 2016). The Q_F influence on midday turbulent heat fluxes and temperature are compared in Section 4.5.3. Section 4.5.4 assesses the changes in response temperature T_{2m} between the three methods, and Section 4.5.5 discusses the impact of the sub-daily diurnal Q_F patterns on Q_H and T_{2m}.

In Section 4.5.2 prior SUEWS evaluation results are used to evaluate the SUEWS-DASH and SUEWS model performance, using runs D2, V1 and U1. Ward et al. (2016) (hereon referred to as W16)

evaluated the SUEWS performance using radiation and eddy covariance observations during 2011-2013 in central London (King's College, Kc_{W16}) and residential Swindon (Sw_{W16}). Two OAs from the current study (Kc_{OA}, Sw_{OA}) with similar characteristics (i.e. land cover, roughness element heights and population) to the eddy covariance footprint areas for Kc_{W16} and Sw_{W16} are chosen for comparison of fluxes (Table 4-2). The areas are not the same and hence differences will occur due to surface characteristics. Daytime ($K_{\downarrow}$ > 5 W m^{-2}) median (DM) values are determined for each flux, which are averaged by the median over each month. ΔQ_S is not compared as this is modelled. The energy partitions β_{DM} ($Q_{H,DM}$ / $Q_{E,DM}$), $Q_{H,DM}$ / Q^*_{DM} and $Q_{E,DM}$ / Q^*_{DM} are calculated to account for differences in Q_F and meteorology.

Table 4-2: Characteristics of specific output areas analysed including two with observations (W16 - Ward et al., 2016, Kc_{W16} and Sw_{W16}) and OA selected to be similar (Kc_{OA} and Sw_{OA}, Section 4.3.5). Kc_{W16} and Sw_{W16} ρ_{pop} values workday and non-workday values not distinguished but the Q_F estimates in Ward et al. (2016) differ between the two day types. $\boldsymbol{z_H}$: mean building height, $\boldsymbol{z_{tr}}$: mean tree height, $\boldsymbol{z_m}$: measurement height.

		Kc_{W16}	Kc_{OA}	Sw_{W16}	Sw_{OA}
Output area (OA)		-	E00004229	-	E00018409
Fraction	Paved	0.43	0.39	0.33	0.35
	Buildings	0.38	0.47	0.16	0.15
	Evergreen trees/shrubs	0.00	0.00	0.01	0.0
	Deciduous trees/shrubs	0.02	0.01	0.08	0.12
	Grass	0.03	0.02	0.36	0.38
	Bare soil	0.00	0.00	0.06	0.00
	Water	0.14	0.11	0.00	0.00
ρ_{pop} (cap ha^{-1}) WD		204.58	238.1	47.63	61.3
ρ_{pop} (cap ha^{-1}) WE		204.58	126.3	47.63	68.0
z_H (m)		22.0	14.7	4.2	5.6
z_{tr} (m)		3.1	5.3	6.2	5.3
z_m (m)		49.6	57.3	10.6	75.5
Centre location		51°30' N 0°07' W	51°32' N 0°08' W	51°35' N 1°48' W	51°36' N 0°02' E

As W16 is for a different period, we use the Frobenius norm (Harris et al., 2020) for each day (1 October 2014 - 30 September 2015) to select the "closest" meteorological day from W16 to the meteorological forcing for this study (Figure K-4Figure K-1: Comparison of ERA5 data (Hersbach et al., 2020) to 1981-2010 climate Normals from Hampstead, Greater London (Met Office, 2020) and differences (ERA5 - Normal) for monthly mean maximum temperature (°C), monthly mean minimum temperature (°C) and monthly rainfall (mm).). Given the daytime turbulent heat fluxes are to be compared, daily mean $K_{\downarrow}$ (W m^{-2}), daily range in soil moisture deficit (SMD) normalised by the period range in SMD, rainfall (mm) and air temperature (°C) are chosen as the metrics to identify days that best ensure similar representation of fluxes (Best and Grimmond, 2014). In W16 Q_F fluxes are

calculated top-down, using GQF (Section 2.3) for Kc_{W16} and directly from energy consumption statistics (Ward et al., 2013) for Sw_{W16}.

4.4 Spatial characteristics of Q_F and variability of U and V-scheme parameters

Analysis of the DASH D1 (Table 4-1) model run with land cover characteristics (Figure 4-2) provides an indication of how Q_F varies across λ_i. DASH does not directly use land cover fractions to estimate the component fluxes, rather it uses occupancy and activity in spaces across the region. From the DASH simulations the changing population densities in the different areas are determined.

4.4.1 Spatial variation and Q_F characteristics

As the proportion of building to paved land cover fraction increases with increasing λ_i (Figure 4-2a), Q_F becomes larger (Figure 4-2c), caused by $Q_{F,B}$ emissions (Figure 4-2c). Transport related emissions are proportionally more important at lower λ_i (Figure 4-2c). However, the transport relation is more complex as the magnitude of $Q_{F,T}$ depends on the traffic flow, which varies (e.g. with road type) and is more substantial when considered by road area instead of spatial unit area (e.g. Figure 3-10c.ii). Population densities and land cover medians are similar between $\lambda_{i,25\text{-}75}$ (Figure 4-2b). Residential populations are much larger than workplace in this range. In these suburban areas, domestic $Q_{F,B}$ is the dominant source, with day of week (workday vs non-workday) causing differences in occupancy level. Median Q_F increases steadily with increasing λ_i despite little change in population size until $\lambda_{i,70}$. The U and V-scheme parameters would ideally capture this variability of controls on anthropogenic heat emission as the relative roles of $Q_{F,B}$ and $Q_{F,T}$ change across the city.

Assessment of whether the critical temperatures are spatially variable or fixed for the region suggests (from analysis of D1 data) that T_h may vary with land cover fraction (not shown). However, as only one forcing temperature is used (Table 4-1) it is assumed that T_h is a regional, rather than neighbourhood, characteristic (Section 4.3.4) for ease of application. With more detailed building stock information and a wider range of climate conditions modelled, T_h could vary (e.g. λ_i, day-type) but for wider applicability for both across the city and for other study areas, that variability is removed. Hence, in this study it is assumed that only land cover influences the base coefficients (i.e. a_{f0}, eq. 4-2; b_b, eq. 4-3). In future work this could be explored further using D2 type model runs with atmospheric feedback.

From analysis of the D1 daily OA median Q_F and mean occupancy results, space heating starts when the mean daily air temperature (T_{av}) goes below ~13.5°C (Figure 4-1b, i.e. T_h Figure 4-1a). At cooler

temperatures, the clear slope shows the expected general space heating response to temperature (Fig Figure 4-1b, i.e. A_h, a_{F2} Figure 4-1). In D1 air conditioning is not implemented. Although Choudhary (2012) suggest 35% to 47% of non-domestic buildings in Greater London have cooling systems fitted, no evidence of Q_F temperature dependency at higher temperatures has been found through analysis as to indicate widespread use of space cooling (Hamilton et al., 2009; Iamarino et al., 2012; Kotthaus and Grimmond, 2014; Dong et al., 2017; Ward and Grimmond, 2017). Coefficients A_c, b_c (U-scheme) and $a_{F,1}$ (V-scheme) are therefore set to 0. With no evidence of the mean diurnal temperatures going below T_{min} (Figure 4-1b) it is not possible to determine b_h. Future work using more extreme conditions could assess this, but this would require application of DASH to another city with these conditions. Work/non-workdays have different baseline (b_b, $a_{F,0}$ Figure 4-1a, b) values when a comfortable outdoor air temperature is reached (Figure 4-1b). The non-workday baseline values are lower. This is explained by greater intensity of both commercial $Q_{F,B}$ and higher intra-city travel on workdays, as typically seen in the Q_F literature (Section 2.3.1).

4.4.2 Parameters influencing daily per capita anthropogenic heat flux

Parameters are derived for each λ_i class using linear regression between $Q_F \rho_{pop}^{-1}$ and T_{av} (Section 4.3.4.1) for the two day types. For the U-scheme, T_h is set to 13.4 °C based on the lowest overall MAE for $Q_F \rho_{pop}^{-1}$ from the 97 classes of A_h and b_b combinations and day type weighting. With T_h set, the A_h and b_b parameters by λ_i class (1% and 5% resolution) are determined (Figure 4-4). For the V-scheme we retain T_b = 18.2 °C, consistent with the Ward and Grimmond (2017) parameters (Section 4.3.4.1). Given the difference in the two temperature balance points, the impact of using these can be assessed. Again, for consistency (between U and V), we use the same population density data for the U and V-schemes so that output differences between the two schemes are only due to the energy coefficients used.

To facilitate application of the appropriate parameters, lookup tables created from the 5% values (blue points, Figure 4-4) are used to find the parameters for each spatial unit when the U and V-schemes are coupled to SUEWS. Values are interpolated between 5% points to 1% values (cyan line, Figure 4-4). This smooths the erratic nature of the 1% points (red points, Figure 4-4) at extreme λ_i. Using the 1% values directly would be suitable for this study area as they would be used for the areas from which they were derived, but the values then may be less appropriate for use in another study area. 5% resolution values still maintain the dominant trends seen in the 1% classes, giving good spatial variability at low and high λ_i without reflecting the large differences between consecutive λ_i in these areas. Hence, interpolation between the 5% values is used for greater applicability and smoothing.

The base values for workdays, a_{F0} (Figure 4-4b.i, V-scheme) and b_b (Figure 4-4a.i, U-scheme) have a similar pattern but a_{F0} is ~ 0.012 W m^{-2} cap^{-1} ha^{-1} less than b_b throughout, indicating a lower base (i.e. temperature independent) Q_F. A similar average difference of ~ 0.017 W m^{-2} cap^{-1} ha^{-1} occurs for the non-workday values. b_b and a_{F0} increase for both (1% and 5%) λ_i class intervals and both day types when λ_i > 65% (Figure 4-4a.i,iv,b.i,iv), indicating greater energy emission per capita. These areas are densely populated during the workday (Figure 4-2b, c), hence associated with non-domestic energy use with typically more intense building emissions (per m^2) than residential areas (Section 2.3.1), and/or higher traffic flow around the city centre.

The responses to decreasing air temperatures, a_{F2} (Figure 4-4b.ii, V) and A_h (Figure 4-4a.ii, U) (i.e. Q_F ρ_{pop}^{-1} T^{1} gradients) are also similar by day type, with a_{F2} gradients shallower than the respective A_h gradients for all λ_i, indicating a slower response to temperature. However, some differences occur at higher λ_i. Non-workday values have a slightly broader range, as the A_h and a_{F2} patterns (Figure 4-4a.v, b.v) are like their respective workday patterns (Figure 4-4a.ii, b.ii) until $\lambda_{i,60}$ after which values become more negative, whilst workday values become less negative after λ_{60}. Non-merchant workplaces are typically fully or partially closed during non-workdays, whilst shops remain open with a greater energy intensity per worker. This causes a greater Q_F ρ_{pop}^{-1} in more commercial areas. On the other hand, the workday response above $\lambda_{i,60}$ implies better energy efficiency as λ_i increases, as the denser population are using less space heating per capita. Non-workday a_{F2} values (Figure 4-4b.v) show a lower range at higher λ_i cf. A_h (Figure 4-4a.v); i.e. smaller changes with temperature ($\lambda_{i,60\rightarrow93}$: ΔA_h = 0.0053, cf. Δa_{F2} = 0.0042 W m^{-2} cap^{-1} ha K^{-1}). For both day types A_h values decrease slightly at $\lambda_{i,15\text{-}20}$ (both 1% and 5% classes). The only apparent distinctive characteristic for these areas is a smaller difference between the mean and median residential population (Figure 4-2b). Domestic buildings in DASH are more responsive to immediate environmental forcing due to the differences in heating setpoint temperature control, which may result in steeper A_h slopes.

The Q_F ρ_{pop}^{-1} MAE (Figure 4-4.iii, v.i) when using both class parameters for the V-scheme (Figure 4-4b) is about twice that for U-scheme (Figure 4-4a) for both day types but less than 0.01 W m^{-2} cap^{-1} ha. This is due to the value of T_b, which was chosen from past studies and not to fit the training data (Section 4.3.4.1). Therefore, the V-scheme is expected to deviate more in the coupled model evaluation (Section 4.5). The slightly higher MAE on non-workdays for both schemes may be caused by their lower frequency throughout the year. λ_i classes with fewer OA (Figure 4-4c) have both larger MAE (Figure 4-4a.vi,b.vi) and less consistent 1% λ_i class A_h and b_b values at both low and high λ_i.

Given the linear nature of the U and V-schemes, the use of different critical temperatures and parameter values will cause the schemes to over/under-estimate relative to each other with T_{av} (Figure

4-1a, shading). Figure 4-5 shows the resultant linear relations (offline) for the U and V-schemes for three selected λ_i. For all λ_i shown, the A_h and a_{F2} lines cross when T_{av} is below 5 °C, and at ~17 °C a_{F2} intersects b_b (Figure 4-5). Between these temperatures Q_F will be greater when estimated by the V than by the U-scheme, and outside of this range the U scheme will produce larger values (red and blue zones, resp., Figure 4-1a). The greatest disparities between the two schemes occur when T_{av} is at 13.4 °C, e.g. 0.022 and 0.032 W m^{-2} cap^{-1} ha for workday and non-workday λ_{99} (resp.) and 0.031 W m^{-2} cap^{-1} ha for workday λ_{33} (similar for non-workday). Areas of high λ_i will likely have a very high ρ_{pop} (residential and/or workplace, depending on day type), resulting in a large difference in total $Q_{F,d}$. Given a peak frequency of temperatures at ~13.4 °C (Figure 4-5), these large differences will occur frequently. On a few warm days (> ~17 °C) the U scheme exceeds the V-scheme, though b_b and a_{F0} lines are of similar magnitude (Figure 4-5), so this will have only a small effect (though for total Q_F this is also dependent on ρ_{pop}). Temperatures below 5 °C are more common, so the intersections around 5 °C could impact, but as they are linked to the λ_i extremes they are spatially less common (Figure 4-4c). As expected, λ_{99} non-workday A_h and b_b lines are greater than the maximum workday lines.

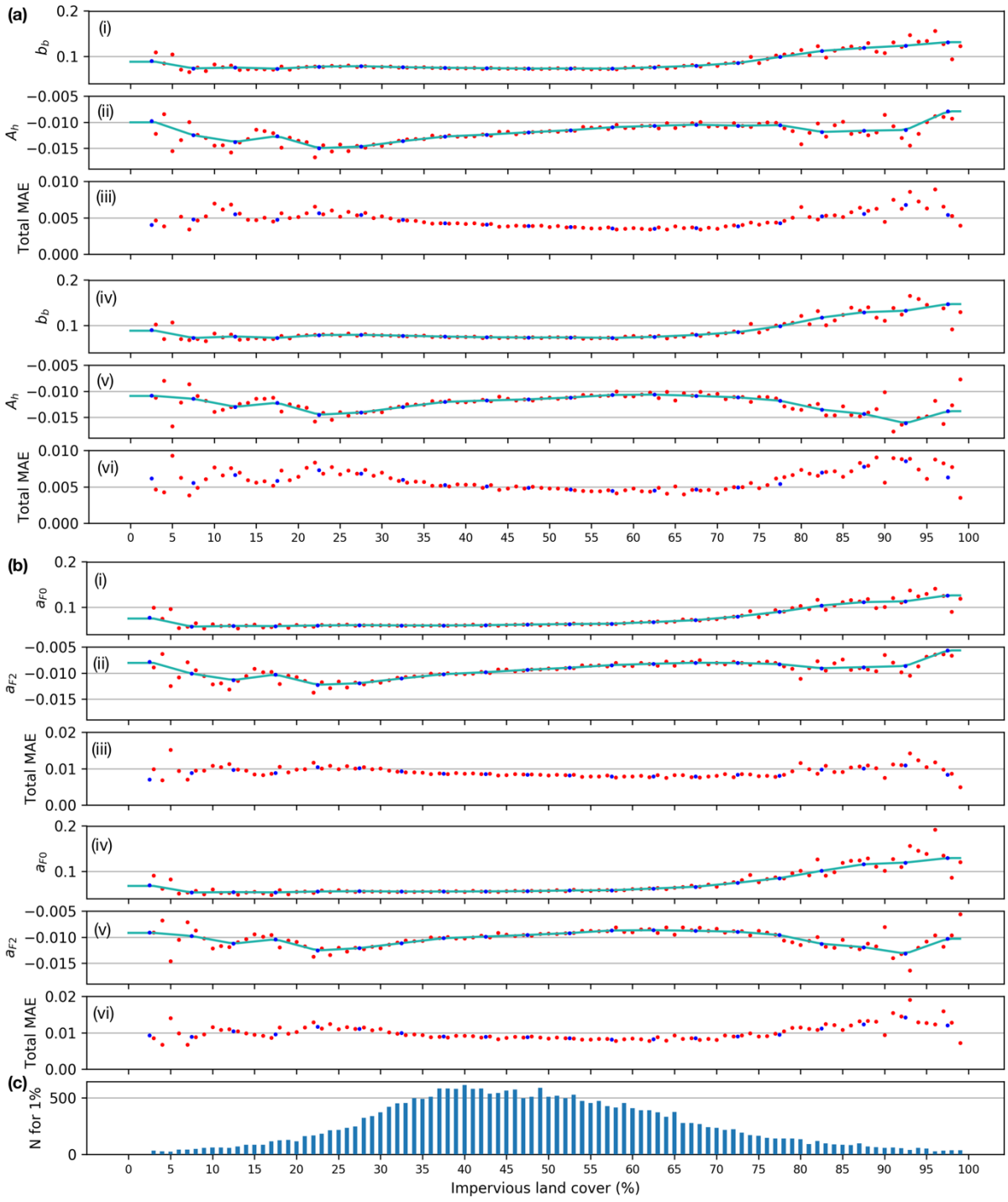

Figure 4-4: Parameters (and assessment) derived for (**i-iii)** workdays and (**iv-vi**) non-workdays for the (**a**) U- and (**b**) V-schemes for impervious land cover (λ_i) classes (1% red, 5% blue) with lookup values interpolated from 5% classes (cyan line), (**c**) number of OA per λ_i 1% (note there are no OA with < 3% λ_i). The assessment is the (**iii, vi**) total mean absolute error (MAE) for $Q_F\ r_{pop}^{-1}$ (W m^{-2} cap^{-1} ha^{-1}) (note: y-axis scales differ between a and b). The parameters for (**a**) U scheme are: (**i**,**iv**) b_b, (**ii**,**v**) A_h with T_h = 13.4°C; and for (**b**) V scheme: (**i**,**iv**) a_{F0}, (**ii**,**v**) a_{F2} with T_b = 18.2°C; see Section 4.2 for equations.

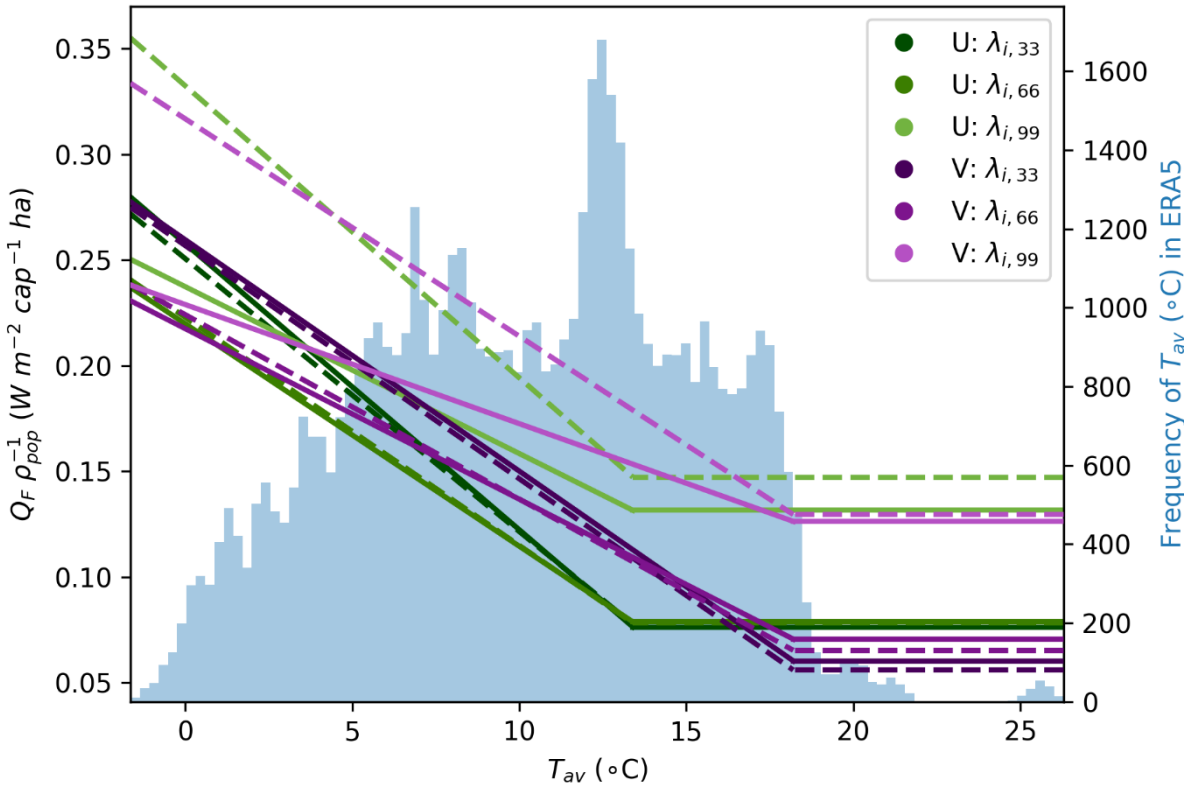

Figure 4-5: Difference in U (green) and V (purple) scheme $Q_F\ \rho_{pop}^{-1}$ (W m^{-2} cap^{-1} ha) with T_{av} (°C) relation for workdays (solid lines) and non-workdays days (dashed lines) for three impervious land cover fractions ($\lambda_{i,33}$, $\lambda_{i,66}$, $\lambda_{i,99}$, chosen to represent spread across all land covers whilst showing differences between coefficients, Figure 4-4), with frequency of forcing T_{av} (blue) during the year across all 22 ERA5 grids (Table 4-1 C model runs) and measurement heights used within OA (i.e. not weighted for number of neighbourhoods for heights used).

4.4.3 Diurnal profiles

For many applications (e.g. NWP) sub-daily values of Q_F are needed (eq. 4-1). For the V-scheme, we use the Ward and Grimmond (2017) profiles that vary with day type (work-, non-work-day) but not with land cover or forcing temperature (Figure 4-6a.i,b.i).

For the U-scheme, the diurnal profiles are derived from the D1 data (Section 4.3.4.2). Independent of λ_i and T_{av}, all profiles have a morning peak as people wake up and use appliances, heating (during cooler temperatures) and transport (Figure 4-6). A second peak occurs around 15:00 as transport use increases again, non-domestic power demand changes (notably in OA with $\lambda_{i,80\text{-}100}$), and domestic appliance and heating use increase. The sharp decline in workday Q_F around 18:00 in OA with higher λ_i (Figure 4-6a.v) is associated with heating and appliance use decreasing as people leave workplaces.

At colder temperatures, the diurnal profiles vary less as heating needs dominate. At warmer temperatures, peaks associated with appliance use are evident. The V-scheme profiles are lower overnight than all the U-scheme values and higher after noon. These differences could go on to impact some variables (e.g. atmospheric stability) as periods with low Q_H will be impacted even by small differences in Q_F as it is always a positive flux (e.g. cf. Q_F schemes) as $Q_{F,d}$ causes differences across the day. For example (assuming the same daily mean Q_F), U-scheme Q_F values will be greater overnight, enhancing Q_H and therefore outdoor air temperature (cf. V-scheme). In the afternoon, V-scheme Q_F values will be greater than U-scheme values.

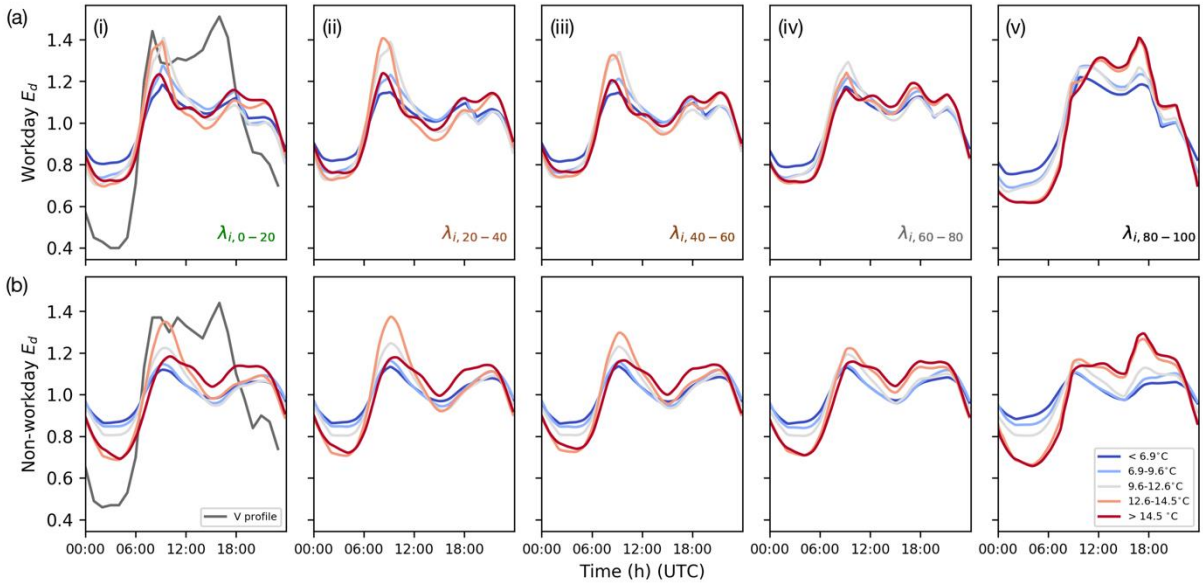

Figure 4-6: Normalised daily Q_F profiles (all adjusted for UTC) for V (grey, 1 hr time steps, Ward and Grimmond, 2017) and U-scheme (rest, 10 min time steps, Section 4.4.3) for (**a**) non-workdays and (**b**) workdays for the U scheme five λ_i classes: (**i**) 0 - 20%, (**ii**) 20 - 40 %, (**iii**) 40 - 60%, (**iv**) 60 - 80%, (**v**) 80 - 100%; and five temperature ranges (colours). See Figure K-3 for temperature ranges described in Section 4.3.4.2.

4.5 SEB fluxes of the coupled models

4.5.1 Variation of Q_F between the three schemes

Comparison of the three schemes to each other uses the following metrics: mean, median, interquartile range (IQR), and mean bias error (MBE). The three comparisons are defined as:

(i) VD = V1-D2

(ii) UD = U1-D2

(iii) UV = U1-V1

As discussed, U1 and V1 are expected to under/over-estimate compared to D2 given the simplifications made (Figure 4-1, Section 4.3).

4.5.1.1 Q_F across Greater London

The annual mean 30 min areally weighted Q_F for Greater London for the coupled DASH (D2) run (8.4 W m^{-2}) is 30 % greater than the equivalent uncoupled DASH Q_F (D1) (Table 4-3) results. As no other configurations were altered between D1 and D2, this is due to the differences in meteorological forcing between the two runs (Figure K-2). The meteorological forcing data include the influence of urban effects (e.g. Q_F, ΔQ_S, surface roughness) as KSSW data are from observations and ERA5 data are urbanised within SUEWS (to multiple levels from $T_{4.6-6.8z_H}$ on average in the Central and West regions, Appendix H, Section 4.3.3.2). Figure K-2 compares the forcing provided by the two sources. The KSSW observed temperatures (used in D1, $T_{\sim 3z_H}$) are warmer than the median monthly mean SUEWS/ERA5 $T_{0.5z_H}$ values across the year in both regions, as is the annual mean (of the median for ERA5 C and W: KSSW- C = +1.24 K, KSSW-W= +1.70 K). The two ERA5 areas have similar mean forcing air temperature (urbanised difference of 0.1 K (W - C)). Hence, the D2 results differ from D1 (e.g. via STEBBS conduction). The KSSW wind speeds are greater for SUEWS/ERA5 $U_{0.5z_H}$, again impacting STEBBS (e.g. convective heat exchange, Appendix B). $K_{\downarrow}$ values are similar to KSSW. The two runs have very similar frequency distributions of annual mean OA data (Figure 4-7), both in shape and magnitude.

The U1 and V1 annual areally weighted Q_F means across Greater London (GL) are smaller than the D2 mean, but medians and IQRs across individual spatial units are larger (Table 4-3). The frequency distributions for U1 and V1 annual average OA values are skewed towards higher values cf. D2 (Figure 4-7, Table 4-3), associated with a general overestimation of the fast schemes. Whereas the D2 GL mean and OA median are quite similar (0.11 W m^{-2}, 1% difference, Table 4-3), the medians for U1 and V1 are both 48% larger than their own means. Overall, the U1 results are more similar to D2 than the V1 results (Table 4-3). Differences are expected between the three runs, as the U1 and V1 coefficients will not capture the extreme Q_F values across λ_i and T_{av} (Section 4.4.2). For example, the U1 and V1 areally weighted annual means across the Central region (where Q_F is most intense: Figure 3-13) are smaller than D2. One possible reason for these differences is that the meteorological response is only to T_{av} for the U and V schemes, whilst DASH $Q_{F,B}$ also responds to wind speed (i.e. convective heat exchanges between the external wall and outdoor environment, Appendix B) and radiation (Section 4.3.3.2, 4.3.4.1).

Table 4-3: Annual (1 October 2014 - 30 September 2015) Greater London (GL), output area (OA), central (C) and west (W) ERA5 region mean (areally weighted by OA area, N= 25053), median and interquartile range (for OA, not weighted) of Q_F (W m^{-2}) for model runs D1, D2, V1 and U1 (Table 4-1). Note, some areas are amalgamated in runs D2, V1 and U1 (Section 4.3.1).

	GL	OA			C	W
	Mean	25th	50th	75th	Mean	Mean
D1	6.43	5.71	8.54	13.03	18.13	5.98
D2	8.37	5.73	8.48	12.75	22.98	6.17
V1	7.44	7.22	11.03	16.70	18.90	5.94
U1	6.68	6.46	9.89	14.99	17.00	5.32

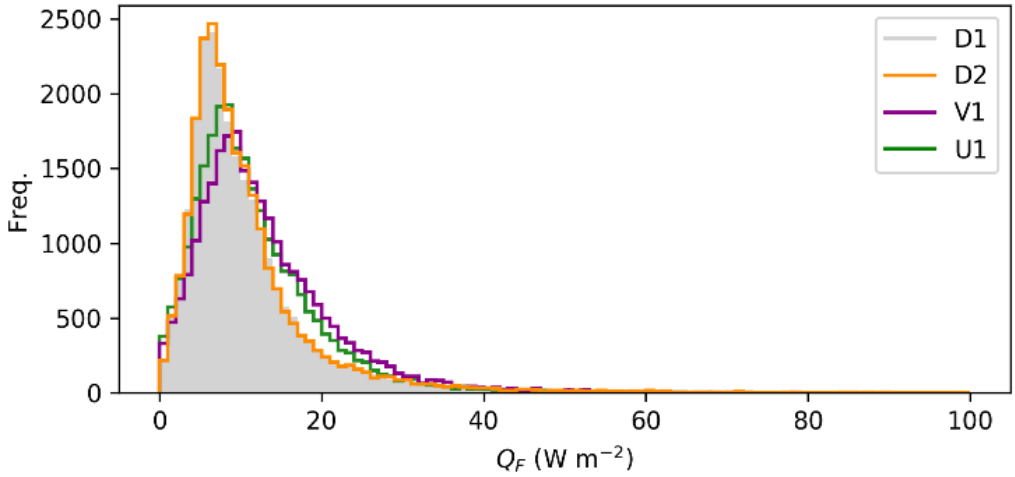

Figure 4-7: Frequency distributions (100 bins) of annual (1 October 2014 - 30 September 2015) average Q_F at OA resolution for runs D1, D2, V1, and U1 for all OA in Greater London (Q_F capped at 100 W m^{-2} to remove large outliers for visualisation).

4.5.1.2 Q_F MBE for VD, UD and UV

All areas and comparisons have a narrow IQR of MBE considered across all temperatures (Figure 4-8a, b, d, e). The IQR for both VD and UD are mostly within positive values (VD: 91 - 95% of IQR; UD: 75 - 95 % of IQR), indicating a slight bias towards V1 and U1, though there is no overwhelming bias according to the p_1 and p_{99} lines (Figure 4-8a.ii, b.ii, d.ii, e.ii; Table I-1). IQR positive bias is slightly less for UD in Central (75%), suggesting that U1 performs better than V1 in this region (Figure 4-8b). Median MBE values are close to zero for both regions for the VD and UD comparisons (Figure 4-8a.i, b.i, d.i, e.i; Table I-1). In areas with low λ_i (green, Fig 6) MBE are closer to zero than for areas with mid (brown) and high (grey) λ_i (Figure 4-9a.ii,b.ii). For the VD comparison, 98% of $Q_{F,d}$ values lie within ±33 W m^{-2} of D2 values for the Central region (Figure 4-8a, b), and ±16 W m^{-2}

for the West region (Figure 4-8d, e). For UD 98% of values lie within ± 29 W m^{-2} for Central and ± 14 W m^{-2} for West.

Given the larger Q_F emissions in the city centre associated with the larger ρ_{pop} and higher λ_i, the Central region has a greater range (Table I-2) of values (Figure 4-8a.ii,b.ii) than the lower West (Figure 4-8d.ii, e.ii). The largest positive outlying values for both VD and UD for the West region are attributed to a single area with a high population density (651 - 704 cap ha^{-1}). For this area the V1 and U1 schemes overestimate $Q_{F,d}$ (MBE up to 150 W m^{-2}) during colder and milder temperatures (MBE ~40 W m^{-2}). As this in turn impacts the other SEB fluxes and street level temperature, these schemes (or parameter values) may not be appropriate in areas with high population density with λ_i the only characteristic considered (Appendix J). As the amalgamation of areas was minimal this may be improved by a more systematic approach, for example using a consistent grid size.

The VD MBE varies more (cf. UD) with forcing temperature (Figure 4-8a.i, b.i). $Q_{F,d}$ is more biased towards the V1 scheme than D2 during colder temperatures for the Central region (Figure 4-8a.i). VD Central median MBE reduces when T_{av} > 13 °C, reaching 0 W m^{-2} at 19 °C (Figure 4-8a.i). The U1 results do not show these trends (median MBE 1 to 2.5 W m^{-2} when T_{av} > 6 °C, Figure 4-8b.i). Median MBE varies for both comparisons at low (T_{av} < 5 °C) and warm (T_{av} > 20 °C) temperature extremes, likely related to small samples. In the West region, VD median MBE decreases slightly with increasing temperature (Figure 4-8d.i), whilst UD median MBE lack a trend (Figure 4-8e.i), with values very close to 0 W m^{-2} once T_{av}. > 8 °C.

Comparison UV of the two fast schemes across the forcing temperatures (Figure 4-8c, f), shows U1 values exceed V1 at low and high temperatures, as expected (Figure 4-5). Median MBE patterns do not indicate a large exceedance of U1 at lower temperatures (Figure 4-8c.i, f.i), despite U1 exceeding V1 from below 7 °C in some high λ_i OA. The U1 values generally are greater than V1 values for T_{av} > 18 °C in both areas (Figure 4-8c.i, f.i), which is approximately where a_{F2} intersects b_b (Figure 4-5). The U1 exceedances have little impact across all λ_i and T_{av}, (e.g. negative skew of the 1st and 99th percentiles in both regions). The V1 bias occurs at milder temperatures, with maximum difference occurring between 9 - 14 °C (Figure 4-8c.i, f.i) consistent (Figure 4-8c.ii, f.ii) with the MBE increasing with λ_i. Although mostly biased towards V1, the difference between the two schemes is quite low across all temperatures (e.g. density of points, Figure 4-8c.iii, f.iii) and percentile lines.

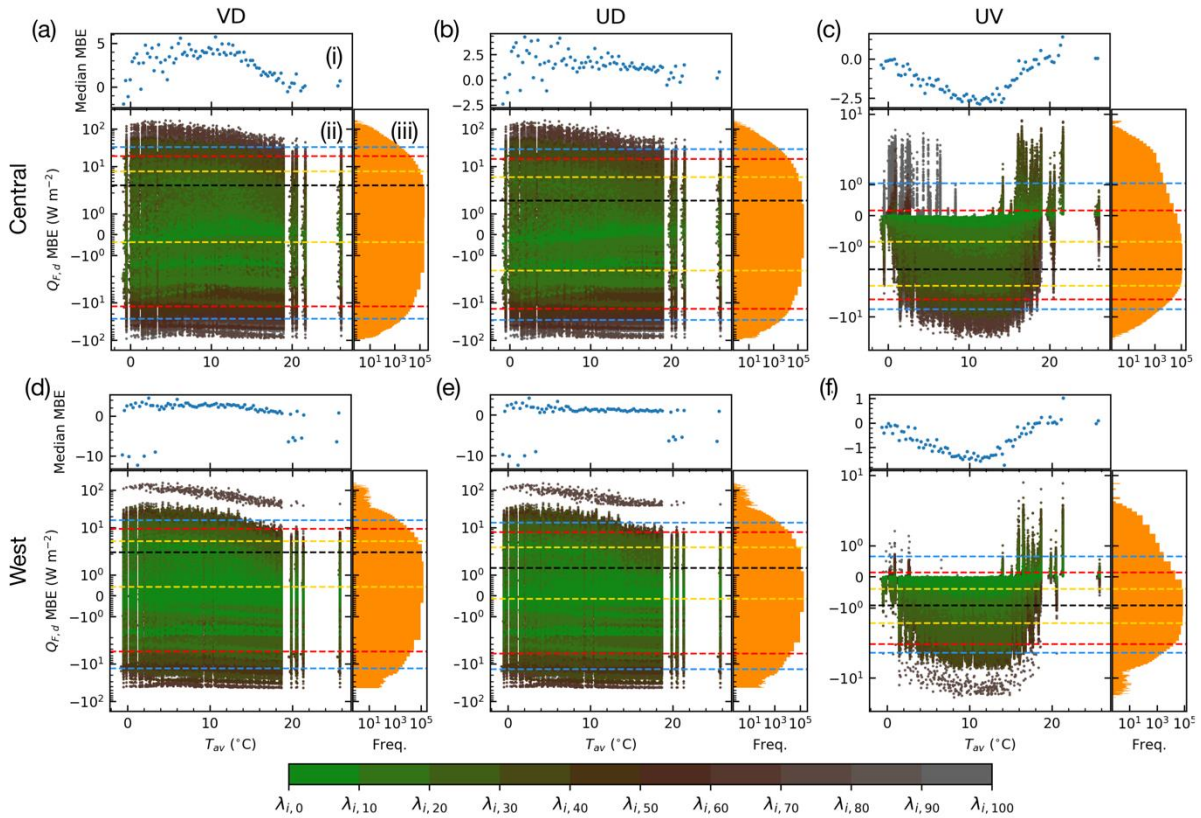

Figure 4-8: MBE of $Q_{F,d}$ for all areas in (**a**-**c**) Central and (**d**-**f**) West for (**a**, **d**) VD, (**b**, **e**) UD and (**c**, **f**) UV. Subplots consist of (**i**) median MBE with T_{av} in 100 ΔT bins, (**ii**) all MBE (log scale) against T_{av} shaded by λ_i (increasing 10% classes), (**iii**) frequency of MBE across all T_{av} (both axes log scale). (**ii**, **iii**) MBE percentiles across all T_{av}: p_1 and p_{99} (blue); p_5 and p_{95} (red); p_{25} and p_{75} (yellow); and median (black) (Table I-1). Y-scale is the same for **ii** and **iii** for VD, UD, likewise for UV.

As expected from the earlier results, comparison of the VD and UD MBE across all λ_i shows VD to be biased towards V1, whereas UD shows more of a bias towards D2 (Figure 4-9). When both fast schemes simultaneously show positive (negative) MBE, i.e. are both biased towards themselves (D2), VD values are larger than the equivalent UD values. This is consistent with the greater spread of V1 values and the overwhelming bias of UV towards V1 (Figure 4-8c, f). This occurs across all λ_i, though low λ_i areas lie closer to the 1:1 line (Figure 4-9). For both comparisons and both regions, mean MAE increases with λ_i (Figure 4-9a.ii, b.ii). This is expected as in high λ_i areas increased ρ_{pop} amplifies the error between the calculated coefficients and true values (Section 4.4.2) in total Q_F.

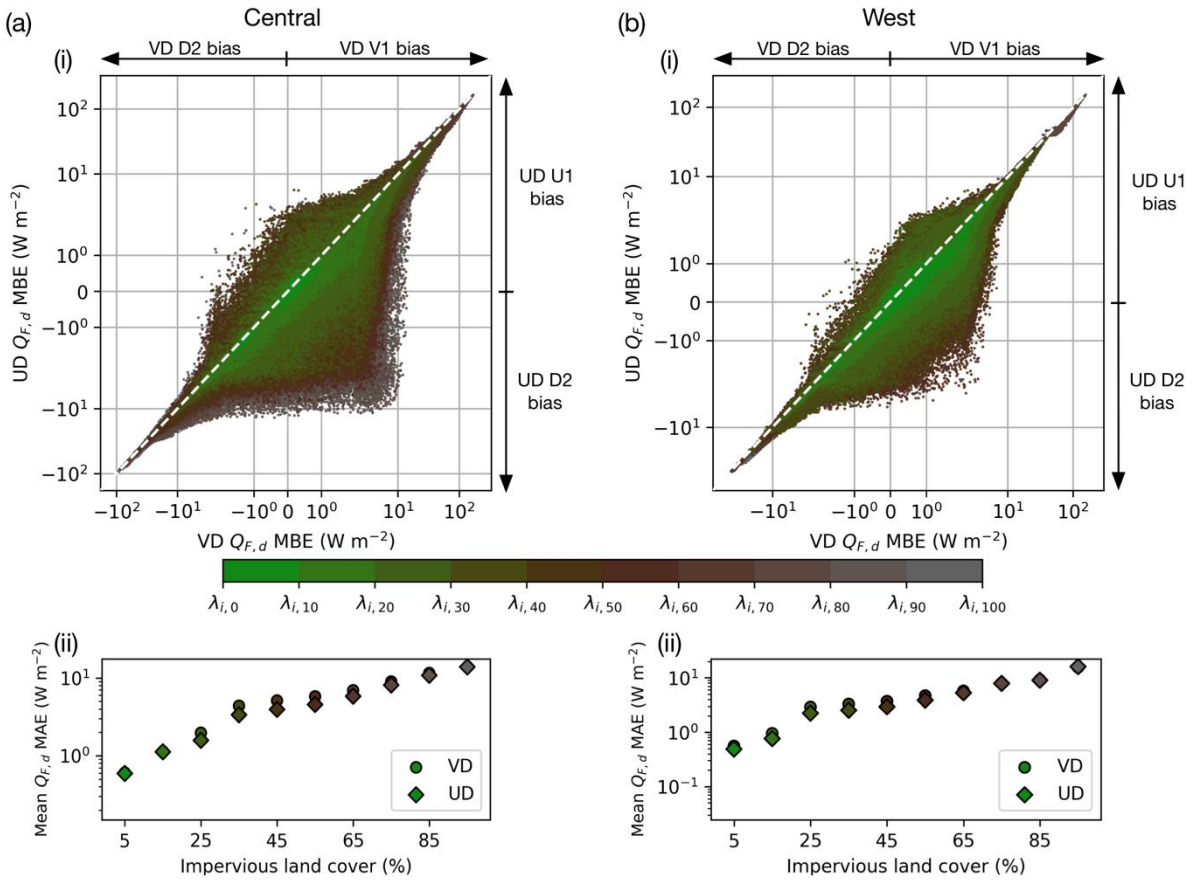

Figure 4-9: VD (V1 - D2) average daily Q_F MBE vs. UD (U1 - D2) $Q_{F,d}$ MBE (both axes log scale) for (**a**) Central and (**b**) West regions shaded by λ_i (increasing 10% classes: green → brown → grey). White dashed line shows 1:1. The directions of the biases towards each of the three schemes are given along the axes.

4.5.1.3 Annual daily IQR of Q_F

$Q_{F,d}$ clearly varies with temperature for all three schemes, which each follow similar seasonal patterns (Figure 4-10). Larger values occur in the winter as buildings respond to heating needs (Section 2.3.2.1, Figure 3-12). Summer values are smaller as no space temperature control is implemented. U1 and V1 are clearly sensitive to T_{av}, displaying similar daily peaks and troughs to D2.

Autumn and winter (2014/10/01 - 2015/02/28) U1 and V1 values exceed D2 in most areas, especially in $\lambda_{i,30\text{-}70}$ (Figure 4-10a.iv-vii, b.iv-vii). For the Central region, U1 median values averaged over this period and λ_i categories are greater than D2, whilst V1 values are even more so (Table 4-4). This also occurs in the West region. In summer (2015/06/01 - 2015/08/31) U1 and V1 still tend to exceed D2, but overall differences are smaller (Table 4-4).

Table 4-4: Seasonal differences in average median $Q_{F,d}$ (Figure 4-10) between V1 & U1 and D2 (%: V1÷D2, U1÷D2; Magnitude, W m^{-2}: V1 - D2, U1 - D2) for areas $\lambda_{i,30\text{-}70}$.

Period	***Temp range* (°C)**	***Region***	***V1***		***U1***	
			%	***Magnitude* (W m^{-2})**	**%**	***Magnitude* (W m^{-2})**
Oct 2014 - Feb 2015	-0.8 - 17.3	C	23 - 28	2.8 - 4.5	12 - 17	1.4 - 2.7
		W	10 - 46	1.3 - 3.5	0 - 32	0.1 - 2.4
June - Aug 2015	10.2 - 26.0	C	16 - 25	1.4 - 2.1	6 - 16	0.6 - 1.3
		W	2 - 47	0.1 - 1.7	-7 - 38	-5.8 - 1.38

Across the year, $Q_{F.d}$ for both U1 and V1 are more similar to D2 at $\lambda_{i,70\text{-}100}$ (Figure 4-10a.viii-x, b.ix-x). This is however dependent on the spatial units sampled. For example, at Central $\lambda_{i,70\text{-}80}$ areas $Q_{F,d}$ values for the fast schemes are similar to D2 (Figure 4-10a.viii) but at West $\lambda_{i,70\text{-}80}$, U1 and V1 underestimate D2 throughout the year (Figure 4-10b.viii). Such disparities also occur between regions at $\lambda_{i,0\text{-}20}$ (Figure 4-10a.i-ii,b.i-ii). This is due to the profile of spatial units specific to the Central/West regions within λ_i. Under-/overestimation will occur if specific sampled OA U1 and V1 parameter values lie above/below the 5% interpolated values (Section 4.4.2). Furthermore, these 5% interpolated values are derived from highly variable, low sampled data at extreme λ_i (Figure 4-4).

$Q_{F,d}$ from V1 model runs exceeds U1, except for the warmest (July - August) and coldest (midwinter) temperatures across all λ_i, when U1 medians equal or exceed V1. This reflects expectations from Figure 4-5, and results shown in Figure 4-8, though the occurrences of temperatures where U1 exceeds V1 are seldom (Figure 4-5). Consistent with offline (Figure 4-5) and MBE analysis (Figure 4-8) results, the greatest differences occur during mid-range temperatures.

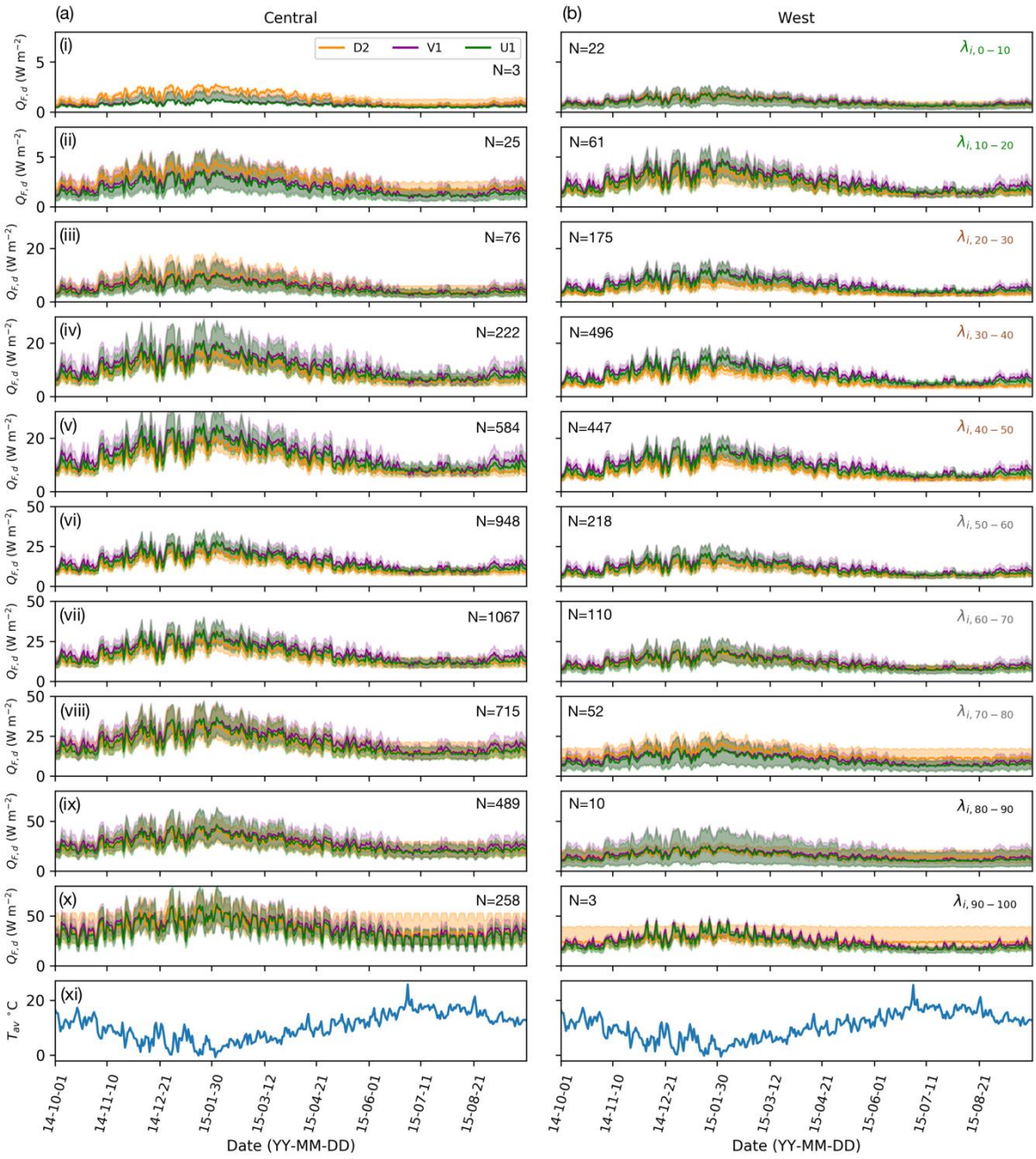

Figure 4-10: D2 (orange), U1 (green), and V1 (purple) (Table 4-1) model results for (**a**) Central and (**b**) West, stratified in to 10 λ_i classes (**i-x**) daily median (line) and IQR (shaded) $Q_{F,d}$ and (**xi**) forcing T_{av} (°C) for each region (median across measurement heights). N denotes number of OA in each λ_i class. Note Y-axes differ between **i-ii, iii-v, vi-viii** and **ix-x**.

4.5.2 Comparison with previous SUEWS results

Kc_{OA} and Sw_{OA} monthly diurnal fluxes are compared to modelled and observed values for Kc_{W16} and Sw_{W16} to determine SUEWS-DASH and SUEWS model performance with regards to the Q_F schemes used. Similar forcing conditions between comparisons are ensured (Section 4.3.5).

Q_F values at Kc_{W16} (W16 obs, Section 4.3.5) are much greater than those at Kc_{OA} for runs U1, V1, D2 (Figure 4-11a) as different models were used to estimate Q_F between the two studies. W16 Q_F values are derived from GQF (Gabey et al., 2019) and were adjusted for energy balance closure against observations of other fluxes at the site (Kotthaus and Grimmond, 2014; Ward et al., 2016). GQF itself has also been shown to produce higher Q_F values than DASH (Section 3.5, Capel-Timms et al., 2020b). This results in higher Q_H values at Kc_{W16} as the additional available energy is partitioned. At Sw, the magnitudes of Q_F are more similar across the year (Figure 4-11a). Summer values are higher for W16 obs, though there is less annual variation. V1 is generally higher than U1 and D2, following trends seen in Figure 4-8 and 4-9.

As Q_F contributes mostly towards sensible heat across a city, Q_H is analysed first. Kc_{W16} $Q_{H,DM}$ / Q^*_{DM} generally follows a similar pattern to U1 and V1 though at a higher magnitude (Figure 4-11b). This is likely due to the higher Q_F providing more available energy to Q_H. All results show elevated winter values compared to the rest of the year. This is due to the common phenomenon of $Q_F > Q^*$ in mid-high latitude cities during low temperatures. In Sw, $Q_{H,DM}$ / Q^*_{DM} has a narrower range due to the higher fraction of vegetated land cover (Figure 4-11b). Q_H will be less dependent on Q_F, as values are smaller in the suburban area. Results modelled for this study (U1, V1, D2) show a decrease for May followed by much higher values for June and July. In May there is a steep increase in leaf area index, which would lead to more evapotranspiration and therefore a greater proportion of available energy partitioned into Q_E, though leaf area index does not decrease in June or July to cause an increase in $Q_{H,DM}$ / Q^*_{DM}. There is also a greater increase in Q^* during this month, accounting for smaller $Q_{H,DM}$ / Q^*_{DM}. Though it is difficult to compare due to differences in forcing meteorology, results for W16 over 2012-2013 (not adjusted for similar meteorology) also show a decrease followed by a sharp increase around a similar time, though this is less extreme.

The magnitudes of Kc winter $Q_{E,DM}$ / Q^*_{DM} for W16 observations are more similar to values simulated for U1, V1 and D2 than those simulated by SUEWS for W16, though over summer W16 values are closer to U1, V1 and D2. All results show a gradual decrease from late winter to spring. Sw results for U1, V1 and D2 show more erratic results from May to July, in tandem with values seen for $Q_{H,DM}$ / Q^*_{DM}. The dominance of Q_E in May is again likely due to the sudden increase in leaf area index (and

therefore evapotranspiration) in this month. The sudden decrease from May to June is also shown in W16 2012-2013 simulated actual results from June to July.

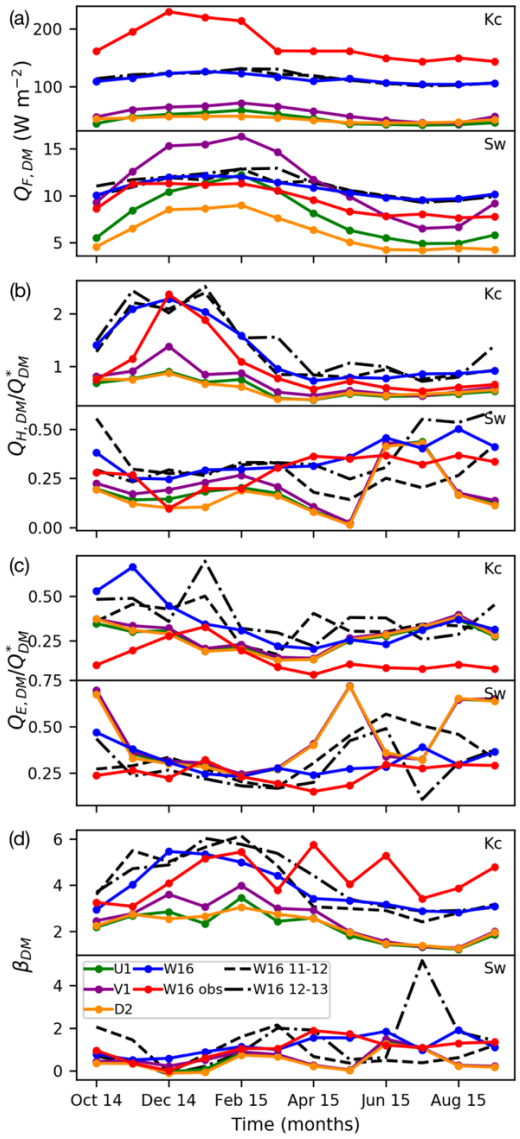

Figure 4-11: Fluxes and flux partitioning at Kc and Sw (Section 4.3.5) for monthly daytime ($K_{\downarrow}$ > 5 W m^{-2}) medians of (**a**) $Q_{F,DM}$ (W m^{-2}), (**b**) $Q_{H,DM}$ / Q^*_{DM}, (**c**) $Q_{E,DM}$ / Q^*_{DM} and (**d**) β_{DM}. W16 refers to values simulated within SUEWS, whilst W16 obs refers to eddy covariance observation values (Ward et al., 2016). Both W16 and W16 obs are arranged for equivalent forcing meteorology to 2014/10/01 - 2015/09/30 ERA5 forcing for Greater London (Section 4.3.5), whilst W16 11-12, W16 12-13 are direct Oct. - Sept. values for 2011-2012 and 2012-2013 resp.. W16 obs Q_F is used for surface energy balance calculations in Ward et al. (2016) and taken from GQF (Kc, adjusted values) or energy consumption statistics (Sw), whilst W16 Q_F (also reflected in W16 11-12, W16 12-13) is simulated via the integrated SUEWS population-based V-scheme but not used for other fluxes.

Bowen ratios are greater in Kc than in Sw across the year for all models (Figure 4-10d) despite a higher water land cover fraction at this site. This is likely due to the constant presence of much higher Q_F values, especially in winter, providing energy to Q_H. No models reflect the monthly alternating pattern of W16 obs values in Kc between March and August, though this is due to small fluctuations in Q_H and Q_E (Figure 4-11b, c). W16 simulated results are generally greater than U1, V1 and D2, with more annual variation. At Sw, the patterns in summer $Q_{H,DM}$ and $Q_{E,DM}$ for U1, V1 and D2 are reflected.

4.5.3 Influence of Q_F on the turbulent heat fluxes

As Q_F influences the turbulent heat fluxes, the resultant errors of each scheme for midday (1100-1400) median sensible ($Q_{H,MM}$) and latent ($Q_{E,MM}$) heat fluxes are investigated. These two fluxes are key to understanding the implications of the three Q_F methods to changes in the urban meteorology, particularly with regard to the development of the urban heat island and boundary layer stability (not explored here) (Section 2.1.3).

4.5.3.1 $Q_{H,MM}$ MBE for VD, UD and UV

The IQR of the MBE density across all comparisons and areas remains narrow for $Q_{H,MM}$ (Figure 4-12a, b, d, e; Table I-1). UD MBE IQR is narrower than for VD by 31% for the Central region and 40% for the West. Furthermore, the IQRs for VD are entirely biased towards V1, whilst UD IQRs span biases for U1 and D2 (73 - 90% towards U1), with medians closer to zero by 2.39 - 4.56 W m^{-2} (Figure 4-12a, b, d, e; Table I-1). This implies that U1 provides closer estimations than V1 across the Central and West regions. This is expected as Q_F is also slightly overestimated by the two fast schemes in most areas (Figure 4-8) and Q_F contributes to Q_H. The biases become less substantial for p_{99}, p_{95}, p_5 and p_1 for both UD and VD (Figure 4-12a.ii, b.ii, d.ii, e.ii; Table I-1). The spread of MBE values increases with λ_i, similar to the patterns seen for Q_F (Section 4.5.1.2). This is confirmed by the positive median MBE in all cases.

Figure 4-12c, f show that U1 $Q_{H,MM}$ is generally lower than that of V1 for both areas, confirming the expectation that higher Q_F estimation leads to higher Q_H. Nevertheless, the breadth and position of the UV IQR of MBE values implies that this may not greatly affect Q_H values in the terms of the diurnal Q_H magnitude. As U1 diurnal profiles are derived from D1 and change with temperature range, it is expected that U1 $Q_{H,MM}$ is closer to D2 than V1, which uses default SUEWS profiles not derived from the study area (Section 4.4.3).

There is little relation between median MBE and T_{av} for the UD comparison (Figure 4-12b.i, e.i); the majority of values are between 0 and 2.5 W m^{-2} for both regions. VD shows a clear relation, as median MBE decreases as T_{av} increases, ranging from 0-10 W m^{-2} for the Central region (Figure 4-12a.i) and 0 – 8 W m^{-2} for the West region (Figure 4-12d.i). VD Q_F median MBE shows a decreasing relation when T_{av} > 13 °C (Figure 4-8a.i, d.i), though differences in $Q_{H,MM}$ could also be symptomatic of the diurnal profiles used for Q_F (Section 4.4.3), as a greater proportion for daily Q_F is shared across midday for V1 (Figure 4-6a.i, b.i).

A particular feature of $Q_{H,MM}$ MBE is a sudden increase at mild temperatures (10 - 18°C) in some areas, indicating overestimation by U1 and V1 (Figure 4-12a.ii, b.ii, d.ii, e.ii), and contributing to the high magnitude of p_{99} values. These areas were found to predominantly be those with a high ρ_{pop} but relatively low λ_i which produce erroneously large $Q_{F,d}$ results (Appendix J.2). Whilst this pattern is not directly reflected in the $Q_{F,d}$ results (Figure 4-8), this appears to have a substantial effect on $Q_{H,MM}$. As $Q_{F,d}$ overestimation in these areas will occur at all temperatures (particularly during colder seasons) this may be due to the diurnal profiles used for both U1 and V1 (Section 4.4.3). There is also the possibility that these areas are too small for SUEWS to physically resolve the resultant high Q_F. This highlights a possible need for the U and V schemes to be implemented at a lower spatial resolution.

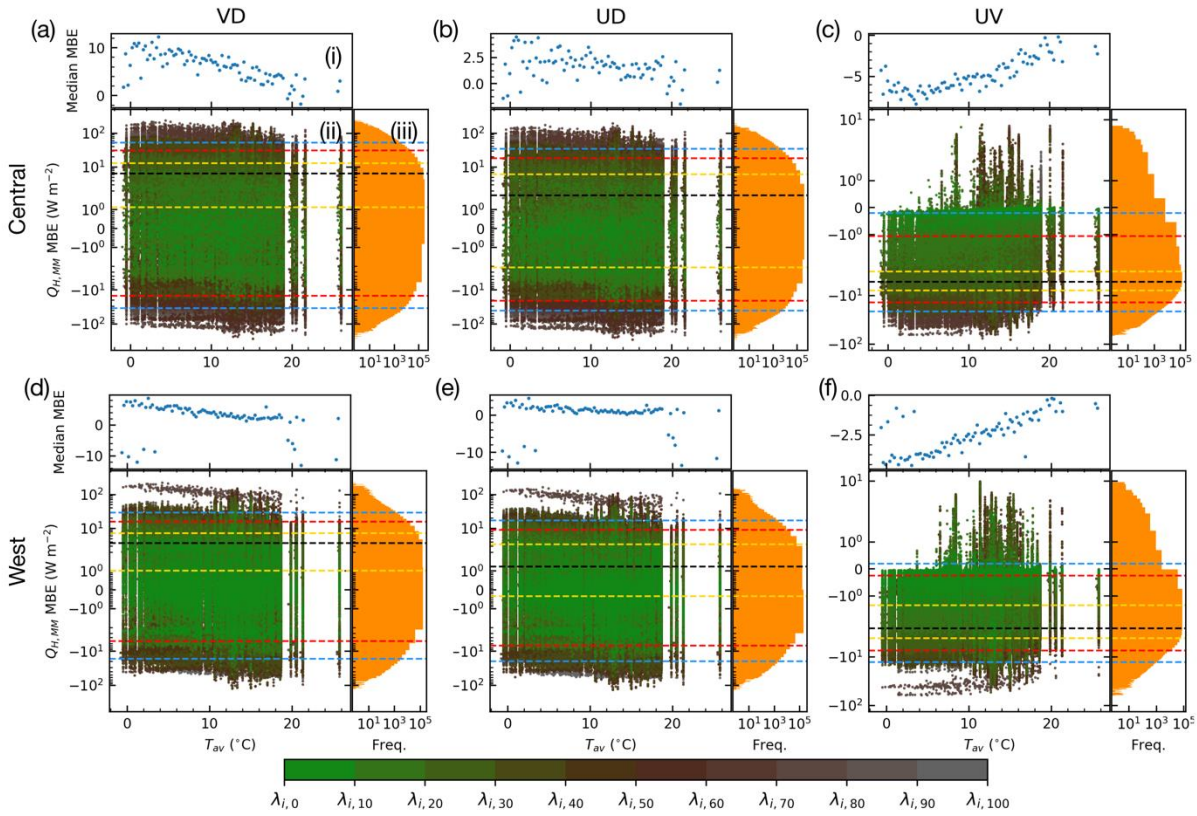

Figure 4-12: MBE of average daily $Q_{H,MM}$ for all areas in (**a**-**c**) Central and (**d**-**f**) West for (**a**, **d**) VD, (**b**, **e**) UD and (**c**, **f**) UV. Subplots consist of (**i**) median MBE against T_{av} in 100 ΔT bins, (**ii**) MBE (log scale) against T_{av}, coloured by λ_i (increasing 10% classes), (**iii**) frequency of MBE across all T_{av} (both axes log scale). (**ii**, **iii**) MBE percentiles across all T_{av}: p_1 and p_{99} (blue); p_5 and p_{95} (red); p_{25} and p_{75} (yellow); and median (black) (Table I-1). Y-scale is the same for **ii** and **iii** for VD, UD, likewise for UV.

4.5.3.2 $Q_{E,MM}$ MBE for VD, UD and UV

$Q_{E,MM}$ MBE have narrower IQRs than $Q_{H,MM}$ (Table I-1). This is partly due to most areas in the city having low vegetated or water land cover, resulting in less opportunity for evaporation. Extreme negative MBE (Figure 4-13a.ii, b.ii, d.ii, e.ii), indicating underestimation of $Q_{E,MM}$ in U1 and V1, occurs at the same temperatures and λ_i as the overestimation of $Q_{H,MM}$ by the fast schemes (Figure 4-12aii, bii, cii, dii). Median MBE therefore shows a relation with temperature, with an apparent move towards a D2 bias for both fast schemes when T_{av} > 12 °C (Figure 4-12a.i, b.i, d.i, e.i). The IQR (Central: 1.4 W m^{-2}, West: 1.1 W m^{-2}) and $p_{5\text{-}95}$ (Central: 6.5 W m^{-2}, West: 4.8 W m^{-2}) point densities for the UV comparisons are narrow, (Figure 4-13c.ii,iii, f.ii,iii; Table I-1), implying little difference between the two fast schemes in most areas, though the p_{25}, p_{75} and median lines show a slight bias towards V1. U1 shows greater $Q_{E,MM}$ at milder temperatures for a few areas with medium to low λ_i.

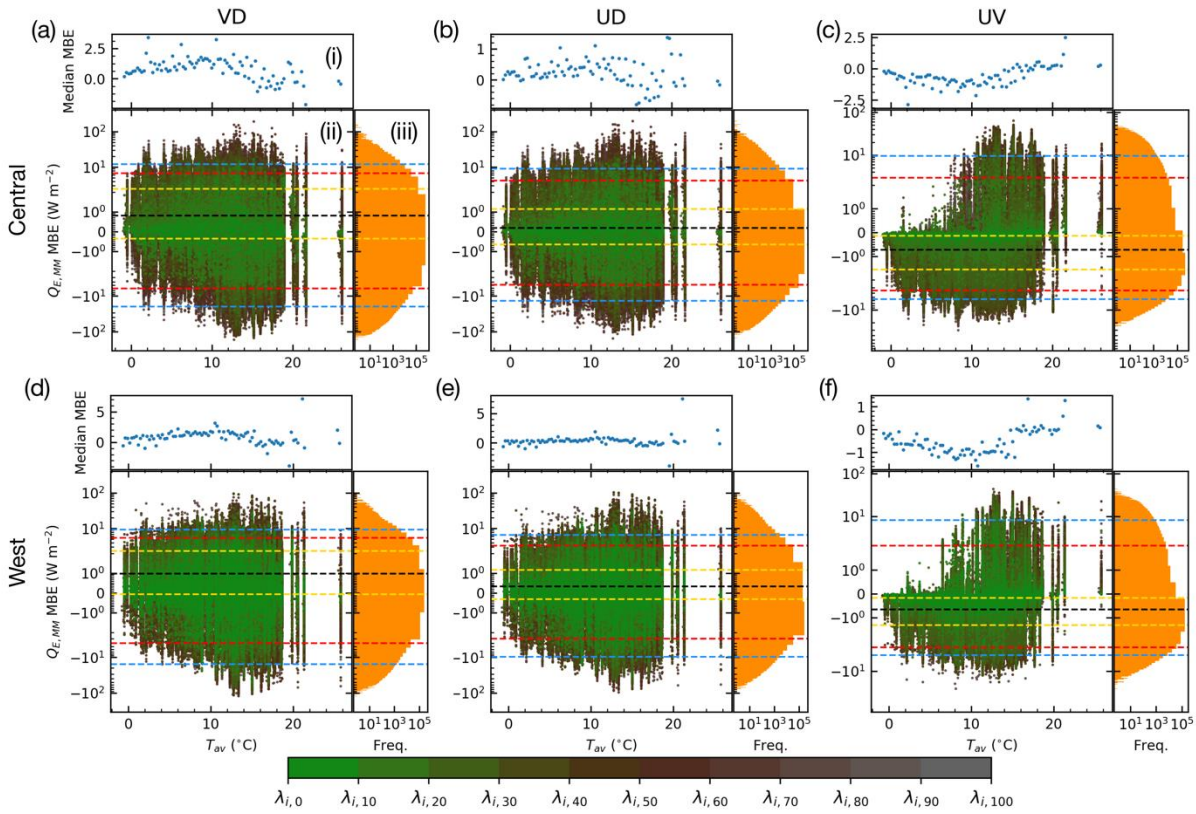

Figure 4-13: MBE of average daily $Q_{E,MM}$ for all areas in (**a**-**c**) Central and (**d**-**f**) West for (**a**, **d**) VD, (**b**, **e**) UD and (**c**, **f**) UV. Subplots consist of (**i**) median MBE against T_{av} in 100 ΔT bins, (**ii**) MBE (log scale) against T_{av}, coloured by λ_i (increasing 10% classes), (**iii**) frequency of MBE across all T_{av} (both axes log scale). (**ii**, **iii**) MBE percentiles across all T_{av}: p_1 and p_{99} (blue); p_5 and p_{95} (red); p_{25} and p_{75} (yellow); and median (black) (Table I-1). Y-scale is the same for **ii** and **iii** for VD, UD, likewise for UV.

4.5.4 T_{2m} MBE for comparisons VD, UD and UV

Under or overestimation of Q_F may lead to changes in air temperature, as Q_F contributes to the warming of the outdoor environment and outgoing longwave radiation (Section 2.1.3.2). These changes in Q_F and T_{2m} must be accounted for and mitigated if using the schemes in applications such as urban weather forecasting and heat stress studies. Again, all IQR and *p* values reference Table I-1.

Both VD and UD comparisons show extremely narrow MBE IQRs in both regions (< 0.055 °C in all cases), with MBE medians very close to zero (< ± 0.012 °C) (Figure 4-14a,b,d,e; Table I-1). For the Central region, both V1 and U1 estimate daily average T_{2m} to within ±0.87 °C of D2 values for at least 98 % of values (Figure 4-14a,b). $p_{1\text{-}99}$ spread is broader for the West region, and slightly broader for UD than for VD (Central: by 3%, West: 11%) (Figure 4-14d.ii,iii, e.ii,iii). $p_{1\text{-}99}$ values indicate that V1 has a very slight tendency to underestimate T_{2m} (52 - 60% values are biased to D2) (Figure 4-14a.i, d.i) whilst U1 only very slightly overestimates T_{2m} (55 - 58 % biased to U1) (Figure 4-14b.ii, e.ii). Central

median MBE does not show a strong pattern but varies more when T_{av} < ~8 °C (Figure 4-14a.i,b.i). This implies that U1 and V1 $Q_{F,d}$ deviate more from D2 (Figure 4-8a,b,d,e) as the fast schemes become more sensitive to temperature (Figure 4-1a) and errors relative to the training data (Section 4.4.2) accumulate.

The comparison UV shows that U1 simulates a higher T_{2m} than V1, though the IQR is below 0.06 °C for both the Central and West regions and centred narrowly around zero (Figure 4-14c, e). Median MBE again shows a trend with T_{av}, becoming biased towards U1 when T_{av} < ~8 °C (Figure 4-14c.i, f.i), though in some areas U1 bias occurs when T_{av} < 12 °C (Figure 4-14cii, fii). This reflects the MBE biases towards D2 and U1 for the VD and UD comparisons resp.. This is likely due to greater proportions of $Q_{F,d}$ distributed during low temperature night times in the U-scheme cf. the V scheme by the E_d profiles. Overnight, V-scheme E_d reaches as low as 0.4, whilst U-scheme E_d only goes as low as 0.75 for the highest λ_i category (Figure 4-6a.i, b.i).

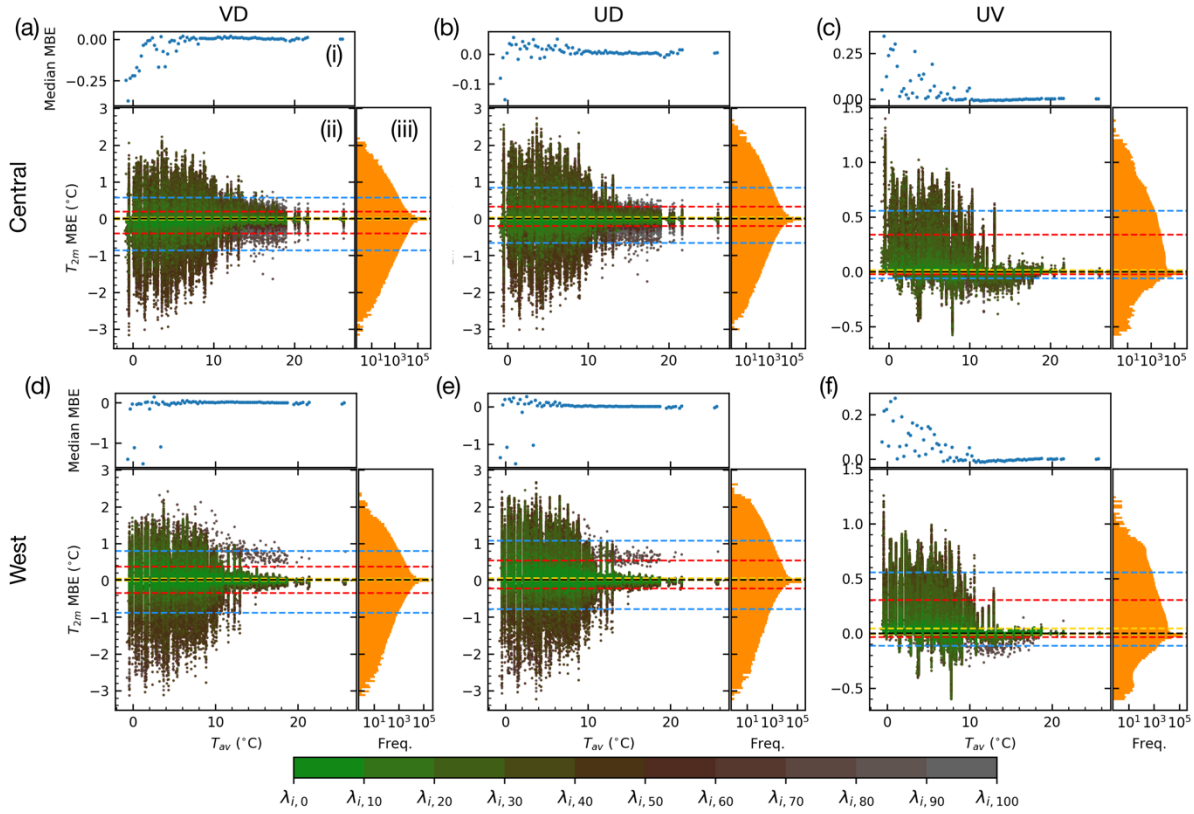

Figure 4-14: MBE of average daily T_{2m} for all areas in (**a**-**c**) Central and (**d**-**f**) West, for (**a**, **d**) VD, (**b**, **e**) UD and (**c**, **f**) UV. Subplots consist of (**i**) median MBE with T_{av} in 100 ΔT bins, (**ii**) MBE against T_{av}, coloured by λ_i (increasing 10% classes), (**iii**) frequency (x-axis log scale) of MBE across all T_{av}. (**ii**, **iii**) MBE percentiles across all T_{av}: p_1 and p_{99} (blue); p_5 and p_{95} (red); p_{25} and p_{75} (yellow); and median (black) (Table I-1). Y-scale is the same for **ii** and **iii** for VD, UD, likewise for UV.

4.5.5 Impact of diurnal profiles on T_{2m} and Q_H

The diurnal Q_F profile of any scheme alters the responses of outdoor air temperature (here two-metre air temperature T_{2m}, which in SUEWS responds to Q_F forcing) and the turbulent heat fluxes. To demonstrate the importance of E_d for U1 and V1, Figure 15 shows the IQR diurnal profiles of Q_F across the Central and West regions, alongside the differences ΔQ_H and ΔT_{2m} (°C) between the three schemes. Days are classified across three T_{av} ranges (from the temperatures used for U1 E_d, Figure 4-6, Section 4.3.4.2), to determine relations between T_{av}, E_d shape and resultant T_{2m} MBE.

Q_F emissions are most intense when $T_{av} \leq 6.9$ °C due to the heating response (Figure 4-15a.i, d.i), and hence diminish as T_{av} increases (Figure 4-15b.i, c.i, e.i, f.i). This is reflected in the decreasing ΔQ_H and ΔT_{2m} with T_{av}. The diurnal Q_F patterns for U1 and D2 are similar, though U1 values are slightly greater than D2 in most cases. This is expected from previous results (Figure 4-7, 4-8). Across the three T_{av} ranges, the diurnal mean of median U1 Q_F values are 12 - 14% greater cf. D2 in the Central region, and 25 - 30% greater in the West region. V1 values are lower than U1 and D2 overnight, but much greater in the daytime. Overall diurnal values are greater than D2. V1 diurnal mean median values are 20 - 29% greater than D2 in the Central region, and 36 - 49% greater in the West region.

$\Delta T_{2m,UV}$ is consistently greater and positive (biased to U1) during the night as U1 Q_F is greater than V1 Q_F. In the daytime, $\Delta T_{2m,UV}$ is zero, or slightly negative when the two peaks in V1 occur (07:00, 17:00, Figure 4-6a,bi). Greater magnitudes in $\Delta T_{2m,UV}$ occur overnight (median values up to 0.7 °C) because Q_F has a greater proportional effect when $K_{\downarrow}$ is zero and the depth of the boundary layer is shallower (Section 2.1.3.2). $K_{\downarrow}$ is stronger at higher T_{av}, so Q_F will have less of an influence on T_{2m} in these temperature ranges. Hence, the T_{2m} MBE for the UV comparison is more sensitive at lower T_{av}, and negligible elsewhere (Figure 4-14c, f). This pattern is not reflected in the comparisons of $Q_{F,d}$ (Figure 4-8) and the turbulent fluxes (Figure 4-12, 4-13) as they are averaged across the whole day and midday, resp.. Differences in surface characteristics and building morphology (e.g. z_H in Central is 4.7 m greater than in West area) cause the differences in $\Delta T_{2m,UV}$ between the two grids (e.g. Figure 4-15a.iii,d.iii). Due to the similarities between U1 and D1 Q_F, $\Delta T_{2m,VD}$ patterns are similar to $\Delta T_{2m,UV}$.

ΔQ_H patterns follow ΔT_{2m} overnight but are more responsive to Q_F in the daytime. This is most noticeable in the patterns for $\Delta Q_{H,VD}$, $\Delta Q_{H,UV}$ where distinctions between Q_F schemes are greater. ΔT_{2m} is less affected by Q_F in the daytime for the inverse of the night-time reasons stated above.
UD ΔT_{2m} and ΔQ_H show better performance cf. VD. This is partly due to U1 providing closer $Q_{F,d}$ estimates (Figure 4-7, 4-8, 4-9), but also shows the importance of maintaining similar sub-daily

profiles as values are close to zero throughout the $\Delta T_{2m,UD}$ and $\Delta Q_{H,UD}$ profiles. Median values for $\Delta Q_{H,UD}$ range from -0.32 to 3.25 W m^{-2} and -0.026 to 0.20 °C for $\Delta T_{2m,UD}$.

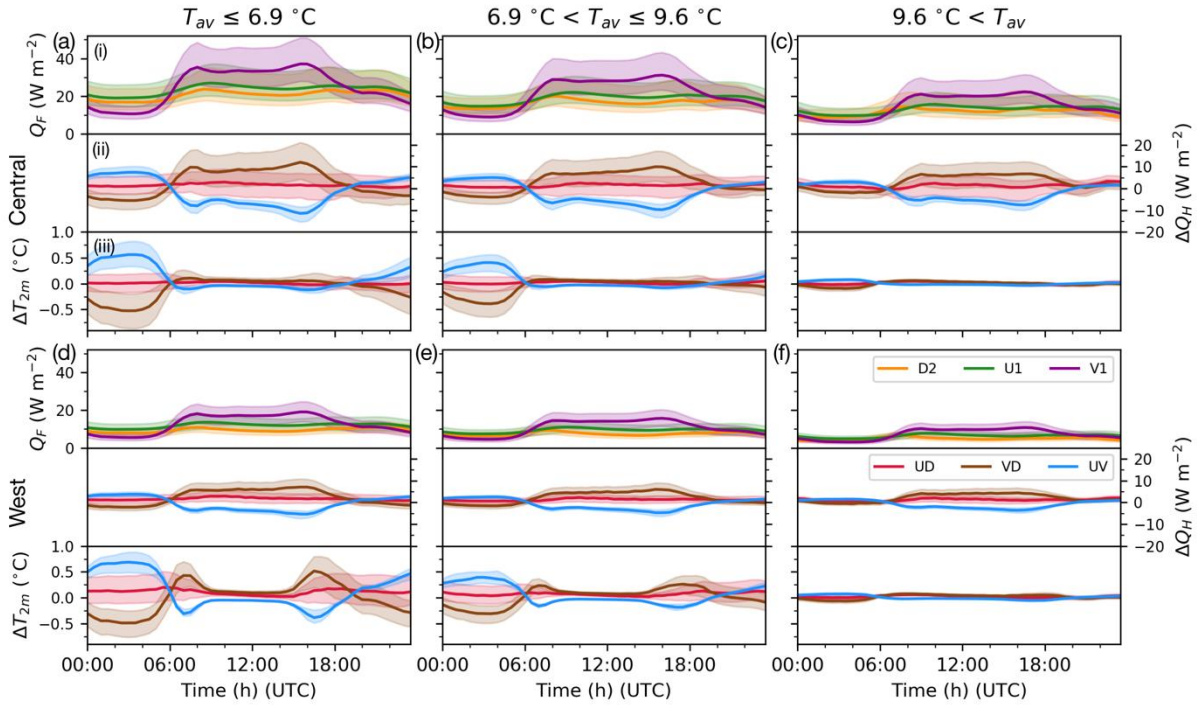

Figure 4-15: Medians (solid line) and IQRs (shading) of (**i**) Q_F estimations, (**ii**) ΔQ_H (UD: U1-D2, VD: V1 - D2, UV: U1 - V1), (**iii**) response temperature ΔT_{2m} (°C; UD, VD, UV) for all days (01 October 2014 - 30 September 2015) categorised by forcing temperature (°C) (**a**, **d**) T_{av} < 6.9 °C, (**b**, **e**) 6.9 < T_{av} < 9.6 °C, (**c**, **f**) 9.6 °C < T_{av} (determined from Figure 4-6 ranges) for all spatial units in the (**a**, **b**, **c**) Central and (**d**, **e**, **f**) West regions. Results at 30 min time steps.

4.6 Conclusions

Parameters for two computationally fast (Table F-1) anthropogenic heat flux estimation methods are derived using a more complex model (DASH), that reacts directly to environmental forcing, behaviours and characteristics of the study area. The V-scheme (eq. 4-2) uses a single temperature balance point based on human thermal comfort temperatures. The U-scheme (eq. 4-3) considers a range of temperatures for which Q_F is independent from outdoor air temperature, using parameters that can be found from analysis of energy consumption data or established Q_F estimations. Diurnal profiles for the U-scheme are derived from the complex model and vary both spatially and by temperature. Coefficients are distributed by fraction of impervious land cover for both schemes, as this showed variability in populations and Q_F intensities. This allowed for a spatially diverse allocation of parameters. All three runs showed similar magnitudes in monthly mean fluxes when compared to established results, though whilst attempts were made to mitigate differences in forcing meteorology, it was difficult to compare seasonal patterns.

Comparisons between the two fast schemes and DASH have shown that both the U- and V-schemes have a tendency to overestimate Q_F, especially during colder temperatures. Annual median Q_F across all spatial units from the V-scheme exceeded DASH estimates by 30%, whilst the U-scheme values exceeded DASH by 16%. Across the autumn and winter period, V-scheme seasonally averaged median daily Q_F in areas of 30-70% impervious land cover were up to 46% greater than for DASH. Though overall difference in Q_F magnitude was small, the U-scheme overestimated DASH by up to only 32% across the same areas and period. Mean bias error in Q_F between DASH and the fast schemes was found to increase with impervious land cover, though this was expected given the related increase in population density and therefore error amplification. Errors were biased towards the fast schemes, though more so for the V-scheme than the U-scheme, which showed less spread in daily error at the highest spatial resolution.

The schemes were also analysed for other elements of the surface energy balance and urban meteorology. Midday Q_H and Q_E MBEs between DASH and U, V showed general biases towards the fast schemes due to the overestimations in Q_F, though these were small for the majority of areas. The V-scheme again showed greater error than the U-scheme, but this could partly be due to midday differences in the Q_F diurnal profiles.

Hence, the U-scheme was found to perform better across most temperature ranges and spatial distributions. This is due to better representation of the Q_F response to forcing temperature, as the temperature balance point was chosen based on analysis of training data as opposed to assumptions on heating/cooling use and a lack of a human thermal comfort range (as seen in previous literature). Through challenging this *a priori* method of temperature balance point selection, it can be assumed that the V-scheme would show similar overestimations (cf. the U-scheme) at higher temperatures within the thermal comfort range of cities that widely use both heating and cooling.

Comparisons of the diurnal Q_H and response temperature patterns highlighted a need for sub-daily Q_F profiles to be derived from the behavioural characteristics of the study area. The U-scheme estimations benefitted from using dynamic Q_F diurnal profiles derived from the behavioural characteristics of Q_F, particularly at lower forcing temperatures. Diurnal profiles are estimated across ranges of T_{av} and λ_i and therefore miss some fine-resolution characteristics (e.g. differences in energy use due to demographics of a specific area, Section 3.4) but results show low differences in median sub-daily values across all areas and temperature ranges. The V-scheme profiles were not tailored to the study area and showed large differences in response temperature during night-time (median up to 0.7 °C), as well as greatly varying Q_H patterns (though median magnitudes were small) throughout the day when

compared to DASH and U. This would have implications for use in forecasting or, for example, heat stress studies.

By distributing coefficients via land cover characteristics, the fast schemes could be adaptable to other cities, without the need for re-estimation. The training and study areas would need to have similar energy use patterns, such as energy intensity per capita (or building volume), diurnal profiles (behavioural characteristics) and thermal comfort ranges. However, using the current method Q_F is overestimated by both fast schemes in spatial units with a small area and dense population. This has consequences for other fluxes. This issue could be resolved by using different metrics to better represent spatial variation of behavioural dynamics. For example, spatial units could be classified as a function of both population density and impervious land cover, instead of solely impervious land cover. It may also be beneficial to lower the spatial resolution of all schemes when coupling with an urban land surface model, allowing for other fluxes to be better resolved. Results have shown that careful analysis into Q_H, Q_E and air temperature results will need to be undertaken before implementing either scheme into other aspects of urban climate modelling or forecasting. Nonetheless, both schemes are suitable for providing efficient Q_F estimations.

Deriving parameters from DASH for simpler schemes has allowed for spatial (relation with land cover characteristics, dynamic population densities) and temporal (diurnal profiles that vary by behaviour according to land cover and forcing temperature) variability to be included within more efficient models. The spatial and temporal aspects of Q_F behaviour and its implications are therefore reflected. The multiple temperature responses of the U-scheme require more pre-analysis and parameters, but their inclusion benefits estimations at a range of temporal resolutions cf. the V-scheme. The U-scheme also shows smaller errors when compared to DASH and is therefore preferred to the V-scheme. The feasibility and efficiency of the U and V-schemes provides a solution to the lack of high resolution Q_F in numerical weather prediction models and some urban SEB studies. If the schemes were to be used extensively in urban climate modelling and weather forecasting, such high spatial resolutions as demonstrated in this study may not be required, likely removing some of the error seen across the SEB. In this case areas would need to be analysed to find a suitable scale that provides enough information without loss of the representation of behavioural characteristics.

Chapter 5 Conclusions, contributions and recommendations

Detailed knowledge of urban meteorology is critical for the wellbeing of city inhabitants, especially as populations continue to increase and urban effects become more prominent. Previous studies of urban meteorology demonstrate that Q_F can affect the near-surface air temperatures and atmospheric stability, with implications for heat stress, air pollution and weather prediction. Despite these impacts on urban meteorology, high resolution anthropogenic heat flux is underrepresented in many NWP-ULSMs; values currently used for urban areas neither respond to immediate forcing nor account for aspects of human activity beyond population density and/or static diurnal profiles. Current modelling techniques could be used to supply estimates, but they are not able to adapt to scenarios on a city-wide scale, so unexpected consequences of changes in behaviour cannot be determined.

As human behavioural practices and actions are fundamental to Q_F, any changes can have major impacts on heat emissions. These can occur on diurnal, weekly, seasonal or yearly time scales, affecting emissions from local areas to the entire urban extent (Chapter 2). It is therefore essential that these processes are properly represented in Q_F modelling in order to account for future changes.

This thesis contributes a novel dynamic approach for modelling anthropogenic heat fluxes that considers human practices and actions at its foundation. This will allow scenarios to be investigated in response to the activity and needs of a city's population, and, given the availability of the required data, will be adaptable to multiple cities. Multiple influences on Q_F were identified and have been incorporated into the model to demonstrate the spatial and temporal variability of Q_F. The development and evaluation of the model is demonstrated, as well as its application to more efficient schemes that are appropriate for integration with NWP-ULSMs.

5.1 Main conclusions and contributions

5.1.1 Application of human behaviour to Q_F modelling

The **D**ynamic **A**nthropogenic activitie**S** impacting **H**eat emissions (DASH) agent-based model simulates the heat emissions of an entire city with regards to human behaviour, involving many processes at individual, cohort (age group, household size), building, city and societal levels. Low-level activities such as building occupancy, use of appliances and thermal interaction with the outdoor environment were used to represent agent response. These activities were used to define the level of detail necessary for each process involved directly in Q_F. Secondary influencing factors were then determined, and processes were modelled from the bottom up. For example, energy consumption is a

direct source of Q_F. Secondary influencing factors include the energy subsector (e.g. domestic or workplace), time of activities and appliances involved. Further influences include the household size. Broader processes governing agent interaction were modelled using large-scale statistics, in particular the movement of occupants across the city. Aspects of current modelling approaches motivated the inclusion of behaviours. For example, the use of static populations with only user-defined transitions gave rise to the needs in modelling the dynamics of movement. The fine-scale details found in traditional bottom-up models motivated the inclusion of building energy models and occupant activities.

DASH (Chapter 3) addresses the need for a local-scale anthropogenic heat model that reacts to human behaviour. Incorporated transport and building energy models are used to reflect all three Q_F sectors. Using a bottom-up, agent-based framework DASH allows for Q_F patterns to evolve through interactions and responses between heterogeneous agents, including:

- movement patterns of city inhabitants across the urban extent depending on diurnal human activity patterns, city populations within various building use types, age groups and transport needs. This is the agent-agent interaction.
- $Q_{F,T}$ emission, driven by exchange of occupants during agent-agent interaction. DASH simulates its own traffic flows in accordance with the movement of inhabitants, with vehicles distributed across the transport network. Journey times are a function of vehicle mode, speed and road capacity.
- the inclusion of low-level activities and appliance characteristics in $Q_{F,B}$. This forms part of the agent response. In the domestic sub-sector, activities attributed to appliance use (assumed to be temperature independent) depend on the occupancy levels of households within an area agent. This is similar for non-domestic energy consumption, but energy demand by floor area of non-domestic type is used instead of individual activities. This adopts methods used within bottom-up modelling, but allows for dynamic occupancy levels instead of static profiles and scaling. Contributions from different end uses can be recorded as output (Appendix E) as opposed to bulk at sub-sector as seen in top-down inventory models.
- the building energy model STEBBS, which allows for response of $Q_{F,B}$ to local meteorology (temperature, solar irradiance, wind speed). The building stock is represented by multiple archetypes which vary by age and dwelling type to account for the thermal properties of buildings across the city.
- $Q_{F,M}$ of inhabitants. This varies with activity (currently awake/sleeping) and or transport mode chosen (when travelling).

These account for secondary effects and behaviours, such as:

- occupancy levels within a variety of building uses. The dynamic movement of city inhabitants successfully emulates expected building occupancy levels when compared against population data across building uses. Top-down inventory approaches use static residential and workplace populations with subjective transitions across the study extent. This fails to account for any city-scale variability in movement due to work shift or commutes, or movement to other building use types such as school and leisure. Bottom-up simulation approaches use occupancy profiles depending on building use, improving simulations at the building scale but not varying across the city. DASH allows for movement between building uses at all times, constrained only by time use data.
- local-scale area occupancy variation by demographic. Areas with different dominant resident age groups are shown to have very different diurnal occupancy profiles, which would have consequences for $Q_{F,B}$ via active and heating/cooling energy demand.
- the influence of road capacity and route choice on travel journey times. Part of the movement allows for the time between origin and destination to vary depending on road capacity. This allows for some of the spatial variation in the occupancies of building use types (domestic/non-domestic) across the urban extent.

The evaluation of DASH was undertaken at a range of spatial and temporal scales against GQF (Gabey et al., 2018) (an established top-down inventory model), energy consumption data and population data. DASH reproduced characteristics of diurnal Q_F patterns seen in GQF, for example morning and evening peaks, though had more variation due to high-resolution response to meteorological forcing. The model compares well at a range of scales, though there is some underestimation in annual mean Q_F across Greater London compared to GQF: DASH - 6.43 W m^{-2}, GQF - 7.97 W m^{-2}. This was mostly due to differences in $Q_{F,B}$. Seasonal patterns observed in DASH, such as heating responses, reflect those seen in national energy consumption statistics, as the model is able to respond to forcing at each time step. Further analysis could address differences seen during warmer months. Expected spatial patterns of energy consumption can be observed across the city, for example Q_F increases towards the centre of the city as population densities increase. When compared to energy consumption statistics, non-domestic Q_F is frequently overestimated by DASH in areas outside of the city centre, though this may be partly due to low overall non-domestic activity in these areas, as energy consumption compares well in the city centre where commercial activity is greater. The spatial variation of non-domestic energy consumption agrees well for the majority of areas. Domestic values tend to be underestimated by DASH, though they are more accurate than for non-domestic.

5.1.2 Adaptation for use in NWP-ULSM

Urban land surface models and numerical weather predictions currently lack high resolution Q_F estimations. Values used currently do not respond to immediate forcing nor account for aspects of human activity beyond population density and/or static diurnal profiles. As demonstrated, DASH accounts for human activity in estimations of Q_F but the model is computationally expensive and requires a lot of input data, making it unsuitable for coupling with large scale climate models. DASH was therefore used to derive parameters for two efficient schemes, the V-scheme and the U-scheme, which both produce Q_F estimates based on average daily temperature and population density. The U-scheme was previously introduced for Q_F estimation (Ao et al., 2018), but this thesis provides the first case study analysing it in comparison with the more established V-scheme (Sailor and Vasireddy, 2006), or adapting it to include detailed aspects of variation attributed to human behaviour.

These approaches are computationally inexpensive and therefore more suitable for model integration. Behavioural variation is spatially accounted for as coefficients are derived by fraction of impervious land cover, λ_i. This is also the case for the sub-daily normalised Q_F profiles in the U-scheme, which also vary by forcing temperature to allow for changes in profile due to heating/cooling. Population density is calculated using the dynamic occupancy levels simulated by DASH for each spatial unit, as opposed to static population data across coarse resolutions as seen in previous studies.

Both DASH and the fast schemes were coupled with the urban land surface model SUEWS, allowing for the urbanisation of meteorological forcing and the inclusion of the interaction of Q_F with the turbulent heat fluxes and outdoor temperature response (U, V, DASH), and related feedbacks (DASH only). The Q_F-temperature feedbacks between DASH and SUEWS allow Q_F-induced changes in outdoor temperature to affect heating and cooling needs within the STEBBS model, providing more realistic interactions with the outdoor environment.

Both schemes generally overestimated Q_F when compared to the coupled DASH run across all λ_i. Whilst the annual mean for the entire city was highest for the DASH run (due to large outliers), median annual average values across spatial units were 2.55 W m^{-2} greater for the V-scheme and 1.48 W m^{-2} greater for the U-scheme. Lower Q_F values were less common for the U and V schemes, and large outliers seen in the DASH run were not present. Spatially averaged (for areas within two analysed regions) mean absolute error of daily mean Q_F increased by fraction of impervious land cover: 0.50 (U) and 0.56 (V) for $\lambda_{i,0\text{-}10}$, and 13.88 (U) and 13.95 (V) for $\lambda_{i,90\text{-}100}$. Seasonal and daily mean Q_F patterns compared well, though overestimation by the two fast schemes persisted. The U-

scheme performed best across all compared fluxes, showing lower mean bias errors for Q_F, midday turbulent heat fluxes and response temperature. Errors in the U-scheme were also less dependent on forcing temperature than those for the V-scheme. Excess Q_F overestimation had consequences for the turbulent fluxes, which would have implications for atmospheric stability when coupled with a boundary layer model.

The two fast schemes are able to replicate temperature responses for both heating and cooling. Only the heating response was explored as there was no cooling implemented in the DASH run used to derive models, with previous studies showing negligible to zero cooling demand in London. Due to the symmetry of the fast schemes, it may be assumed that similar errors may occur when cooling demand is present.

Variability in diurnal profiles (across ranges of T_{av} and λ_i , estimated from DASH results) for the U-scheme was shown to produce changes in response to outdoor air temperature by up to 0.7 °C (peak night-time difference between medians at cold forcing temperature) when compared to the static profile used for the V-scheme. This effect was strongest at colder forcing temperatures due to the dominance of anthropogenic emissions as a heat source (stronger space heating, less warming by solar irradiance). This demonstrates the importance of including high spatial resolution human activity at sub-daily time scales when estimating Q_F, and the consequences on urban meteorology. Differences also manifested in the diurnal patterns of Q_H. For both Q_H and response temperature, U showed the lowest differences across the diurnal patterns when compared to DASH. This demonstrates the advantages over using diurnal Q_F patterns based on national statistics of energy consumption sectors at local scale, a method frequently employed by top-down inventory approaches.

The U-scheme, which allows for a range in forcing temperature during which there is no heating response, provided Q_F estimates closer to DASH than the V-scheme. This, along with its efficiency and the inclusion of spatially variable behaviours, makes a DASH derived U-scheme approach suitable for inclusion in NWP-ULSMs.

5.2 Recommendations for future work

5.2.1 Further development of DASH

Further development could resolve some of the limitations and assumptions within the current evaluation of DASH. For example, the representation of building stock could be enhanced by including more archetypes with a wider range of thermal properties. When refining a model, it is

important to consider which components are worthy of development. A sensitivity analysis could be conducted to aid efficiency in development and provide more insight into the model's functionality, as this would allow for the investigation of multiple factors and their interactions (Saltelli et al., 2009). A sensitivity analysis of DASH in particular would challenge the assumptions that were made when building DASH and STEBBS, and further establish confidence in the model's validity beyond the existing evaluation. It would provide worthwhile information about the interactions within the model that would otherwise not necessarily arise, specifically the association between input and output. Uncertainties within parameters could be quantified, and parameters of little influence could be identified and rejected/generalised if they are shown to have negligible or no influence. Furthermore, a sensitivity analysis would aid understanding into which factors of human activity most influence resultant Q_F, especially with regards to low-level processes.

As DASH is a complex model with multiple modules and associations, it would be best analysed in separate parts, for example:

- STEBBS (Section 3.2.4.3, Appendix B): to investigate the sensitivity of HVAC needs to each building input variables and component parameters. This would require testing under a variety of meteorological scenarios and could be completed using multiple building archetypes. Results would provide some insight into the amount of variation in building parameters (i.e. archetypes) needed to thoroughly represent building stock and find a balance between research needs and accuracy of output. Sensitivity analyses are commonly carried out for BEMs using traditional methods (Tian, 2013).
- Transport and travel agency behaviour (Section 3.2.4.2): this component of DASH is more complex as it includes more second-order (and beyond) effects. As traffic volume is so closely governed by road length, a less systematic analysis could involve altering road length over a reduced study area, e.g. a few boroughs. Changes in route could be investigated across large spatial extents to investigate wider effects across a city (e.g. road capacity). Changing parameters such as fuel consumption and heat of combustion will only display a linear change in Q_F. A sensitivity analysis of travel agency behaviour would involve alteration of Markov transition matrices at each time step. Unlike STEBBS and most aspects of the transport component, structure of the travel agency behaviour does not use parameters that can be individually altered, but Markov matrices and other socio-physical input factors. This would require very complex analysis.
- Household occupant behaviour (Section 3.2.4.3): Like the travel agency behaviour component, household occupant behaviour (i.e. energy activity profiles) is dependent on

weightings. Factors that influence the time of activities, such as household size and occupancy levels, may be investigated by standard sensitivity analysis methods.

To provide further areas of study, DASH agent-agent interaction could be modified to include feedbacks between local weather and human behaviour. For example, local weather might alter patterns of movement between activity subareas, or modes used (e.g. Cools et al., 2010; Saneinejad et al., 2012; Tsapakis et al., 2013).

In the current iteration of DASH the agent-based interaction is focused on the movement of city inhabitants. Low-level processes, such as activities within buildings and transport mode choice, have been included in detail in order to allow for scenario development. Some low-level behavioural practices and actions have been modelled using ABM (Section 2.4.1), for example evolution of building stock and introduction of electric vehicles. ABM sub-models could therefore be used within these to investigate the development of trends across long time periods.

5.2.2 Future study

DASH could be used for multiple purposes. DASH and STEBBS output data include the energy consumption of different building types and end uses (Appendix E), which could find use in the investigation of city-scale energy consumption as a response to activity and movement patterns.

Using the DASH-SUEWS coupling, the benefits of including meteorological feedbacks could be explored in more detail, such as the differences seen in SEB fluxes and outdoor air temperature between coupled and uncoupled runs under the same initial and forcing conditions. This could also be used to address the impacts of including highly detailed Q_F in ULSMs. This has been investigated using monthly mean values (Best and Grimmond, 2016), but it was noted that better temporal and spatial resolutions could be used, such that human behaviour and local meteorological forcing could be taken into account. This could be particularly critical for ULSM performance in areas of greater Q_F intensity and under conditions where Q_F contributes more to the SEB (Hertwig et al., 2020). This could then be used to promote better representation of Q_F in NWP-ULSMs.

The DASH-SUEWS coupling (Chapter 4) could also be used for heat stress studies to explore the effects of local temperature increase due to Q_F on human health. Such studies do exist, but DASH would be able to provide simulation at fine spatial and temporal scales across a city to better highlight local inequalities and hotspots.

The flexibility of agent-based modelling provides many opportunities to study different Q_F scenarios. It is particularly important that scenarios are evaluated when large-scale change is likely to occur, for example population growth or climate change. Scenario development and analysis could support or drive mitigations for any adverse effects that may be found. It could also be used to measure the value of any policy changes that could occur and highlight any unwanted responses in meteorology.

Ward and Grimmond (2017) provide some examples which DASH will be able to re-examine in more detail with the advantage of behavioural response and the inclusion of secondary effects. The functionality of DASH allows for detailed investigation into the impact of scenarios on Q_F beyond first-order effects. Scenarios could be designed to investigate:

- population change, and its implications for building land cover/volume, demographics and households. As DASH simulated residential occupancy profiles have shown variation by age demographic, the type of population increase would need to be considered, e.g. aging population, increased birth rate or equal proportion across all ages. This would affect movement across the city (transport capacity), housing needs and workplace densities.
- replenishment of building stock. The location of buildings and their thermal properties should be considered. For example, whether existing buildings replaced/retrofitted, or if land use changes.
- road closure, with impacts seen across the transport network at different scales.
- evolution of technology, e.g. change of transport fleet to include more electric vehicles. Potential changes to consider include power demand, loss/gain of human activities, changes to journey times, technology uptake.

Overall, the modelling approaches presented in this thesis provide the ability to capture behaviourally motivated anthropogenic heat fluxes at a range of scales. This is achieved through a complex, agent-based model which considers the movement of populations across a city and the subsequent response of energy consumption. Interactions with the environment are included. The application of computationally efficient approaches to the output from the fine resolution, behaviourally responsive Q_F from DASH allows for integration into broader urban studies and weather models. It is hoped that the original and derived models will be used in ways that benefit urban modelling, both for the sake of progressing forecasting methods and driving studies that improve the wellbeing of city inhabitants.

Appendix A Creation of Markov chains

A Markov transition matrix (Hermanns, 2003; Sericola, 2013) is built from the probabilities of transition from one state to another in the next time step, with *n* states forming an $n \times n$ Markov transition matrix (Table A-1a). Entries are the probabilities *p* of transitioning from one state at time step *t* (row) to another at time step *t + 1* (column) (e.g. Table A-1b,c). Stationary distribution for state 1:

$$\pi(t) = [p(t)_{1,1}, p(t)_{1,2}, p(t)_{1,3}, p(t)_{1,4}, p(t)_{1,5}, p(t)_{1,6}] \quad \text{(A-1)}$$

The transition matrices created for this model are time inhomogeneous, reflecting a realistic diurnal profile with changes in likelihood state through the day. If state transition *n, n* is chosen, the state does not change. Markov transition matrices may exclude entry to particular states by setting the column and row of a restricted state to zero.

As there is no way to determine the states prior to the start of a model run and to ensure no spin-up is required, the stationary distribution for the first-time step in the run is given by the diagonal of the matrix (e.g. based on Table A-1 six states):

$$\pi(t) = [p(t)_{1,1}, p(t)_{2,2}, p(t)_{3,3}, p(t)_{4,4}, p(t)_{5,5}, p(t)_{6,6}] \quad \text{(A-2)}$$

This represents the distribution across states that are not in transition during the previous or the current time step.

For travel (Section 3.2.4.2) at *t*=1, O_C are distributed using a weighted choice with the diagonal of the transition matrix (eq. A-2) for that time step and age group as the weight distribution. At each subsequent time step, the origin A_N has a choice to keep each O_C or release them into another a_S^N, according to weighted choice using the transition probabilities dictated by the origin a_S^N's stationary distribution (eq. A-1) at *t* as ω. The A_N destination depends on the destination a_S^N selected. If a_S^N for the next time step is the same as the previous time step, the A_N does not release the O_C.

Table A-1: Markov transition matrix (**a**) general for six states (rows and columns) (**b**) data for a single time step and (**c**) transition probabilities for the data in (**b**) (Gershuny and Sullivan, 2017)

a)	1	2	3	4	5	6
1	$p(t)_{1,1}$	$p(t)_{1,2}$	$p(t)_{1,3}$	$p(t)_{1,4}$	$p(t)_{1,5}$	$p(t)_{1,6}$
2	$p(t)_{2,1}$	$p(t)_{2,2}$	$p(t)_{2,3}$	$p(t)_{2,4}$	$p(t)_{2,5}$	$p(t)_{2,6}$
3	$p(t)_{3,1}$	$p(t)_{3,2}$	$p(t)_{3,3}$	$p(t)_{3,4}$	$p(t)_{3,5}$	$p(t)_{3,6}$
4	$p(t)_{4,1}$	$p(t)_{4,2}$	$p(t)_{4,3}$	$p(t)_{4,4}$	$p(t)_{4,5}$	$p(t)_{4,6}$
5	$p(t)_{5,1}$	$p(t)_{5,2}$	$p(t)_{5,3}$	$p(t)_{5,4}$	$p(t)_{5,5}$	$p(t)_{5,6}$
6	$p(t)_{6,1}$	$p(t)_{6,2}$	$p(t)_{6,3}$	$p(t)_{6,4}$	$p(t)_{6,5}$	$p(t)_{6,6}$

b)	Domestic	Workplace	Shops	Other
Domestic	270	46	2	4
Workplace	1	170	0	1
Shops	0	0	5	0
Other	0	1	1	18

c)	Domestic	Workplace	Shops	Other
Domestic	270/320	46/320	2/320	4/320
Workplace	1/172	170/172	0	1/172
Shops	0	0	1	0
Other	0	1/20	1/20	18/20

Appendix B Heat exchange within STEBBS

STEBBS employs a nodal approach (Foucquier et al., 2013) as found in commonly used simulation tools such as TrnSys (Klein et al., 2017) and EnergyPlus (Crawley et al., 2000). Each node represents a homogeneous layer within a specified component of the building, with heat transfer equations solved between each node (Figure B-1). STEBBS' eight nodes are 2-layers for wall-roof, ground floor and windows; plus a bulk air node and an all internal mass node (calculated as a percentage of total volume). Additionally, there are six nodes associated with the domestic hot water (DHW) system. There are 2-layers for the hot water tank walls and a bulk DHW distribution system, plus a bulk water node for the storage and a distribution node. Effective thermal properties are applied to each component (i.e. a wall cavity and insulation layers are not modelled separately). As this is computationally cheap, it allows multiple instances for each A_N at high temporal resolution. The only latent heat consideration is that of people from metabolic processes (Section 3.2.4.1).

The STEBBS considers heat exchanges by convection, conduction, and radiation, and heat gain from solar insolation and casual heat sources (Figure B-1). The convective flux, q_{cv}, between a fluid *f* and a surface *s* (Bergman et al., 2017) is:

$$q_{cv} = h\,A(T_f - T_s) \tag{B-1}$$

where T_f and T_s are the temperatures of the fluid (*f*) and surface (*s*), respectively, and *A* the surface area of the building. Convective fluxes occur between indoor (outdoor) air and internal (external) wall/window/floor surface as well as the internal mass surface. For DHW, eq. B-1 calculates convective flux between water and hot water tank/vessel walls. Forced convection *h* is experienced on external walls as a function of wind speed *ws* (m s^{-1}) at roof height, so is variable whilst internal values are held constant (Cole and Sturrock, 1977):

$$h = 5.8 + 4.1ws \tag{B-2}$$

Conduction between internal and external surfaces of a component (i.e. wall, window, floor, hot water tank/vessel, and ground floor to ground) is:

$$q_{cd} = k_e\,A\,\frac{T_{si} - T_{so}}{L} \tag{B-3}$$

where k_e is the effective conductivity of a building component with 1 to *n* layers of thickness L_n (sum to *L*) and conductivity k_n:

$$k_e = \frac{L}{\frac{L_1}{k_1} + \frac{L_2}{k_2} + \cdots + \frac{L_n}{k_n}} \tag{B-4}$$

and T_{si}, T_{so} are the component's inside and outside surface temperatures, respectively. This is calculated for inside surfaces of a wall, ceiling, window, floor, hot water tank and hot water vessel

components and their respective outside surfaces, as well as the point of contact between the ground floor and the external ground.

Shortwave insolation ($K_{\downarrow}$) is considered on building walls/roof and windows, with transmitted proportion through windows added to internal heat gain and absorbed proportion contributing to wall/roof/window gains (Underwood and Yik, 2004). Windows have an effective shortwave transmissivity (τ) and albedo (Θ), whereas walls/roof depend only on their albedo. Solar internal heat gain (q_{si}) as:

$$q_{si} = \tau \cdot K_{\downarrow} \tag{B-5}$$

and solar gain to external wall (q_{se}^{a}) and window (q_{se}^{i}) as:

$$q_{se}^{a} = (1 - \Theta)\, K_{\downarrow} \text{ and } q_{se}^{i} = (1 - \tau - \Theta)\, K_{\downarrow} \tag{B-6}$$

The net longwave radiation (Q_{L*}) exchange between building surfaces (walls or windows) and surfaces (including sky) in their view is found using Bergman et al. (2017):

$$Q_{L*} = A \sum_{i=1}^{n} \left[\Psi_i\, \sigma\, \varepsilon \left({T_{so}}^4 - {T_{s,i}}^4\right)\right] \tag{B-7}$$

where σ is the Stefan-Boltzmann constant (5.67×10^{-8} W m^{-2} K^{-4}), ε is the wall/window emissivity and surface temperature. $T_{s,i}$ is the temperature of the surface (i) in view.

The three view factors (ψ_i) for external wall/window surfaces (sky ψ_s, buildings ψ_b, and ground ψ_g) will sum to 1. Currently, neither short nor longwave radiation are ψ accounted for (i.e. uniform temperature is assumed). This could be improved when coupled with more detailed morphology data and urban meteorology as ψ varies across a city with height (building facet) and density of buildings (Grimmond et al., 2001). Internal wall radiative exchanges are currently not considered.

Energy for heating (cooling) is controlled by setpoint temperature with energy added (removed) directly from the indoor air node that is controlled according to a maximum power rating and set system efficiency. The temperature setpoints can change at each timestep allowing both automated and human control to be accounted for. The level of heating (cooling) is further controlled by the difference between indoor air and setpoint temperatures. Internal gains are accounted for as a bulk gain to the indoor air node.

The BESTEST Case 600 single zone building case is used with EnergyPlus (v.9.3.0). to evaluate STEBBS[5]. The EnergyPlus BESTEST model downloaded from the EnergyPlus helpserve website (EnergyPlus, 2020) is modified to run with v9.3.0. Observed London weather data for 2012 (Kotthaus and Grimmond, 2014) are generated using SuPy (Sun and Grimmond, 2019) at an hourly resolution for EnergyPlus and STEBBS. Although EnergyPlus indicates it interpolates sub-hourly weather data for consistency we use both with a 1-hour timestep.

Following EnergyPlus Engineering Reference, the STEBBS external convection coefficient is changed to the DOE-2 method (U.S. Department of Energy, 2020) for consistency between the models. Note, this is found to have little impact on the results. The internal mass and DHW in STEBBS are reduced in volume to ensure they have negligible impact on results (see https://doi.org/10.5281/zenodo.3745523 for BESTEST setup). The bulk building thermal properties in STEBBS are calculated using the BESTEST Case 600 values as presented in ASHRAE 140 (ASHRAE, 2017). Building dimensions for STEBBS are set to give consistent total indoor volume, wall-roof surface area, window area, and floor area. As STEBBS has only one pair of nodes (i.e. 2-layer wall, Figure B-1), building geometry and orientation are not represented in STEBBS.

The EnergyPlus annual and inter-day heating and cooling dynamics are captured in STEBBS (Figure B-2). Both models control the indoor air temperature to within the setpoint limits of 20 (heating) and 27 (cooling). EnergyPlus simulates a higher heating and cooling load with more times when the indoor temperature is between (rather than at) the setpoint temperatures. EnergyPlus also simulates a cooling requirement during the heating season, which STEBBS does not.

The modal hourly heating/cooling load differences between the two models are relatively small (Figure B-2). Although the distribution range is large, the differences are perhaps best attributed to a difference in load control. The EnergyPlus BESTEST case uses the maximum heating (cooling) capacity to add (remove) thermal energy to (from) the building that is likely to result in the observed indoor temperature overshoots, the higher frequency of switching (on-off) for heating and cooling, and need for cooling during heating season as heating and cooling power are set high (100 kW). Whereas to prevent this type of behaviour, STEBBS uses the difference between air and setpoint temperature to help control the heating and cooling power.

[5] This analysis was undertaken by co-author Stefán Smith for Capel-Timms et al., 2020b

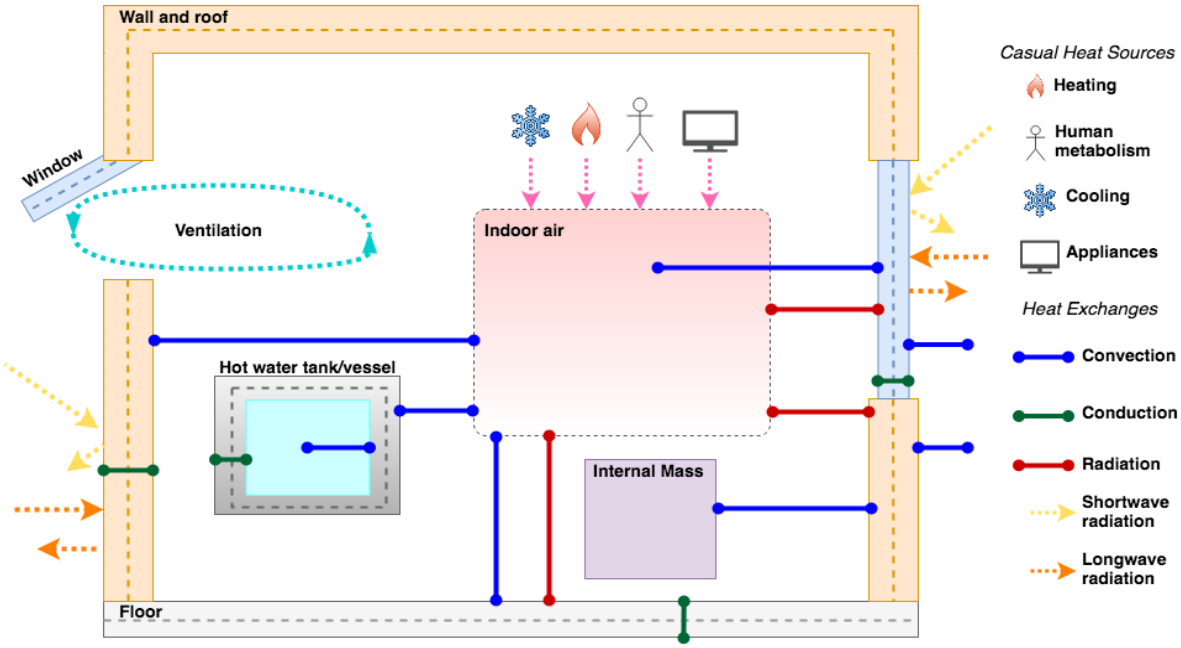

Figure B-1: STEBBS 1-D model simulates building facets/nodes (dots), casual heat sources and heat exchanges. Longwave radiation is absorbed by building facets from the outdoor environment, and shortwave radiation from direct, diffuse and reflected sources.

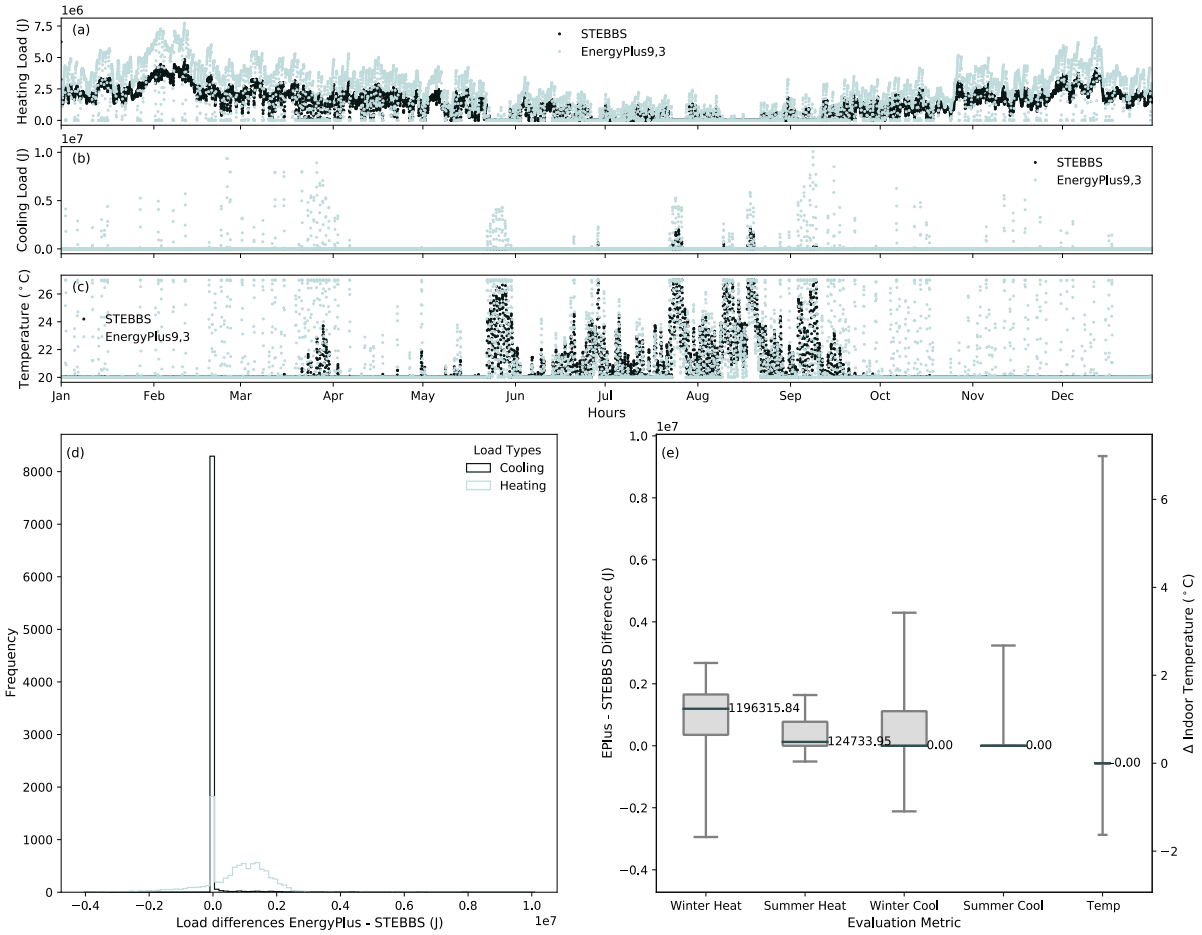

Figure B-2: BESTEST Case 600 is used with London weather data to evaluate STEBBS relative to EnergyPlus at an hourly time scale for 2012 (**a**) heating and (**b**) cooling loads (J), (**c**) indoor air temperature (**d**) frequency distribution of hourly differences between EnergyPlus and STEBBS for heating and cooling loads, (**e**) inter quartile range of hourly differences in winter (Jan, Feb, Mar, Oct, Nov, Dec) and summer (May, Jun, Jul, Aug) loads, and indoor temperatures (whiskers 1% and 99%).

Appendix C DASH building energy parameter values

Table C-1: Appliances used in domestic and workplace subareas and their attributes. Usage categories: Active only (AO) consume energy as a results of user activities; Active with standby (AS) consume less when not in active use (standby); Continuous (C) have constant power consumption independent of human activity (cycling appliance power converted to continuous). See Table 3-3 for references.

Appliance	***Attributed activity***	***Usage category***	***Power rating (W)***	***Standby power rating (W)***	***Proportion on standby***	***Market permeation***
Domestic appliances						
Oven	Food preparation	AO	2125	-	-	0.616
TV	Watching TV	AS	124	3	1	0.977
Desktop	Computer use	AS	100	20	1	0.35
Laptop	Computer use	AS	70	10	1	0.71
Iron	Ironing	AO	1000	-	-	0.9
Washing machine	Laundry	AS	792	1	0.5	0.93
Chest fridge	-	C	38	-	-	1
Small appliance (generic)	-	C	2	-	-	
Lighting (single bulb)	Active	AO	43	-	-	-
Workplace appliances						
Office “desk”	At work	AS	250	25	0.5	per worker
Office background (e.g. IT equipment)	-	C	230	-	-	per worker
Lighting	At work	AS	120	120	0.5	per worker

Table C-2: Properties used in STEBBS vary by property age (<1965, > 1965), type (HB - house & bungalow; flat), component (roof etc) for (**a**) building fabric, (**b**) DHW and (**c**) external ground. $\boldsymbol{L}$: thickness (m); $\boldsymbol{\varepsilon}$: emissivity; $\boldsymbol{\tau}$: effective transmissivity; $\boldsymbol{\Theta}$: surface albedo; $\boldsymbol{k_e}$: effective thermal conductivity (W m^{-1} K^{-1}); $\boldsymbol{\rho}$: density (kg m^{-3}); $\boldsymbol{c_p}$: specific heat capacity (J kg^{-1} K^{-1}) (Internal Air 1005); $\boldsymbol{h}$: convection coefficient (Int: internal, Ext: external) (W m^{-2} K^{-1}); $\boldsymbol{V_{FR}}$: volumetric flow rate of DHW per water user (dom: domestic, n-dom: non-domestic) (10^{-3} m^3 s^{-1}); $\boldsymbol{V_R}$: ventilation rate (10^{-3} m^3 s^{-1}); $\boldsymbol{V_T}$: DHW tank volume (m^3); **WWR**: window-to-wall ratio (0.4). Vessels: all other storage of DHW. For data sources refer to Table 3-3. [a] varies with wind speed. [b] per water user.

(a) Building fabric		*Roof & wall*		*Window*	*Ground Floor*	*Internal Mass*
		HB	*Flat*			
L	< 1965	0.241	0.327	0.005	0.5	-
	> 1965	0.373	0.373	0.02	0.5	-
k_e	< 1965	0.835	0.837	1.05	0.752	0.121
	> 1965	0.104	0.104	0.041	0.690	0.121
ρ	< 1965	1690	1692	2500	1540	873.7
	> 1965	1076	1076	1000.7	1470	873.7
c_p	< 1965	804.1	803.1	840	1012.8	967.9
	> 1965	865.9	865.9	902.4	1016	967.9
h	Int.	3	3	3	2.8	3
	Ext.	var[a]	var[a]	var[a]	-	-
Θ		0.4	0.4	0.05	-	0
ε		0.9	0.9	0.88	-	0.91
τ		0	0	0.9	-	0
V_R		600				

(b) DHW		*Tank*	*Vessel*	*People residence^{-1}*	*V_T (m^3)*
L (m)		0.055	0.0047	1	0.115
ε		0.9	0.91	2	0.115
k_e		0.0275	0.16	3	0.125
ρ		745.55	1380	4	0.148
c_p		1380	1380	5	0.17
h	Int.	243	243	6	0.18
	Ext.	3	3	*(c)*	*Ground*
V_{FR}[b]	dom	0.183	0.1372	L	2
	n-dom	0.15	0.1125	k_e	1.28

Appendix D Code availability/Data availability

All code and data are deposited at https://doi.org/10.5281/zenodo.3745523.

Table D-1: Data examples. More details (example structure, units, raw data source, location in repository and location of use in code) can be found at https://doi.org/10.5281/zenodo.3745523.

Filename		File type	Definition
(i) Population			
a	age_groups	csv	Population of each age group in each A_N
b	allworkers	csv	Residential and workplace spatial unit relation
c	area_hierarchy	csv	List of A_N in the larger, containing, spatial unit (B)
d	daytype	csv	Dates used by run and corresponding day of year and day type
e	SchoolWorkShopcap	csv	School and workplace populations and shops and 'other' subarea capacities for each A_N
(ii) Transport			
a	SpatialUnitRoadLengths	csv	L_r in each B
b	average_passengers	csv	Average number of people in a single *m* vehicle
c	distance_freqs	csv	Journey distance categories and their respective mode weightings
d	fuel_consumption	csv	Average urban fuel consumption for urban roads for vehicle stock (g km^{-1})
e	fuel_ratio	csv	Proportions of each *m* using each *f*
f	IntraBorDist/*x*matrix	csv	Distance matrix for distance between A_N centroids in B
g	IndivBor/*x*h_wsorted	csv	Proportions of people using each mode to travel from home to work
h	IndivBor/*x*w_hsorted	csv	Proportions of people using each mode to travel from work to home
i	MeanSpeedLimits	csv	Mean $v_{r,lim}$ for each *r* in each B
j	RoadAADTMeansLengthWeighted	csv	AADT means of each *r*, mode for each B
k	routes_distances	csv	List of route segment distances for each spatial unit traversed for each route
l	routes_int	csv	List of routes between each start-destination pair, including the spatial units traversed for each route
m	route_reference_matrix	csv	Reference matrix for route numbers
n	ShopsGravity	csv	Gravity weightings (eq. 3-3) for travel to shops and other subareas
o	speed_fuel_ratio_func	pickle	Functions of normalised speed - fuel consumption relation for each *m*
p	traveltime_functions	pickle	Functions relating distance to time travelled for each mode
q	vehicle_length (in settings.nml)	-	Length of representative vehicle
(iii) Area			
a	env_vars	csv	Environmental variables used for each time step
b	IndustrialOAs	csv	Location of industrial land use around the study area

c	OA_area_details	csv	Population, road length, building stock and dimensions, floor plan area data for each A_N
(iv) Buildings			
a	CommBuildingArchetype	nml	Multiple *.nml* lists for each commercial building archetype and their STEBBS parameters
b	CommTypes	nml	Multiple *.nml* lists for each school/shops/other land use type and their parameters
c	DomApplianceList	nml	Multiple *.nml* lists for appliances used by occupants in domestic buildings, and their parameters
d	DomBuildingArchetype	nml	Multiple *.nml* lists for each commercial building archetype and their STEBBS parameters
e	domlighting	nml	Parameters for domestic lighting
f	WorkApplianceList	nml	Multiple *.nml* lists for appliances used by occupants in commercial buildings, and their parameters
g	*x*personactiveweekend/day	csv	Proportions of people active (awake and present) in households with *x* people present at each time step
h	*x*personweekend/day	csv	Proportions of people who belong to household of size *x* present in household at each time step, given that someone is present

Appendix E DASH output files

Table E-1: Output files generated by a DASH run for the movementtravel and energyQfcalcs DASH components (Appendix F). Some files are for each day of year (DOY) or date (YYYY-MM-DD)

	Filename	**File type**	**Definition**
(i) Movement and travel			
a	{DOY}results.pkl	pkl	Number of people in each A_N and a_S^N (two-level index, rows) at each time step (columns) for DOY.
b	{DOY}travel.pkl	csv	Dictionary of number of passengers. Keys are mode names, values are number of passengers using such mode for each spatial unit (row) and time step (columns) for DOY.
c	{DOY}density.pkl	csv	Matrix of vehicle density (veh km^{-1}) for each spatial unit (rows) and time step (columns) for DOY.
(ii) Q_F estimation			
a	<YYYY-MM-DD>results.nc	netcdf4	(primarily) Q_F results. Variables are detailed in Table E-2
b	nhood_list	csv	Order of A_N IDs used for run in Q_F output (Table E-2.iia)
c	run_settings	nml	Copy of the input setting file

Table E-2: Variables within the main output file (Table E-1.iia).

Variable		Units	Definition
(i) Movement and travel			
a	qfb_dom_air	W m^{-2}	$Q_{F,B}$ through domestic building fabric to the outdoor air
b	qfb_dom_gr	W m^{-2}	$Q_{F,B}$ through domestic building fabric to the ground
c	*qfb_dom_tot*	W m^{-2}	Total $Q_{F,B}$ through domestic building fabric to the outdoor environment
d	*qfm_dom*	W m^{-2}	$Q_{F,M}$ within domestic buildings
e	*qfb_work_air*	W m^{-2}	$Q_{F,B}$ through non-domestic building fabric to the outdoor air
f	*qfb_work_gr*	W m^{-2}	$Q_{F,B}$ through non-domestic building fabric to the ground
g	*qfb_work_tot*	W m^{-2}	Total $Q_{F,B}$ through non-domestic building fabric to the outdoor environment
h	*qfm_work*	W m^{-2}	$Q_{F,M}$ within non-domestic buildings
i	*qft*	W m^{-2}	Total $Q_{F,T}$
j	*qfmt*	W m^{-2}	$Q_{F,M}$ from passengers in transport
k	*dom_energy*	W	Power demand of appliances and lighting in domestic buildings
l	*work_energy*	W	Power demand from appliances and lighting in non-domestic buildings
m	*qheat_dom*	W	Heating power demand in domestic buildings
n	*qcool_dom*	W	Cooling power demand in domestic buildings
o	*qheat_work*	W	Heating power demand in non-domestic buildings
p	*qcool_work*	W	Cooling power demand in non-domestic buildings
q	*qfb_dhw*	W	Power demand from hot water use in domestic buildings
r	*qfb_work_hw*	W	Power demand from hot water use in non-domestic buildings

Appendix F Flow diagrams of DASH operation

The following diagrams demonstrate the operation of DASH for the implementations used in this thesis (Chapter 3). The model comprises four main components (Figure 3-2Figure 3-2): data processing (Figure F-1), which converts the appropriate raw data to input data for other components (1.dataprocessing); agent interaction (Section 3.2.2, 3.2.3, 3.2.4.2) through the exchange of O_C across the city, as well as resultant travel (2.movementtravel, Figure 3-3a, F-2, F-5); agent response to occupancy levels (Section 3.2.4.2) through the energy use and its release (via STEBBS, Appendix B) to the outdoor environment (3.energyQfcalcs, Figure 3-3b, F-3, F-4, F-6); and visualisation of results (4.visualisation). The agent interaction and response components are separated in order to facilitate quicker running times.

Table F-1: Simulation run times for DASH model components for runs involving 25053 agents across Greater London. Full simulation requires results from both components, which may be run separately so that results from 2.movementtravel can be used in multiple simulations for 3.energyQfcalcs. Multiple cores should be used to run multiple days (DASH) or spatial units (U and V-schemes).

Component	Spin-up simulation days	Simulated days	Total simulated days	Run time (HH:MM:SS)	No. of spatial units
2.movementtravel	-	3	3	01:13:14	25053
3.energyQfcalcs	1	2	3	03:11:04	25053
SUEWS: U-scheme	365	365	730	00:06:00	1
SUEWS: V-scheme	365	365	730	00:01:53	1

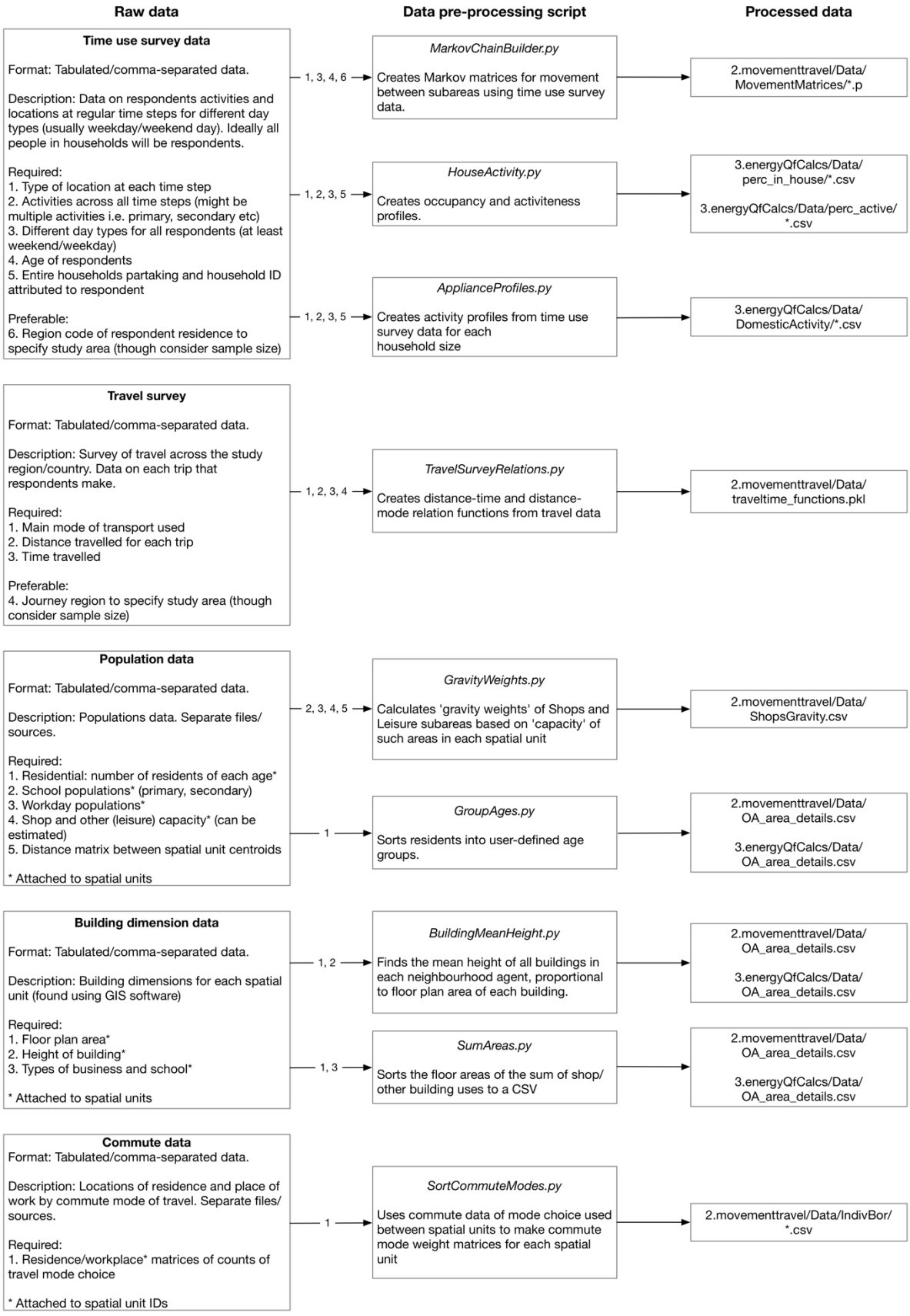
Raw data
Data pre-processing script
Processed data
Time use survey data
Format: Tabulated/comma-separated data.
Description: Data on respondents activities and locations at regular time steps for different day types (usually weekday/weekend day). Ideally all people in households will be respondents.
Required:
1. Type of location at each time step
2. Activities across all time steps (might be multiple activities i.e. primary, secondary etc)
3. Different day types for all respondents (at least weekend/weekday)
4. Age of respondents
5. Entire households partaking and household ID attributed to respondent
Preferable:
6. Region code of respondent residence to specify study area (though consider sample size)
1, 3, 4, 6
MarkovChainBuilder.py
Creates Markov matrices for movement between subareas using time use survey data.
2.movementtravel/Data/MovementMatrices/*.p
1, 2, 3, 5
HouseActivity.py
Creates occupancy and activiteness profiles.
3.energyQfCalcs/Data/perc_in_house/*.csv
3.energyQfCalcs/Data/perc_active/*.csv
1, 2, 3, 5
ApplianceProfiles.py
Creates activity profiles from time use survey data for each household size
3.energyQfCalcs/Data/DomesticActivity/*.csv
Travel survey
Format: Tabulated/comma-separated data.
Description: Survey of travel across the study region/country. Data on each trip that respondents make.
Required:
1. Main mode of transport used
2. Distance travelled for each trip
3. Time travelled
Preferable:
4. Journey region to specify study area (though consider sample size)
1, 2, 3, 4
TravelSurveyRelations.py
Creates distance-time and distance-mode relation functions from travel data
2.movementtravel/Data/traveltime_functions.pkl
Population data
Format: Tabulated/comma-separated data.
Description: Populations data. Separate files/sources.
Required:
1. Residential: number of residents of each age*
2. School populations* (primary, secondary)
3. Workday populations*
4. Shop and other (leisure) capacity* (can be estimated)
5. Distance matrix between spatial unit centroids
* Attached to spatial units
2, 3, 4, 5
GravityWeights.py
Calculates 'gravity weights' of Shops and Leisure subareas based on 'capacity' of such areas in each spatial unit
2.movementtravel/Data/ShopsGravity.csv
1
GroupAges.py
Sorts residents into user-defined age groups.
2.movementtravel/Data/OA_area_details.csv
3.energyQfCalcs/Data/OA_area_details.csv
Building dimension data
Format: Tabulated/comma-separated data.
Description: Building dimensions for each spatial unit (found using GIS software)
Required:
1. Floor plan area*
2. Height of building*
3. Types of business and school*
* Attached to spatial units
1, 2
BuildingMeanHeight.py
Finds the mean height of all buildings in each neighbourhood agent, proportional to floor plan area of each building.
2.movementtravel/Data/OA_area_details.csv
3.energyQfCalcs/Data/OA_area_details.csv
1, 3
SumAreas.py
Sorts the floor areas of the sum of shop/other building uses to a CSV
2.movementtravel/Data/OA_area_details.csv
3.energyQfCalcs/Data/OA_area_details.csv
Commute data
Format: Tabulated/comma-separated data.
Description: Locations of residence and place of work by commute mode of travel. Separate files/sources.
Required:
1. Residence/workplace* matrices of counts of travel mode choice
* Attached to spatial unit IDs
1
SortCommuteModes.py
Uses commute data of mode choice used between spatial units to make commute mode weight matrices for each spatial unit
2.movementtravel/Data/IndivBor/*.csv

Figure F-1 continued next page

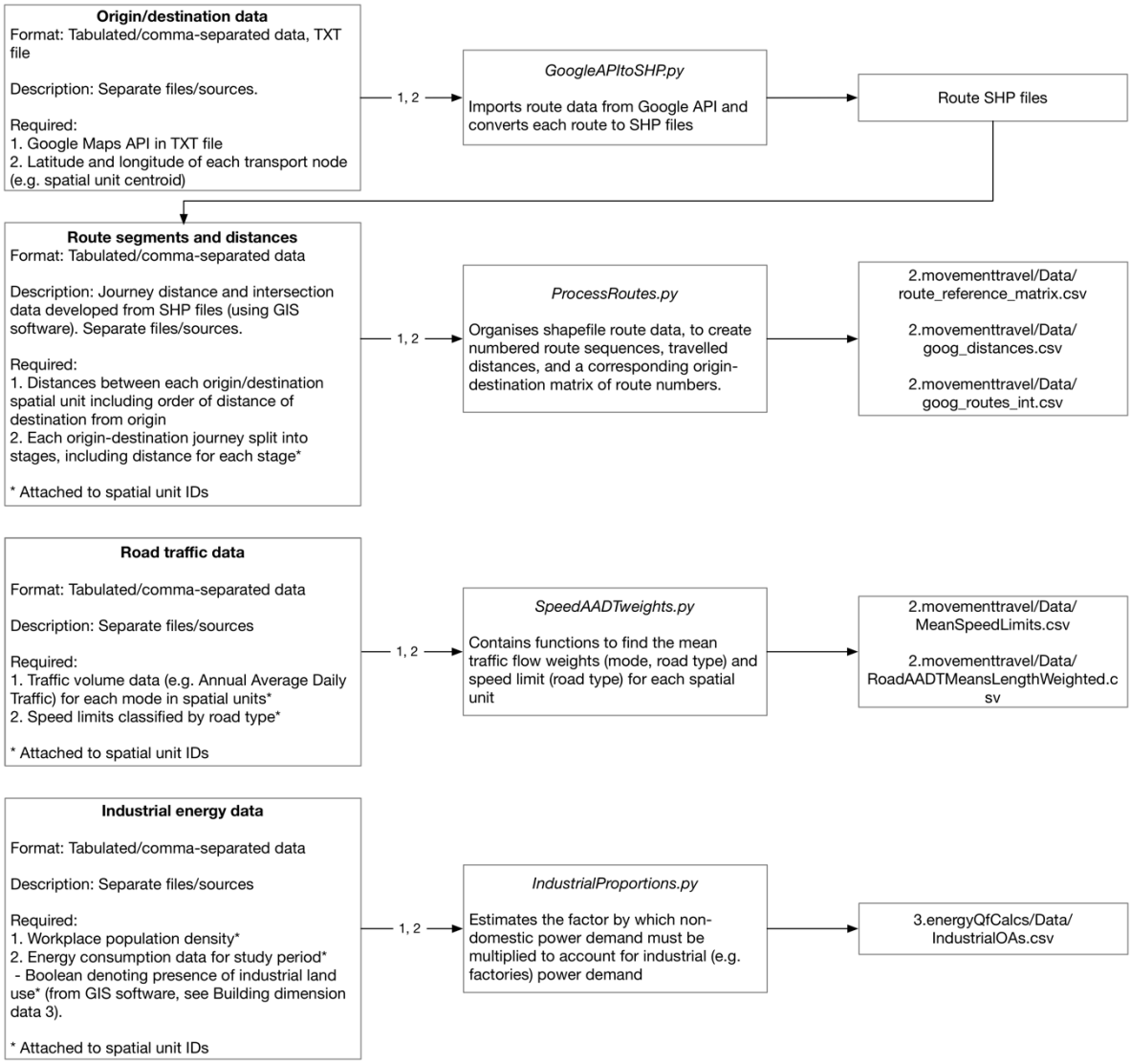

Figure F-1: All data processed in the 1.dataprocessing component. Raw data information (left column) includes required format, description of data, and required and preferable data. Data pre-processing script (middle column) information includes the script name (within the 1.dataprocessing component) and definition of processes within. Processed data (right data) shows the filepath and name of processed data.

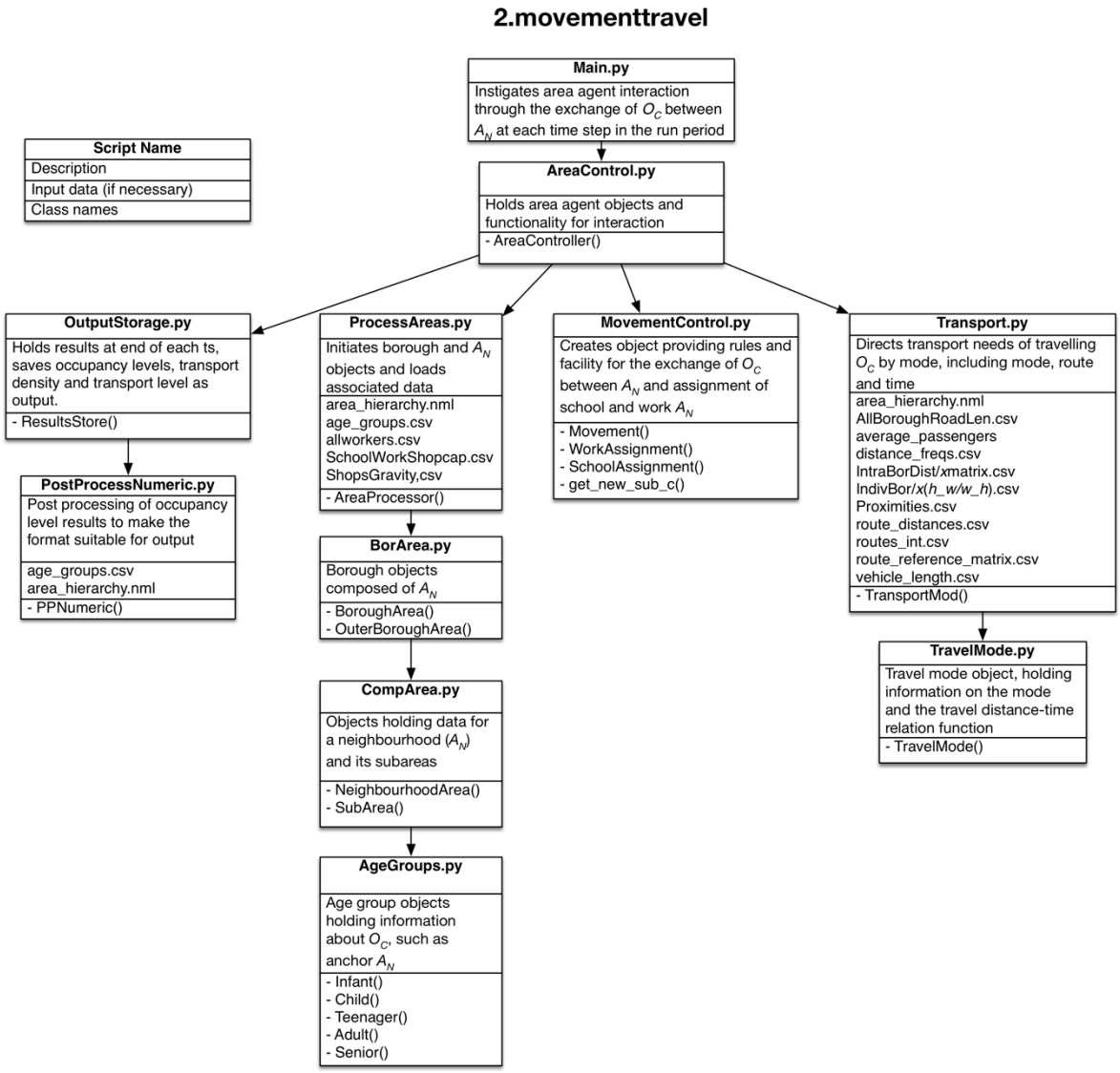

Figure F-2: Dependency diagram of scripts within the 2.movementtravel component, including description of script functionality, input data required by script and names of class objects within.

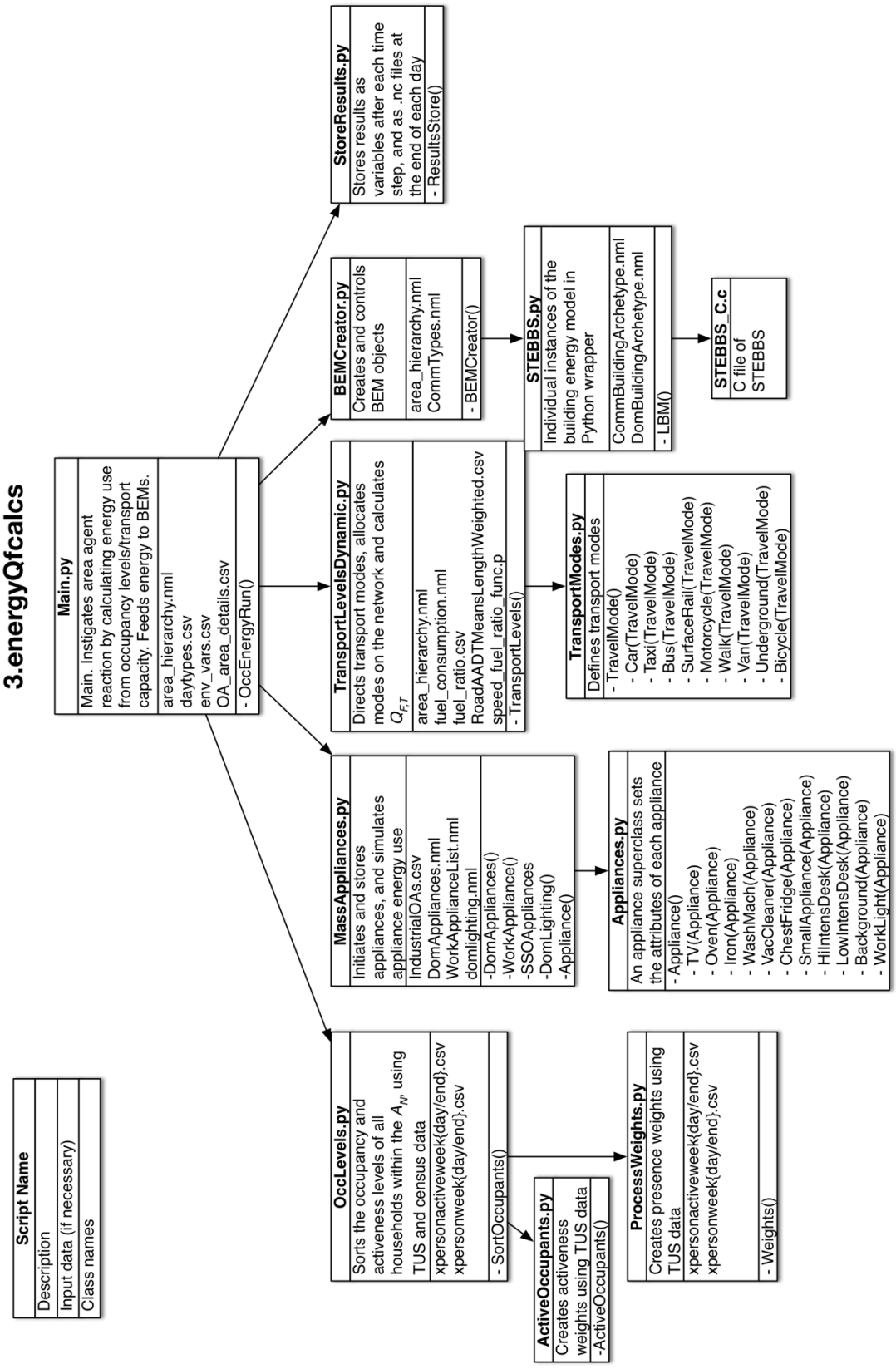

Figure F-3: Dependency diagram of scripts within the 3.energyQfcalcs component, including description of script functionality, input data required by script and names of class objects within.

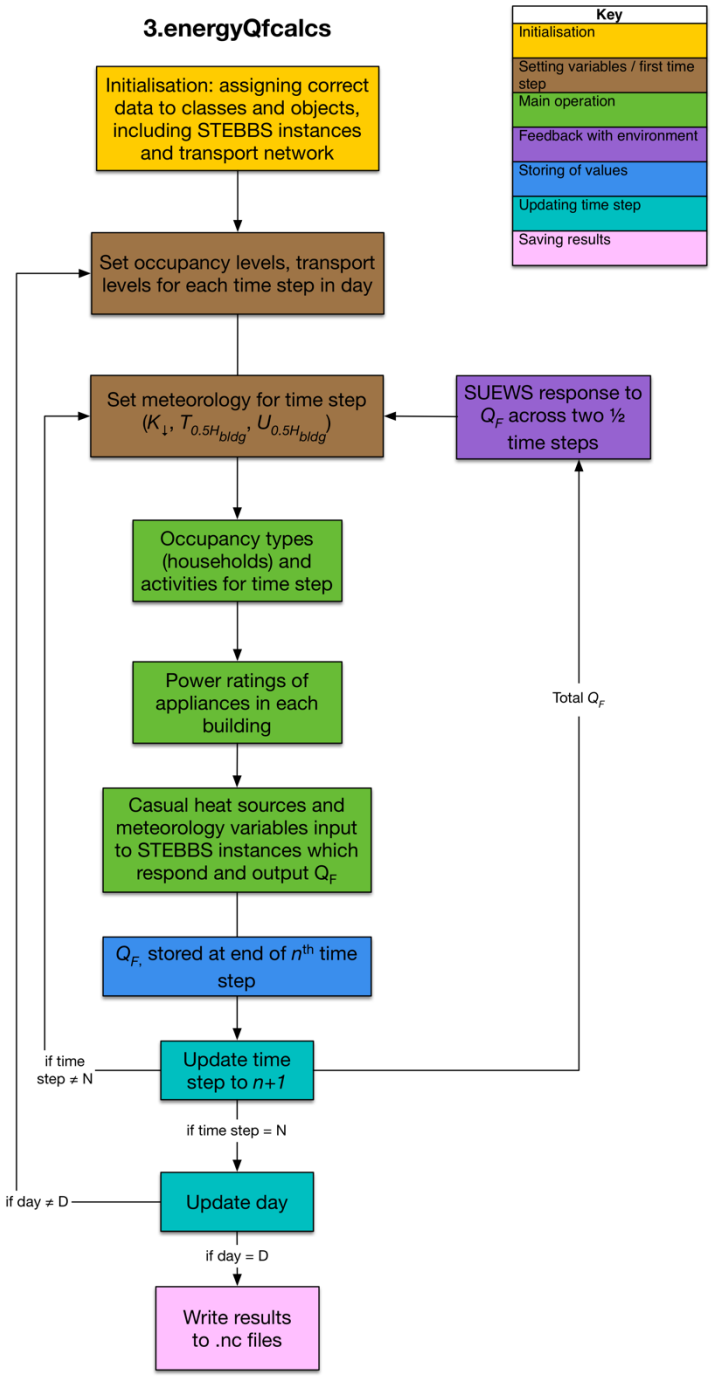

Figure F-4: Flow diagram of the basic processes within a total run of the agent reaction component 3.energyQfcalcs through N time steps and D days (DASH v1.1), including the coupling with SUEWS (Figure 4-3). This coupling provides feedbacks between Q_F and outdoor air temperature and wind speed, both at half building height (Section 4.3.3.2). Each process step is colour-coded by process type.

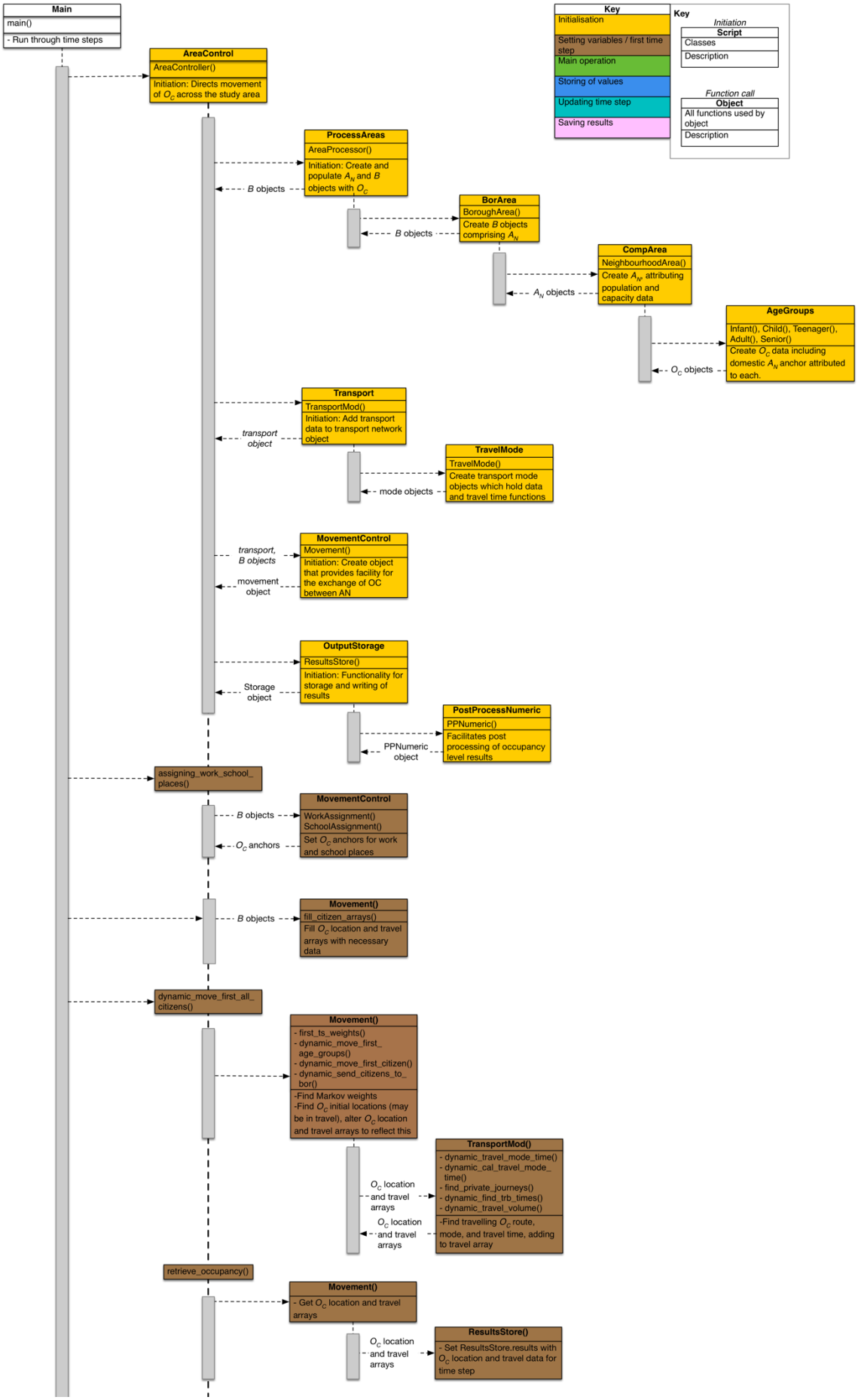
Main
main()
- Run through time steps
AreaControl
AreaController()
Initiation: Directs movement of O_C across the study area
ProcessAreas
AreaProcessor()
Initiation: Create and populate A_N and B objects with O_C
B objects
BorArea
BoroughArea()
Create B objects comprising A_N
B objects
CompArea
NeighbourhoodArea()
Create A_N, attributing population and capacity data
A_N objects
AgeGroups
Infant(), Child(), Teenager(), Adult(), Senior()
Create O_C data including domestic A_N anchor attributed to each.
O_C objects
Transport
TransportMod()
Initiation: Add transport data to transport network object
transport object
TravelMode
TravelMode()
Create transport mode objects which hold data and travel time functions
mode objects
transport, B objects
MovementControl
Movement()
Initiation: Create object that provides facility for the exchange of OC between AN
movement object
OutputStorage
ResultsStore()
Initiation: Functionality for storage and writing of results
Storage object
PostProcessNumeric
PPNumeric()
Facilitates post processing of occupancy level results
PPNumeric object
assigning_work_school_places()
MovementControl
WorkAssignment()
SchoolAssignment()
Set O_C anchors for work and school places
B objects
O_C anchors
Movement()
fill_citizen_arrays()
Fill O_C location and travel arrays with necessary data
B objects
dynamic_move_first_all_citizens()
Movement()
- first_ts_weights()
- dynamic_move_first_age_groups()
- dynamic_move_first_citizen()
- dynamic_send_citizens_to_bor()
-Find Markov weights
-Find O_C initial locations (may be in travel), alter O_C location and travel arrays to reflect this
TransportMod()
- dynamic_travel_mode_time()
- dynamic_cal_travel_mode_time()
- find_private_journeys()
- dynamic_find_trb_times()
- dynamic_travel_volume()
-Find travelling O_C route, mode, and travel time, adding to travel array
O_C location and travel arrays
O_C location and travel arrays
retrieve_occupancy()
Movement()
- Get O_C location and travel arrays
O_C location and travel arrays
ResultsStore()
- Set ResultsStore.results with O_C location and travel data for time step
Key
Initialisation
Setting variables / first time step
Main operation
Storing of values
Updating time step
Saving results
Key
Initiation
Script
Classes
Description
Function call
Object
All functions used by object
Description

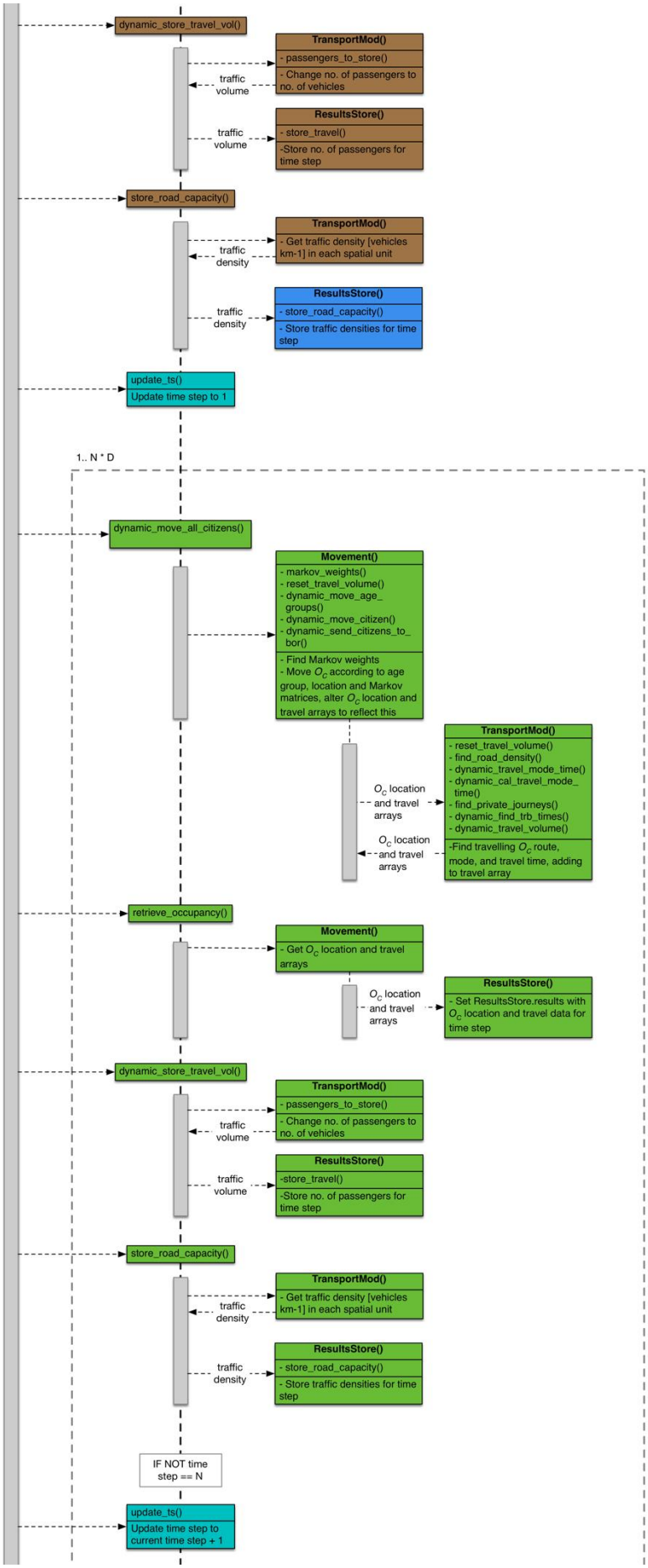
dynamic_store_travel_vol()
TransportMod()
- passengers_to_store()
- Change no. of passengers to no. of vehicles
traffic volume
ResultsStore()
- store_travel()
-Store no. of passengers for time step
traffic volume
store_road_capacity()
TransportMod()
- Get traffic density [vehicles km-1] in each spatial unit
traffic density
ResultsStore()
- store_road_capacity()
- Store traffic densities for time step
traffic density
update_ts()
Update time step to 1
1.. N * D
dynamic_move_all_citizens()
Movement()
- markov_weights()
- reset_travel_volume()
- dynamic_move_age_groups()
- dynamic_move_citizen()
- dynamic_send_citizens_to_bor()
- Find Markov weights
- Move O_C according to age group, location and Markov matrices, alter O_C location and travel arrays to reflect this
O_C location and travel arrays
TransportMod()
- reset_travel_volume()
- find_road_density()
- dynamic_travel_mode_time()
- dynamic_cal_travel_mode_time()
- find_private_journeys()
- dynamic_find_trb_times()
- dynamic_travel_volume()
-Find travelling O_C route, mode, and travel time, adding to travel array
O_C location and travel arrays
retrieve_occupancy()
Movement()
- Get O_C location and travel arrays
O_C location and travel arrays
ResultsStore()
- Set ResultsStore.results with O_C location and travel data for time step
dynamic_store_travel_vol()
TransportMod()
- passengers_to_store()
- Change no. of passengers to no. of vehicles
traffic volume
ResultsStore()
-store_travel()
-Store no. of passengers for time step
traffic volume
store_road_capacity()
TransportMod()
- Get traffic density [vehicles km-1] in each spatial unit
traffic density
ResultsStore()
- store_road_capacity()
- Store traffic densities for time step
traffic density
IF NOT time step == N
update_ts()
Update time step to current time step + 1

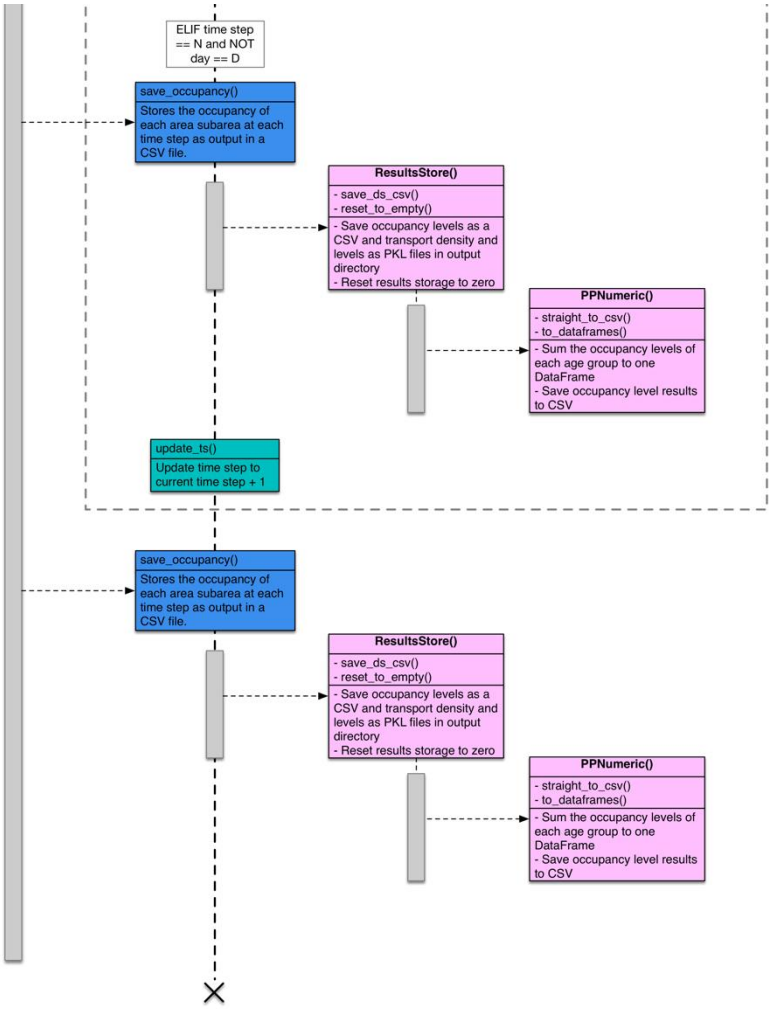

Figure F-5: Sequence diagram of processes in DASH (v1.0; Capel-Timms et al., 2020a) agent interaction component 2.movementtravel, detailing each function and interactions through N time steps and D days. Each process step is colour-coded by process type.

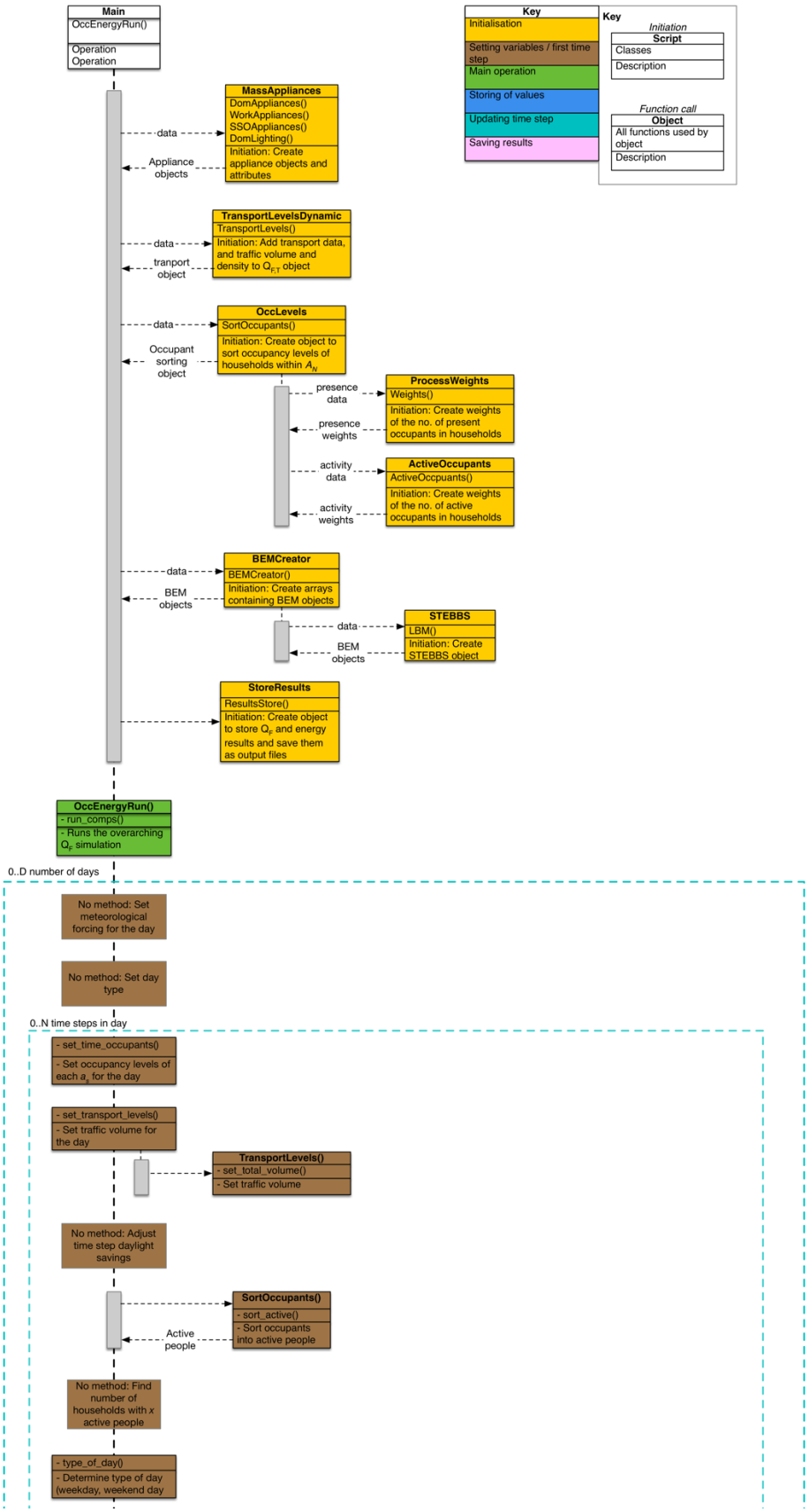
Main
OccEnergyRun()
Operation
Operation
Key
Initialisation
Setting variables / first time step
Main operation
Storing of values
Updating time step
Saving results
Key
Initiation
Script
Classes
Description
Function call
Object
All functions used by object
Description
MassAppliances
DomAppliances()
WorkAppliances()
SSOAppliances()
DomLighting()
Initiation: Create appliance objects and attributes
data
Appliance objects
TransportLevelsDynamic
TransportLevels()
Initiation: Add transport data, and traffic volume and density to $Q_{E,T}$ object
data
tranport object
OccLevels
SortOccupants()
Initiation: Create object to sort occupancy levels of households within A_N
data
Occupant sorting object
ProcessWeights
Weights()
Initiation: Create weights of the no. of present occupants in households
presence data
presence weights
ActiveOccupants
ActiveOccpuants()
Initiation: Create weights of the no. of active occupants in households
activity data
activity weights
BEMCreator
BEMCreator()
Initiation: Create arrays containing BEM objects
data
BEM objects
STEBBS
LBM()
Initiation: Create STEBBS object
data
BEM objects
StoreResults
ResultsStore()
Initiation: Create object to store Q_E and energy results and save them as output files
OccEnergyRun()
- run_comps()
- Runs the overarching Q_E simulation
0..D number of days
No method: Set meteorological forcing for the day
No method: Set day type
0..N time steps in day
- set_time_occupants()
- Set occupancy levels of each a_x for the day
- set_transport_levels()
- Set traffic volume for the day
TransportLevels()
- set_total_volume()
- Set traffic volume
No method: Adjust time step daylight savings
SortOccupants()
- sort_active()
- Sort occupants into active people
Active people
No method: Find number of households with x active people
- type_of_day()
- Determine type of day (weekday, weekend day

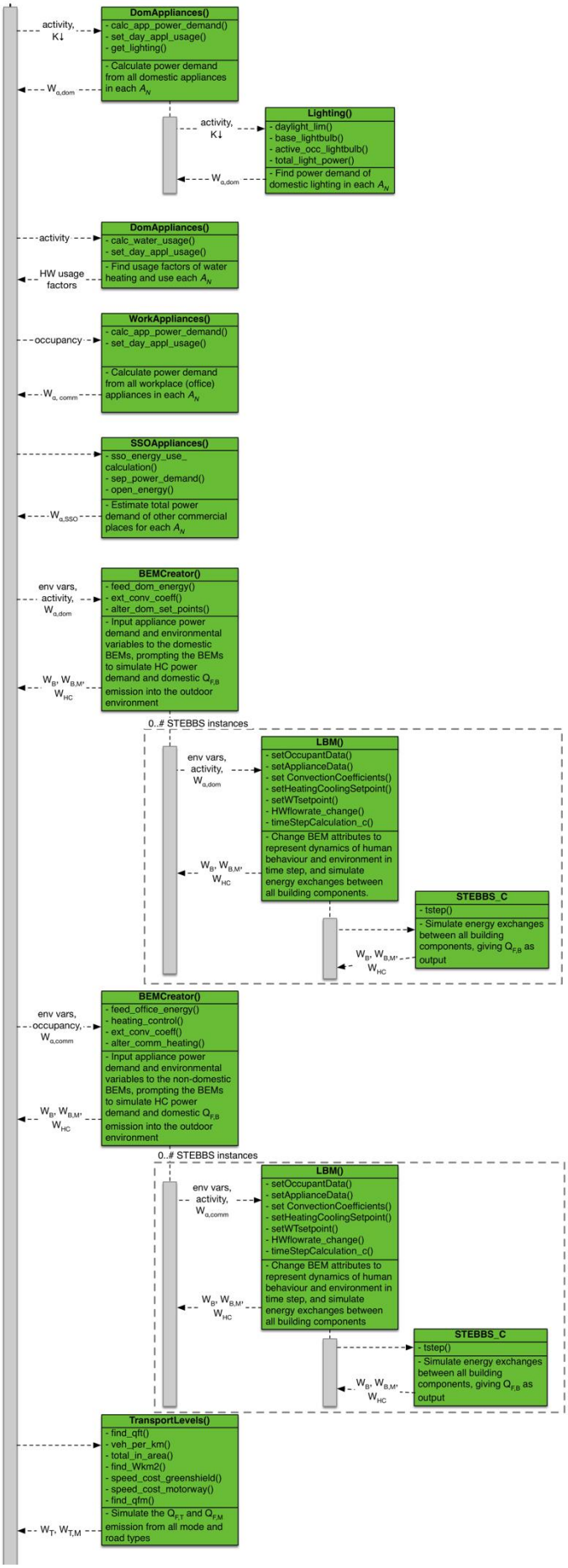
DomAppliances()
- calc_app_power_demand()
- set_day_appl_usage()
- get_lighting()
- Calculate power demand from all domestic appliances in each A_N
activity, K↓
$W_{a,dom}$
Lighting()
- daylight_lim()
- base_lightbulb()
- active_occ_lightbulb()
- total_light_power()
- Find power demand of domestic lighting in each A_N
DomAppliances()
- calc_water_usage()
- set_day_appl_usage()
- Find usage factors of water heating and use each A_N
activity
HW usage factors
WorkAppliances()
- calc_app_power_demand()
- set_day_appl_usage()
- Calculate power demand from all workplace (office) appliances in each A_N
occupancy
$W_{a, comm}$
SSOAppliances()
- sso_energy_use_ calculation()
- sep_power_demand()
- open_energy()
- Estimate total power demand of other commercial places for each A_N
$W_{a,SSO}$
BEMCreator()
- feed_dom_energy()
- ext_conv_coeff()
- alter_dom_set_points()
- Input appliance power demand and environmental variables to the domestic BEMs, prompting the BEMs to simulate HC power demand and domestic $Q_{F,B}$ emission into the outdoor environment
env vars, activity, $W_{a,dom}$
W_B, $W_{B,M}$, W_{HC}
0..# STEBBS instances
LBM()
- setOccupantData()
- setApplianceData()
- set ConvectionCoefficients()
- setHeatingCoolingSetpoint()
- setWTsetpoint()
- HWflowrate_change()
- timeStepCalculation_c()
- Change BEM attributes to represent dynamics of human behaviour and environment in time step, and simulate energy exchanges between all building components.
env vars, activity, $W_{a,dom}$
W_B, $W_{B,M}$, W_{HC}
STEBBS_C
- tstep()
- Simulate energy exchanges between all building components, giving $Q_{F,B}$ as output
W_B, $W_{B,M}$, W_{HC}
BEMCreator()
- feed_office_energy()
- heating_control()
- ext_conv_coeff()
- alter_comm_heating()
- Input appliance power demand and environmental variables to the non-domestic BEMs, prompting the BEMs to simulate HC power demand and domestic $Q_{F,B}$ emission into the outdoor environment
env vars, occupancy, $W_{a,comm}$
W_B, $W_{B,M}$, W_{HC}
0..# STEBBS instances
LBM()
- setOccupantData()
- setApplianceData()
- set ConvectionCoefficients()
- setHeatingCoolingSetpoint()
- setWTsetpoint()
- HWflowrate_change()
- timeStepCalculation_c()
- Change BEM attributes to represent dynamics of human behaviour and environment in time step, and simulate energy exchanges between all building components
env vars, activity, $W_{a,comm}$
W_B, $W_{B,M}$, W_{HC}
STEBBS_C
- tstep()
- Simulate energy exchanges between all building components, giving $Q_{F,B}$ as output
W_B, $W_{B,M}$, W_{HC}
TransportLevels()
- find_qft()
- veh_per_km()
- total_in_area()
- find_Wkm2()
- speed_cost_greenshield()
- speed_cost_motorway()
- find_qfm()
- Simulate the $Q_{F,T}$ and $Q_{F,M}$ emission from all mode and road types
W_T, $W_{T,M}$

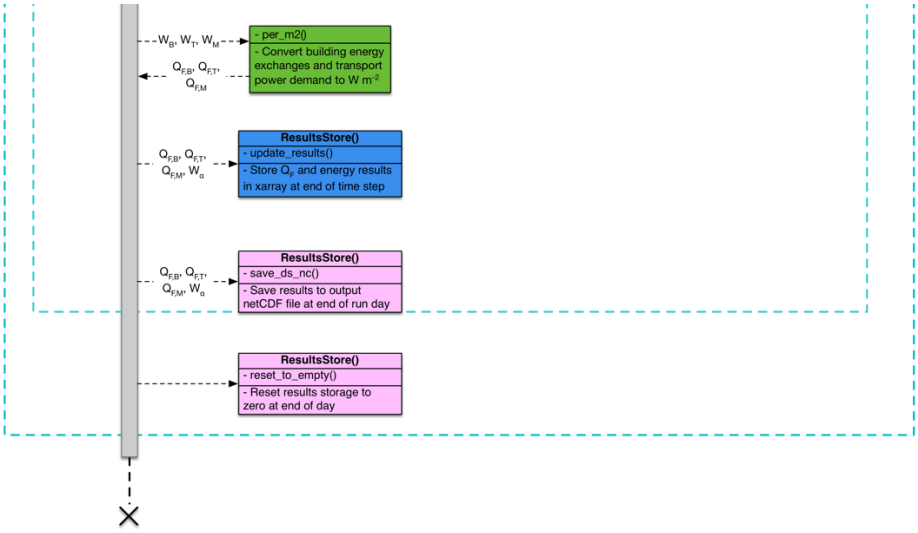

Figure F-6: Sequence diagram of processes in DASH (v1.0; Capel-Timms et al., 2020a) agent interaction component 3.energyQfcalcs, detailing each function and interactions through N time steps and D days. Each process step is colour-coded by process type.

Appendix G Construction of building components used in STEBBS

Table G-1: Thermal properties of separate materials in composite building components used in STEBBS for DASH (v1.0, 1.1). For data sources and total values see Table 3-4

Material	**Length (mm)**	**Density (kg m^{-3})**	**Effective conductivity (W m^{-1} K^{-1})**	**Specific heat capacity (J kg^{-1} K^{-1})**
Pre-1965 house external wall				
Exposed brick	216	1700	0.84	800
Lime plaster	25	1600	0.8	840
Pre-1965 flat external wall				
Exposed brick	302	1700	0.84	800
Lime plaster	25	1600	0.8	840
Post-1965 external wall				
Exposed brick	105	1750	0.77	1000
Air cavity	75	1.23	0.025	1004
Concrete medium weight block	180	1150	0.40	840
Gypsum plaster	13	1200	0.51	960
Ground floor pre-1965				
Carpet & underlay	10	200	0.6	1300
Screed	75	1200	0.46	1000
Cast concrete	150	1800	1.13	1000
Ground floor pre-1965				
Carpet & underlay	10	200	0.6	1300
Screed	75	1200	0.46	1000
Cast concrete	100	1800	1.13	1000
Internal wall				
Plaster	22	720	0.23	840
Aggregate block	175	600	0.2	840
Internal floor				
Carpet	4	200	0.6	1300
Screed	60	1200	0.46	1000
Insulation	140	12	0.042	1030
Concrete	180	1760	0.66	840
Acoustic tile	20	290	0.057	1340
Single glazed window (pre -1965)				
Soda lime glass	5	2500	1.05	840
Double glazed window (post -1965)				
Soda lime glass	8	2500	1.05	840
Air	12	1.23	0.025	1004
Domestic hot water tank				
Steel	5	8000	16	840
Polyurethane foam	50	30	0.025	1470

Appendix H Meteorological data used to force SUEWS

ERA5 data (Hersbach et al., 2020) are available at multiple vertical levels (user-defined) at 0.125° × 0.125° (~8.6 km × ~13.8 km in London) horizontal resolution and 1 h temporal resolution (Hersbach et al., 2020). These are downscaled to 5 min by SuPy using linear interpolation between the 1 h values for all variables except rainfall, for which the hourly value is evenly distributed across the 5 min timesteps for that hour. After linear interpolation of $K_{\downarrow}$, values are checked to ensure energy is conserved.

As SUEWS is a local scale urban land surface model, the forcing data need to be provided at a forcing height z_m above the roughness sublayer (RSL), which extends from ground level to 2–5z_H (where z_H is mean building height) and is characterised by the turbulent flow caused by roughness elements (e.g. buildings and trees). Above the RSL (at blending height z_r), and within the inertial sublayer (ISL), measurements are considered spatially averaged (Oke, 1988). z_m must be found for each spatial unit ($z_{m,s.u.}$) to account for spatial differences in height.

Both the ground elevation and building height vary across London, so it is inappropriate to use a single height above the surface. To estimate where the model forcing should be, one could use estimations via roughness element heights (such as 2–5z_H), but this is unreasonable for changing building densities (Raupach et al., 1991; Claussen, 1995). Therefore this spacing is taken into account (Raupach et al., 1980):

$$z_r = z_H + 1.5(\overline{D_x} - \overline{L_x}) \quad \text{(m)} \tag{H-1}$$

where z_r is the height of the RSL, z_H is the mean building height, and, for number of buildings n_{bldg}, area of spatial unit A and building land cover fraction λ_p:

$$D_x = \sqrt{\frac{A}{n_{bldg}}} \; and \; L_x = \sqrt{\lambda_p \cdot \frac{A}{n_{bldg}}} \tag{H-2}$$

Figure H-1 shows that this scheme fails for some building densities (plotted as a function of λ_p and building frontal area index λ_f). This typically when λ_p is below 0.13, as the flow regime changes from isolated to wake interference flow (Hussain and Lee, 1980; Grimmond and Oke, 1999a). Hence, two schemes are used with the condition:

$$z_{m,s.u.}\,(\text{m}) = \begin{cases} 3z_H + z_s \; when \; \lambda_p \leq 0.13 \\ z_{r(eq.\text{A}-1)} + z_s \; when \; \lambda_p > 0.13 \end{cases} \tag{H-3}$$

where z_s is the height of the spatial unit above sea level. $3z_H$ is a "rule of thumb" value for z_r. Additionally, z_m is capped at the maximum z_m for grids where z_H is greater than 40 m (red points, Figure H-1):

$$ERA5_{diag} = z_{m,s.u.} + z_s \quad \text{(H-4)}$$

Each ERA5 grid is diagnosed at multiple heights. The closest diagnosis height above the estimated RSL height is chosen for each SUEWS grid.

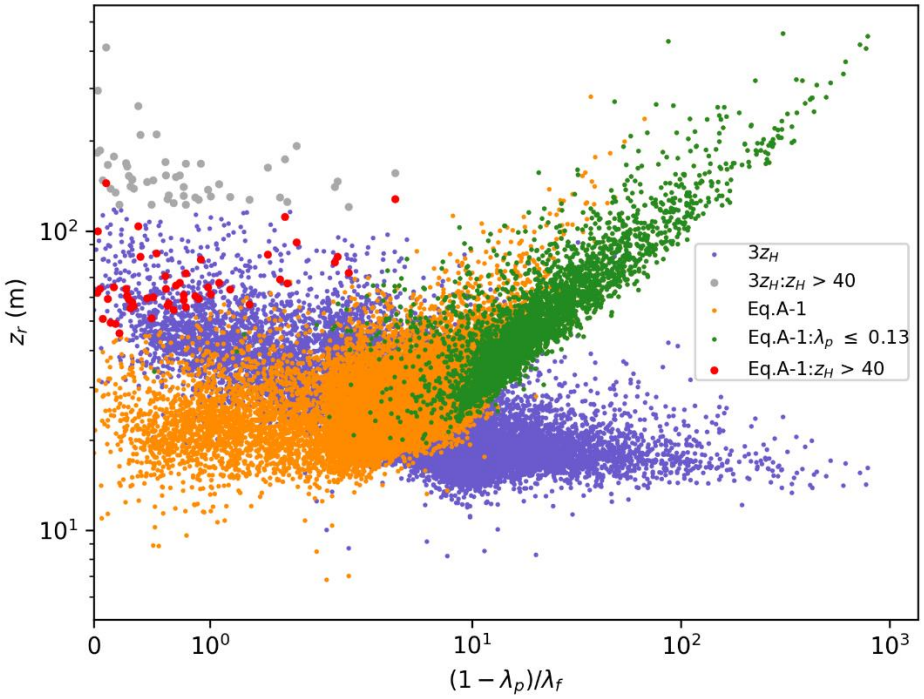

Figure H-1: Comparison of two z_m estimation methods using eq. H-3.

Appendix I MBE density percentiles and IQRs between comparisons VD, UD and UV

The tables in this appendix relate to the percentile lines of MBE density in Figure 4-8 ($Q_{F,d}$), 4-11 ($Q_{H,MM}$), 4-12 ($Q_{E,MM}$ and 4-13 (T_{2m}).

Table I-1: MBE density percentiles (p:1st, 5th, 25th, 75th, 95th and 99th), medians and IQRs for Q_F (W m^{-2}, Figure 4-8), $Q_{H,MM}$ (W m^{-2}, Figure 4-12), $Q_{E,MM}$ (W m^{-2}, Figure 4-13), T_{2m} (°C, Figure 4-14) across comparisons VD, UD and UV in the Central (C) and West (W) regions.

Q_F		p_1	p_{99}	p_5	p_{95}	p_{25}	p_{75}	***Median***	**IQR**
VD	*C*	-26.5	33.0	-12.7	18.9	-0.366	7.48	3.18	7.84
	W	-13.3	15.6	-4.74	9.27	0.416	4.34	2.18	3.92
UD	*C*	-28.7	29.1	-14.6	15.6	-1.72	5.18	1.63	6.90
	W	-14.0	13.7	-5.36	7.65	-0.140	3.01	1.32	3.15
UV	*C*	-7.31	1.04	-4.87	0.166	-2.77	-0.844	-1.73	1.93
	W	-3.56	0.649	-2.46	0.138	-1.49	-0.394	-0.920	1.10
$Q_{H,MM}$		p_1	p_{99}	p_5	p_{95}	p_{25}	p_{75}	***Median***	**IQR**
VD	*C*	-35.1	52.2	-14.9	30.4	1.13	13.0	6.32	11.9
	W	-17.0	28.6	-5.02	15.6	1.00	7.14	3.62	6.14
UD	*C*	-41.8	34.2	-20.9	18.2	-2.17	6.05	1.76	8.22
	W	-19.9	17.1	-7.00	8.58	-0.341	3.36	1.23	3.70
UV	*C*	-21.4	-0.211	-14.0	-1.07	-7.91	-3.24	-5.30	4.66
	W	-13.0	0.191	-7.49	-0.260	-4.16	-1.35	-2.64	2.81
$Q_{E,MM}$		p_1	p_{99}	p_5	p_{95}	p_{25}	p_{75}	***Median***	**IQR**
VD	*C*	-20.2	12.2	-6.08	6.76	-0.365	2.45	0.803	2.81
	W	-15.8	9.32	-4.02	5.47	-0.0623	2.33	0.980	2.39
UD	*C*	-13.7	9.00	-4.79	4.15	-0.647	1.15	0.177	1.79
	W	-9.58	6.61	-2.98	3.28	-0.322	1.17	0.330	1.49
UV	*C*	-5.64	9.62	-3.55	2.94	-1.57	-0.140	-0.722	1.43
	W	-4.25	8.27	-2.74	2.09	-1.31	-0.177	-0.667	1.13
T_{2m}		p_1	p_{99}	p_5	p_{95}	p_{25}	p_{75}	***Median***	**IQR**
VD	*C*	0.867	0.577	-0.408	0.196	-0.0236	0.0274	0.00538	0.0510
	W	-0.882	0.796	-0.350	0.368	-0.00957	0.0484	0.0116	0.0580
UD	*C*	-0.663	0.836	-0.198	0.326	-0.0112	0.0321	0.0433	0.0058
	W	-0.785	1.08	-0.226	0.542	-0.00407	0.0564	0.0122	0.0605
UV	*C*	-0.0614	0.555	-0.0243	0.336	-0.00711	0.0161	-0.0016	0.0232
	W	-0.112	0.556	-0.0335	0.303	-0.00940	0.0454	-0.0008	0.0548

Table I-2: Ranges of $Q_{F,d}$ MBE for comparisons VD and UD across Central and West regions. Also included is West region omitting the anomalous area (Section 4.5.1, 4.5.3)

	VD	**UD**
Central	261.7	259.4
West	199.4	195.3
West, omitting anomaly	91.1	88.7

Appendix J Monthly IQR of diurnal fluxes in individual spatial units for runs D2, V1 and U1

J.1 Monthly diurnal patterns of Q_F and turbulent heat fluxes at Kc_{OA} and Sw_{OA}

Figure J-1 compares monthly diurnal IQR flux profiles for U1, V1 and D2 at Kc_{OA} and Sw_{OA} (Section 4.3.5, Table 2-1) to judge the impacts that differences in the Q_F profiles (Section 4.4.3, Figure 4-6) have on the diurnal profiles of the turbulent heat fluxes.

Kc_{OA} and Sw_{OA} diurnal Q_F profiles differ between the three approaches. At Kc_{OA}, V1 daytime Q_F is greater than U1 and D2 throughout winter and spring (Figure J-1a Nov-Apr), with median V1 Q_F up to 20 W m^{-2} greater than D2 (Figure J-1a Feb). During summer and autumn, V1 values are slightly closer to D2 than U1 values (Figure J-1a Oct, May-Sep). These elevated Q_F values may be the cause of a slight increase in V1 Q_H over the other two schemes (Figure J-1b). Q_E patterns between the three schemes are almost identical (Figure J-1c). It is expected that Q_F is partitioned more into Q_H than Q_E. U1 Q_F values are close to D2 throughout the year, though underestimations occur during summer months (Figure J-1a). The U1 diurnal pattern tends to be close to D2 until early evening, after which it does not decline as quickly.

In Sw_{OA}, U1 Q_F is much more similar to D2 than V1 throughout the year (Figure J-1d). Unlike at Kc_{OA}, V1 Q_F remains higher than the other two schemes regardless of time of year. This may in part be explained by Figure 4-5, which shows that areas with lower λ_i have a broader range of temperatures during which V Q_F estimates are greater than U, as would be the case when comparing Sw_{OA} and Kc_{OA}. The turbulent heat fluxes between the three schemes show very similar patterns (Figure J-1e, f). There are however differences in the partitioning of Q_H and Q_E between the two areas. Due to the greater vegetated land cover at Sw_{OA}, Q_E is much higher throughout the year than at Kc_{OA} (Figure J-1c, f). The greatest Q_E values at Sw_{OA} occur in May (Figure J-1f), reflecting the patterns seen in Figure 4-11b, c. U1 patterns in both areas can be seen to change throughout the year as they respond to temperature, as per the changing E_d profiles.

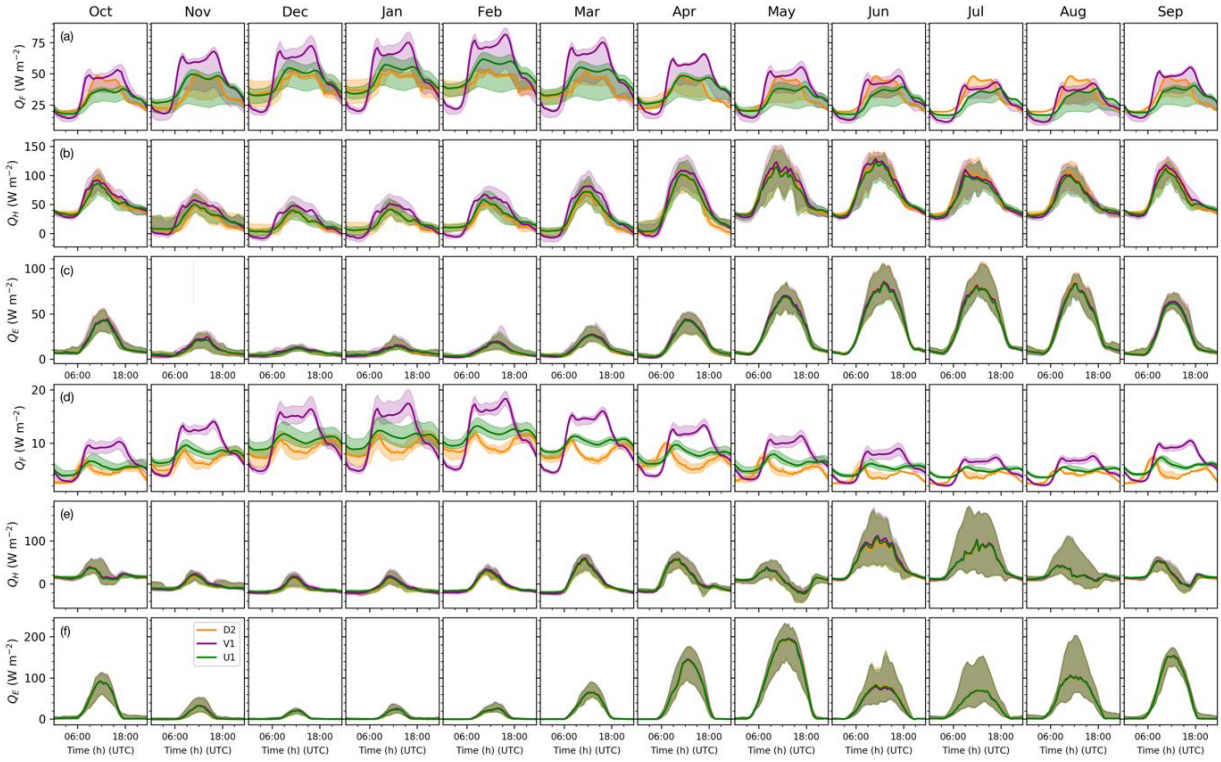

Figure J-1: Monthly diurnal median (lines) and interquartile range (IQR) (shaded) (**a**, **d**) Q_F, (**b**, **e**) Q_H, (**c**, **f**) Q_E, for (**a-c**) Kc_{OA} and (**d-f**) Sw_{OA} for runs D2 (orange), V1 (purple), U1 (green).

J.2 Densely populated areas with low λ_i

Some spatial units may show anomalous values due to the method used to find U and V scheme coefficients (Section 4.3.4), as median values of $Q_F\ \rho_{pop}^{-1}$ are used to find the coefficients across λ_i. This method excludes extreme areas, for example areas with a low λ_i but high ρ_{pop} as would be seen in areas with high rise buildings and urban green spaces. These are likely to produce U1 and V1 Q_F values much greater than those estimated in run D2, as the coefficients are not calibrated for high ρ_{pop} with lower $Q_F\ \rho_{pop}^{-1}$ (e.g. buildings with a high population density are expected to be more thermally efficient due to low exposed wall to volume ratio). The IQR of Q_F for each scheme is presented to analyse the seasonal responses between each approach and to provide visual comparison (Figure J-2). Veg_{OA} (Table J-1) is an example of such an area, with workday ρ_{pop} 340.5 cap ha^{-1} and λ_i 0.39, with low paved land cover fraction (0.04), representative of an area with high density housing surrounded by green areas. In run D2, median Q_F peaks at around 40 W m^{-2} during winter months (Figure J-2a Feb), yet for the V1 and U1 runs median values reach 100 and 80 W m^{-2} at the same time of day. This has consequences for the Q_H in this area (Figure J-2b), as U1 and V1 Q_H values are elevated compared to D2 throughout the year. This would have implications for boundary layer stability and height estimation if used for numerical weather prediction or boundary layer modelling.

Table J-1: Characteristics of a highly vegetated and densely populated OA, Veg_{OA}. z_H: mean building height, z_{tr}: mean tree height, z_m: measurement height, z_0: roughness length, z_d: displacement height.

		Veg_{OA}
Output area (OA)		E00166758
Fraction	Paved	0.04
	Buildings	0.35
	Evergreen trees/shrubs	0.0
	Deciduous trees/shrubs	0.27
	Grass	0.33
	Bare soil	0.0
	Water	0.01
ρ_{pop} (cap ha^{-1}) WD		340.5
ρ_{pop} (cap ha^{-1}) WE		378.8
z_H(m)		24.0
z_{tr} (m)		8.0
z_m (m)		75.5
Centre location		51°31' N 0°06' W

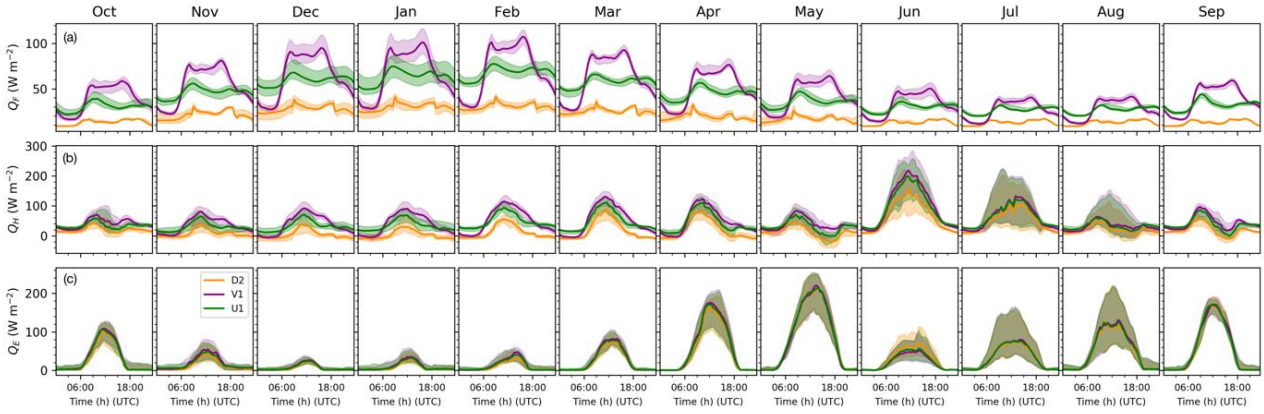

Figure J-2: Monthly diurnal median (solid lines) and IQR (filled areas) of (**a**) Q_F, (**b**) Q_H, (**c**) Q_E at Veg_{OA} (Table J-1) for runs D2 (orange), V1 (purple), (**iii**) U1 (green).

Appendix K Chapter 4 supplementary material

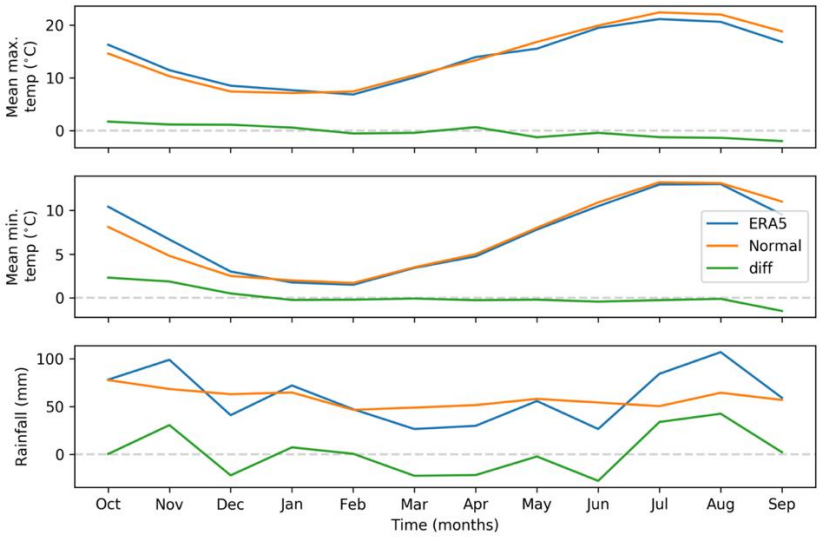

Figure K-1: Comparison of ERA5 data (Hersbach et al., 2020) to 1981-2010 climate Normals from Hampstead, Greater London (Met Office, 2020) and differences (ERA5 - Normal) for monthly mean maximum temperature (°C), monthly mean minimum temperature (°C) and monthly rainfall (mm).

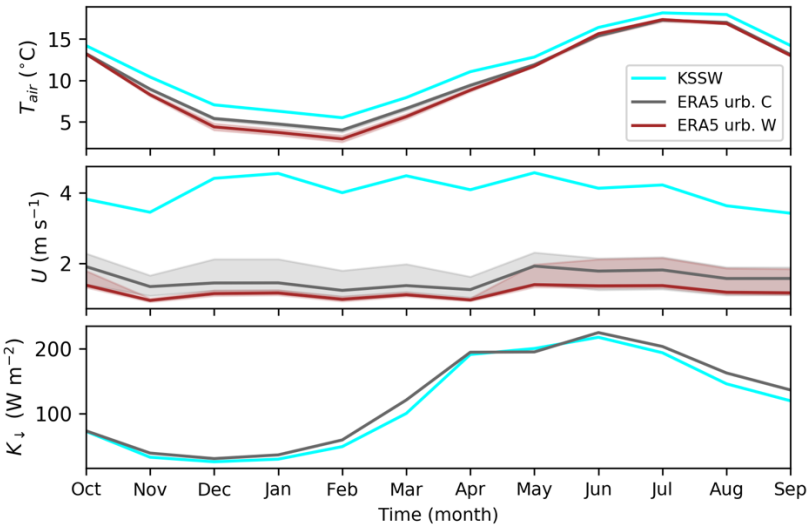

Figure K-2: Monthly mean forcing meteorology for: KSSW, used for D1; ERA5 urb., spatial IQRs of monthly mean ERA5 urbanised by SUEWS for the Central (C) and West (W) regions, i.e. $T_{0.5z_H}$, $U_{0.5z_H}$ (Section 4.3.5) that provide forcing to STEBBS in run D2. Meteorological variables shown are those that are used for input into the STEBBS submodel, and therefore directly affect $Q_{F,B}$.

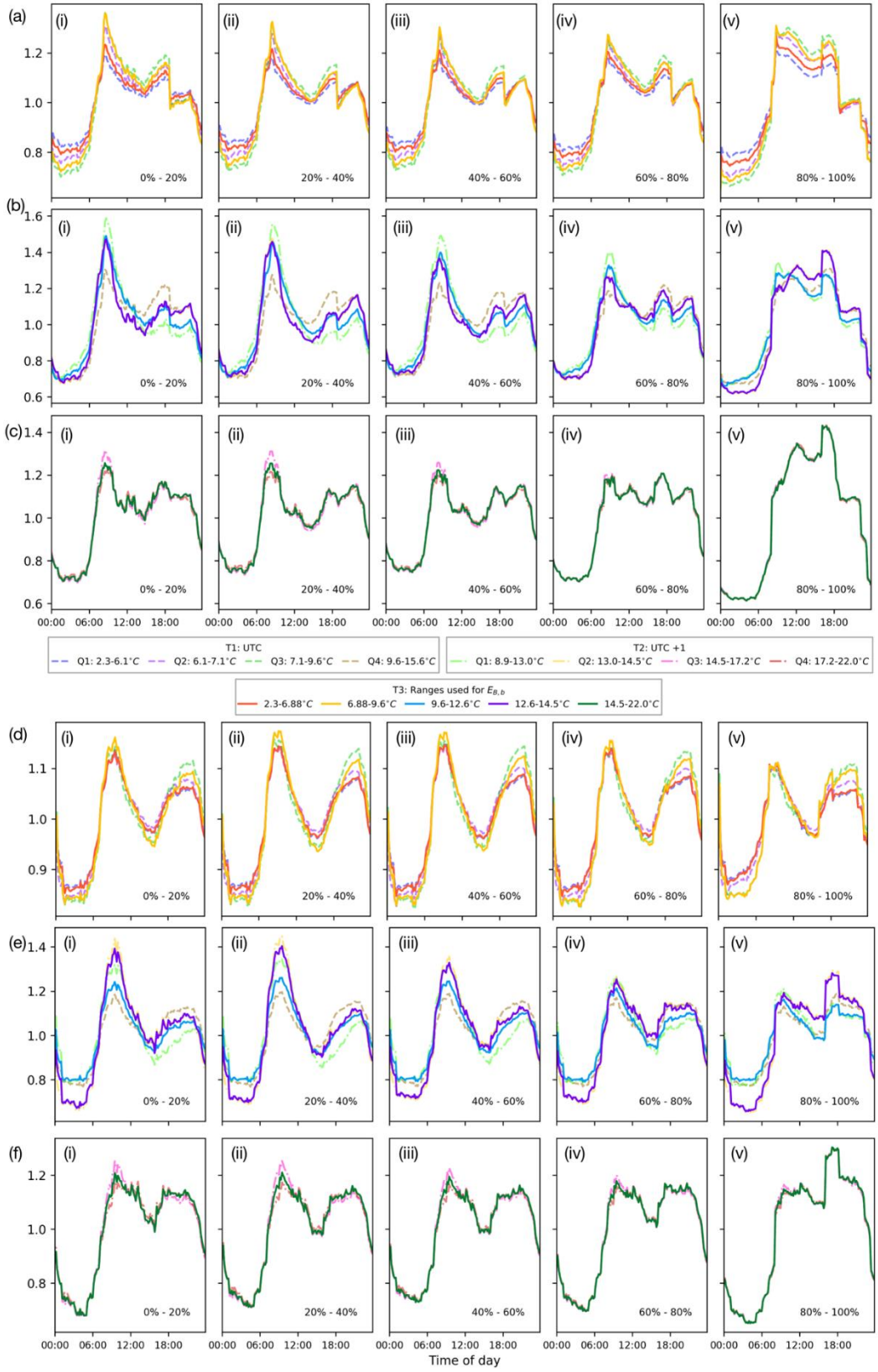

Figure K-3: Normalised Q_F profiles, averaged for T1 (dashed, 26 October 2014 - 28 March 2015), T2 (dot-dashed, plotted as UTC, 1 October 2014 - 25 October 2014 and 29 March 2015 - 30 September 2015) and T3 (solid, temperature ranges used as T1 and T2 combined) for **a-c** workdays and **d-f** non-workdays for five λ_i classes: (**i**) 0 - 20%, (**ii**) 20 - 40 %, (**iii**) 40 - 60%, (**iv**) 60 - 80%, (**v**) 80 - 100%; and three temperature ranges: (**a,d**) $0.28 \leq T_{a5} < 9.6$ ℃, (**b,e**) $9.6 \leq T_{a5} < 15.6$ ℃, (**c,f**) $14.5 \leq T_{a5} < 22.0$ ℃. See text for definitions.

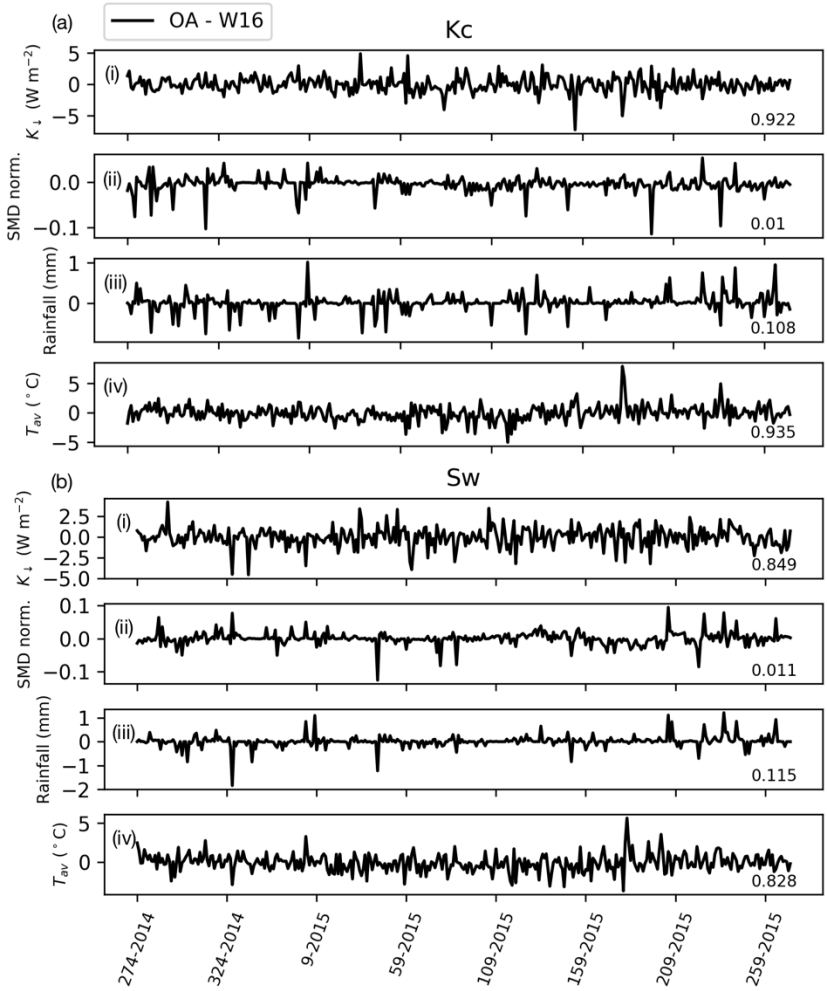

Figure K-4: Differences between forcing data (1 Oct 2014 - 30 Sept 2015 ERA5) and chosen W16 days (section 3.5) at (**a**) Kc and (**b**) Sw for metrics: (**i**) $K_{\downarrow}$, (**ii**) daily (d) range in soil moisture deficit (SMD) normalised by the whole period (p) SMD range $\left[\frac{SMD_{max,d} - SMD_{min,d}}{SMD_{max,p} - SMD_{min,p}}\right]$, (**iii**) rainfall and (**v**) daily mean air temperature (T_{av}). The annual mean annual error (MAE) between the ERA5 and the observed data selected determined for the daily data is given in the lower right corner (units are as for each variable).

References

Allen, L., Lindberg, F. and Grimmond, C. S. B.: Global to city scale urban anthropogenic heat flux: Model and variability, Int. J. Climatol., 31(13), 1990–2005, doi:10.1002/joc.2210, 2011.

Andersen, P. D., Iversen, A., Madsen, H. and Rode, C.: Dynamic modeling of presence of occupants using inhomogeneous Markov chains, Energy Build., 69, 213–223, doi:10.1016/j.enbuild.2013.10.001, 2014.

Ao, X., Grimmond, C. S. B., Ward, H. C., Gabey, A. M., Tan, J., Yang, X. Q., Liu, D., Zhi, X., Liu, H. and Zhang, N.: Evaluation of the Surface Urban Energy and Water Balance Scheme (SUEWS) at a dense urban site in Shanghai: Sensitivity to anthropogenic heat and irrigation, J. Hydrometeorol., 19(12), 1983–2005, doi:10.1175/JHM-D-18-0057.1, 2018.

Arguez, A., Durre, I., Applequist, S., Squires, M., Vose, R., Yin, X. and Bilotta, R.: NOAA's U.S. Climate Normals (1981-2010), NOAA Natl. Centers Environ. Inf., doi:10.7289/V5PN93JP, 2010.

Arnfield, A. J.: Two decades of urban climate research: A review of turbulence, exchanges of energy and water, and the urban heat island, Int. J. Climatol., 23(1), 1–26, doi:10.1002/joc.859, 2003.

ASHRAE: ANSI/ASHRAE Standard 140-2017, Standard Method of Test for the Evaluation of Building Energy Analysis Computer Programs., 2017.

Azar, E. and Menassa, C. C.: Agent-based modeling of occupants and their impact on energy use in commercial buildings, J. Comput. Civ. Eng., 26(4), 506–518, doi:10.1061/(ASCE)CP.1943-5487.0000158, 2012.

Azevedo, J. A., Chapman, L. and Muller, C. L.: Critique and suggested modifications of the degree days methodology to enable long-term electricity consumption assessments: A case study in Birmingham, UK, Meteorol. Appl., 22(4), 789–796, doi:10.1002/met.1525, 2015.

Baetens, R. and Saelens, D.: Modelling uncertainty in district energy simulations by stochastic residential occupant behaviour, J. Build. Perform. Simul., 9(4), 431–447, doi:10.1080/19401493.2015.1070203, 2016.

Barlow, J. F.: Progress in observing and modelling the urban boundary layer, Urban Clim., 10(P2), 216–240, doi:10.1016/j.uclim.2014.03.011, 2014.

Batty, M.: Agents, cells, and cities: New representational models for simulating multiscale urban dynamics, Environ. Plan. A, 37(8), 1373–1394, doi:10.1068/a3784, 2005.

BCO: Guide to Specification 2009, British Council for Offices., 2009.

Beijing Construction Bureau: Design standard for energy efficiency of public buildings, China Architecture and Building Press. [online] Available from: http://bbs.topenergy.org/redirect.php, 2005.

BEIS: Department for Business, Energy & Industrial Strategy: Sub-national electricity consumption data, [online] Available from: https://www.gov.uk/government/collections/%0Asub-national-electricity-consumption-data#lsoa/msoa-data (Accessed 14 July 2017a), 2017.

BEIS: Department for Business, Energy & Industrial Strategy: Sub-national gas consumption data, [online] Available from: https://www.govuk/government/collections/sub-national-gas-consumption-data (Accessed 14 July 2017b), 2017.

BEIS: Department for Business, Energy & Industrial Strategy: Sub-national total final energy consumption data, 2017c.

BEIS: Department for Business, Energy & Industrial Strategy: Sub-National Consumption Statisitics: Methodology and guidance booklet., 2018.

Bergman, T. L., Lavine, A. S., Incropera, F. P. and DeWitt, D. P.: Fundamentals of Heat and Mass Transfer, 8th ed., Wiley Global Education., 2017.

Best, M. J. and Grimmond, C. S. B.: Importance of initial state and atmospheric conditions for urban land surface models' performance, Urban Clim., 10(P2), 387–406, doi:10.1016/j.uclim.2013.10.006, 2014.

Best, M. J. and Grimmond, C. S. B.: Key conclusions of the first international urban land surface model comparison project, Bull. Am. Meteorol. Soc., 96(5), 805–819, doi:10.1175/BAMS-D-14-00122.1, 2015.

Best, M. J. and Grimmond, C. S. B.: Investigation of the impact of anthropogenic heat flux within an urban land surface model and PILPS-urban, Theor. Appl. Climatol., 126, 51–60, doi:10.1007/s00704-015-1554-3, 2016.
Björkegren, A. and Grimmond, C. S. B.: Net carbon dioxide emissions from central London, Urban Clim., 23, 131–158, doi:10.1016/j.uclim.2016.10.002, 2018.
Blitzstein, J. K. and Hwang, J.: Introduction to Probability, 2nd ed., Chapman and Hall, CRC Press., 2019.
Block, A., Keuler, K. and Schaller, E.: Impacts of anthropogenic heat on regional climate patterns, Geophys. Res. Lett., 31(12), 2–5, doi:10.1029/2004GL019852, 2004.
Böcker, L., Prillwitz, J. and Dijst, M.: Climate change impacts on mode choices and travelled distances: a comparison of present with 2050 weather conditions for the Randstad Holland, J. Transp. Geogr., 28, 176–185, doi:10.1016/j.jtrangeo.2012.11.004, 2013.
Bohnenstengel, S. I., Evans, S., Clark, P. A. and Belcher, S. E.: Simulations of the London urban heat island, Q. J. R. Meteorol. Soc., 137(659), 1625–1640, doi:10.1002/qj.855, 2011.
Bohnenstengel, S. I., Hamilton, I., Davies, M. and Belcher, S. E.: Impact of anthropogenic heat emissions on London's temperatures, Q. J. R. Meteorol. Soc., 140(679), 687–698, doi:10.1002/qj.2144, 2014.
Bruhns, H. and Wyatt, P.: A data framework for measuring the energy consumption of the non-domestic building stock, Build. Res. Inf., 39(3), 211–226, doi:10.1080/09613218.2011.559704, 2011.
BSI: British Standards Institutution, BS 6700: Specification for Design, installation, testing and maintenance of services supplying water for domestic use within buildings and their curtilages, British Standards Institutution., 1997.
Bueno, B., Pigeon, G., Norford, L. K., Zibouche, K. and Marchadier, C.: Development and evaluation of a building energy model integrated in the TEB scheme, Geosci. Model Dev., 5(2), 433–448, doi:10.5194/gmd-5-433-2012, 2012.
Busby, J.: UK shallow ground temperatures for ground coupled heat exchangers, Q. J. Eng. Geol. Hydrogeol., 2015–077, doi:10.1144/qjegh2015-077, 2015.
Busch, J., Roelich, K., Bale, C. S. E. and Knoeri, C.: Scaling up local energy infrastructure; An agent-based model of the emergence of district heating networks, Energy Policy, 100(October 2016), 170–180, doi:10.1016/j.enpol.2016.10.011, 2017.
Bustos-Turu, G., Van, D. K. H., Acha, S., Markides, C. N. and Shah, N.: Simulating residential electricity and heat demand in urban areas using an agent-based modelling approach, 2016 IEEE Int. Energy Conf., doi:10.1109/ENERGYCON.2016.7514077, 2016.
Butcher, K., Ed.: CIBSE Guide K: Electricity in buildings, Chartered Institution of Building Services Engineers., 2004.
Butcher, K., Ed.: CIBSE Guide F: Energy Efficiency in Buildings, Chartered Institution of Building Services Engineers., 2012.
Butcher, K., Ed.: CIBSE Guide G: Public health and plumbing engineering, Chartered Institution of Building Services Engineers., 2014.
Butcher, K. and Craig, B., Eds.: CIBSE Guide A: Environmental Design, Chartered Institution of Building Services Engineers, London., 2016.
Calhoun, C., Ed.: Dictionary of the Social Sciences, Oxford University Press., 2002.
Capel-Timms, I., Smith, S. T., Sun, T. and Grimmond, C. S. B.: Dynamic Anthropogenic activitieS impacting Heat emissions (DASH v1.0): Development and evaluation, [online] Available from: https://doi.org/10.5281/zenodo.3936025, 2020a.
Capel-Timms, I., Smith, S. T., Sun, T. and Grimmond, S.: Dynamic Anthropogenic activitieS impacting Heat emissions (DASHv1.0): Development and evaluation, Geosci. Model Dev., 13(10), 4891–4924, doi:10.5194/gmd-13-4891-2020, 2020b.
Castellani, B., Barbrook-Johnson, P. and Schimpf, C.: Case-based methods and agent-based modelling: bridging the divide to leverage their combined strengths, Int. J. Soc. Res. Methodol., 22(4), 403–416, doi:10.1080/13645579.2018.1563972, 2019.
Chen, F., Yang, X. and Zhu, W.: WRF simulations of urban heat island under hot-weather synoptic

conditions: The case study of Hangzhou City, China, Atmos. Res., 138, 364–377, doi:10.1016/j.atmosres.2013.12.005, 2014.
Chen, Y., Liang, X., Hong, T. and Luo, X.: Simulation and visualization of energy-related occupant behavior in office buildings, Build. Simul., 10(6), 785–798, doi:10.1007/s12273-017-0355-2, 2017.
Choudhary, R.: Energy analysis of the non-domestic building stock of Greater London, Build. Environ., 51, 243–254, doi:10.1016/j.buildenv.2011.10.006, 2012.
Christen, A. and Vogt, R.: Energy and radiation balance of a central European city, Int. J. Climatol., 24(11), 1395–1421, doi:10.1002/joc.1074, 2004.
Chrysoulakis, N. and Grimmond, C. S. B.: Understanding and reducing the anthropogenic heat emission, in Urban Climate Mitigation Techniques, edited by M. Santamouris and D. Kolokotsa, pp. 27–40, Routledge, London, UK., 2016.
Chrysoulakis, N., Grimmond, S., Feigenwinter, C., Lindberg, F., Gastellu-Etchegorry, J. P., Marconcini, M., Mitraka, Z., Stagakis, S., Crawford, B., Olofson, F., Landier, L., Morrison, W. and Parlow, E.: Urban energy exchanges monitoring from space, Sci. Rep., 8, 1–8, doi:10.1038/s41598-018-29873-x, 2018.
Clarke, J. A., Johnstone, C. M., Kim, J. M. and Tuohy, P. G.: Energy, carbon and cost performance of building stocks: Upgrade analysis, energy labelling and national policy development, Adv. Build. Energy Res., 3(1), 1–20, doi:10.3763/aber.2009.0301, 2009.
Claussen, M.: Estimation of regional heat and moisture fluxes in homogeneous terrain with bluff roughness elements, J. Hydrol., 166(3–4), 353–369, doi:10.1016/0022-1694(94)05089-G, 1995.
Cleveland, W. S.: LOWESS : A Program for Smoothing Scatterplots by Robust Locally Weighted Regression, Am. Stat., 35(1), 54, 1988.
Coffey, B., Borgeson, S., Selkowitz, S., Apte, J., Mathew, P. and Haves, P.: Towards a very low-energy building stock: Modelling the US commercial building sector to support policy and innovation planning, Build. Res. Inf., 37(5–6), 610–624, doi:10.1080/09613210903189467, 2009.
Cole, R. J. and Sturrock, N. S.: The convective heat exchange at the external surface of buildings, Build. Environ., 12(4), 207–214, doi:10.1016/0360-1323(77)90021-X, 1977.
Cools, M., Moons, E., Creemers, L. and Wets, G.: Changes in travel behavior in response to weather conditions: Do type of weather and trip purpose matter?, Transp. Res. Rec., (2157), 22–28, doi:10.3141/2157-03, 2010.
Coutts, A. M., Beringer, J. and Tapper, N. J.: Impact of increasing urban density on local climate: Spatial and temporal variations in the surface energy balance in Melbourne, Australia, J. Appl. Meteorol. Climatol., 46(4), 477–493, doi:10.1175/JAM2462.1, 2007.
Crawford, B., Grimmond, C. S. B., Ward, H. C., Morrison, W. and Kotthaus, S.: Spatial and temporal patterns of surface–atmosphere energy exchange in a dense urban environment using scintillometry, Q. J. R. Meteorol. Soc., 143(703), 817–833, doi:10.1002/qj.2967, 2017.
Crawley, D. B., Lawrie, L. K., Pedersen, C. O. and Winkelmann, F. C.: EnergyPlus: Energy Simulation Program, ASHRAE J., 42, 49–56 [online] Available from: https://energyplus.net/, 2000.
Crooks, A., Castle, C. and Batty, M.: Key challenges in agent-based modelling for geo-spatial simulation, Comput. Environ. Urban Syst., 32(6), 417–430, doi:10.1016/j.compenvurbsys.2008.09.004, 2008.
Crooks, A. T. and Heppenstall, A. J.: Introduction to Agent-Based Modelling, in Agent-Based Models of Geographical Systems, pp. 85–105, Springer., 2012.
Day, T.: TM41: Degree-days: theory and application, The Chartered Institution of Building Services Engineers., 2006.
DECC: Department of Energy and Climate Change: The Non-Domestic National Energy Efficiency Data-Framework: Energy Statistics 2006-12, Department of Energy and Climate Change., 2015.
DECC and BRE: Department of Energy and Climate Change and Building Research Establishment: Energy Follow Up Survey (EFUS) 2011, , doi:10.5255/UKDA-SN-7471-3, 2016.
Delzendeh, E., Wu, S., Lee, A. and Zhou, Y.: The impact of occupants' behaviours on building energy analysis: A research review, Renew. Sustain. Energy Rev., 80(September 2016), 1061–1071, doi:10.1016/j.rser.2017.05.264, 2017.

Department for Transport: National Travel Survey, 2002-2016 (12th Edition), , doi:10.5255/UKDA-SN-5340-8, 2017.
DfE: Department for Education: Schools, Pupils and their Characteristics: January 2019 - Accompanying Table, [online] Available from: https://www.gov.uk/government/statistics/schools-pupils-and-their-characteristics-january-2019 (Accessed 11 February 2020), 2019.
DfT: Department for Transport, TRA0203 - Motor vehicle traffic (vehicle kilometres) by road class and region and country in Great Britain, annual 2014, [online] Available from: https://www.gov.uk/government/statistical-data-sets/tra02-traffic-by-road-class-and-region-kms (Accessed 10 February 2016a), 2016.
DfT: Department for Transport, TRA0204 - Road traffic (vehicle kilometres) by vehicle type and road class in Great Britain, annual 2014, [online] Available from: https://www.gov.uk/government/statistical-data-sets/road-traffic-statistics-tra (Accessed 10 February 2016b), 2016.
DfT: Department for Transport. National Travel Survey, 2002-2016. [data collection]. 12th Edition. UK Data Service. SN: 5340, 2017.
DfT and DVLA: Department for Transport (DfT) and Driver and Vehicle Licensing Agency (DVLA). Data on all licensed and registered vehicles (VEH01), 2019.
Ding, Z., Hu, T., Li, M., Xu, X. and Zou, P. X. W.: Agent-based model for simulating building energy management in student residences, Energy Build., 198, 11–27, doi:10.1016/j.enbuild.2019.05.053, 2019.
Dong, Y., Varquez, A. C. G. and Kanda, M.: Global anthropogenic heat flux database with high spatial resolution, Atmos. Environ., 150, 276–294, doi:10.1016/j.atmosenv.2016.11.040, 2017.
Druckman, A. and Jackson, T.: Household energy consumption in the UK: A highly geographically and socio-economically disaggregated model, Energy Policy, 36(8), 3167–3182, doi:10.1016/j.enpol.2008.03.021, 2008.
Dziedzic, J. W., Yan, D., Sun, H. and Novakovic, V.: Building occupant transient agent-based model – Movement module, Appl. Energy, 261(7491), 114417, doi:10.1016/j.apenergy.2019.114417, 2020.
e-Stat Statistics of Japan: Japanese census data resolution, [online] Available from: https://www.e-stat.go.jp/en (Accessed 15 January 2018), 2017.
Elkhafif, M. A. T.: An iterative approach for weather-correcting energy consumption data, Energy Econ., 18(3), 221–230, doi:10.1016/0140-9883(96)00010-2, 1996.
Ellison, R. B., Greaves, S. P. and Hensher, D. A.: Five years of London's low emission zone: Effects on vehicle fleet composition and air quality, Transp. Res. Part D Transp. Environ., 23, 25–33, doi:10.1016/j.trd.2013.03.010, 2013.
EnergyPlus: Knowledgebase: Downloads, Testing and valida- tion, ANSI/ASHRAE Standard 140 models, Knowledge- base Downloads, [online] Available from: http://energyplus.helpserve.com/Knowledgebase/List/Index/49 (Accessed 30 June 2020), 2020.
Eurostat: Complete Energy Balances (nrg_bal_c), 2019.
Evans, S., Liddiard, R. and Steadman, P.: Modelling a whole building stock: domestic, non-domestic and mixed use, Build. Res. Inf., 47(2), 156–172, doi:10.1080/09613218.2017.1410424, 2019.
Evins, R., Orehounig, K. and Dorer, V.: Variability between domestic buildings: the impact on energy use, J. Build. Perform. Simul., 1493(July), 1–14, doi:10.1080/19401493.2015.1006526, 2015.
Falasca, S., Catalano, F. and Moroni, M.: Numerical study of the daytime planetary boundary layer over an idealized urban area: Influence of surface properties, anthropogenic heat flux, and geostrophic wind intensity, J. Appl. Meteorol. Climatol., 55(4), 1021–1039, doi:10.1175/JAMC-D-15-0135.1, 2016.
Fan, H. and Sailor, D. J.: Modeling the impacts of anthropogenic heating on the urban climate of Philadelphia: A comparison of implementations in two PBL schemes, Atmos. Environ., 39(1), 73–84, doi:10.1016/j.atmosenv.2004.09.031, 2005.
Ferreira, M. J., de Oliveira, A. P. and Soares, J.: Anthropogenic heat in the city of São Paulo, Brazil, Theor. Appl. Climatol., 104, 43–56, doi:10.1007/s00704-010-0322-7, 2011.
Field, J.: TM46: Energy Benchmarks., 2008.

Firth, S., Lomas, K., Wright, A. and Wall, R.: Identifying trends in the use of domestic appliances from household electricity consumption measurements, Energy Build., 40(5), 926–936, doi:10.1016/j.enbuild.2007.07.005, 2008.
Fisher, K. and Gershuny, J.: Coming full circle - introducing the multinational Time Use Study Simple File, Electron. Int. J. od Time Use Res., 10(1), 91–96, doi:10.1016/j.physbeh.2017.03.040, 2013.
Flamco: Indirect Water Heaters (mains water systems), [online] Available from: https://flamcogroup.com/media/files/documentation/EXP17_PSTEST_LR_v09022017_Chapter_6.pdf (Accessed 11 March 2019), 2017.
Flanner, M. G.: Integrating anthropogenic heat flux with global climate models, Geophys. Res. Lett., 36(2), doi:10.1029/2008GL036465, 2009.
Foucquier, A., Robert, S., Suard, F., Stéphan, L. and Jay, A.: State of the art in building modelling and energy performances prediction: A review, Renew. Sustain. Energy Rev., 23, 272–288, doi:10.1016/j.rser.2013.03.004, 2013.
Fu, G., Dawson, R., Khoury, M. and Bullock, S.: Interdependent networks: Vulnerability analysis and strategies to limit cascading failure, Eur. Phys. J. B, 87(7), doi:10.1140/epjb/e2014-40876-y, 2014.
Gabey, A. M., Grimmond, C. S. B. and Capel-Timms, I.: Anthropogenic heat flux: advisable spatial resolutions when input data are scarce, Theor. Appl. Climatol., (ii), 1–2, doi:10.1007/s00704-018-2431-7, 2018.
Gabey, A. M., Grimmond, C. S. B. and Capel-Timms, I.: Anthropogenic heat flux: advisable spatial resolutions when input data are scarce, Theor. Appl. Climatol., 135(1–2), 791–807, doi:10.1007/s00704-018-2431-7, 2019.
Gaetani, I., Hoes, P. J. and Hensen, J. L. M.: Occupant behavior in building energy simulation: Towards a fit-for-purpose modeling strategy, Energy Build., 121, 188–204, doi:10.1016/j.enbuild.2016.03.038, 2015.
Gershuny, J. and Sullivan, O.: United Kingdom Time Use Survey, 2014-2015, SN: 8128, UK Data Serv., doi:10.5255/UKDA-SN-8128-1, 2017.
Ginzburg, A. S. and Demchenko, P. F.: Air temperature and energy consumption feedbacks within urbanized areas, Izv. - Atmos. Ocean Phys., 53(5), 487–494, doi:10.1134/S000143381705005X, 2017.
GLA: Greater London Authority, Statistical GIS Boundary Files for London, [online] Available from: https://data.london.gov.uk/dataset/ statistical-gis-boundary-files-london (Accessed 11 February 2020), 2011.
GLA: Greater London Authority, London Schools Atlas, [online] Available from: https://data.london.gov.uk/dataset/london-schools-atlas (Accessed 5 May 2017), 2014.
Google: Google Directions API, [online] Available from: https://developers.google.com/maps/documentation/directions/start (Accessed 4 May 2019), 2019.
Greenshields, B., Bibbins, J., Channing, W. and Miller, H.: A Study of Traffic Capacity, in Proceedings of the highway research board (Highway Research Board, Washington, D. C.), pp. 14: 448–477., 1935.
Grimmond, C. S. B.: The Suburban Energy Balance : Methodological Considerations and Results for a Mid-Latitude West, Int. J. Climatol., 12, 481–497, doi:10.1002/joc.3370120506, 1992.
Grimmond, C. S. B. and Oke, T. R.: Aerodynamic properties of urban areas derived from analysis of surface form, J. Appl. Meteorol., 38(9), 1262–1292, doi:10.1175/1520-0450(1999)038<1262:APOUAD>2.0.CO;2, 1999a.
Grimmond, C. S. B. and Oke, T. R.: Heat Storage in Urban Areas: Local-Scale Observations and Evaluation of a Simple Model, J. Appl. Meteorol., 38, 922–940, doi:10.1175/1520-0450(1999)038<0922:HSIUAL>2.0.CO;2, 1999b.
Grimmond, C. S. B., Cleugh, H. A. and Oke, T. R.: An objective urban heat storage model and its comparison with other schemes, Atmos. Environ., 25B(3), 311–326, 1991.
Grimmond, C. S. B., Potter, S. K., Zutter, H. N. and Souch, C.: Rapid methods to estimate sky view factors applied to urban areas, Int. J. Clim., 21, 903–913, doi:10.1002/joc.659, 2001.
Grimmond, C. S. B., Best, M., Barlow, J., Arnfield, A. J., Baik, J. J., Baklanov, A., Belcher, S., Bruse, M., Calmet, I., Chen, F., Clark, P., Dandou, A., Erell, E., Fortuniak, K., Hamdi, R., Kanda, M.,

Kawai, T., Kondo, H., Krayenhoff, S., Lee, S., Limor, A., Martilli, A., Masson, V., Miao, S., Mills, G., Moriwaki, R., Oleson, K., Porson, A., Sievers, U., Tombrou, M., Voogt, J. and Williamson, T.: Urban surface energy balance models: model characteristics and methodology for a comparison study, in Meteorological and Air Quality Models for Urban Areas, pp. 97–123, Springer., 2009.
Guerra Santin, O., Itard, L. and Visscher, H.: The effect of occupancy and building characteristics on energy use for space and water heating in Dutch residential stock, Energy Build., 41(11), 1223–1232, doi:10.1016/j.enbuild.2009.07.002, 2009.
HABITAT-III: The New UN Urban Agenda A/RES/71/256, Quito, Ecuador. [online] Available from: https://habitat3.org/the-new-urban-agenda, 2016.
Hamilton, I. G., Davies, M., Steadman, P., Stone, A., Ridley, I. and Evans, S.: The significance of the anthropogenic heat emissions of London's buildings: A comparison against captured shortwave solar radiation, Build. Environ., 44(4), 807–817, doi:10.1016/j.buildenv.2008.05.024, 2009.
Hamilton, I. G., Steadman, P. J., Bruhns, H., Summerfield, A. J. and Lowe, R.: Energy efficiency in the British housing stock: Energy demand and the Homes Energy Efficiency Database, Energy Policy, 60, 462–480, doi:10.1016/j.enpol.2013.04.004, 2013.
Harris, C. R., Millman, K. J., van der Walt, S. J., Gommers, R., Virtanen, P., Cournapeau, D., Wieser, E., Taylor, J., Berg, S., Smith, N. J., Kern, R., Picus, M., Hoyer, S., van Kerkwijk, M. H., Brett, M., Haldane, A., Fernández del Río, J., Wiebe, M., Peterson, P., Gérard-Marchant, P., Sheppard, K., Reddy, T., Weckesser, W., Abbasi, H., Gohlke, C. and Oliphant, T. E.: Array programming with NumPy, Nature, 585, 357–362, doi:10.1038/s41586-020-2649-2, 2020.
Hasan, S., Schneider, C. M., Ukkusuri, S. V. and González, M. C.: Spatiotemporal Patterns of Urban Human Mobility, J. Stat. Phys., 151(1–2), 304–318, doi:10.1007/s10955-012-0645-0, 2013.
Hattam, L. and Greetham, D. V.: Green neighbourhoods in low voltage networks: measuring impact of electric vehicles and photovoltaics on load profiles, J. Mod. Power Syst. Clean Energy, 5(1), 105–116, doi:10.1007/s40565-016-0253-0, 2017.
Hatvani-Kovacs, G., Bush, J., Sharifi, E. and Boland, J.: Policy recommendations to increase urban heat stress resilience, Urban Clim., 25(November 2017), 51–63, doi:10.1016/j.uclim.2018.05.001, 2018.
Hawkins, G.: Rules of Thumb, Guidelines for Building Services., 2011.
HCA: Employment Densities Guide: 2nd Edition, Homes and Communities Agency, [online] Available from: https://www.gov.uk/government/publications/employment-densities-guide (Accessed 7 September 2020), 2010.
Heaviside, C., Vardoulakis, S. and Cai, X.-M.: Attribution of mortality to the urban heat island during heatwaves in the West Midlands, UK., Environ. Health, 15((Suppl 1)), 50–59, doi:10.1186/s12940-016-0100-9, 2016.
Heiple, S. and Sailor, D. J.: Using building energy simulation and geospatial modeling techniques to determine high resolution building sector energy consumption profiles, Energy Build., 40(8), 1426–1436, doi:10.1016/j.enbuild.2008.01.005, 2008.
Heppenstall, A., Malleson, N. and Crooks, A.: "Space, the Final Frontier": How Good are Agent-Based Models at Simulating Individuals and Space in Cities?, Systems, 4(1), 9, doi:10.3390/systems4010009, 2016.
Hermanns, H.: Interactive Markov Chains: The Quest for Quantified Quality, Springer., 2003.
Hersbach, H., Bell, B., Berrisford, P., Hirahara, S., Horányi, A., Muñoz-Sabater, J., Nicolas, J., Peubey, C., Radu, R., Schepers, D., Simmons, A., Soci, C., Abdalla, S., Abellan, X., Balsamo, G., Bechtold, P., Biavati, G., Bidlot, J., Bonavita, M., De Chiara, G., Dahlgren, P., Dee, D., Diamantakis, M., Dragani, R., Flemming, J., Forbes, R., Fuentes, M., Geer, A., Haimberger, L., Healy, S., Hogan, R. J., Hólm, E., Janisková, M., Keeley, S., Laloyaux, P., Lopez, P., Lupu, C., Radnoti, G., de Rosnay, P., Rozum, I., Vamborg, F., Villaume, S. and Thépaut, J.-N.: The ERA5 global reanalysis, Q. J. R. Meteorol. Soc., 146(730), 1999–2049, doi:10.1002/qj.3803, 2020.
Hertwig, D., Grimmond, S., Hendry, M. A., Saunders, B., Wang, Z., Jeoffrion, M., Vidale, P. L., McGuire, P. C., Bohnenstengel, S. I., Ward, H. C. and Kotthaus, S.: Urban signals in high-resolution weather and climate simulations: role of urban landsurface characterisation, Theor. Appl. Climatol., In press, doi:10.1007/s00704-020-03294-1, 2020.

Highways Agency: Traffic Capcity of Urban Roads. Design Manual for Roads and Bridges: TA 79/99, Highways Agency., 2017.
Hinkel, K. M., Nelson, F. E., Klene, A. E. and Bell, J. H.: The urban heat island in winter at Barrow, Alaska, Int. J. Climatol., 23(15), 1889–1905, doi:10.1002/joc.971, 2003.
Hoes, P., Hensen, J. L. M., Loomans, M. G. L. C., de Vries, B. and Bourgeois, D.: User behavior in whole building simulation, Energy Build., 41(3), 295–302, doi:10.1016/j.enbuild.2008.09.008, 2009.
Hor, C. L., Watson, S. J. and Majithia, S.: Analyzing the impact of weather variables on monthly electricity demand, IEEE Trans. Power Syst., 20(4), 2078–2085, doi:10.1109/TPWRS.2005.857397, 2005.
Huebner, G. M., Hamilton, I., Chalabi, Z., Shipworth, D. and Oreszczyn, T.: Explaining domestic energy consumption - The comparative contribution of building factors, socio-demographics, behaviours and attitudes, Appl. Energy, 159, 589–600, doi:10.1016/j.apenergy.2015.09.028, 2015.
Hussain, M. and Lee, B. E.: A wind tunnel study of the mean pressure forces acting on large groups of low-rise buildings, J. Wind Eng. Ind. Aerodyn., 6(3), 207–225, doi:https://doi.org/10.1016/0167-6105(80)90002-1, 1980.
Iamarino, M., Beevers, S. and Grimmond, C. S. B.: High-resolution (space, time) anthropogenic heat emissions: London 1970-2025, Int. J. Climatol., 32(11), 1754–1767, doi:10.1002/joc.2390, 2012.
Ichinose, T., Shimodozono, K. and Hanaki, K.: Impact of anthropogenic heat on urban climate in Tokyo, Atmos. Environ., 33(24–25), 3897–3909, doi:10.1016/S1352-2310(99)00132-6, 1999.
Ihara, T., Genchi, Y., Sato, T., Yamaguchi, K. and Endo, Y.: City-block-scale sensitivity of electricity consumption to air temperature and air humidity in business districts of Tokyo, Japan, Energy, 33(11), 1634–1645, doi:10.1016/j.energy.2008.06.005, 2008.
IOP: Plumbing Services Engineering Design Guide, Institute of Plumbing., 2002.
IPCC: Climate change 2014 impacts, adaptation and vulnerability: Part A: Global and sectoral aspects: Working group II contribution to the fifth assessment report of the intergovernmental panel on climate change, edited by C. B. Field, V. R. Barros, D. J. Dokken, K. J. Mach, M. D. Mastrandrea, T. E. Bilir, M. Chatterjee, K. L. Ebi, Y. O. Estrada, R. C. Genova, B. Girma, E. S. Kissel, A. N. Levy, S. MacCracken, P. R. Mastrandrea, and L. L. White, Cambridge University Press., 2014.
Järvi, L., Grimmond, C. S. B. and Christen, A.: The Surface Urban Energy and Water Balance Scheme (SUEWS): Evaluation in Los Angeles and Vancouver, J. Hydrol., 411(3–4), 219–237, doi:10.1016/j.jhydrol.2011.10.001, 2011.
Järvi, L., Havu, M., Ward, H. C., Bellucco, V., McFadden, J. P., Toivonen, T., Heikinheimo, V., Kolari, P., Riikonen, A. and Grimmond, C. S. B.: Spatial Modeling of Local-Scale Biogenic and Anthropogenic Carbon Dioxide Emissions in Helsinki, J. Geophys. Res. Atmos., 124(15), 8363–8384, doi:10.1029/2018JD029576, 2019.
Jenkins, K., Hall, J., Glenis, V., Kilsby, C., McCarthy, M., Goodess, C., Smith, D., Malleson, N. and Birkin, M.: Probabilistic spatial risk assessment of heat impacts and adaptations for London, Clim. Change, 124(1–2), 105–117, doi:10.1007/s10584-014-1105-4, 2014.
Jin, K., Wang, F. and Wang, S.: Assessing the spatiotemporal variation in anthropogenic heat and its impact on the surface thermal environment over global land areas, Sustain. Cities Soc., 63(August), 102488, doi:10.1016/j.scs.2020.102488, 2020.
Joint Research Centre (JRC) and European Environment Agency (EEA): Heating and cooling degree days, [online] Available from: https://www.eea.europa.eu/data-and-maps/indicators/heating-degree-days-2 (Accessed 17 September 2020), 2019.
Jones, R. V., Fuertes, A. and Lomas, K. J.: The socio-economic, dwelling and appliance related factors affecting electricity consumption in domestic buildings, Renew. Sustain. Energy Rev., 43, 901–917, doi:10.1016/j.rser.2014.11.084, 2015.
Karatasou, S. and Santamouris, M.: Socio-economic status and residential energy consumption: A latent variable approach., Energy Build., 198, 100–105, doi:10.1016/j.enbuild.2019.06.013, 2019.
Kato, S. and Yamaguchi, Y.: Analysis of urban heat-island effect using ASTER and ETM+ Data: Separation of anthropogenic heat discharge and natural heat radiation from sensible heat flux, Remote Sens. Environ., 99(1–2), 44–54, doi:10.1016/j.rse.2005.04.026, 2005.

Kelly, M. J.: Retrofitting the existing UK building stock, Build. Res. Inf., 37(2), 196–200, doi:10.1080/09613210802645924, 2009.
Kikegawa, Y., Genchi, Y., Yoshikado, H. and Kondo, H.: Development of a numerical simulation system toward comprehensive assessments of urban warming countermeasures including their impacts upon the urban buildings' energy-demands, Appl. Energy, 76(4), 449–466, doi:10.1016/S0306-2619(03)00009-6, 2003a.
Kikegawa, Y., Genchi, Y., Yoshikado, H. and Kondo, H.: Development of a numerical simulation system toward comprehensive assessments of urban warming countermeasures including their impacts upon the urban buildings' energy-demands, Appl. Energy, 76(4), 449–466, doi:10.1016/S0306-2619(03)00009-6, 2003b.
Kikegawa, Y., Tanaka, A., Ohashi, Y., Ihara, T. and Shigeta, Y.: Observed and simulated sensitivities of summertime urban surface air temperatures to anthropogenic heat in downtown areas of two Japanese Major Cities, Tokyo and Osaka, Theor. Appl. Climatol., 117(1), 175–193, doi:10.1007/s00704-013-0996-8, 2014.
Kim, Y. S. and Srebric, J.: Impact of occupancy rates on the building electricity consumption in commercial buildings, Energy Build., 138, 591–600, doi:10.1016/j.enbuild.2016.12.056, 2017.
Kipping, A. and Trømborg, E.: Modeling hourly consumption of electricity and district heat in non-residential buildings, Energy, 123, 473–486, doi:10.1016/j.energy.2017.01.108, 2017.
Klein, S. A., Duffie, J. A. and Mitchell, J. C.: TRNSYS 18: A Transient System Simulation Program, Solar Energy Laboratory, University of Wisconsin, [online] Available from: https://sel.me.wisc.edu/trnsys/, 2017.
Klimenko, V. V., Ginzburg, A. S., Demchenko, P. F., Tereshin, A. G., Belova, I. N. and Kasilova, E. V.: Impact of urbanization and climate warming on energy consumption in large cities, Dokl. Phys., 61(10), 521–525, doi:10.1134/s1028335816100050, 2016.
Kłysik, K.: Spatial and seasonal distribution of anthropogenic heat emissions in Lodz, Poland, Atmos. Environ., 30(20), 3397–3404, doi:10.1016/1352-2310(96)00043-X, 1996.
Knudsen, S.: Heat transfer in a 'tank in tank' combi store, BYG Rapport, No. R-025., 2002.
Koman, P. D., Romo, F., Swinton, P., Mentz, G. B., de Majo, R. F., Sampson, N. R., Battaglia, M. J., Hill-Knott, K., Williams, G. O., O'Neill, M. S. and Schulz, A. J.: MI-Environment: Geospatial patterns and inequality of relative heat stress vulnerability in Michigan, Heal. Place, 60(March), 102228, doi:10.1016/j.healthplace.2019.102228, 2019.
Kondo, H. and Kikegawa, Y.: Temperature variation in the urban canopy with anthropogenic energy use, Pure Appl. Geophys., 160(1–2), 317–324, doi:10.1007/s00024-003-8780-9, 2003.
Kotthaus, S. and Grimmond, C. S. B.: Identification of Micro-scale Anthropogenic CO2, heat and moisture sources - Processing eddy covariance fluxes for a dense urban environment, Atmos. Environ., 57, 301–316, doi:10.1016/j.atmosenv.2012.04.024, 2012.
Kotthaus, S. and Grimmond, C. S. B.: Energy exchange in a dense urban environment - Part I: Temporal variability of long-term observations in central London, Urban Clim., 10(P2), 261–280, doi:10.1016/j.uclim.2013.10.002, 2014.
Krpo, A., Salamanca, F., Martilli, A. and Clappier, A.: On the Impact of Anthropogenic Heat Fluxes on the Urban Boundary Layer: A Two-Dimensional Numerical Study, Boundary-Layer Meteorol., 136, 105–127, doi:10.1007/s10546-010-9491-2, 2010.
Kunze, C. and Hecht, R.: Semantic enrichment of building data with volunteered geographic information to improve mappings of dwelling units and population, Comput. Environ. Urban Syst., 53, 4–18, doi:10.1016/j.compenvurbsys.2015.04.002, 2015.
Lee, S. H., Song, C. K., Baik, J. J. and Park, S. U.: Estimation of anthropogenic heat emission in the Gyeong-In region of Korea, Theor. Appl. Climatol., 96(3–4), 291–303, doi:10.1007/s00704-008-0040-6, 2009.
LGA: Local Government Association website, [online] Available from: https://www.local.gov.uk/about/what-local-government (Accessed 26 November 2019), 2019.
Li, C., Cao, Y., Zhang, M., Wang, J., Liu, J., Shi, H. and Geng, Y.: Hidden benefits of electric vehicles for addressing climate change, Sci. Rep., 5, 1–5, doi:10.1038/srep09213, 2015.
Li, D. H. W., Yang, L. and Lam, J. C.: Impact of climate change on energy use in the built

environment in different climate zones - A review, Energy, 42(1), 103–112, doi:10.1016/j.energy.2012.03.044, 2012.
Liddiard, R.: Room-scale profiles of space use and electricity consumption in non-domestic buildings, Build. Res. Inf., 3218, doi:10.1080/09613218.2013.817112, 2013.
Lindberg, F., Grimmond, C. S. B., Yogeswaran, N., Kotthaus, S. and Allen, L.: Impact of city changes and weather on anthropogenic heat flux in Europe 1995-2015, Urban Clim., 4(2013), 1–15, doi:10.1016/j.uclim.2013.03.002, 2013.
Lindberg, F., Olofson, K. F. G., Sun, T., Grimmond, C. S. B. and Feigenwinter, C.: Urban storage heat flux variability explored using satellite, meteorological and geodata, Theor. Appl. Climatol., 141(1–2), 271–284, doi:10.1007/s00704-020-03189-1, 2020.
Lipson, M. J., Thatcher, M., Hart, M. A. and Pitman, A.: A building energy demand and urban land surface model, Q. J. R. Meteorol. Soc., 144(714), 1572–1590, doi:10.1002/qj.3317, 2018.
Liu, X., Huang, Y., Xu, X., Li, X., Li, X., Ciais, P., Lin, P., Gong, K., Ziegler, A. D., Chen, A., Gong, P., Chen, J., Hu, G., Chen, Y., Wang, S., Wu, Q., Huang, K., Estes, L. and Zeng, Z.: High-spatiotemporal-resolution mapping of global urban change from 1985 to 2015, Nat. Sustain., 3(7), 564–570, doi:10.1038/s41893-020-0521-x, 2020.
Liu, X. H. and Andersson, C.: Assessing the impact of temporal dynamics on land-use change modeling, Comput. Environ. Urban Syst., 28(1–2), 107–124, doi:10.1016/S0198-9715(02)00045-5, 2004.
London Datastore: London Atmospheric Emissions Inventory (LAEI) 2013 - Supporting information: key GIS geographies and road traffic flows and vehicle-kilometres, 2014.
Lowe, R. (Ed. .: Climate Change: National Building Stocks [Special Issue], Build. Res. Inf., 35(4) [online] Available from: https://www.tandfonline.com/toc/rbri20/35/4, 2007.
Lu, Y., Wang, Q., Zhang, Y., Sun, P. and Qian, Y.: An estimate of anthropogenic heat emissions in China, Int. J. Climatol., 36(3), 1134–1142, doi:10.1002/joc.4407, 2016.
Luo, X., Lam, K. P., Chen, Y. and Hong., T.: Performance Evaluation of an Agent-based Occupancy Simulation Model., Build. Environ., 115, 42–53, 2017.
Ma, S., Pitman, A., Hart, M., Evans, J. P., Haghdadi, N. and MacGill, I.: The impact of an urban canopy and anthropogenic heat fluxes on Sydney's climate, Int. J. Climatol., 37(February), 255–270, doi:10.1002/joc.5001, 2017.
Macal, C. and North, M.: Tutorial on agent-based modelling and simulation, J Simul, 4(3), 151–162, doi:10.1057/jos.2010.3, 2010.
Mansouri, I., Newborough, M. and Probert, D.: Energy consumption in UK households: Impact of domestic electrical appliances, Appl. Energy, 54(3 SPEC. ISS.), 211–285, doi:10.1016/0306-2619(96)00001-3, 1996.
Martilli, A.: Numerical study of urban impact on boundary layer structure: Sensitivity to wind speed, urban morphology, and rural soil moisture, J. Appl. Meteorol., 41(12), 1247–1266, doi:10.1175/1520-0450(2002)041<1247:NSOUIO>2.0.CO;2, 2002.
Martilli, A.: Current research and future challenges in urban mesoscale modelling, Int. J. Climatol., (27), 1909–1918, doi:10.1002/joc.1620, 2007.
Martilli, A., Clappier, A. and Rotach, M. W.: An urban surface exchange parameterisation for mesoscale models, Boundary-Layer Meteorol., 104(2), 261–304, doi:10.1023/A:1016099921195, 2002.
Masson, V., Lemonsu, A., Hidalgo, J. and Voogt, J.: Urban Climates and Climate Change, Annu. Rev. Environ. Resour., 45(1), 411–444, doi:10.1146/annurev-environ-012320-083623, 2020.
Mavrogianni, A., Wilkinson, P., Davies, M., Biddulph, P. and Oikonomou, E.: Building characteristics as determinants of propensity to high indoor summer temperatures in London dwellings, Build. Environ., 55, 117–130, doi:10.1016/j.buildenv.2011.12.003, 2012.
McKenna, E., Krawczynski, M. and Thomson, M.: Four-state domestic building occupancy model for energy demand simulations, Energy Build., 96, 30–39, doi:10.1016/j.enbuild.2015.03.013, 2015.
Met Office: UK Climate Projections 2009, 2009.
Met Office: UK climate averages, [online] Available from: https://www.metoffice.gov.uk/research/climate/maps-and-data/uk-climate-averages/ (Accessed 29

October 2020), 2020.
Moriwaki, R., Kanda, M., Senoo, H., Hagishima, A. and Kinouchi, T.: Anthropogenic water vapor emissions in Tokyo, Water Resour. Res., 44(11), doi:10.1029/2007WR006624, 2008.
De Munck, C., Pigeon, G., Masson, V., Meunier, F., Bousquet, P., Tréméac, B., Merchat, M., Poeuf, P. and Marchadier, C.: How much can air conditioning increase air temperatures for a city like Paris, France?, Int. J. Climatol., 33(1), 210–227, doi:10.1002/joc.3415, 2013.
MWS: McDonald Water Storage Ltd: Hot Water Tanks Specifications and Sizing, 2019.
Nägeli, C., Jakob, M., Catenazzi, G. and Ostermeyer, Y.: Towards agent-based building stock modeling: Bottom-up modeling of long-term stock dynamics affecting the energy and climate impact of building stocks, Energy Build., 211, doi:10.1016/j.enbuild.2020.109763, 2020.
Narumi, D., Kondo, A. and Shimoda, Y.: Effects of anthropogenic heat release upon the urban climate in a Japanese megacity, Environ. Res., 109(4), 421–431, doi:10.1016/j.envres.2009.02.013, 2009.
National Bureau of Statistics of China: http://www.stats.gov.cn/english/statisticaldata/censusdata/, [online] Available from: http://www.stats.gov.cn/english/statisticaldata/censusdata/ (Accessed 5 January 2017), 2017.
NG: National Grid: Transmission operational data, [online] Available from: https://www.nationalgridgas.com/data-and-operations/ transmission-operational-data (Accessed 28 November 2015), 2015.
Nie, W. S., Sun, T. and Ni, G. H.: Spatiotemporal characteristics of anthropogenic heat in an urban environment: A case study of Tsinghua Campus, Build. Environ., 82, 675–686, doi:10.1016/j.buildenv.2014.10.011, 2014.
O'Sullivan, D. and Haklay, M.: Agent-based models and individualism: Is the world agent-based?, Environ. Plan. A, 32(8), 1409–1425, doi:10.1068/a32140, 2000.
O'Sullivan, D., Millington, J., Perry, G. and Wainwright, J.: Agent-Based Models - Because They're Worth It?, in Agent-Based Models of Geographical Systems, pp. 109–123., 2012.
Offerle, B., Grimmond, C. S. B. and Fortuniak, K.: Heat storage and anthropogenic heat flux in relation to the energy balance of a central European city centre, Int. J. Climatol., 25(10), 1405–1419, doi:10.1002/joc.1198, 2005.
Office for National Statistics: WP101EW Population (Workplace population), [online] Available from: https://www.nomisweb.co.uk/query/construct/summary.asp?reset=yes&mode=construct&dataset=1300&version=0&anal=1&initsel=%0D, 2014.
Office for National Statistics: Mid-2015 Population Estimates for Census Output Areas in London by Single Year of Age and Sex, [online] Available from: https://www.ons.gov.uk/peoplepopulationandcommunity/populationandmigration/populationestimates/datasets/censusoutputareaestimatesinthelondonregionofengland (Accessed 24 May 2018), 2015.
Office for National Statistics: Census Geography, [online] Available from: https://www.ons.gov.uk/methodology/geography/ukgeographies/censusgeography (Accessed 8 October 2020), 2020.
Ohashi, Y., Suido, M., Kikegawa, Y., Ihara, T., Shigeta, Y. and Nabeshima, M.: Impact of seasonal variations in weekday electricity use on urban air temperature observed in Osaka, Japan, Q. J. R. Meteorol. Soc., 142(695), 971–982, doi:10.1002/qj.2698, 2016.
Oikonomou, E., Davies, M., Mavrogianni, A., Biddulph, P., Wilkinson, P. and Kolokotroni, M.: Modelling the relative importance of the urban heat island and the thermal quality of dwellings for overheating in London, Build. Environ., 57(July 2006), 223–238, doi:10.1016/j.buildenv.2012.04.002, 2012.
Oke, T. R.: Boundary Layer Climates, 2nd ed., Routledge., 1987.
Oke, T. R.: The urban energy balance, Prog. Phys. Geogr., 12(4), 471–508, doi:10.1177/030913338801200401, 1988.
Oke, T. R., Mills, G., Christen, A. and Voogt, J. A.: Energy Balance, in Urban Climates, pp. 156–196, Cambridge University Press., 2017a.
Oke, T. R., Mills, G., Christen, A. and Voogt, J. A.: Urban Climates, 1st ed., Cambridge University Press., 2017b.

Omidvar, H., Sun, T., Grimmond, S., Bilesback, D., Black, A., Chen, J., Duan, Z., Gao, Z., Iwata, H. and McFadden, J. P.: Surface [Urban] Energy and Water Balance Scheme (v2020a) in non-urban areas: developments, parameters and performance (under review), Geosci. Model Dev. Discuss. [preprint], doi:10.5194/gmd-2020-148, 2020.
ONS: Office for National Statistics, QS406EW - Household size, [online] Available from: https://www.nomisweb.co.uk/census/2011/qs406ew (Accessed 10 February 2020), 2011.
ONS: Office for National Statistics: WP101EW Population (Workplace population), [online] Available from: https://www.nomisweb.co.uk/query/construct/summary.asp?reset=yes&mode=construct&dataset=1300&version=0&anal=1&initsel=%0D (Accessed 31 January 2020a), 2014.
ONS: Office for National Statistics: WU03UK Location of usual residence and place of work by method of travel to work, [online] Available from: https://www.nomisweb.co.uk/query/construct/summary.asp?reset=yes&mode=construct&dataset=1207&version=0& anal=1&initsel= (Accessed 31 January 2020b), 2014.
ONS: Office for National Statistics: Mid-2015 Population Estimates for Census Output Areas in London by Single Year of Age and Sex, [online] Available from: https://www.ons.gov.uk/peoplepopulationandcommunity/populationandmigration/populationestimates/datasets/censusoutputareaestimatesinthelondonregionofengland (Accessed 25 May 2016), 2015.
ONS: Office for National Statistics: Census Geography, [online] Available from: https://www.ons.gov.uk/methodology/geography/ukgeographies/censusgeography (Accessed 5 January 2017), 2017.
ONS: Estimated average calorific values of fuels 2017 - Digest of UK Energy Statistics (DUKES): calorific values, 2018.
OpenStreetMap: OpenStreetMap data of Greater London, [online] Available from: https://www.openstreetmap.org (Accessed 31 January 2017), 2017.
OS: Ordnance Survey: OS MasterMap®, [online] Available from: http://digimap.edina.ac.uk (Accessed 11 October 2016), 2014.
OS: London digital speed limit map and private communication, Ordnance Survey., 2015.
OS: Ordnance Survey (GB): OS Open Roads, [online] Available from: https://www.ordnancesurvey.co.uk/opendatadownload/products.html (Accessed 30 August 2016a), 2016.
OS: OS Open Roads, 2016b.
Page, J., Robinson, D., Morel, N. and Scartezzini, J. L.: A generalised stochastic model for the simulation of occupant presence, Energy Build., 40(2), 83–98, doi:10.1016/j.enbuild.2007.01.018, 2008.
Palmer, E., Ed.: CIBSE Guide B1 - Heating, Chartered Institution of Building Services Engineers., 2016.
Park, C., Schade, G. W., Werner, N. D., Sailor, D. J. and Kim, C. H.: Comparative estimates of anthropogenic heat emission in relation to surface energy balance of a subtropical urban neighborhood, Atmos. Environ., 126, 182–191, doi:10.1016/j.atmosenv.2015.11.038, 2016.
Pedregosa, F., Varoquaux, G., Gramfort, A., Michel, V., Thirion, B., Grisel, O., Blondel, M., Prettenhofer, P., Weiss, R., Dubourg, V., Vanderplas, J., Passos, A., Cournapeau, D., Brucher, M., Perrot, M. and Duchesnay, É.: Scikit-learn: Machine Learning in Python (v 0.21.3), J. Mach. Learn. Res., 12, 2825–2830 [online] Available from: https://scikit-learn.org/stable/whats_new/v0.21.html, 2011.
Pérez-Lombard, L., Ortiz, J. and Pout, C.: A review on buildings energy consumption information, Energy Build., 40(3), 394–398, doi:10.1016/j.enbuild.2007.03.007, 2008.
Perez, L. and Dragicevic, S.: An agent-based approach for modeling dynamics of contagious disease spread, Int. J. Health Geogr., 8(1), 1–17, doi:10.1186/1476-072X-8-50, 2009.
Phan, D. and Varenne, F.: Agent-Based Models and Simulations in Economics and Social Sciences : From Conceptual Exploration to Distinct Ways of Experimenting, J. Artif. Soc. Soc. Simul., 13(1),

1–11, 2010.
Pigeon, G., Legain, D., Durand, P. and Masson, V.: Anthropogenic heat release in an old European agglomeration (Toulouse, France), Int. J. Climatol., 27, 1969–1981, doi:10.1002/joc.1530, 2007.
Psiloglou, B. E., Giannakopoulos, C., Majithia, S. and Petrakis, M.: Factors affecting electricity demand in Athens, Greece and London, UK: A comparative assessment, Energy, 34(11), 1855–1863, doi:10.1016/j.energy.2009.07.033, 2009.
Quah, A. K. L. and Roth, M.: Diurnal and weekly variation of anthropogenic heat emissions in a tropical city, Singapore, Atmos. Environ., 46, 92–103, doi:10.1016/j.atmosenv.2011.10.015, 2012.
Raupach, M. R., Thom, A. S. and Edwards, I.: A wind-tunnel study of turbulent flow close to regularly arrayed rough surfaces, Boundary-Layer Meteorol., 18, 373–397, doi:10.1007/BF00119495, 1980.
Raupach, M. R., Antonia, R. A. and Rajagopalan, S.: Rough wall turbulent boundary layers., Appl. Mech. Mater., 44(1), 1–25, doi:10.1115/1.3119492, 1991.
Ravetz, J.: State of the stock-What do we know about existing buildings and their future prospects?, Energy Policy, 36(12), 4462–4470, doi:10.1016/j.enpol.2008.09.026, 2008.
Reilly, W. J.: The Law of Retail Gravitation, 2nd ed., Pilsbury Publishers, New York., 1953.
Richardson, I., Thomson, M. and Infield, D.: A high-resolution domestic building occupancy model for energy demand simulations, Energy Build., 40(8), 1560–1566, doi:10.1016/j.enbuild.2008.02.006, 2008.
Richardson, I., Thomson, M., Infield, D. and Delahunty, A.: Domestic lighting: A high-resolution energy demand model, Energy Build., 41(7), 781–789, doi:10.1016/j.enbuild.2009.02.010, 2009.
Richardson, I., Thomson, M., Infield, D. and Clifford, C.: Domestic electricity use: A high-resolution energy demand model, Energy Build., 42(10), 1878–1887, doi:10.1016/j.enbuild.2010.05.023, 2010.
Ryu, Y. H. and Baik, J. J.: Quantitative analysis of factors contributing to urban heat island intensity, J. Appl. Meteorol. Climatol., 51(5), 842–854, doi:10.1175/JAMC-D-11-098.1, 2012.
Sailor, D. J.: Relating residential and commercial sector electricity loads to climate - Evaluating state level sensitivities and vulnerabilities, Energy, 26(7), 645–657, doi:10.1016/S0360-5442(01)00023-8, 2001.
Sailor, D. J.: A review of methods for estimating anthropogenic heat and moisture emissions in the urban environment, Int. J. Climatol., 31, 189–199, doi:10.1002/joc.2106, 2011.
Sailor, D. J. and Hart, M.: An anthropogenic heating database for major US cities, 86th AMS Annu. Meet., (January 2006), 2006.
Sailor, D. J. and Lu, L.: A top-down methodology for developing diurnal and seasonal anthropogenic heating profiles for urban areas, Atmos. Environ., 38(17), 2737–2748, doi:10.1016/j.atmosenv.2004.01.034, 2004.
Sailor, D. J. and Vasireddy, C.: Correcting aggregate energy consumption data to account for variability in local weather, Environ. Model. Softw., 21, 733–738, doi:10.1016/j.envsoft.2005.08.001, 2006.
Sailor, D. J., Brooks, A., Hart, M. and Heiple, S.: A bottom-up approach for estimating Anthropogenic heat flux, in Proceedings of 7th Symposium on the Urban Environment, San Diego, CA., 2007.
Salamanca, F., Krpo, A., Martilli, A. and Clappier, A.: A new building energy model coupled with an urban canopy parameterization for urban climate simulations-part I. formulation, verification, and sensitivity analysis of the model, Theor. Appl. Climatol., 99(3–4), 331–344, doi:10.1007/s00704-009-0142-9, 2010.
Salamanca, F., Georgescu, M., Mahalov, A., Moustaoui, M. and Wang, M.: Anthropogenic heating of the urban environment due to air conditioning, J. Geophys. Res. Atmos., 5949–5965, doi:10.1002/2013JD021225, 2014.
Salamanca, F., Zhang, Y., Barlage, M., Chen, F., Mahalov, A. and Miao, S.: Evaluation of the WRF-Urban Modeling System Coupled to Noah and Noah-MP Land Surface Models Over a Semiarid Urban Environment, J. Geophys. Res. Atmos., 123(5), 2387–2408, doi:10.1002/2018JD028377, 2018.
Saltelli, A., Chan, K. and Scott, E. M.: Sensitivity Analysis, Wiley., 2009.

Salter, R. J.: The relationship between speed, flow and density of a highway traffic stream, in Highway Traffic Analysis and Design, pp. 119–120, Palgrave Macmillan., 1989.
Saneinejad, S., Roorda, M. J. and Kennedy, C.: Modelling the impact of weather conditions on active transportation travel behaviour, Transp. Res. Part D Transp. Environ., 17(2), 129–137, doi:10.1016/j.trd.2011.09.005, 2012.
Santamouris, M., Papanikolaou, N., Livada, I., Koronakis, I., Georgakis, C., Argiriou, A. and Assimakopoulos, D. .: On the impact of urban climate on the energy consumption of buildings, Sol. Energy, 70(3), 201–216, doi:10.1016/S0038-092X(00)00095-5, 2001.
Schechtman, E., Bar-Gera, H. and Musicant, O.: Driver views on speed and enforcement, Accid. Anal. Prev., doi:10.1016/j.aap.2015.12.028, 2016.
Schoetter, R., Masson, V., Bourgeois, A., Pellegrino, M. and Lévy, J. P.: Parametrisation of the variety of human behaviour related to building energy consumption in the Town Energy Balance (SURFEX-TEB v. 8.2), Geosci. Model Dev., 10(7), 2801–2831, doi:10.5194/gmd-10-2801-2017, 2017.
Seabold, S. and Perktold, J.: statsmodels: Econometric and statistical modeling with python, in Proceedings of the 9th Python in Science Conference., 2010.
Sellers, W. D.: Physical Climatology, 4th ed., Univeristy of Chicago Press, Ltd., 1972.
Sericola, B.: Markov chains: theory, algorithms and applications, John Wiley & Sons, Inc., 2013.
Smith, C., Lindley, S. and Levermore, G.: Estimating spatial and temporal patterns of urban anthropogenic heat fluxes for UK cities: The case of Manchester, Theor. Appl. Climatol., 98(1–2), 19–35, doi:10.1007/s00704-008-0086-5, 2009.
Spitler, J. D.: Thermal Load and Energy performance prediction, in Building performance simulation for design and operation, edited by J. L. Hensen and R. Lamberts, Spon Press., 2011.
Statistics Canada: Statistical Area Classification (SAC), [online] Available from: http://www12.statcan.gc.ca/census-recensement/2011/ref/dict/geo045-eng.cfm (Accessed 15 January 2018), 2017.
Steadman, P., Bruhns, H. R. and Rickaby, P. A.: An introduction to the national Non-Domestic Building Stock database, Environ. Plan. B Plan. Des., 27(1), 3–10, doi:10.1068/bst2, 2000.
Stewart, I. D. and Kennedy, C. A.: Metabolic heat production by human and animal populations in cities, Int. J. Biometeorol., 61(7), 1159–1171, doi:10.1007/s00484-016-1296-7, 2017.
Stewart, I. D. and Oke, T. R.: Local climate zones for urban temperature studies, Bull. Am. Meteorol. Soc., 93(12), 1879–1900, doi:10.1175/BAMS-D-11-00019.1, 2012.
Sun, T. and Grimmond, S.: A Python-enhanced urban land surface model SuPy (SUEWS in Python, v2019.2): Development, deployment and demonstration, Geosci. Model Dev., 12(7), 2781–2795, doi:10.5194/gmd-12-2781-2019, 2019.
Sun, T., Järvi, L., Omidvar, H., Theeuwes, N., Lindberg, F., Li, Z. and Grimmond, S.: Urban-Meteorology-Reading/SUEWS: 2020a Release (Version 2020a): EmissionsMethod, , doi:10.5281/zenodo.3828525, 2020a.
Sun, T., Järvi, L., Omidvar, H., Theeuwes, N., Lindberg, F., Li, Z. and Grimmond, S.: Urban-Meteorology-Reading/SUEWS: 2020a Release (Version 2020a): Input files, , doi:10.5281/zenodo.3828525, 2020b.
Sun, T., Järvi, L., Omidvar, H., Theeuwes, N., Lindberg, F., Li, Z. and Grimmond, S.: Urban-Meteorology-Reading/SUEWS: 2020a Release (Version 2020a): Wind, Temperature and Humidity Profiles in the Roughness Sublayer, [online] Available from: http://doi.org/10.5281/zenodo.3828525 (Accessed 8 December 2020c), 2020.
Sun, Z., Lorscheid, I., Millington, J. D., Lauf, S., Magliocca, N. R., Groeneveld, J., Balbi, S., Nolzen, H., M??ller, B., Schulze, J. and Buchmann, C. M.: Simple or complicated agent-based models? A complicated issue, Environ. Model. Softw., 86(3), 56–67, doi:10.1016/j.envsoft.2016.09.006, 2016.
Takane, Y., Kikegawa, Y., Hara, M. and Grimmond, C. S. B.: Urban warming and future air-conditioning use in an Asian megacity: importance of positive feedback, npj Clim. Atmos. Sci., 2(1), 1–11, doi:10.1038/s41612-019-0096-2, 2019.
Tang, Y., Sun, T., Luo, Z., Omidvar, H., Theeuwes, N., Xie, X., Xiong, J., Yao, R. and Grimmond, S.: Urban typical meteorological year (uTMY) for building energy modelling (under review), , 1–31,

2021.
Taylor, J. W. and Buizza, R.: Using weather ensemble predictions in electricity demand forecasting, Int. J. Forecast., 19(1), 57–70, doi:10.1016/S0169-2070(01)00123-6, 2003.
TfL: Bus service usage: passengers and kilometres operated by route (2014 - 2015), [online] Available from: https://tfl.gov.uk/corporate/publications-and-reports/buses#on-this-page-1 (Accessed 11 February 2020), 2018.
TfL: Number of Buses by Type of Bus in London, [online] Available from: https://data.london.gov.uk/dataset/number-buses-type-bus-london (Accessed 11 February 2020), 2019.
Thorsson, S., Rocklöv, J., Konarska, J., Lindberg, F., Holmer, B., Dousset, B. and Rayner, D.: Mean radiant temperature - A predictor of heat related mortality, Urban Clim., 10(P2), 332–345, doi:10.1016/j.uclim.2014.01.004, 2014.
Tian, W.: A review of sensitivity analysis methods in building energy analysis, Renew. Sustain. Energy Rev., 20, 411–419, doi:10.1016/j.rser.2012.12.014, 2013.
Torriti, J.: Understanding the timing of energy demand through time use data: Time of the day dependence of social practices, Energy Res. Soc. Sci., 25, 37–47, doi:10.1016/j.erss.2016.12.004, 2017.
Tsapakis, I., Cheng, T. and Bolbol, A.: Impact of weather conditions on macroscopic urban travel times, J. Transp. Geogr., 28, 204–211, doi:10.1016/j.jtrangeo.2012.11.003, 2013.
U.S. Department of Energy: EnergyPlusVersion 9.3.0: Engineering Reference., 2020.
UK Statutory Instruments: The Building Regulations 1965 SI 1965/1373, [online] Available from: https://www.legislation.gov.uk/uksi/1965/1373/made (Accessed 9 October 2020), 1965.
Underwood, C. P. and Yik, F. W. H.: Modelling Methods for Energy in Buildings, Blackwell Publishing Ltd., 2004.
United Nations: World Urbanization Prospects. The 2018 Revision, Methodology ESA/P/WP/252, New York. [online] Available from: https://population.un.org/wup/Publications/Files/WUP2018-Methodology.pdf, 2018.
US Census Bureau: US Census Geography, [online] Available from: https://www.census.gov/programs-surveys/geography.html (Accessed 28 November 2019), 2019.
Valuation Office Agency: Dwellings by Property Build Period and Type, [online] Available from: https://data.london.gov.uk/dataset/property-build-period-lsoa (Accessed 29 January 2018), 2015.
Wang, X., Feng, W., Cai, W., Ren, H., Ding, C. and Zhou, N.: Do residential building energy efficiency standards reduce energy consumption in China? – A data-driven method to validate the actual performance of building energy efficiency standards, Energy Policy, 131(February 2018), 82–98, doi:10.1016/j.enpol.2019.04.022, 2019.
Ward, H. C. and Grimmond, C. S. B.: Assessing the impact of changes in surface cover, human behaviour and climate on energy partitioning across Greater London, Landsc. Urban Plan., 165, 142–161, 2017.
Ward, H. C., Evans, J. G. and Grimmond, C. S. B.: Multi-season eddy covariance observations of energy, water and carbon fluxes over a suburban area in Swindon, UK, Atmos. Chem. Phys., 13(9), 4645–4666, doi:10.5194/acp-13-4645-2013, 2013.
Ward, H. C., Kotthaus, S., Järvi, L. and Grimmond, C. S. B.: Surface Urban Energy and Water Balance Scheme (SUEWS): Development and evaluation at two UK sites, Urban Clim., 18, 1–32, doi:10.1016/j.uclim.2016.05.001, 2016.
Ward, I. C.: What are the energy and power consumption patterns of different types of built environment?, Energy Policy, 36(12), 4622–4629, doi:10.1016/j.enpol.2008.09.066, 2008.
Widén, J. and Wäckelgård, E.: A high-resolution stochastic model of domestic activity patterns and electricity demand, Appl. Energy, 87(6), 1880–1892, doi:10.1016/j.apenergy.2009.11.006, 2010.
Widén, J., Nilsson, A. M. and Wäckelgård, E.: A combined Markov-chain and bottom-up approach to modelling of domestic lighting demand, Energy Build., 41(10), 1001–1012, doi:10.1016/j.enbuild.2009.05.002, 2009a.
Widén, J., Lundh, M., Vassileva, I., Dahlquist, E., Ellegård, K. and Wäckelgård, E.: Constructing load profiles for household electricity and hot water from time-use data-Modelling approach and

validation, Energy Build., 41(7), 753–768, doi:10.1016/j.enbuild.2009.02.013, 2009b.
Widén, J., Molin, A. and Ellegård, K.: Models of domestic occupancy, activities and energy use based on time-use data: deterministic and stochastic approaches with application to various building-related simulations, J. Build. Perform. Simul., 5(1), 27–44, doi:10.1080/19401493.2010.532569, 2012.
Willmott, C. J., Robeson, S. M. and Matsuura, K.: Climate and other models may be more accurate than reported, Eos (United States), 98(9), 13–14, doi:10.1029/2017eo074939, 2017.
Wood, G. and Newborough, M.: Dynamic energy-consumption indicators for domestic appliances: Environment, behaviour and design, Energy Build., 35(8), 821–841, doi:10.1016/S0378-7788(02)00241-4, 2003.
Wright, A.: What is the relationship between built form and energy use in dwellings?, Energy Policy, 36(12), 4544–4547, doi:10.1016/j.enpol.2008.09.014, 2008.
Wu, N.: A new approach for modeling of Fundamental Diagrams, Transp. Res. B, 36(10), 867–884, doi:10.1016/S0965-8564(01)00043-X, 2000.
Xie, M., Zhu, K., Wang, T., Feng, W., Gao, D., Li, M., Li, S., Zhuang, B., Han, Y., Chen, P. and Liao, J.: Changes in regional meteorology induced by anthropogenic heat and their impacts on air quality in South China, Atmos. Chem. Phys., 16(23), 15011–15031, doi:10.5194/acp-16-15011-2016, 2016a.
Xie, M., Liao, J., Wang, T., Zhu, K., Zhuang, B., Han, Y., Li, M. and Li, S.: Modeling of the anthropogenic heat flux and its effect on air quality over the Yangtze River Delta region, China, Atmos. Chem. Phys. Discuss., 15(22), 32367–32412, doi:10.5194/acpd-15-32367-2015, 2016b.
Yan, D., O'Brien, W., Hong, T., Feng, X., Burak Gunay, H., Tahmasebi, F. and Mahdavi, A.: Occupant behavior modeling for building performance simulation: Current state and future challenges, Energy Build., 107, 264–278, doi:10.1016/j.enbuild.2015.08.032, 2015.
Yohanis, Y. G., Mondol, J. D., Wright, A. and Norton, B.: Real-life energy use in the UK: How occupancy and dwelling characteristics affect domestic electricity use, Energy Build., 40(6), 1053–1059, doi:10.1016/j.enbuild.2007.09.001, 2008.
Yu, M., Carmichael, G. R., Zhu, T. and Cheng, Y.: Sensitivity of predicted pollutant levels to anthropogenic heat emissions in Beijing, Atmos. Environ., 89, 169–178, doi:10.1016/j.atmosenv.2014.01.034, 2014.
Zhang, J. and Wu, L.: Influence of human population movements on urban climate of Beijing during the Chinese New Year holiday, Sci. Rep., 7(August 2016), 1–8, doi:10.1038/srep45813, 2017.
Zhang, Y., Balzter, H. and Wu, X.: Spatial-temporal patterns of urban anthropogenic heat discharge in Fuzhou, China, observed from sensible heat flux using Landsat TM/ETM+ data, Int. J. Remote Sens., 34(4), 1459–1477, doi:10.1080/01431161.2012.718465, 2013.
Zheng, Y. and Weng, Q.: High spatial- and temporal-resolution anthropogenic heat discharge estimation in Los Angeles County, California, J. Environ. Manage., 206, 1274–1286, doi:10.1016/j.jenvman.2017.07.047, 2017.